STUDIES OF METAL ION - PHOSPHINE OXIDE AND ARSINE OXIDE INTERACTIONS

A thesis presented for the degree of

Doctor of Philosophy in Chemistry

in the University of Canterbury,

Christchurch, New Zealand.

by

NG YEW SUN

1977

With three accompanying pamphlets

in back pocket

To

My Mother

And

Mandy

ACKNOWLEDGEMENTS

I wish to express my sincere appreciation to my Supervisors, Drs. W.T. Robinson and G.A. Rodley, for their advice and assistance throughout the course of this work. Thanks are also due to Dr. R.G.A.R. Maclagan who assisted in the strain-energy calculations, to Dr. F.C. March for his helpful comments on the solution of the dinuclear structure and to my colleagues for many helpful discussions and proof-reading various parts of this thesis. I am also grateful to my family for the support and encouragement which enabled me to further my studies. The award of a Teaching Fellowship is appreciated.

CONTENTS

LIST OF FIGURES

LIST OF TABLES

ABBREVIATIONS

M	metal
L	ligand
Bu_3PO	tributylphosphine oxide
Me_3PO	trimethylphosphine oxide
Me_3AsO	trimethylarsine oxide
Ph_3PO	triphenylphosphine oxide
Ph_3Aso	triphenylarsine oxide
Ph_2MePO	diphenylmethylphosphine oxide
Ph_2MeAsO	diphenylmethylarsine oxide
HMPA	hexamethylphosphoramide
MORPO	morpholinophosphine oxide
diphos	diphenylphosphine
diars	dialkylarsine
THF	tetrahydrofuran
THT	tetrahydrothiophene
TPP	tetraphenylporphine
MgP_c	dipyridinated magnesium phthalocyanin
Meso	mesoporphyrin
DPEP	deoxo-phylloerythroetioporphyrin
TpivPP	picket-fence porphyrin
acac	acetylacetonate
AcO	acetate
act	acetamide
ala	alanine
apy	antipyrine
cit	citrate
catec	o-dihydroxobenzene
DBA	bis(1,3,5-triketone)

en	ethylenediamine
eSace	ethylenedithioacetate
gly	glycine
imp	inosine 5'-monophosphate
mis	myo-inositol
mpq	substituted quinoline
picox	2-picoline N-oxide
py	pyridine
sar	sarcosine
tren	tris(2-aminoethyl)amine
T_2	tropolonate ion
taz	1,2,4-triazole
Sal-NR	N-alkyl-salicylideneiminate
Sal-dipa	bis(salicylidene-γ-iminopropyl)amine
SalMeDPT	bis(salicylidene-γ-iminopropyl)methylamine
bdhe	N,N-bis(2-diethylaminoethyl)-2-hydroxyethylamine
bddae	N,N-bis(2-diethylaminoethyl)-2-diphenyl-arsinoethylamine
CR	tetrazabicyclo-heptadeca-pentaene derivative
dacoDA	1,5-diazacyclo-octane N,N'-diacetate
dmp	2,9-dimethyl-1,10-phenanthroline
DMF	dimethylformamide
DPP	1,3-diphenyl-1,3-propenedione
mpdo	1-(o-methoxyphenyl)-2,6-diazaoctane
Medabco	N-methyl-diazabicyclo-octonium derivative
Me_2dtp	bis(o,o'-dimethyl-dithiophosphate)
Me_6tren	tris(2-dimethylaminoethyl)amine
osdd	1-oxo-7,10-dithio-4,13-diazacyclopentadecane
tet	N,N'-bis(3-aminopropyl)piperazine
tpen	N,N,N'-tris(2-(2'-pyridyl)ethyl)ethylenediamine

ABSTRACT

This thesis reports a study of metal complexes of trimethylphosphine and trimethylarsine oxides. X-ray crystal structure determinations and other physical studies, notably infrared and nmr, were used to assess the factors that influence the stereochemistries of these complexes.

It was observed that the compounds, $(Mg(Me_3AsO)_5)(ClO_4)_2$, $(Ni(Me_3AsO)_5)(ClO_4)_2$ and $(Mg(Me_3PO)_5)(ClO_4)_2$, readily adopt the square-pyramidal geometry. Two unusual features have been found in these complexes. The axial metal-oxygen bonds are consistently shorter than the corresponding basal metal-oxygen bonds, and the penultimate atoms (phosphorus and arsenic) of the basal ligands are coplanar with the square-base of the pyramid. This latter feature produces a large space in the region of the vacant sixth coordination site. The shorter axial metal-oxygen bond is discussed in terms of a stronger π interaction in the axial direction while the stability of the square-pyramidal geometry is explained in terms of electrostatic interactions between adjacent basal oxygen and arsenic atoms. Further evidence of this type of interaction was obtained from coulombic calculations.

The crystal structures of $(Mg(Me_3PO)_5)(ClO_4)_2$ and $(Mg(Me_3PO)_5H_2O)(ClO_4)_2$ enable the influence of a sixth ligand on the coordination geometry to be assessed. The significance of the formation of the five-coordinate square-pyramidal geometry and the stereochemical effects of the binding of a sixth ligand are discussed in relation to the possible importance of these geometrical features in the biological function of calcium and magnesium ions.

Comparisons between the donor powers of the phosphine oxide and arsine oxide are made. While arsine oxide has a greater σ donor strength, phosphine oxide is capable of a stronger π interaction.

An interesting dinuclear structure was determined for a calcium arsine oxide complex. This complex, $(Ca_2(Me_3AsO)_9)(ClO_4)_4$, was found to be bridged by arsine oxide ligands. The different donor capacities of the terminal and bridging ligands are discussed in relation to X-ray and nmr results.

CHAPTER 1

INTRODUCTION

1.1 GENERAL INTRODUCTION

In this work, the crystal structures of some selected complexes of calcium, magnesium and nickel having trimethylphosphine oxide and trimethylarsine oxide ligands were determined. Changes in stereochemistry resulting from varying either the metal ions or the ligands were compared in order to obtain information concerning the nature of the coordinate bonds. The precise data obtained from X-ray single crystal structure determinations enabled the influences of metal ions and ligands on the coordination geometry of the complexes to be investigated thoroughly. Although this work was mainly concerned with more detailed knowledge of the coordination chemistry of calcium and magnesium, consideration was also given to the possibility of relating the structural features of the present compounds to the nature of the metal coordination sites in biological systems.

1.2 A SUMMARY OF THE PRESENT WORK

The crystal structures of five chemically and structurally related compounds were determined. Throughout this thesis these five compounds will be referred to by their formulae, thus conveniently distinguishing the changes in metal and ligand atoms in discussion. Three of these compounds, $(Ni(Me_3AsO)_5)(ClO_4)_2$, $(Mg(Me_3AsO)_5)(ClO_4)_2$ and $(Mg(Me_3PO)_5)(ClO_4)_2$, were found to be five-coordinate and isomorphous. The fourth compound was $(Mg(Me_3PO)_5H_2O)(ClO_4)_2$, a six-coordinate mono aquo adduct of

$(Mg(Me_3PO)_5)(ClO_4)_2$. The fifth compound was a novel dinuclear complex, $(Ca_2(Me_3AsO)_9)(ClO_4)_4$, with a confacial bi-octahedral geometry. Apart from $(Mg(Me_3AsO)_5)(ClO_4)_2$, crystals suitable for X-ray diffraction had to be recrystallized from powder samples. A considerable amount of effort was spent in obtaining suitable crystals of anhydrous $(Mg(Me_3PO)_5)(ClO_4)_2$, since this complex is extremely sensitive to moisture. Since different substituents on the phosphorus or arsenic atoms may affect the ligation properties, only methyl substituted phosphine and arsine oxides were used in order to simplify comparisons.

In Chapter 2 a general description of the experimental and computing methods employed in the structure solutions is given. Departures from standard procedures are explicitly noted in the appropriate chapters. Non-standard Patterson methods such as the difference Patterson (Chapter 3) and the Patterson projection (Chapter 5) were used to obtain trial models when more usual procedures did not yield solutions readily. These models were refined by least-squares techniques. For isomorphous structures, the coordinates from one structure were used as a starting set for the other.

Analyses of the crystal structures of the two isomorphous compounds, $(Mg(Me_3AsO)_5)(ClO_4)_2$ and $(Ni(Me_3AsO)_5)(ClO_4)_2$ [1] are reported in Chapter 3. In each case the metal atom is in a five-coordinate square-pyramidal environment provided by five oxygen atoms of the donor ligands. Two notable features observed in these complexes are:

(i) a shorter M-O axial than M-O basal bond, and

(ii) the co-planarities of the basal arsenic and oxygen atoms with the square base of the pyramid.

Similarities in the detailed geometry of the transition metal ion Ni(II) and the non-transition metal ion Mg(II) provide insight into the factors which influence the coordination polyhedron; both steric and electronic factors are discussed.

Chapter 4 is concerned with the crystal structure analyses of the five-coordinate anhydrous $(Mg(Me_3PO)_5)(ClO_4)_2$ complex and its six-coordinate hydrated adduct $(Mg(Me_3PO)_5H_2O)(ClO_4)_2$. $(Mg(Me_3PO)_5)(ClO_4)_2$ is isomorphous with $(Mg(Me_3AsO)_5)(ClO_4)_2$ and $(Ni(Me_3AsO)_5)(ClO_4)_2$, while $(Mg(Me_3PO)_5H_2O)(ClO_4)_2$ crystallizes in a non-centrosymmetric orthorhombic space group. Further stereochemical insights can be obtained by examining the changes induced on coordination by a sixth ligand. Consistent trends in the structural variations have been observed and discussed.

The interesting dinuclear complex, $(Ca_2(Me_3AsO)_9)(ClO_4)_4$, is discussed [2] in Chapter 5. It crystallizes in a hexagonal space group. The two, octahedrally coordinated, calcium atoms are triply-bridged by oxygen atoms of three trimethylarsine oxide molecules giving rise to a confacial bi-octahedral geometry which is similar to a range of dinuclear complexes of the type $M_2X_9^{3-}$ where M = Cr, Mo, W and X = halides [3-5]. Factors influencing the stereochemistry are discussed and in addition, comparisons with other calcium complexes are made.

Chapter 6 summarizes some chemical investigations related to this

work and includes a brief summary of five-coordination chemistry. Emphasis is placed on factors determining stereochemistry in these situations. Infrared and nmr data on phosphine and arsine oxide metal complexes are discussed with reference to the structural parameters obtained. Strain-energy minimization calculations for several coordination geometries of the $(Mg(Me_3AsO)_5)^{2+}$ cation were performed. Their relative stabilities are analysed. The last section of this chapter presents a tentative bonding scheme for the metal complexes.

Chapter 7 suggests a relevance of these investigations of calcium and magnesium complexes to proposed mechanisms for muscle contraction and photosynthesis, respectively.

1.3 A BRIEF REVIEW OF PHOSPHORYL AND ARSENYL METAL COMPLEXES

Coordinate compounds of phosphine oxide were described as early as 1861 by Hoffmann[6] who prepared $ZnI_2(Et_2PO)_2$. In the century that followed, however, few additional investigations were made [7-9]. It was not until the late 1950's when a strong interest in metal complexes having neutral, substituted phosphine and arsine oxide (R_3XO, X = P, As) ligands was again developed [10-14]. Since then, numerous metal complexes have been synthesized and, to a much lesser extent, structurally characterized [15].

Originally, interest was focused on which atom of the phosphoryl group acted as the electron donor (Lewis base) towards the inorganic electron acceptor (Lewis acid). A classic example was the controversy over the two possible formulations of $SbCl_5(Cl_3PO)$ [16]. Sheldon and

Tyree [10] studied the infrared spectra of phosphoryl ligands and observed, invariably, a negative shift in the P-O stretching vibrational frequency upon metal complex formation. They suggested that the phosphoryl group coordinates to the metal ion through the oxygen atom. This suggestion was subsequently substantiated by the crystal structure determination of $SbCl_5(Cl_3PO)$ [17].

A hindrance to the study of phosphine and arsine oxide metal complexes has been a tendency of these complexes to be decomposed by water. Synthetic methods, involving the use of organic dehydrating agents, such as triethyl orthoformate or 2,2-dimethoxypropane were introduced in 1969 [18,19]. In this work, triethyl orthoformate was used extensively as a dehydrating agent [1,2].

Of the studies undertaken to date, the majority have concentrated on transition metal ions [20-61]. Most of such complexes can be classified into the formulation of ML_nX_m, where usually:

M = Ti, V, Cr, Mn, Fe, Co, Ni, Cu, Zn, Pt, Pd(II);

L = Ph_3PO, Ph_3AsO, Me_3PO, Me_3AsO, Ph_2MePO, Ph_2MeAsO etc.;

X = Cl, Br, I, ClO_4, NO_3, NCS, BF_4, and

m and n = 2-4.

The stereochemistry of transition metal cationic complexes of phosphine and arsine oxides has been a challenging subject for study [11, 33, 34, 38-41]. These metal complexes normally involve coordination of four or five ligand molecules to the central metal ion. Often, the bulkiness of the ligand molecules has been considered the overriding factor in determining the stereochemistry. However,

two octahedral complexes $(M(HMPA)_6)(ClO_4)_3$, (M = Cr, Fe; HMPA = hexamethylphosphoramide) have been reported [62]. In addition, de Bolster et al were able to prepare complexes of the type $(M(Ph_3PO)_5BF_4)BF_4$, (M = Co, Ni) [57]. They noted that other factors, such as overlap between metal and ligand and choice of solvent may play important roles in determining the structure of a given compound [57].

A number of lanthanide and actinide complexes with phosphine and arsine oxides have also been reported in recent years [63-73]. By contrast, compounds with lanthanide and actinide ions usually display coordination numbers (C.N.) higher than six; due probably to the larger cationic sizes. By assuming that the NO_3^- ion acts as a bidentate ligand, some complexes have been assigned the following compositions: $M(NO_3)_3(Ph_3PO)_2EtOH$, C.N. = 9; $M(NO_3)_3(Ph_3PO)_3$, C.N. = 9; $M(NO_3)_3(Ph_3PO)_4$, C.N. = 10 and $(M(NO_3)_2(Ph_3PO)_4)(NO_3)$, C.N. = 8, (M = Y, La-Lu, except Pm, Yb)[64]. Crystal structure determinations of compounds of empirical formula $UO_2(CH_3COO)_2L$; L = Ph_3PO, Ph_3AsO, show that both structures are dimeric [74]. The uranium atom is seven-coordinated and the dimeric units are bridged by acetato groups. In $UO_2((C_2H_5)_2NCS)_2L$; L = Ph_3PO, Ph_3AsO, the uranium atom is similarly found to exist in a seven-coordinate pentagonal-bipyramidal environment [75].

With non-transition elements, less extensive studies were undertaken [43, 46, 57, 58, 76-82]. A number of adducts of lithium and sodium salts with Ph_3PO have been prepared; some of which have the formula of $MX \cdot 5L$ [83]. The crystal structure of the adduct $LiI \cdot 5Ph_3PO$ has been determined [84]. The oxygen atoms of four ligand

molecules are tetrahedrally coordinated to the lithium ion and the iodide ions occupy isolated positions distant from the lithium. The fifth Ph_3PO is enclosed by the rest of the structure. Previous work with phosphine oxide complexes of calcium and magnesium has been an appendage to studies of transition metal ions. Complexes of MORPO [58] (MORPO = morpholinophosphine oxide), Ph_3PO [46] and Bu_3PO [43] with calcium and magnesium have been prepared. Other papers have presented the coordination chemistry of In [78], Sn [76, 77, 79] and Sb [27] halides with phosphine and arsine oxides. More recently, Jameson and Rodley reported various phosphine and arsine oxide complexes of calcium and magnesium [85, 86].

In some studies, for example, complexes of $MCl_6L_3 \cdot xH_2O$ (M = Nd(III) and Sm(III), L = 1, 2-ethylene-bisdiphenylphosphine and arsine oxide), the bidentate ligands act as bridging groups and give polymeric compounds [67]. This, however, is not an exclusive property of bidentate ligands. Monodentate ligands have similarly been suggested to be involved in forming polymers, such as $(Mg(Ph_3PO)_4)_n(ClO_4)_{2n}$ [46], $(Cu(Bu_3PO)_{4n})(ClO_4)_{2n}$ [43], $(M(Ph_3PO)_2(SO_4)_2)_n$ where M = Fe, Ni [59], and the dinuclear $(Ca_2(Me_3AsO)_9)^{4+}$ cation to be described in Chapter 5.

CHAPTER 2

EXPERIMENTAL PROCEDURES IN X-RAY STRUCTURE DETERMINATIONS

2.1 INTRODUCTION

Discussion in this chapter is confined to a brief, general overview of some of the common procedures employed in crystal structure analyses. Details of their application to specific analyses are given in later chapters.

Of the five compounds studied, the structures of pentakis-(trimethylarsine oxide)magnesium(II) diperchlorate, $(Mg(Me_3AsO)_5)(ClO_4)_2$, and its nickel(II) analogue, $(Ni(Me_3AsO)_5)(ClO_4)_2$, were solved [1] by difference Patterson syntheses and standard Fourier methods. The structure of the pentakis(trimethylphosphine oxide)monoaquo magnesium(II) diperchlorate complex, $(Mg(Me_3PO)_5H_2O)(ClO_4)_2$, was determined using direct methods. Its anhydrous analogue, $(Mg(Me_3PO)_5)(ClO_4)_2$, is isomorphous with the $(Mg(Me_3AsO)_5)(ClO_4)_2$ and $(Ni(Me_3AsO)_5)(ClO_4)_2$ structures. The tri-μ-(trimethylarsine oxide)-hexakis(trimethylarsine oxide)-dicalcium(II) tetraperchlorate structure, $(Ca_2(Me_3AsO)_9)(ClO_4)_4$, was solved [2] via its Patterson projection.

2.2 EXPERIMENTAL DETAILS

A structure investigation commences with the determination of cell parameters and crystallographic space group. The next stage is the collection of intensity data which are necessary for the

elucidation of detailed crystal structures. This section deals with some particulars of these procedures.

2.2.1 Primary Crystal Data

Preliminary Weissenberg and precession photographs were used to establish approximate unit cell constants and possible space groups. The densities of $(Ni(Me_3AsO)_5)(ClO_4)_2$ and $(Mg(Me_3PO)_5)(ClO_4)_2$ were not measured because of their extreme sensitivities to moisture. The densities of other air-stable compounds were measured by the flotation method [87]. Crystals of suitable quality for data collection were selected after examining precession photographs. Single crystals were mounted on goniometer heads in random orientations to minimize incidence of multiple reflections [88]. The air-sensitive compounds were sealed in capillary tubes which were then glued onto the goniometer heads.

2.2.2 Collection Of Intensity Data

Initially two or more reflections were indexed on precession photographs before the crystal was transferred to the Hilger and Watts computer controlled four-circle diffractometer for full three-dimensional data collection. After accurately centering the crystal for rotational movement using the diffractometer telescope, these indexed reflections were used to provide an initial matrix for finding intense reflections in reciprocal space.

Unit cell and crystal orientation parameters were obtained by least-squares refinements [89] using the setting angles of twelve reflections accurately centred in a 5.0 mm diameter collimator with its circular receiving aperture set at 230 mm from the crystal.

Parameters were considered to have converged to best values when the difference between the observed and calculated setting angles for the twelve reflections was less than 0.03° and estimated standard deviations (esd's) for the diffractometer orientation defining angles were less than 0.01°. The diffracted beam collimator allowed both the K_{α_1} and K_{α_2} maxima in the diffracted beams to be recorded and hence the wavelength used in all refinements was $K_{\bar{\alpha}}$, the weighted mean of the K_{α_1} and K_{α_2} components.

The mosaicity of each crystal was examined by means of open-counter ω-scans [90] at a take-off angle of 3°, and was judged to be very good when peak widths at half-height for strong low angle reflections were in the range of 0.05° to 0.2°. Intensities of all reflections were recorded using the ω-2θ scan techniques. The incident X-radiation was filtered with the appropriate β-filters. The scans were symmetric and centred on the peak position calculated from the wavelength of $K_{\bar{\alpha}}$ radiation. Scan steps were set at 0.02° in 2θ and 0.01° in ω whereas scan widths were determined experimentally for each crystal. Stationary crystal, stationary counter background counts were taken at both ends of the scan range.

Calibrated attenuators were used to bring strong reflections within the linear response range of the scintillation counter whenever rates exceeded 8,000 counts/sec. Throughout the data collections three strong reflections were measured regularly and subsequently used to correct data for non-statistical variations in intensity due, for example, to crystal decomposition.

2.2.3 Reduction Of Intensity Data

Data processing was carried as described by Corfield, Doedens and Ibers [91]. The integrated intensity was given by

$$I = C-0.5(t_c/t_b)(B_1+B_2)$$

where C is the scan count, t_c and t_b are scan and background times and B_1 and B_2 are the background counts. The standard deviation for each measured intensity was

$$\sigma(I) = (C+0.25(t_c/t_b)^2(B_1+B_2)+(pI)^2)^{\frac{1}{2}}$$

and p is a factor initially assigned a value of 0.05 and is an adjustable factor used to avoid overweighting more intense reflections [92]. Lorentz-polarization effects were applied to I and $\sigma(I)$ to obtain values of F_o^2 and $\sigma(F_o^2)$.

In cases where more than one equivalent member of the form were collected, these data were averaged. F_o^2 values of these data were taken as the weighted mean of the individual observations. The standard deviation of F_o^2, $\sigma(F_o^2)$, was taken either as the average of the individual standard deviations of the equivalent forms or as a value estimated from the range of the F_o^2 values of the equivalent forms, whichever was larger [91]. All esd's were finally multiplied by $(N/NEQ)^{\frac{1}{2}}$ where N was the number of equivalent sets of reflections collected and NEQ was the number of times a reflection was actually observed [93].

The standard deviation of each reflection intensity was required

to compute a weighting factor, $w = 4F_o^2/\sigma(F_o^2)^2$, which was used in the least-squares minimization of the function

$$\Sigma w(|F_o|-|F_c|)^2$$

where $|F_o|$ and $|F_c|$ are the observed and calculated structure factor amplitudes. Weights were adjusted so that the function showed as small as possible dependence on $|F_o|$, $\sin\theta/\lambda$ and reflection indices [94].

Absorption corrections were applied, where necessary, using Gaussian integration performed by the program DABS [95*]. Input to this program consisted of indices of boundary faces of the crystal and perpendicular distances of these faces from any defined origin within the crystal.

2.3 SOLUTION AND REFINEMENT PROCEDURES

The elucidations of the structures described in this thesis were either by way of Patterson syntheses, or direct methods, combined with Fourier techniques and full-matrix least-squares refinements. These procedures are discussed separately below.

2.3.1 The Patterson Function

The Patterson function [96], which involves only the square of the amplitudes and not the phases of the structure factor, is

---

* A list of the computer program used in these structure determinations is given in Appendix A. All calculations were performed on a Burroughs B6718 computer.

commonly written in the Fourier series form as

$$P(u,v,w) = V^{-1}\sum_{hkl}\sum\sum|F(hkl)|^2\cos 2\pi(hu+kv+lw)$$

where V is the volume of the unit cell. This function shows maxima at uvw, corresponding to interatomic vectors between atoms in the unit cell at x_1, y_1, z_1 and x_2, y_2, z_2 such that

$$u = x_1 - x_2$$
$$v = y_1 - y_2$$
$$w = z_1 - z_2.$$

If a unit cell contains N atoms, there are N^2 vectors in the Patterson function. N of these vectors are of zero magnitude, being vectors from each atom to itself and coalesced at u = v = w = 0. There are thus N^2-N non-origin peaks in a Patterson calculation. Because of the requirement to pack N^2-N rather than N peaks in the unit cell, there is a greater degree of overlap among the peaks of a Patterson map than of an electron density map. This effect is further accentuated by the larger intrinsic breadth of the Patterson peaks. To improve the resolution, use is made of the sharpening process (program SHNORM [97]), which involves modification of $F^2(hkl)$ such that dependence of the atomic scattering factors on $\sin\theta/\lambda$, and the effects of thermal vibrations are removed [98-100].

2.3.2 Direct Methods

The essence of direct methods is to derive the phases of the structure factors directly by means of mathematical relationships [101, 102]. Developments of these methods were due mainly to Harker and Kasper [103],

Sayre [104], Cochran [105], Zachariasen [106] and Karle and Hauptmann [107]. More recently, Karle and Karle [108] and Main and Woolfson [109] and their co-workers have extended these methods to handle most space groups.

The program MULTAN [110] was used in the solution of the structure of $(Mg(Me_3PO)_5H_2O)(ClO_4)_2$. Input into the program consisted of h, k, l and $|E|$ values. The normalized structure factor magnitudes, $|E|$'s expressed by the formula[101]

$$|E_h|^2 = \frac{|F_h|^2}{\varepsilon \sum_{j=1}^{N} f_j(h)}$$

where $|F_h|$ is the structure factor magnitude, f_j is the atomic scattering factor for j^{th} atom in a unit cell containing N atoms and ε is a number which corrects for space group extinctions, are calculated by the program SHNORM [97].

The program searches for sets of reflections satisfying the Σ_2 relationships

$$\phi_h \simeq \phi_{h'} + \phi_{h-h'}$$

where ϕ_h is the phase associated with the normalized structure factor E_h.

The next section of the program selects a starting set of

reflections. This starting set is made up of three types of reflections:

(i) High |E| reflections whose phases are derived from the Σ_1 relation of the general form

$$S(E_{2h2k2l}) \simeq S(|E_{hkl}|^2 - 1)$$

where $S(E_{hkl})$ means the sign of E_{hkl}

(ii) Origin and enantiomorph (in cases of non-centrosymmetric crystals) defining reflections whose phases are fixed by the restrictions imposed by the space group symmetry and,

(iii) Reflections were chosen, as far as possible, from different parity groups (eee, oee, eoe, eeo, ooe, oeo, eoo and ooo for e = even and o = odd hkl indices) to facilitate the propagation of phase combinations. Phases for these reflections are assigned with all possible combinations of the values $\pm \pi/4$ and $\pm 3\pi/4$ or in the case of centric reflections, 0 and π are used.

Beginning with the starting set, phases of other reflections are determined and refined using the weighted tangent formula [111]

$$\tan\phi_h = \frac{\sum_{h'} w_{h'} w_{h-h'} |E_{h'} E_{h-h'}| \sin(\phi_{h'} + \phi_{h-h'})}{\sum_{h'} w_{h'} w_{h-h'} |E_{h'} E_{h-h'}| \cos(\phi_{h'} + \phi_{h-h'})} = \frac{T_h}{B_h}$$

where w_h is the weight associated with the phase ϕ_h and each weight is computed from

$w_h = \tanh(\frac{1}{2}\alpha_h)$ and

$\alpha_h = |E_h|(T_h^2 + B_h^2)^{\frac{1}{2}}$.

Several iterative cycles using the tangent formula finally lead to convergence on the phases assigned to the data.

For each set of phases determined, figures of merit, which are measures of the reliabilities of the phases assigned, are computed. Data sets with high figures of merit can be used to calculate E-maps using the $|E|$'s with their best refined phase angles as coefficients for the Fourier synthesis. In a correct E-map, the high peaks usually indicate atomic positions. A structure factor calculation or a least-squares refinement can be initiated using these positional parameters.

2.3.3 Difference Fourier Synthesis

In any difference Fourier synthesis, the coefficients used are the differences between observed and calculated structure factors $|F_o|$ and $|F_c|$ and α_c is the phase angle computed from the trial structure. This may be expressed in the form

$$\Delta\rho(x,y,z) = V^{-1}\sum_{hkl}\sum\sum(|F_o|-|F_c|)\exp(i\alpha_c)\exp(-2\pi i(hx+ky+lz)).$$

All Fourier syntheses were calculated in three dimensions and the function was evaluated for unique asymmetric units in sections through the cell. Points were usually sampled at regular intervals, about 0.3Å, parallel to each unit cell axis. Peak positions and peak heights were listed by program FOURIER [112]. Alphanumeric plots and contour were optional routines in the program. Difference Fourier syntheses were used routinely throughout these structure solving processes.

2.3.4 Observed Fourier Synthesis

This method was used in the solution of the $(Mg(Me_3PO)_5H_2O)$-$(ClO_4)_2$ complex. The Fourier series used for computing electron densities is

$$\rho(x,y,z) = V^{-1}\sum_{hkl}\sum\sum|F_o|\exp(i\alpha_c)\exp(-2\pi i(hx+ky+lz))$$

and the terms are as defined before.

The electron density thus evaluated may yield positions of atoms which can be added to the trial model and least-squares refinement can then follow.

2.3.5 Structure Factor Calculations And Least-Squares Refinements

The method of least-squares used in the structure refinements involved minimizing the weighted sum of the squares of the differences between the observed and calculated structure factor amplitudes respectively:

$$\Sigma w(|F_o|-|F_c|)^2$$

where w is the weight calculated as $4F_o^2/\sigma(F_o^2)^2$. The conventional R factors, which are convenient parameters for measuring the correctness of a structure, are defined as

$$R_1 = \Sigma||F_o| - |F_c||/\Sigma|F_o| \text{ and}$$

$$R_2 = (\Sigma w(|F_o| - |F_c|)^2/\Sigma w|F_o|^2)^{\frac{1}{2}}.$$

Positional and thermal parameters of atoms, located by the

process of inspection of Patterson or E-map syntheses, were refined by the full-matrix least-squares methods. Model building proceeded by successive difference Fourier or observed Fourier syntheses to locate further atoms and intermediate least-squares refinement cycles.

The equation for the structure factor may be expressed as

$$F_c(S) = \sum_{j=1}^{N} f_j(S)T_j(S)\exp(2\pi i S r_j)$$

where $f_j(S)$ is the atomic scattering factor, $T_j(S)$ is the thermal effects, and vector r_j is the position of the j^{th} atom respectively in the unit cell and S is the scattering vector. Structure factor calculations and least-squares computations were performed by program CUCLS [113].

(a) Atomic Scattering Factors of Atoms - Atomic scattering factors of non-hydrogen atoms were obtained from Cromer and Mann [114] and those for hydrogen atoms were from Stewart et al [115]. The effects of anomalous scattering

$$f_a = f_o + \Delta f' + \Delta f''$$

were applied in this work. The real and imaginary contributions of anomalous scattering, $\Delta f'$ and $\Delta f''$, were obtained from Cromer's tabulation [116] and f_o is the normal scattering factor. Anomalous scattering effects were used to distinguish the absolute configuration of the pentakis(trimethylphosphine oxide)monoaquo magnesium(II) diperchlorate complex.

(b) Thermal Vibrations of Atoms - Atoms were assumed to be vibrating in harmonic potential fields, and assigned either isotropic or anisotropic thermal parameters as appropriate. For the isotropic case the expression is

$$T_i(S) = \exp(-\tfrac{1}{4}B(2\sin\theta/\lambda)^2)$$

where $B = 8\pi^2\bar{u}^2$ and $\bar{u}^2$ is the root-mean square amplitude of vibration. For anisotropic vibrations, the temperature factor is

$$T_i(S) = \exp(-2\pi^2(u_{11}h^2a^{*2} + u_{22}k^2b^{*2} + u_{33}l^2c^{*2} + 2u_{12}hka^*b^* + 2u_{13}hla^*c^* + 2u_{23}klb^*c^*)$$

where u_{ij} are the thermal parameters in terms of mean-square amplitudes of vibration in Angstroms.

CHAPTER 3

CRYSTAL STRUCTURES OF THE PENTAKIS(TRIMETHYLARSINE OXIDE)-METAL(II) PERCHLORATE $(Ni(Me_3AsO)_5)(ClO_4)_2$ AND $(Mg(Me_3AsO)_5)(ClO_4)_2$

3.1 INTRODUCTION

It is now recognised that monodentate oxo ligands of the type R_3XO (X = P, As) readily form five-coordinate complexes with metal(II) perchlorates [33, 34, 40, 41, 44, 49, 57]. Two basic compositions are obtained: $(M(R_3XO)_4ClO_4)ClO_4$ [34] and $(M(R_3XO)_5)(ClO_4)_2$ [117]. Both geometries have been shown to be square-pyramidal using spectral, magnetic and, in some cases, X-ray techniques.

For simple five-coordinate compounds, the trigonal-bipyramidal structure is predicted on the basis of a valence-shell electron-pair repulsion (VSEPR) model [118, 119]. On the other hand, crystal field calculations indicated that the stabilization energies favour the square-pyramidal structure [120]. The interconversion energy between the trigonal-bipyramid and the alternative square-pyramidal structure may be relatively small, of the order of a few kJ/mole [120]. Intermediate geometries are often observed. Generally, it is not possible to decide a priori which geometry a five-coordinate chromophore will adopt [121]. The present study using monodentate oxo ligands (R_3XO, X = P, As) removed the steric restrictions otherwise imposed by multidentate chelating ligands on the geometry [120, 122]; and allowed an assessment on the reasons for the formation of the square-pyramidal geometry in such systems.

In this Chapter, detailed studies of the square-pyramidal compound $(Ni(Me_3AsO)_5)(ClO_4)_2$ [1, 117] and its magnesium analogue [1] using accurate diffractometer data sets are presented. By comparison with other reported five-coordinate structures, factors that govern their stereochemistry - repulsion between bonding electron pairs, ligand field stabilization energies, steric requirements of the ligands, packing forces in the solid state and electronic configurations of the metal ion and ligand - are analysed.

While octahedral coordination may be the most common geometry for magnesium ions, other coordination numbers of three [123], four [124-126], five [127-130] and eight [131] around the magnesium atom have been observed. Ligand systems with appropriate properties (electronic as well as steric) readily produce five-coordinate Ca(II) and Mg(II) complexes. The magnesium structure discussed in this chapter provides detailed information on a magnesium complex which is representative of a range of five-coordinate complexes of Ca(II) and Mg(II) recently prepared with oxo ligands [85, 86].

The formation of five-coordinate complexes of calcium and magnesium has not been studied extensively. However, this geometry could be of considerable importance in biological systems. Basically similar square-pyramidal chlorophyll-like compounds such as aquomagnesium tetraphenylporphyrin [132], magnesium phthalocyanin [133] and ethyl chlorophyllide a hydrate [134] have been found from X-ray analyses. Five-coordinate species for certain chlorophyll systems have also been indicated from infrared and nmr studies [135]. More recently, the involvement of five-coordinate nickel atoms in enzymatic systems was discussed [136, 137]. These considerations point

to the possibility that in biological systems, hydrophobic regions of protein structures may participate in reducing coordination numbers from six through the elimination of water from the coordination sphere.

3.2 EXPERIMENTAL

3.2.1 Preparation

(a) $(Ni(Me_3AsO)_5)(ClO_4)_2$ Crystals - A powder sample of $(Ni(Me_3AsO)_5)(ClO_4)_2$ was prepared [138] by adding a five-fold excess of trimethylarsine oxide dissolved in acetone to a solution of nickel perchlorate in acetone-triethyl orthoformate [18]. Suitable orange, plate-shaped crystals were obtained by dissolving the complex in acetonitrile-triethyl orthoformate solution, and allowing the solution to reduce in volume on standing over dried ether vapour in a closed vessel. The crystals, being moisture-sensitive, were sealed in Lindemann glass capillaries under a stream of dry nitrogen.

(b) $(Mg(Me_3AsO)_5)(ClO_4)_2$ Crystals - Colourless, transparent, plate-shaped crystals of $(Mg(Me_3AsO)_5)(ClO_4)_2$ were provided by Mr G.B. Jameson [139].

3.2.2 Crystal Data

The crystals were examined by Weissenberg and precession photography using CuK_α radiation. They showed systematic absences uniquely consistent with the monoclinic space group $P2_1/c$ but it was found convenient to solve both the structures using the unconventional setting $P2_1/n$ (equivalent positions: x, y, z; -x, -y, -z; $\frac{1}{2}$+x, $\frac{1}{2}$-y, $\frac{1}{2}$+z; $\frac{1}{2}$-x, $\frac{1}{2}$+y, $\frac{1}{2}$-z). The density of the nickel complex

was not measured because the crystals were extremely moisture-sensitive. The density of the magnesium complex was determined by flotation in a mixture of bromobenzene and dibromoethane [87]. The experimental figure confirmed that there were four molecules in the unit cell. Stoichiometrically it seemed unlikely crystallographic symmetry would be imposed on individual molecules.

Diffraction data were collected from well-formed, plate-shaped crystals. During data collection, the intensities of the three monitored standard reflections for the nickel complex decreased to 63% of their starting values while no great fluctuations in the standard reflections occurred for the magnesium complex. All reflections for each complex were placed on the same relative scale by the method described in Chapter 2, Section 2.2.2.

Important crystal data are given in Table 3.1 and Table 3.2 presents a summary of data collection and processing details. Throughout this thesis the figures given in parentheses are estimated standard deviations in the least significant digits quoted and were usually derived from the inverse matrix in the course of normal least-squares refinement calculations.

3.3 SOLUTION AND REFINEMENT

In the original structure analysis of $(Ni(Me_3AsO)_5)(ClO_4)_2$ using the symbolic addition method, the R factor converged at 0.13 with 1171 film data [117]. However, these atom parameters did not lead to satisfactory refinements with the present diffractometer data sets and were thus abandoned.

Table 3.1

Crystal Data

	$(Ni(Me_3AsO)_5)(ClO_4)_2$	$(Mg(Me_3AsO)_5)(ClO_4)_2$
Formula weight	937.74	903.34
a/Å	11.301(3)	11.330(5)
b/Å	27.256(6)	27.562(6)
c/Å	11.294(5)	11.328(6)
β/deg	90.41(3)	90.58(5)
V_c/Å^3	3478.8	3537.5
d_{measd}/g cm^{-3}		1.73
d_{calcd}/g cm^{-3}	1.79	1.70
Z	4	4
Max crystal dimension/mm	0.5	0.43
Min crystal dimension/mm	0.13	0.18

Table 3.2

Experimental Parameters

	$(Ni(Me_3AsO)_5)(ClO_4)_2$	$(Mg(Me_3AsO)_5)(ClO_4)_2$
Mosaicity/deg	0.19	0.18
θ-Scan range/deg	0.72	0.90
Scan time/sec	72	90
Total background time/sec	18	22.5
θ limit/deg	22	50
Total independent reflections	3975	3552
Reflections used in refinement for which $\|F\|^2 \geq 3\sigma(\|F\|^2)$	1890	2413
Range of transmission factors	0.31-0.50	0.04-0.03
Weighting parameter p	0.05	0.05
Primary beam collimator diameter/mm	2.0	2.0
Secondary beam collimator diameter/mm	5.0	5.0
X-radiation	Mo K_α	Cu K_α

Numerous attempts to solve the structures using Patterson and direct methods were unsuccessful, although intramolecular vectors for the heavy atoms were identified. The inherent difficulty was due mainly to the great number of overlapping vectors such that intermolecular Harker peaks necessary to locate the atomic positions were not prominent in the vector maps. Eventually, a solution was obtained by the difference Patterson synthesis. A general description of the method is given below.

3.3.1 The Difference Patterson Method

When two isomorphous crystals are available, in this instance the nickel and magnesium trimethylarsine oxide complexes, subtraction of one Patterson map from that of the other may reveal a partial, or possibly the total structure [99].

Consider two isomorphous crystals MABCD and NABCD where M and N are the different atoms that occupied the same positions in the two structures which are otherwise the same. For simplification, assume there is only one molecule in the unit cell. The individual Patterson map for the two structures consists of peaks given below:

For MABCD, the vectors are:

MM, AA, BB, CC, DD;

MA, MB, MC, MD, AB, AC, AD, BC, BD, CD, and

centrosymmetrical equivalents.

For NABCD, the vectors are:

NN, AA, BB, CC, DD;

NA, NB, NC, ND, AB, AC, AD, BC, BD, CD, and

centrosymmetrical equivalents.

By subtracting the second Patterson from that of the first, the resultant is a difference Patterson map with peaks corresponding to:

MM-NN;
(M-N)A, (M-N)B, (M-N)C, (M-N)D, and
centrosymmetrical equivalents.

The difference Patterson function can therefore be written as:

$$^{M,N}\Delta(u,v,w) = {}^{M}P(u,v,w) - {}^{N}P(u,v,w)$$

$$= V^{-1}\sum_{hkl}\sum\sum (|{}^{M}F|^2 - |{}^{N}F|^2)_{hkl} \exp 2\pi i(hu+kv+lw) .$$

In essence, the difference Patterson map is a map of the crystal structure where the replaceable atoms are moved to the unit cell origin (Figure 3.1).

In structures which have more than one molecule in the unit cell, ambiguity in the interpretation of the difference Patterson map may arise. It is then necessary to locate the true orientation of the structure by considering its conformation with reference to other symmetry related images.

3.3.2 Application Of Difference Patterson Synthesis To The Solution And Refinement Of The Structures

The positions of the central metal atom and the five arsenic atoms were obtained from the difference between Patterson syntheses calculated using diffractometer data sets. Both the unsharpened Patterson maps for the Ni(II) and Mg(II) complexes were placed on the same relative scale by equating average, dominant, equivalent

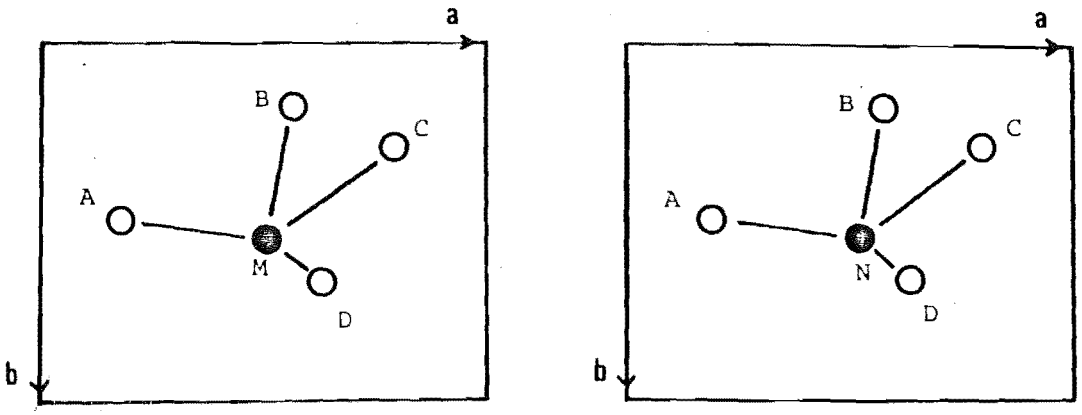

(a)

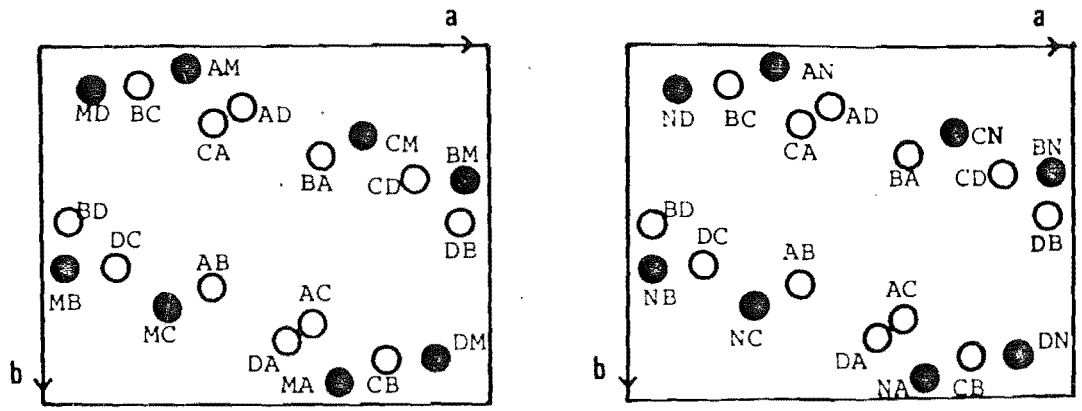

(b)

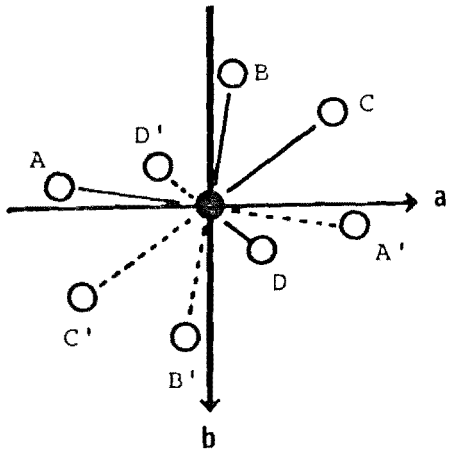

(c)

Figure 3.1 - Diagrams showing the steps involved in deriving a Difference Patterson map (two dimensions)

(a) Unit cells of two structures MABCD and NABCD; M and N are the replaceable atoms.
(b) Vector maps of the two structures.
(c) Difference Patterson map with the replaceable atoms at the origin.

• Peaks involving the replaceable atoms.

As-As vector peak densities. The map for the magnesium complex was subtracted from that of the nickel complex, section by section using the Fourier synthesis. This resultant difference vector map revealed only vectors between the replaceable metal atom and the arsenic atoms. Vectors corresponding to common pairs of atoms in the two structures disappeared because they had the same relative weights and were subtracted. An image of a square-pyramidal arrangement of five arsenic atoms about one metal atom was located with the metal atom at the origin. After tracing the resultant maps, section by section, onto glass plates, a similar arrangement apparently related by a two-fold screw axis, was discerned and served to position the heavy atoms absolutely in real space.

Full-matrix least-squares refinement first began with data from the magnesium complex. The initial least-squares refinements of positional and isotropic thermal parameters for the magnesium and five arsenic atoms led to agreement factors

$$R_1 = 0.366 \text{ and}$$
$$R_2 = 0.445.$$

A difference Fourier synthesis revealed the locations of all the non-hydrogen atoms in the structure except the apical methyl carbon atoms of the cation and oxygen atoms of the perchlorate counter-anions. The remaining atoms were found from subsequent structure factor calculations and difference Fourier synthesis. Refinements in which all atoms were assigned variable isotropic vibrational parameters

converged at

$$R_1 = 0.120 \text{ and}$$
$$R_2 = 0.160.$$

These refined coordinates were transferred to the nickel complex and yielded

$$R_1 = 0.120 \text{ and}$$
$$R_2 = 0.137.$$

A difference Fourier synthesis at this stage showed regions of high electron densities for most atoms in the structure. Accordingly, all atoms in the structure were assigned anisotropic vibrational parameters. However, core storage limitations of the computer permitted only 176 parameters to be varied simultaneously. Therefore, least-squares refinements using anisotropic temperature factors were carried out in two separate blocks for each structure. The scale factor and all parameters for the nickel and axial arsenic atoms were varied in both blocks. The parameters for the perchlorate anions, the four basal arsenic atoms and the axial ligand carbon atoms were varied in the first block. The parameters for all the arsine oxide oxygen and basal methyl carbon atoms were varied in the second block. These refinements converged at

$$R_1 = 0.064 \text{ and}$$
$$R_2 = 0.076$$

for the nickel structure (1890 data with $|F|^2 \geq 3\sigma(|F|^2)$) and

$$R_1 = 0.068 \text{ and}$$
$$R_2 = 0.083$$

for the magnesium structure (2413 data with $|F|^2 \geq 3\sigma(|F|^2)$). Two of the methyl carbon atoms, C(22) and C(42) in the nickel complex only, had non-positive definite temperature factors indicating that the thermal ellipsoid representation for these two atoms was not physically reasonable. Shifts in the last cycle of refinements were all less than 1.1 and 0.8 of the estimated standard deviations for the nickel and magnesium complex parameters, respectively.

Final difference Fourier syntheses did not show electron densities higher than those assigned to highly anisotropic methyl carbon atoms in earlier such calculations. Analyses of average values of the minimized function showed little dependence on $|F_o|$ and $\sin\theta/\lambda$. The weighting schemes were satisfactory. The errors in an observation of unit weight were 1.99 and 2.33 for the nickel and magnesium complexes, respectively.

Final positional and vibrational parameters and their esd's from the final cycle of least-squares refinements are listed in Tables 3.3 and 3.4. Comparison of these values with those obtained in the earlier analysis showed that, although the published $(Ni(Me_3AsO)_5)^{2+}$ cationic structure [117] was correct, the ions were incorrectly located in the unit cell.

In Tables 3.5 and 3.6 are presented the root-mean-square amplitudes of vibrations. Listings of the final values of $|F_o|$ and $|F_c|$ (in electrons) for reflections used in the refinements of both structures are given in Appendices B and C.

Table 3.3

Positional and Thermal Parameters for $(Ni(Me_3AsO)_5)(ClO_4)_2$

Atom	x	y	z	U_{11}[a]	U_{22}	U_{33}	U_{12}	U_{13}	U_{23}
Ni	0.0920(3)	0.1085(1)	0.1382(2)	0.031(2)	0.055(2)	0.029(2)	-0.001(2)	0.004(2)	-0.002(2)
As(1)	0.2558(2)	0.0999(1)	-0.0977(2)	0.034(2)	0.075(2)	0.035(2)	-0.002(2)	0.009(2)	-0.004(2)
As(2)	0.3268(2)	0.0894(1)	0.3056(2)	0.038(6)	0.087(3)	0.036(2)	0.002(2)	-0.004(2)	0.002(2)
As(3)	-0.0777(2)	0.1008(1)	0.3732(2)	0.040(2)	0.089(2)	0.035(2)	0.001(2)	0.006(2)	0.002(2)
As(4)	-0.1443(2)	0.0958(1)	-0.0288(2)	0.035(2)	0.083(2)	0.032(2)	-0.003(2)	-0.002(2)	-0.002(2)
As(5)	0.0897(3)	0.2366(1)	0.1484(2)	0.079(3)	0.056(2)	0.069(2)	0.000(2)	0.009(2)	0.003(2)
O(1)	0.125(1)	0.0914(5)	-0.031(1)	0.04(2)	0.11(2)	0.038(9)	0.01(1)	0.005(8)	-0.001(9)
O(2)	0.257(1)	0.0865(5)	0.175(1)	0.008(9)	0.09(2)	0.047(9)	0.010(8)	0.003(7)	0.012(8)
O(3)	0.054(1)	0.1042(6)	0.311(1)	0.04(2)	0.13(2)	0.035(9)	0.02(2)	0.016(8)	0.010(9)
O(4)	-0.079(1)	0.0950(6)	0.103(1)	0.03(2)	0.10(2)	0.06(1)	0.007(9)	-0.004(9)	0.002(9)
O(5)	0.112(2)	0.1787(6)	0.121(1)	0.16(3)	0.08(2)	0.09(2)	0.02(2)	0.01(2)	-0.00(2)
C(11)	0.352(2)	0.0418(9)	-0.076(2)	0.08(3)	0.09(3)	0.08(2)	0.02(2)	0.01(2)	-0.00(2)
C(12)	0.227(2)	0.1052(9)	-0.265(2)	0.06(2)	0.13(3)	0.02(2)	0.02(2)	-0.01(2)	0.00(2)
C(13)	0.338(2)	0.1572(9)	-0.055(9)	0.06(2)	0.08(2)	0.09(2)	-0.03(2)	0.04(2)	-0.00(2)
C(21)	0.265(2)	0.0394(8)	0.412(2)	0.08(3)	0.06(2)	0.07(2)	0.01(2)	-0.01(2)	0.03(2)
C(22)	0.491(2)	0.074(1)	0.271(2)	0.00(2)	0.27(4)	0.08(2)	0.02(2)	-0.00(2)	-0.03(3)
C(23)	0.314(3)	0.1514(9)	0.378(2)	0.11(3)	0.07(3)	0.10(3)	-0.02(2)	-0.03(2)	0.00(2)

Table 3.3 continued

Atom	x	y	z	U_{11}	U_{22}	U_{33}	U_{12}	U_{13}	U_{23}
C(31)	-0.156(2)	0.0383(9)	0.336(2)	0.10(3)	0.07(3)	0.10(3)	0.00(2)	0.02(2)	-0.04(2)
C(32)	-0.054(2)	0.103(1)	0.541(2)	0.10(3)	0.15(3)	0.02(2)	-0.00(2)	-0.00(2)	0.01(2)
C(33)	-0.186(3)	0.154(1)	0.330(2)	0.09(3)	0.09(3)	0.10(3)	-0.04(2)	0.02(2)	0.02(2)
C(41)	-0.113(2)	0.0367(8)	-0.116(2)	0.06(3)	0.06(2)	0.08(2)	-0.01(2)	0.00(2)	0.03(2)
C(42)	-0.315(2)	0.0996(9)	0.004(2)	-0.00(2)	0.15(3)	0.07(2)	-0.01(2)	-0.01(2)	-0.01(2)
C(43)	-0.104(2)	0.1532(9)	-0.125(2)	0.10(3)	0.09(2)	0.05(2)	-0.01(2)	0.00(2)	-0.03(2)
C(51)	0.084(4)	0.251(1)	0.315(2)	0.31(6)	0.13(4)	0.08(3)	0.05(4)	0.01(3)	-0.04(3)
C(52)	-0.056(3)	0.261(1)	0.086(3)	0.12(4)	0.15(4)	0.24(5)	-0.10(3)	-0.07(4)	0.01(4)
C(53)	0.198(3)	0.274(1)	0.062(4)	0.13(4)	0.05(3)	0.33(6)	-0.02(3)	0.08(4)	0.02(3)
Cl(1)	0.0792(8)	0.4108(3)	0.1499(7)	0.058(6)	0.083(6)	0.067(5)	-0.001(6)	0.003(5)	0.006(5)
Cl(2)	0.085(1)	0.2537(4)	-0.3255(9)	0.114(9)	0.089(8)	0.121(9)	-0.008(7)	-0.005(8)	0.002(6)
O(11)	0.025(3)	0.3749(8)	0.206(2)	0.23(4)	0.08(2)	0.25(3)	-0.05(2)	0.12(3)	-0.01(2)
O(12)	0.131(3)	0.405(1)	0.047(2)	0.20(4)	0.29(4)	0.14(3)	0.07(3)	0.09(3)	-0.01(3)
O(13)	0.161(3)	0.428(1)	0.210(2)	0.30(5)	0.45(6)	0.15(3)	-0.25(5)	-0.18(3)	0.14(3)
O(14)	0.000(3)	0.446(1)	0.138(3)	0.17(4)	0.18(3)	0.32(4)	0.07(3)	0.14(3)	0.11(3)
O(21)	0.046(4)	0.220(1)	-0.396(3)	0.34(6)	0.14(3)	0.31(5)	-0.08(3)	0.02(4)	-0.09(3)
O(22)	0.158(3)	0.236(1)	-0.237(3)	0.20(4)	0.22(2)	0.21(3)	0.02(3)	-0.10(3)	0.07(3)
O(23)	-0.000(4)	0.274(2)	-0.270(4)	0.24(6)	0.48(8)	0.39(7)	0.20(6)	0.05(5)	-0.11(6)
O(24)	0.141(3)	0.287(1)	-0.385(3)	0.26(5)	0.24(5)	0.30(5)	-0.13(4)	-0.12(4)	0.14(4)

[a]The form of the thermal ellipsoid expression is $\exp(-(\beta_{11}h^2+\beta_{22}k^2+\beta_{33}l^2+2\beta_{12}hk+2\beta_{13}hl+2\beta_{23}kl))$; $U_{ij}=\beta_{ij}/2\pi^2 a_i^* a_j^*$ (Å)

Table 3.4

Positional and Thermal Parameters for $(Mg(Me_3AsO)_5)(ClO_4)_2$

Atom	x	y	z	U_{11}	U_{22}	U_{33}	U_{12}	U_{13}	U_{23}
Mg	0.0908(3)	0.1112(1)	0.1381(4)	0.032(3)	0.052(3)	0.039(3)	-0.000(3)	-0.001(2)	-0.000(3)
As(1)	0.2552(1)	0.1014(1)	-0.1009(1)	0.0418(9)	0.077(2)	0.042(1)	-0.0037(9)	0.0045(8)	-0.0049(9)
As(2)	0.3261(1)	0.0876(1)	0.3051(1)	0.042(1)	0.078(2)	0.043(2)	0.0043(9)	-0.0043(8)	-0.0003(9)
As(3)	-0.0794(1)	0.1001(1)	0.3744(1)	0.042(1)	0.093(2)	0.041(2)	0.0007(9)	0.0050(8)	0.0036(9)
As(4)	-0.1461(1)	0.0934(1)	-0.0299(1)	0.0396(9)	0.078(2)	0.041(1)	-0.0031(9)	-0.0052(8)	-0.0009(9)
As(5)	0.0890(2)	0.2394(1)	0.1503(2)	0.075(2)	0.053(1)	0.068(2)	0.001(1)	0.0021(9)	0.0035(9)
O(1)	0.1255(7)	0.0947(4)	-0.0345(7)	0.039(6)	0.095(8)	0.043(6)	-0.003(6)	0.004(5)	-0.018(6)
O(2)	0.2539(7)	0.0859(3)	0.1759(7)	0.038(6)	0.090(8)	0.041(6)	0.008(5)	-0.005(5)	0.002(6)
O(3)	0.0502(8)	0.1025(4)	0.3113(8)	0.043(6)	0.116(9)	0.049(7)	0.007(6)	0.010(5)	-0.001(6)
O(4)	-0.0773(7)	0.0923(4)	0.1030(7)	0.044(6)	0.093(8)	0.036(6)	0.011(6)	-0.011(5)	-0.002(5)
O(5)	0.105(1)	0.1804(4)	0.128(1)	0.13(2)	0.047(7)	0.14(2)	0.022(8)	0.013(9)	-0.007(7)
C(11)	0.351(1)	0.0458(7)	-0.076(2)	0.06(2)	0.13(2)	0.09(2)	0.04(2)	0.017(9)	-0.00(2)
C(12)	0.224(1)	0.1080(7)	-0.267(1)	0.06(2)	0.15(2)	0.05(2)	0.00(2)	-0.000(9)	0.01(2)
C(13)	0.343(1)	0.1574(7)	-0.052(1)	0.06(2)	0.12(2)	0.08(2)	-0.02(2)	0.007(9)	-0.00(2)
C(21)	0.270(1)	0.0387(6)	0.413(1)	0.09(2)	0.10(2)	0.05(1)	-0.01(2)	-0.006(9)	0.029(9)
C(22)	0.490(1)	0.0748(8)	0.271(1)	0.04(1)	0.18(3)	0.07(2)	0.02(2)	-0.011(9)	-0.00(2)
C(23)	0.313(2)	0.1512(5)	0.377(1)	0.11(2)	0.06(2)	0.09(2)	-0.00(2)	-0.04(2)	-0.04(1)
C(31)	-0.157(2)	0.0391(7)	0.338(2)	0.12(2)	0.12(2)	0.08(2)	0.04(2)	0.01(2)	-0.01(2)
C(32)	-0.056(2)	0.1026(9)	0.544(1)	0.09(2)	0.19(3)	0.05(2)	-0.00(2)	0.019(9)	0.01(2)

Table 3.4 continued

Atom	x	y	z	U_{11}	U_{22}	U_{33}	U_{12}	U_{13}	U_{23}
C(33)	-0.182(1)	0.1501(6)	0.327(1)	0.09(2)	0.10(2)	0.08(2)	-0.03(2)	0.02(1)	0.01(2)
C(41)	-0.110(1)	0.0366(6)	-0.117(1)	0.08(2)	0.09(2)	0.07(2)	-0.02(1)	-0.014(9)	0.05(1)
C(42)	-0.315(1)	0.0948(7)	0.000(1)	0.023(8)	0.15(2)	0.07(2)	-0.000(9)	0.001(8)	0.01(2)
C(43)	-0.108(2)	0.1510(6)	-0.121(1)	0.12(2)	0.09(2)	0.04(1)	0.02(2)	-0.021(9)	-0.040(9)
C(51)	0.100(2)	0.2586(8)	0.311(2)	0.25(3)	0.11(2)	0.07(2)	0.02(2)	-0.01(2)	-0.02(2)
C(52)	-0.057(2)	0.2611(9)	0.099(3)	0.12(2)	0.11(2)	0.24(3)	-0.05(2)	-0.08(2)	0.00(2)
C(53)	0.207(2)	0.2734(8)	0.073(3)	0.18(3)	0.10(2)	0.25(4)	-0.00(2)	0.13(3)	0.01(2)
Cl(1)	0.0783(4)	0.4108(2)	0.1484(4)	0.061(3)	0.078(4)	0.074(4)	-0.007(3)	-0.000(3)	0.003(3)
Cl(2)	0.0787(6)	0.2556(2)	-0.3256(6)	0.116(5)	0.097(4)	0.110(5)	-0.003(4)	-0.014(4)	0.009(4)
O(11)	0.033(2)	0.3731(6)	0.210(2)	0.22(2)	0.10(2)	0.27(3)	-0.07(2)	0.12(2)	-0.02(2)
O(12)	0.121(2)	0.403(1)	0.041(2)	0.38(4)	0.34(4)	0.09(2)	0.13(3)	0.07(2)	0.01(2)
O(13)	0.159(2)	0.429(1)	0.206(2)	0.35(4)	0.45(5)	0.25(3)	-0.29(4)	-0.23(3)	0.21(3)
O(14)	-0.003(2)	0.4463(7)	0.139(2)	0.15(2)	0.18(2)	0.38(4)	0.08(2)	0.12(2)	0.12(3)
O(21)	0.038(3)	0.222(1)	-0.398(2)	0.36(4)	0.21(3)	0.23(3)	-0.11(3)	-0.03(3)	-0.03(3)
O(22)	0.153(2)	0.2359(8)	-0.244(2)	0.26(3)	0.20(3)	0.25(3)	0.02(2)	-0.14(3)	0.06(2)
O(23)	-0.006(3)	0.276(2)	-0.266(3)	0.33(4)	0.55(7)	0.25(4)	0.26(5)	0.06(3)	-0.11(4)
O(24)	0.132(3)	0.290(1)	-0.388(2)	0.41(5)	0.25(3)	0.19(3)	-0.16(3)	-0.05(3)	0.04(3)

Table 3.5

Root-Mean-Square Amplitudes of Vibration (Å) for Selected Atoms

$(Ni(Me_3AsO)_5)(ClO_4)_2$

Atom	Min	Intermed	Max
Ni	0.162(5)	0.182(5)	0.234(4)
As(1)	0.162(4)	0.206(4)	0.276(3)
As(2)	0.182(4)	0.203(4)	0.294(4)
As(3)	0.176(4)	0.208(4)	0.299(3)
As(4)	0.176(4)	0.191(4)	0.288(3)
As(5)	0.235(4)	0.254(4)	0.289(4)
O(1)	0.18(3)	0.21(2)	0.33(2)
O(2)	0.08(5)	0.21(2)	0.30(2)
O(3)	0.15(3)	0.22(2)	0.38(2)
O(4)	0.16(3)	0.24(2)	0.32(2)
O(5)	0.26(3)	0.30(2)	0.41(3)
C(51)	0.22(5)	0.38(4)	0.57(5)
C(52)	0.15(7)	0.44(5)	0.55(5)
C(53)	0.19(5)	0.34(5)	0.60(4)
Cl(1)	0.24(1)	0.26(1)	0.29(1)
Cl(2)	0.29(1)	0.34(1)	0.35(1)

Table 3.6

Root-Mean-Square Amplitudes of Vibration (Å) for Selected Atoms

$(Mg(Me_3AsO)_5)(ClO_4)_2$

Atom	Min	Intermed	Max
Mg	0.178(6)	0.200(6)	0.229(6)
As(1)	0.194(2)	0.212(2)	0.279(2)
As(2)	0.194(2)	0.217(2)	0.280(2)
As(3)	0.192(2)	0.214(2)	0.305(2)
As(4)	0.186(2)	0.215(2)	0.279(2)
As(5)	0.229(2)	0.261(2)	0.274(2)
O(1)	0.19(1)	0.20(1)	0.32(1)
O(2)	0.18(1)	0.21(1)	0.30(1)
O(3)	0.19(1)	0.24(1)	0.34(1)
O(4)	0.17(2)	0.22(1)	0.31(1)
O(5)	0.20(2)	0.36(2)	0.38(2)
C(51)	0.24(3)	0.34(3)	0.51(3)
C(52)	0.23(3)	0.37(3)	0.53(3)
C(53)	0.28(3)	0.32(3)	0.58(3)
Cl(1)	0.241(6)	0.270(5)	0.286(5)
Cl(2)	0.303(7)	0.318(7)	0.362(7)

3.4 DESCRIPTION OF THE CRYSTAL STRUCTURES

The two isomorphous structures $(M(Me_3AsO)_5)(ClO_4)_2$ (M = Ni, Mg) contain discrete, well-separated ions. Figure 3.2 is a stereoscopic lattice packing diagram of the contents of the unit cell. The packing appears to be relatively open in the crystal structures; the M-Cl separations being greater than 6.5Å. All interionic contacts for non-hydrogen atoms are greater than 3.3Å. Selected interatomic distances and bond angles are collected in Tables 3.7 and 3.8.

3.4.1 The $(ML_5)^{2+}$ Cation

A perspective view of the complex cation $(Mg(Me_3AsO)_5)^{2+}$ is shown in Figure 3.3 and defines the atom numbering system adopted for both the complexes. Since the crystals are isomorphous, only diagrams of the magnesium complex are given. Another view of the same $(MgL_5)^{2+}$ cation, looking down the crystallographic b axis is presented in Figure 3.4.

(a) Coordination of the Metal Atoms - Each metal atom (Ni, Mg) is coordinated by oxygen atoms to five trimethylarsine oxide ligands in a square-pyramidal environment. Disregarding the axial methyl group, the cation has approximate C_4 symmetry. The oxygen atoms O(1) to O(4), together with the arsenic atoms As(1) to As(4), though not statistically coplanar, are close to their least-squares plane which is taken as the basal plane for a square-pyramid. This square base of the pyramid is parallel to the B face of the unit cell. Table 3.9 defines these planes together with the displacements of selected atoms from them. The fifth axial oxygen atom does not lie directly above the central metal atom (Figure 3.4), being displaced approximately 0.1Å from the normal vector of the basal plane in both complexes.

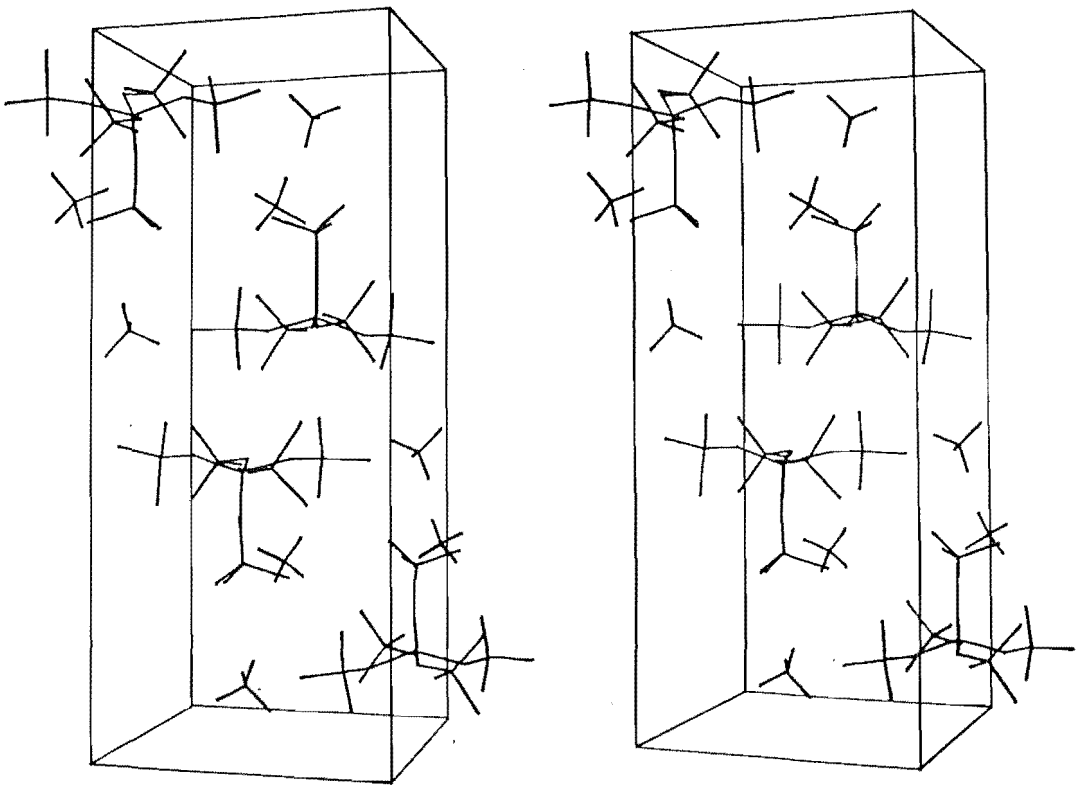

Figure 3.2 - Stereoscopic view showing contents of the unit cell of $(Mg(Me_3AsO)_5)(ClO_4)_2$.

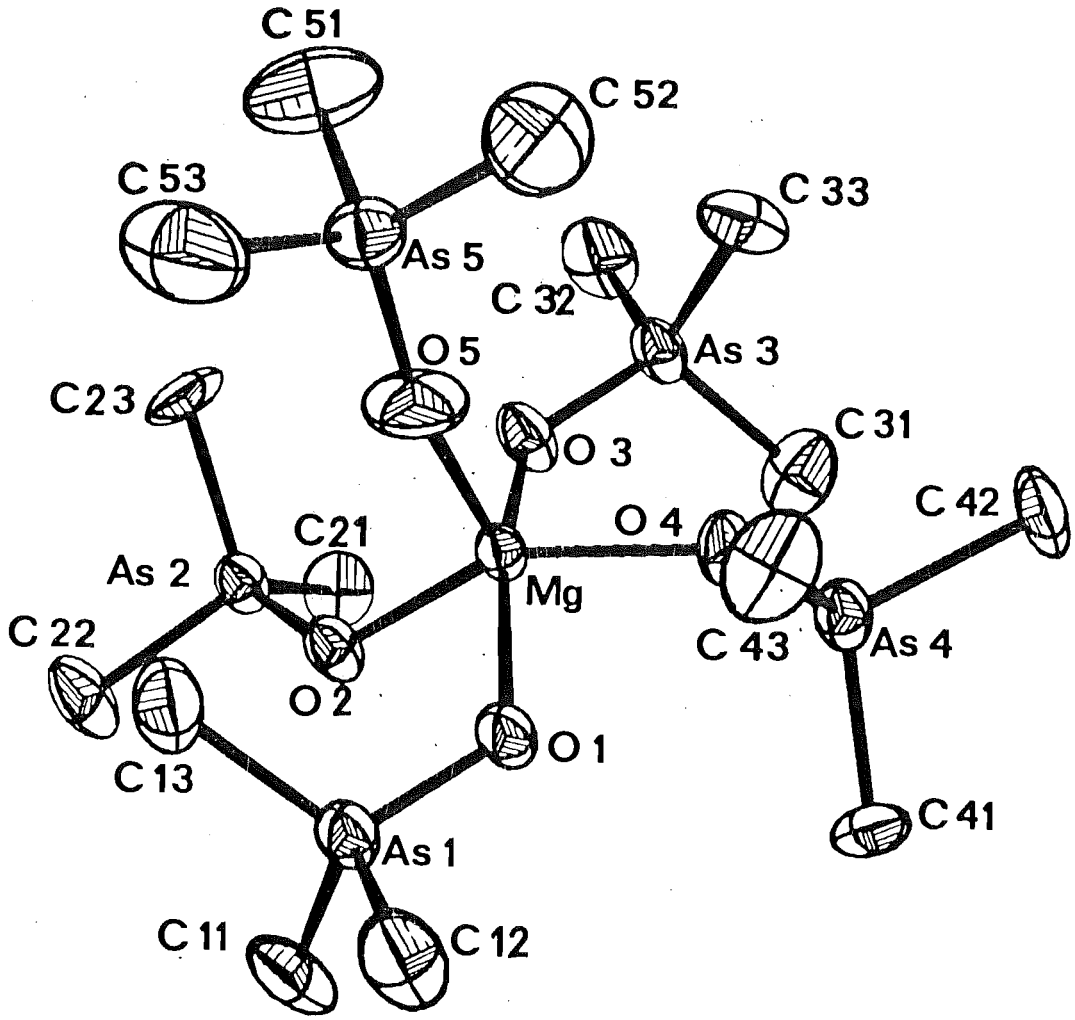

Figure 3.3 - Perspective view of the $(Mg(Me_3AsO)_5)^{2+}$ cation showing 30% probability thermal ellipsoids.

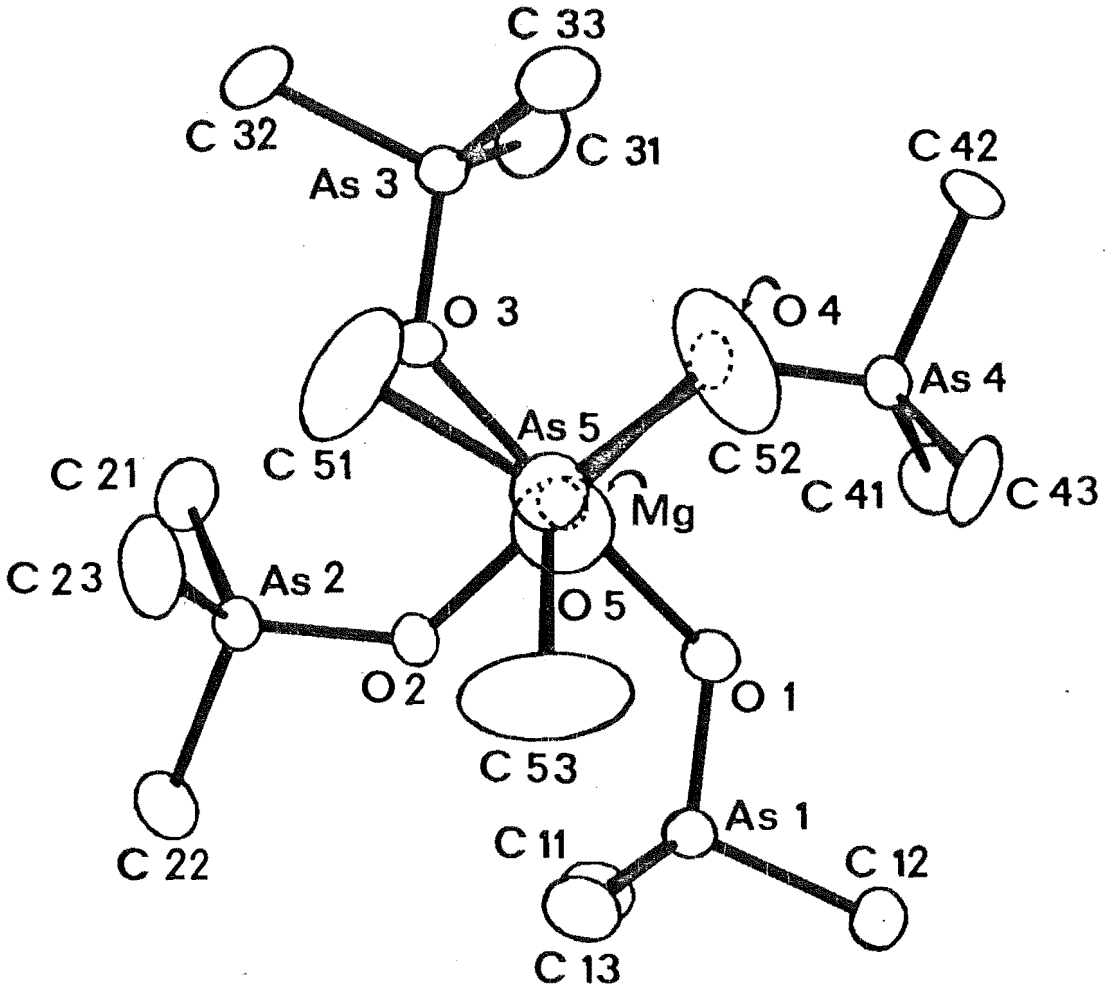

Figure 3.4 - View of the $(Mg(Me_3AsO)_5)^{2+}$ cation looking down the crystallographic b axis.

Table 3.7

Selected Interatomic Distances (Å) in $(M(Me_3AsO)_5)(ClO_4)_2$

Cation	M = Ni	M = Mg
M-O(1)	2.00(1)	2.049(9)
M-O(2)	2.00(1)	2.017(9)
M-O(3)	2.00(1)	2.03(1)
M-O(4)	2.01(1)	2.010(9)
Av	2.00(1)[a]	2.03(2)
M-O(5)	1.94(2)	1.92(1)
As(1)-O(1)	1.68(1)	1.668(8)
As(2)-O(2)	1.67(1)	1.670(8)
As(3)-O(3)	1.65(1)	1.641(9)
As(4)-O(4)	1.66(1)	1.688(8)
Av	1.67(1)	1.67(2)
As(5)-O(5)	1.63(2)	1.65(1)
As(1)-C(11)	1.94(2)	1.90(2)
As(1)-C(12)	1.92(2)	1.92(2)
As(1)-C(13)	1.88(2)	1.91(2)
As(2)-C(21)	1.95(2)	1.93(2)
As(2)-C(22)	1.94(2)	1.93(1)
As(2)-C(23)	1.88(2)	1.94(1)
As(3)-C(31)	1.96(3)	1.94(2)
As(3)-C(32)	1.91(2)	1.94(2)
As(3)-C(33)	1.95(3)	1.90(2)
As(4)-C(41)	1.92(2)	1.90(1)
As(4)-C(42)	1.97(2)	1.95(1)
As(4)-C(43)	1.96(2)	1.94(1)
As(5)-C(51)	1.93(3)	1.90(2)
As(5)-C(52)	1.90(3)	1.85(2)
As(5)-C(53)	1.87(3)	1.86(2)

Table 3.7 continued

Cation	M = Ni	M =Mg
M...As(1)	3.263(4)	3.313(4)
M...As(2)	3.289(4)	3.318(4)
M...As(3)	3.292(4)	3.329(4)
M...As(4)	3.276(4)	3.311(4)
M...As(5)	3.492(4)	3.536(4)
As(1)...O(2)	3.11(1)	3.166(8)
As(2)...O(3)	3.11(1)	3.155(9)
As(3)...O(4)	3.05(1)	3.082(8)
As(4)...O(1)	3.05(1)	3.078(8)
As(1)...As(2)	4.628(4)	4.677(2)
As(2)...As(3)	4.650(4)	4.681(2)
As(3)...As(4)	4.598(4)	4.638(2)
As(4)...As(1)	4.595(4)	4.630(2)
As(5)...O(1)	4.463(15)	4.525(9)
As(5)...O(2)	4.515(13)	4.632(9)
As(5)...O(3)	4.069(16)	4.214(11)
As(5)...O(4)	4.333(15)	4.500(10)
As(5)...As(1)	5.020(4)	5.120(3)
As(5)...As(2)	5.133(4)	5.262(3)
As(5)...As(3)	4.928(4)	4.992(3)
As(5)...As(4)	5.020(4)	5.230(3)
O(1)...O(2)	2.76(2)	2.79(2)
O(2)...O(3)	2.81(2)	2.82(2)
O(3)...O(4)	2.81(2)	2.77(2)
O(4)...O(1)	2.77(2)	2.79(2)
O(5)...O(1)	2.94(2)	3.01(2)
O(5)...O(2)	3.02(2)	3.05(2)
O(5)...O(3)	3.06(2)	3.15(2)
O(5)...O(4)	3.15(2)	3.20(2)

Table 3.7 continued

Anion	M = Ni	M = Mg
Cl(1)-O(11)	1.32(2)	1.35(2)
Cl(1)-O(12)	1.31(2)	1.33(2)
Cl(1)-O(13)	1.23(2)	1.23(2)
Cl(1)-O(14)	1.31(3)	1.35(2)
Cl(2)-O(21)	1.29(3)	1.31(2)
Cl(2)-O(22)	1.38(2)	1.36(2)
Cl(2)-O(23)	1.28(2)	1.32(2)
Cl(2)-O(24)	1.29(3)	1.33(3)

[a]Esd's for average bond lengths were calculated from the expression $\sigma = \Sigma_{i=1}^{i=N} ((l_i-\bar{l})^2/(N-1))^{\frac{1}{2}}$, where l_i is the i^{th} bond length and $\bar{l}$ is the average bond length.

Table 3.8

Selected Bond Angles (deg) in $(M(Me_3AsO)_5)(ClO_4)_2$ (Cation)

Cation	M = Ni	M = Mg
M-O(1)-As(1)	124.6(8)	125.8(5)
M-O(2)-As(2)	127.4(7)	128.0(5)
M-O(3)-As(3)	128.2(8)	129.6(5)
M-O(4)-As(4)	126.6(8)	126.9(5)
M-O(5)-As(5)	157(1)	163.8(8)
O(5)-M-O(1)	96.6(7)	98.6(5)
O(5)-M-O(2)	102.1(7)	106.4(5)
O(5)-M-O(3)	100.3(7)	101.0(5)
O(5)-M-O(4)	105.9(8)	108.9(5)
O(1)-M-O(2)	87.2(5)	86.7(4)
O(2)-M-O(3)	89.1(5)	88.3(4)
O(3)-M-O(4)	88.1(6)	86.4(4)
O(4)-M-O(1)	87.5(6)	86.8(4)
O(1)-M-O(3)	163.1(6)	160.4(5)
O(2)-M-O(4)	151.9(6)	144.7(5)
O(1)-As(1)-C(11)	109.1(9)	110.4(6)
O(1)-As(1)-C(12)	108.1(9)	107.5(6)
O(1)-As(1)-C(13)	115.8(8)	114.7(6)
O(2)-As(2)-C(21)	109.9(8)	111.9(6)
O(2)-As(2)-C(22)	105.3(8)	106.4(6)
O(2)-As(2)-C(23)	112.9(9)	110.7(6)
O(3)-As(3)-C(31)	111.4(10)	110.4(7)
O(3)-As(3)-C(32)	111.4(10)	108.3(6)
O(3)-As(3)-C(33)	107.7(9)	113.2(6)
O(4)-As(4)-C(41)	111.7(9)	110.6(6)
O(4)-As(4)-C(42)	105.2(8)	107.1(5)
O(4)-As(4)-C(43)	113.8(9)	112.5(6)
O(5)-As(5)-C(51)	113.2(10)	114.6(7)
O(5)-As(5)-C(52)	113.9(12)	111.4(8)
O(5)-As(5)-C(53)	109.3(10)	110.1(7)

Table 3.8 continued

Cation	M =Ni	M = Mg
C(11)-As(1)-C(12)	106.1(10)	108.5(8)
C(12)-As(1)-C(13)	105.4(11)	107.1(8)
C(13)-As(1)-C(11)	111.8(11)	108.5(8)
C(21)-As(2)-C(22)	108.8(13)	108.6(8)
C(22)-As(2)-C(23)	110.5(13)	108.9(8)
C(23)-As(2)-C(21)	109.4(11)	110.1(8)
C(31)-As(3)-C(32)	106.9(11)	107.4(9)
C(32)-As(3)-C(33)	108.2(11)	109.5(8)
C(33)-As(3)-C(31)	108.0(12)	107.9(9)
C(41)-As(4)-C(42)	108.9(10)	108.9(7)
C(42)-As(4)-C(43)	107.2(11)	107.4(7)
C(43)-As(4)-C(41)	109.9(10)	110.3(8)
C(51)-As(5)-C(52)	104.3(17)	105.2(12)
C(52)-As(5)-C(53)	100.6(17)	109.5(14)
C(53)-As(5)-C(51)	114.9(18)	105.8(14)

Table 3.9

Reference Least-Squares Planes for $(M(Me_3AsO)_5)^{2+}$ Cations [a]

	Distance of atom from plane/Å	
	Plane I (M = Ni)	Plane II (M = Mg)
For Atoms Included in Least-Squares Planes		
As(1)	0.223(3)	0.232(3)
As(2)	-0.080(3)	-0.119(3)
As(3)	0.047(3)	0.099(3)
As(4)	-0.069(3)	-0.115(3)
O(1)	-0.07(1)	0.00(1)
O(2)	-0.18(1)	-0.19(1)
O(3)	0.20(2)	0.21(1)
O(4)	-0.08(2)	-0.12(1)
For Other Atoms		
M	0.359(3)	0.454(3)
As(5)	3.844(3)	3.985(3)
C(12)	0.38(3)	0.40(2)
C(22)	-0.42(3)	-0.43(2)
C(32)	0.09(3)	0.17(3)
C(42)	-0.04(3)	-0.11(2)

[a] Equations of planes referred to orthorhombic crystallographic axes. X,Y,Z are atomic coordinates in Å: (I) 0.0382X + 0.9992Y -0.0105Z = 2.6188; (II) 0.0276X + 0.9996Y - 0.0020Z = 2.6408.

However, the apical arsenic atom is closely collinear with this normal vector; thus the arrangement of the arsenic atoms is also square-pyramidal.

The nickel atom lies 0.359(3)Å above this basal plane towards the apical atom, O(5). The magnesium atom is similarly displaced 0.454(3)Å above the basal plane. In other high-spin square-pyramidal Ni(II) complexes, the nickel atom has been observed to lie 0.30 - 0.40Å above the basal plane as shown in Table 3.10 [1, 140-150]. In square-pyramidal chlorophyll-like aquomagnesium tetraphenylporphyrin [132], magnesium phthalocyanin [133] and ethyl chlorophyllide a dihydrate [134] structures, the magnesium atom is displaced 0.276Å, 0.39Å and 0.496Å, respectively from the basal plane of nitrogen atoms. These non-planarities of the metal atoms are also exhibited in other five-coordinate metalloporphyrins as shown in Table 3.11 [132-134, 151-156].

M-O distances in the square-pyramid range from 1.94(2) to 2.01(1)Å for M = Ni and from 1.92(1) to 2.05(1)Å for M = Mg. An interesting feature is the shorter axial, compared to the basal, M-O bond. While the M-O basal bond lengths in this investigation are in good agreement with previously published results (Table 3.12 and Table 3.13; references: 1, 141, 144, 157-182; and 1, 183-199), few reported structures have a short M-O distance comparable to the axial M-O bond length in this investigation. From simple steric effects, one would expect an increase in bond length with increase in coordination number due to ligand-ligand repulsion. The values from this work for the axial M-O distance are shorter than those observed in corresponding five-coordinate complexes. This short bond could be significant in view of the fact that the short Ni-O bond of 1.80Å in the planar bis(N-methylsalicylaldimine) nickel(II) compound [157] has been attri-

Table 3.10

Some Geometrical Parameters In High-Spin Square-Pyramidal Nickel(II) Complexes

Compound	Donor Atoms	Basal Dist. (Å)		Axial Dist. (Å)		Displacement from Basal Plane (Å)	References
$Ni(5\text{-}Cl\text{-}SalenNEt_2)_2$	2-O,2-N,1-N[a]	M-O	1.929(16), 1.954(14)	M-N	1.977(17)	0.36	140, 141
		M-N	1.997(2), 2.199(23)				
$Ni(CR)Br_2 \cdot H_2O$	4-N,1-Br	M-N	1.808(14), 1.892(14)	M-Br	2.791(4)	0.17[b]	142
			1.923(16), 1.927(13)				
$(Ni(dmp)Cl_2)_2 2CHCl_3$	3-Cl,1-N,1-N	M-Cl	2.316(3), 2.378(3)	M-N	2.06(1)	0.39	143, 144
			2.394(3)				
		M-N	2.07(1)				
$(Ni(dacoDA)(H_2O))2H_2O$	2-O,2-N,1-OH_2	M-O	2.00, 1.98	M-OH_2	2.01	0.34	145
		M-N	2.02, 2.03				
$Ni(bddae)(NCS)_2$	5-N	M-N	1.97, 2.08	M-N	1.95	0.34	146
			2.18, 2.22				
$(Ni(2,3,2\text{-}tet)Cl)Cl$	4-N,1-Cl	M-N	2.07, 2.07	M-Cl	2.33	0.34	147
			2.11, 2.11				
$Ni(dmp)(Me_2dtp)_2$	3-S,1-N,1-N	M-S	2.31, 2.42	M-N	1.99	0.18[b]	148
			2.58				
		M-N	2.00				
$(Ni(tpen))(ClO_4)_2 MeNO_2$	5-N	M-N	2.100(6), 2.079(6)	M-N	2.011	0.33	149, 150
			2.124(6), 2.061(5)				
$(Ni(Me_3AsO)_5)(ClO_4)_2$	5-O	M-O	2.00(1), 2.00(1)	M-O	1.94(2)	0.359(3)	1, this wor
			2.00(1), 2.01(1)				

[a] The last donor atom for all the compounds refers to the axial donor atom.

[b] Distorted square-pyramid

Table 3.11

Some Geometrical Parameters For Square-Pyramidal Magnesium(II) Complexes And Metalloporphyrins

Compound	Donor Atoms	Basal Dist. (Å)	Axial Dist. (Å)	Displacement from Basal Plane (Å)	References
$Mg(TPP)H_2O$	4-N,1-OH_2	2.072	2.099	0.27	132
MgP_c	4-N,1-OH_2	2.04	2.022(3)	0.496(4)	133
MgEChl a	4-N,1-OH_2	2.09	2.035(6)	0.39	134
MgEChl b	4-N,1-OH_2	2.08	2.012(7)	0.39	151
$(Mg(Me_3AsO)_5(ClO_4)_2$	5-O	2.03(2)	1.92(1)	0.454(3)	1, this work
Five-coordinate Metalloporphyrins					
α-chlorohemin	4-N,1-Cl	2.062(10)	2.218(6)	0.475(10)	152
FeMe—Meso	4-N,1-O	2.073(6)	1.842(4)	0.49	153
VO-DPEP	4-N,1-O	2.08	1.63(2)	0.48	154
Fe(TPP)Cl	4-N,1-Cl	2.049(9)	2.192(12)	0.383(5)	155
$(Fe(TpivPP).OH_2)_n THT_n^*$	4-N,1-O	2.07	2.22	0.283	156

*A semi-coordinated water molecule at the sixth position.

Table 3.12

Comparison Of Nickel-Oxygen Bond Distances (Å)

Compound	Donor Atoms	Ni-O(H_2O)	Ni-O(Ligand)	References
4-Coordination				
$Ni(Sal\text{-}Me)_2$	2-N,2-O		1.80	157
$Ni(Sal\text{-}iPr)_2$	2-N,2-O		1.894(5), 1.898(4)	158
5-Coordination				
Ni(SalMeDPT)[a]	3-N,2-O		1.90	159
$Ni(Medabco^+)Cl_3.H_2O$	3-Cl,1-N,1-OH_2	2.100(6)		160
Ni(Sal-dipa)[a]	3-N,2-O		1.981(5), 2.008(5)	161
$(Ni_2(bdhe)_2)(ClO_4)_2$[b]	3-N,2-O		1.973(8), 1.974(8)	162
Ni(mpdo)Br_2[c]	3-Br,2-N,1-O		2.32(1)	163
$Ni(5\text{-}Cl\text{-}SalenNEt_2)_2$[d]	3-N,2-O		1.93(2), 1.96(2)	141
$(Ni(dacoDA)(H_2O))2H_2O$[d]	2-N,2-O,1-OH_2	2.011(7)	1.997(7), 1.983(6)	144
$Ni(SalenNEt_2)(catec)$[d,e]	2-N,3-O		1.96, 1.98, 2.03	164
$(Ni(Me_3AsO)_5)(ClO_4)_2$[d]	5-O		1.94(2), 2.00(1), 2.00(1), 2.00(1), 2.01(1)	1, this work

[a]Trigonal-bipyramidal. [b]Distorted trigonal-bipyramidal. [c]Intermediate. [d]Square-pyramidal. [e]Two distinct dimer.

Table 3.12 continued

Compound	Donor Atoms	Ni-O(H_2O)	Ni-O(Ligand)	References
6-Coordination				
$Ni(ala)_2.2H_2O$	2-N,2-O,2-OH_2	2.17(3)	2.14(3)	165
$Ni(gly)_2.2H_2O$	2-N,2-O,2-OH_2	2.10	2.06	166
$(Ni(taz)_3.3H_2O)Ni(NO_3)_6(H_2O)_2$	3-N,3-OH_2	2.048(3), 2.069(3) 2.087(2)		167
$(Ni(mpq)_2NO_3)NO_3$	4-N,2-O		2.127	168
$Ni(AcO)_2.4H_2O$	2-O,4-OH_2	2.081(2), 2.048(3)	2.067(3)	169
$Ni(picox)_2.4H_2O$	2-N,2-O,2-OH_2	2.100(11)	2.053(7)	170
$Ni(eSace)_2.2H_2O$	2-S,2-O,2-OH_2	2.036(7)	2.014(7)	171
$Ni(py)_2(NO_3)_2.2H_2O$	2-N,2-O,2-OH_2	2.061(2)	2.101(2)	172
$Ni(act)_4.2H_2O.Cl_2$	4-O,2-OH_2	2.063(1)	2.102(1), 2.044(1)	173
$Ni(py)_2(AcO)_2.2H_2O$	2-N,2-O,2-OH_2	2.102	2.050	174
$Ni.T_2.H_2O$	5-O,1-OH_2	2.097	2.042, 2.007 2.012, 2.035	175
$(Ni(en)_2)_2(C_2O_4)$	4-N,2-O		2.097(4), 2.093(5)	176
$Ni(sar)_2.2H_2O$	2-N,2-O,2-OH_2	2.263(6)	1.880(6)	177
$Ni.Si.F_6.6H_2O$	6-OH_2	2.047(1)		178
$(Ni(osdd)H_2O)(NO_3)_2$	2-S,2-N,1-O,1-OH_2	2.090(3)	2.069(2)	179
$Ni_2(DBA)_2(py)_4.4(py)$	2-N,4-O		2.013(1), 2.042(6) 2.014(6), 2.046(6)	180
$(Ni(imp)(H_2O)_5)(2H_2O)$	1-N,5-OH_2	2.06		181
$Ni(anil)(NO_3)_2$	3-N,3-O		2.027(5), 2.070(4) 2.138(5)	182

Table 3.13

Comparison Of Magnesium-Oxygen Bond Distances (Å)

Compound	Donor Atoms	Mg-O(H_2O)	Mg-O(Ligand)	References
4-Coordination				
$Mg(PO_2(OEt)_2)_2$	4-O		1.901	183
5-Coordination				
$MgMeBr(THF)_3$	1-Br,1-C,3-O		2.06	129
$Mg_4Br_6O(OEt_2)_4$	3-Br,2-O		1.952[a], 2.11	130
$(Mg(Me_3AsO)_5)(ClO_4)_2$	5-O		1.92(1) 2.049(9), 2.017(9) 2.03(1), 2.010(9)	1, this work
5- and 6-Coordination				
α-$Mg_2P_2O_7$: 5-CN	5-O		2.04	186
: 6-CN	6-O		2.14	
$(Mg_2EtCl_3(THF)_3)_2$: 5-CN	3-Cl,1-C,1-O		2.14(2)	187
: 6-CN	4-Cl,2-O		2.07(2)	
$Mg_3(PO_4)_2$: 5-CN	5-O		2.03	188
: 6-CN	6-O		2.12	

[a]Axial bond length

Table 3.13 continued

Compound	Donor Atoms	Mg-O(H_2O)	Mg-O(Ligand)	References
6-Coordination				
$(Mg(H_2O)_6)(MgCit(H_2O))_2.2H_2O$				189
: $Mg(H_2O)_6$	6-OH_2	2.074		
: $MgCit(H_2O)$	5-O,1-OH_2	2.031	2.07	
$Mg(acac)_2.2H_2O$	4-O,2-OH_2	2.148	2.03	190
$Mg(apy)_6(ClO_4)_2$	6-O		2.059(6)	191
$MgBr_2(THF)_4$	2-Br,4-O		2.16	192
$(Mg(CF_3COCHCOCF_3)(C_{14}H_{19}N_2)$	6-O		2.06(2)	193
$Mg(NH_4)_2(PO_3OH_2).4H_2O$	2-O,4-OH_2	2.10(3)	2.07(3)	194
$MgSO_4.5H_2O$	2-O,4-OH_2	2.05	2.09	195
$MgSO_3.6H_2O$	6-OH_2	2.07		196
$Mg(DMF)_2.(DPP)_2$	6-O		2.07	197
$Mg(mis)Cl_2$	2-O,4-OH_2	2.05	2.12	198
$Mg_2P_4O_{12}$: Mg(1)	6-O		2.092	199
: Mg(2)	6-O		2.065	
$MgCr_2O_7\cdot 2(CH_2)_6N_4)\cdot 6H_2O$	6-O	2.10		184
$Mg(OH_2)_6\cdot H_2EDTA$	6-O	2.08		185

buted to involvement of π bonding in the structure.

(b) Conformation of the Ligands - The trimethylarsine oxide (Me_3AsO) ligand moieties retain tetrahedral geometries on coordination. The C-As-C and O-As-C bond angles are in favourable agreement with the other reported tertiary substituted arsine oxide complexes given in Table 3.14 [1, 34, 75, 200-207]. The ligands in the basal plane are in a 'swasticka' arrangement (Figure 3.5), with the three methyl carbon atoms of each ligand placed above, below and on the basal plane (Figure 3.2).

Examination of the bond distances in Table 3.7 reveals that the As-O bonds have multiple characters, being appreciably less than the As-O single bond distance of 1.87Å calculated from covalent radii and the observed As-OH distances of 1.747(8)Å in the two salts of $AsO_3(OH)^{2-}$ [208, 209]. This bonding has been rationalized [204] as arising from the formation of four σ bonds using sp^3 hybrid orbitals of the arsenic atoms, three are directed to the three methyl substituents and the fourth forms a dative $Me_3As \rightarrow O$ bond. The As-O bond length is then shortened by overlap between filled pπ orbitals of the oxygen atom and the unfilled dπ orbitals of the arsenic atom; a similar proposal has been given by Cruickshank [210] to explain bonding in analogous phosphorus and sulphur compounds.

3.4.2 The Perchlorate Anions

There are two crystallographically distinct perchlorate anions in the structure which are well-removed from the square-pyramidal cations. Their positions with respect to the cations are illustrated

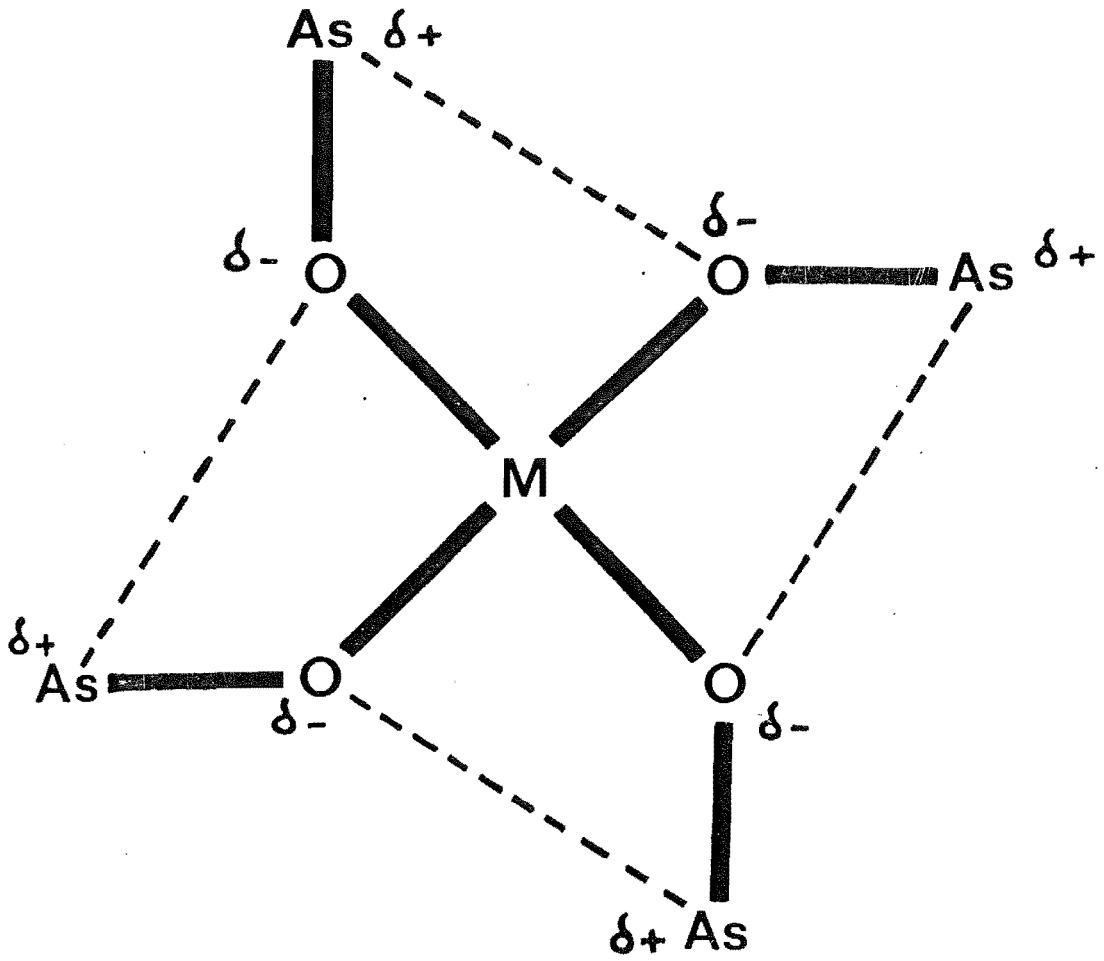

Figure 3.5 - Interactions of oxygen atoms with arsenic atoms of adjacent basal ligands.

Table 3.14

Structural Data For Some Arsenyl Ligands And Their Complexes

Compound	Bond Lengths (Å)			Bond Angles (deg)			References
	M-O	As-O	As-C	M-O-As	O-As-C	C-As-C	
$(Ph_3AsO)_2HgCl_2$	2.35	1.69	1.92	135.6	111.2	107.6	200
$Ph_2As\text{-}O\text{-}AsPh_2$		1.67	1.90		104	100	201
$(Co(Ph_2MeAsO)_4ClO_4)ClO_4$	2.02	1.70	1.96	129			34
$(Ph_3AsOH^+)Hg_2Br_6^{2-}$		1.68					202
$UO_2(NO_3)_2(Ph_3AsO)_2$	2.36	1.65	1.86	153.0	110.5	108.2	203
$Ph_3AsO.H_2O$		1.644	1.91		110.9	108.0	204
$UO_2(Et_2NCS_2)_2Ph_3AsO$	2.30	1.64	1.89	159.0	111.3	107.3	75
$Ph_3AsO.C_6H_4Cl_4O_2$		1.694	1.902		110.6	108.4	205
$(Ph_3AsO)_2CoCl_2$	1.92(1)	1.67(1)	1.907	149.8	109.9	109.1	206
$Ph_3AsO.C_6F_5OH$		1.662	1.908		111.1	107.8	207
$(Ni(Me_3AsO)_5)(ClO_4)_2$	1.94[a]	1.63	1.90	157.0	112.1	106.6	1, this work
	2.00[b]	1.67	1.93	126.7	110.2	108.4	
$(Mg(Me_3AsO)_5)(ClO_4)_2$	1.92[a]	1.65	1.87	163.8	112.1	106.8	1, this work
	2.03[b]	1.67	1.93	127.6	110.3	108.6	

[a]Parameters for the axial ligand. [b]Parameters for the basal ligands.

in the stereoscopic lattice packing diagram (Figure 3.2). Although the anions have relatively high thermal motions, they exhibit no chemically significant deviations from normal tetrahedral geometry. Disorder and large thermal motions are common in perchlorate structures [211-215]. Bond lengths and angles in the perchlorate anions range from 1.23 to 1.32Å and 101.5 to 122.6° for the nickel complex. In the magnesium complex, these values are from 1.23 to 1.36Å and 104.2 to 119.3°.

3.5 DISCUSSION

3.5.1 General Consideration

The occurrence of two closely similar cations, one formed by a transition metal atom and the other a main group element, provides an opportunity to gauge why the square-pyramidal structure is preferred. Moreover, the relatively high accuracy of the parameters attained in the structure analyses permits some significant comparisons to be made. In addition, these data highlight differences in the axial and basal binding ability of the ligands.

The existence of square-pyramidal geometry has been indicated in other studies using phosphine and arsine oxides as ligands in the metal systems. Preliminary X-ray photographic studies of $(Co(Ph_2MeAsO)_4ClO_4)ClO_4$ [34] and $(Ni(Me_3AsO)_5)(ClO_4)_2$ [117] have shown the cations have essentially the same square-pyramidal structures. In $(Co(Ph_2MeAsO)_4ClO_4)^+$ (Figure 3.6a) [34] the cobalt atom lies on the four-fold axis and is displaced 0.32Å above the basal plane formed by the four equivalent Ph_2MeAsO ligands. The apical Co-O bond was found to be slightly longer than the four basal Co-O bonds. The cobalt-

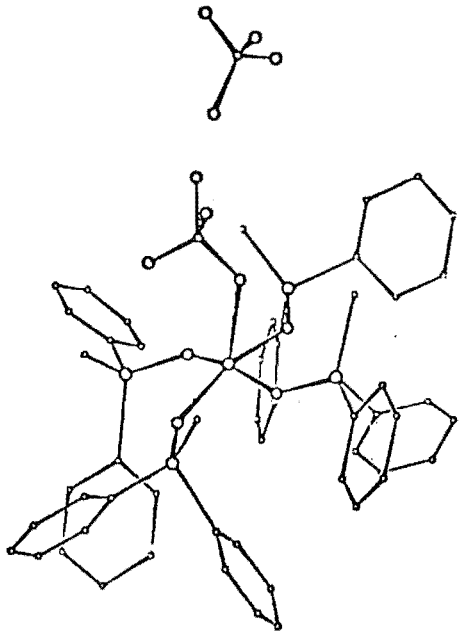

(a)

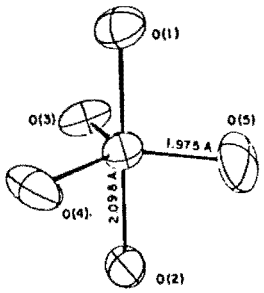

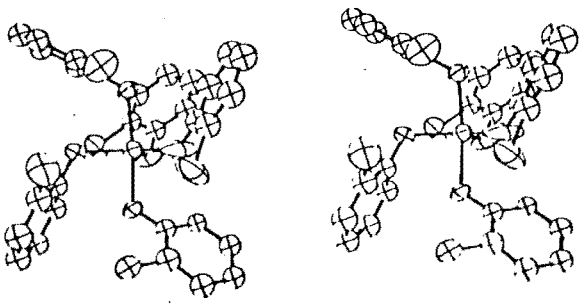

(b)

Figure 3.6 (a) - Perspective view of the $(Co(Ph_2MeAsO)_4ClO_4)\cdot ClO_4$ complex.

(b) - Perspective view of the CoO_5 chromophore in $(Co(picox))^{2+}$ cation and stereoscopic view of the cation.

bonded oxygen atom of the perchlorate anion lies well outside (0.72Å) the normal vector to the basal plane. These effects have been attributed to steric repulsion between the perchlorate ligand and the four basal ligands.

In this section some of the factors considered to govern penta-coordinate geometry, namely (a) crystal packing forces, (b) inter-ligand repulsion and (c) nature of the metal ion, are discussed.

3.5.2 Stabilization Of The Square-Pyramidal Structure

(a) Crystal Packing Forces - A classic example illustrating the influence of crystalline environment on the stereochemistry of five-coordinate molecule in the solid state is $(Cr(en)_3)(Ni(CN)_5)$ [216]. The unit cell contains two crystallographically distinct $Ni(CN)_5^{3-}$ ions. In one of these the nickel has a square-pyramidal geometry. This is apparently stabilized by π-conjugation among the basal ligands as they are more linearly coordinated. In the second it has a distorted trigonal-bipyramidal geometry. It is assumed that weak hydrogen bonding in the crystal may force a stereochemical conversion from the square-pyramidal form to another geometry. Other information suggested that the square-pyramid is the preferred ground state stereochemistry [217].

By contrast, the $(Ni(Me_3AsO)_5)(ClO_4)_2$ and $(Mg(Me_3AsO)_5)(ClO_4)_2$ complexes are unlikely to be stabilized by crystal packing forces. It is apparent from a side-on view of the cation (Figure 3.2) that a characteristic feature of the structure is the absence of a ligand in the sixth coordination site. The nickel(II) complex, though

susceptible to moisture, does not form the octahedral "$(Ni(Me_3AsO)_5H_2O)(ClO_4)_2$" complex [138]. The magnesium(II) complex, on the other hand, is air-stable. Electronic spectra have also shown that square-pyramidal $(Ni(Me_3AsO)_5)^{2+}$ can exist as a stable entity in solution [40].

(b) Inter-Ligand Repulsion - Tertiary phosphine and arsine oxides are capable of forming many five-coordinate complexes. $(ML_4(ClO_4))^+$ or $(ML_5)^{2+}$ complexes have been formed by Ph_2MePO [41], Ph_2MeAsO [33, 41], Ph_3PO [41, 44, 49, 57], Ph_3AsO [41, 44, 49], Me_3PO [40] and Me_3AsO [40] where the anions are ClO_4^-, NO_3^-, BF_4^-, NCS^-, or I^-. The electronic properties of these ligands are presumably quite similar, whereas the steric requirements are expected to increase gradually on passing from the trimethyl to the triphenyl derivatives. The fact that all these ligands are able to form square-pyramidal species shows that steric balance of the ligands is perhaps less critical than it is sometimes assumed.

If ligand-ligand repulsion was important for R_3XO complexes, a different molecular structure from that observed might have been expected. Steric interactions would possibly favour the trigonal-bipyramidal structures as found for the high-spin ML_5 complex $(Co(picox))^{2+}$ (Figure 3.6b) [218]. Furthermore, to minimize steric repulsions, rotation of the Me_3As groupings about the M-O bonds away from the axial ligand would appear to give a more sterically favourable structure.

(c) Other Factors - To a first approximation, the stabilizing effect must be independent of the metal atom as essentially the same

geometrical arrangement is adopted by Mg(II) and Ni(II). Thus some factor(s) in addition to M-O σ bond, crystal packing forces and inter-ligand repulsion might be involved.

The basal M-O-As bond has an angle of ≃ 127°, which is significantly smaller than the corresponding angle for the axial ligand and those found in other arsine oxide complexes (see Table 3.14). It can be envisaged that the oxygen atom has a hybridized orbital close to sp^2, and favourable disposition of the oxygen lone pair towards the proximity of the arsenic atom of a neighbouring ligand. A major stabilizing influence would therefore seem to arise from this interaction. A similarly short, non-bonded interaction between oxygen and tetrahedral arsenic atoms of about the same distance apart, ≃ 3.1Å , has recently been determined for a substituted triphenylarsonium cyclopentadienylide ion [219].

This type of interaction would prevent free rotation of the Me_3As groups about the M-O bond. The closeness of the basal arsenic atoms to the mean plane of the $(OAs)_4$ groupings (Table 3.9) would enhance this type of electrostatic interaction between neighbouring oxygen and arsenic atoms as illustrated in Figure 3.5 (page 58).

A somewhat similar type of interligand interaction had been suggested to account for the occurrence of trigonal-prismatic geometry (Figure 3.7a) in a series of tris(dithiolato) complexes, $M(S_2C_2R_2)_3$ (M = V, Cr, Mo, W, Re) [220, 221]. The stability of trigonal-prismatic coordination over the octahedral coordination was ascribed primarily to the involvement of two types of interactions [220, 221]:

(i) direct pπ-pπ bonding interaction between appropriate molecular orbitals of the interligand systems since the average S...S distance of 3.08Å is nearly constant for a series of tris(dithiolato) complexes (Figure 3.7b), and,

(ii) the involvement of the in-plane ligand π orbitals with metal d_{z2} and p_z orbitals along the C_3 axis of the prism.

Both these effects have since been used to describe the prismatic structure of the $Mo(Se_2C_2(CF_3)_2)_3$ compound [222] where the interligand Se...Se distance is 3.222Å. It should be noted that several recent investigations [223, 225] have questioned the validity of the interligand S...S bonding as a major stabilizing force in determining the trigonal-prismatic structure. The argument was based on the observation that in the $Nb(S_2C_6H_4)_3^-$ complex, the interligand S...S distances are greater than those in $Mo(S_2C_2(CN)_2)_3^{2-}$ and $W(S_2C_2(CN)_2)_3^{2-}$, yet the Nb compound is trigonal-prismatic whereas the dianions are distorted octahedral. But in the case of the dianionic complexes, the additional electrons would necessitate that higher antibonding molecular orbitals to be populated and cause a destabilization of the trigonal-prismatic geometry [223]. Although $(V(S_2C_2(CN)_2)_3)^{2-}$ and $Re(S_2C_2Ph_2)_3$ both have an extra electron in the antibonding molecular orbital, the former is a distorted prism compared with the prismatic $Re(S_2C_2Ph_2)_3$ structure [225]. Gray et al discussed the distortion [224] and called attention to the properties of the ligands as well as the electronic structure of the metal ions as possible factors in stabilizing the prismatic structures.

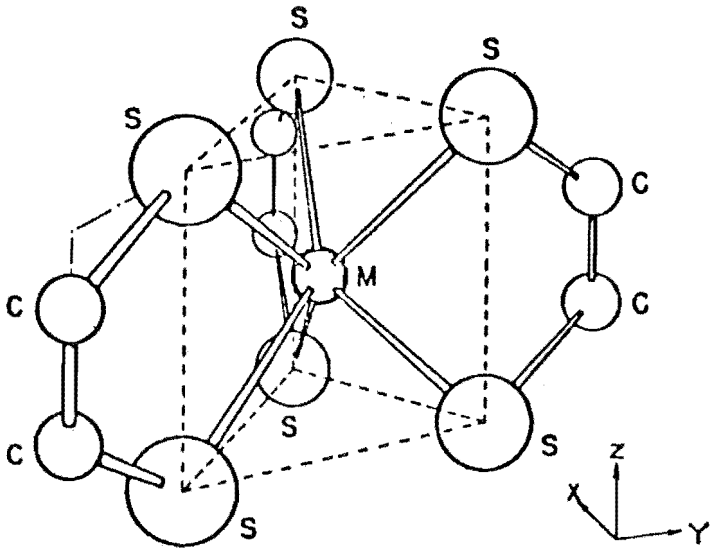

(a)

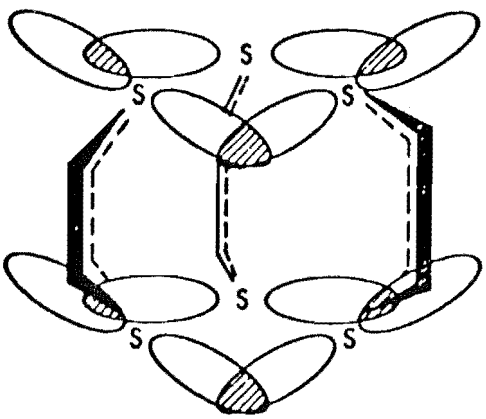

(b)

Figure 3.7 (a) - Idealized structure of a trigonal-prismatic dithiolato complex.

(b) - Interligand interactions in dithiolato complex.

3.5.3 Comparison Of The Nickel And Magnesium Structures

The ionic radii of Ni(II) and Mg(II) are closely similar (0.69Å and 0.65Å, respectively) [226]. A comparison of structural parameters for the two molecules should therefore be a good indication of the influence of the partially filled d shell in the case of Ni(II).

From Tables 3.7 and 3.8 it can be seen that there are generally small differences in corresponding bond lengths and bond angles, only in a few instances are the differences statistically significant. However, there are general and consistent trends indicating

(i) marginally stronger basal M-O bond for the nickel complex and,

(ii) marginally stronger axial M-O bond for the magnesium complex.

The overall differences between nickel and magnesium may be related to contributions from M→L basal, and M←L axial π bonding interactions.

(a) The $(Ni(Me_3AsO)_5)(ClO_4)_2$ Complex - As the nickel structure has consistently shorter M-O bonds in the basal groupings and as the nickel atom is more co-planar with the $(OAs)_4$ groupings, a stabilizing effect appears to be associated with the partially filled metal 3d orbitals in addition to the As...O interaction discussed above.

In the basal ligands, the magnitudes of the Ni-O-As angles suggest that each oxygen atom is approaching a state of sp^2 hybridization, and thus possesses a filled p orbital perpendicular to the basal plane. This oxygen p orbital is firstly involved in forming a π interaction with the empty arsenic d orbital. In addition, it is possible that

overlap of the Ni 3d and oxygen 2p orbitals could occur. The metal $3d_{xz}$ and $3d_{yz}$ orbitals are capable of this overlap (taking the C_4 axis of the square-pyramid as the z axis). However, overlap in the basal plane may not be as significant since the in-plane oxygen sp^2 orbital is directed away from the metal d_{xy} orbital. Similar types of basal M→L π bonding have been suggested for $(Mn(Ph_3PO)_4I)^+$ (Figure 3.8a) [227] and $(Ni(Diars)_2X)^+$ [228].

For the axial ligand, bond angles and bond distances reveal significant differences in bonding. The Ni-O-As angle is greater than the corresponding basal angles. This indicates greater s character for the oxygen hybrid orbitals and that the two lone pairs on the oxygen atom are in approximate p orbitals [229]. An extended π bonding could occur by involving nickel d_{xz}, d_{yz} and two oxygen pπ orbitals. This would give a different (and stronger) Ni←L bonding for the axial group. On the whole, in addition to σ bonding, the axial group appears to have two π interactions (d_{xz}←p_x and d_{yz}←p_z) whereas the basal groups have only one such interaction (d_{xz}→p_z or d_{yz}→p_z).

(b) The $(Mg(Me_3AsO)_5)(ClO_4)_2$ Complex - Interpretation of the structural features of the Mg(II) complex is not as straightforward as in the case for the Ni(II) complex. Involvement of empty magnesium 3d orbitals in bonding is not normally considered because of the high energy of such orbitals. Nevertheless, whether the energy-lowering effect of the electronegative oxygen environment around the magnesium atom could enable dπ-pπ bonding to occur is not clear without detailed molecular orbital calculations being performed.

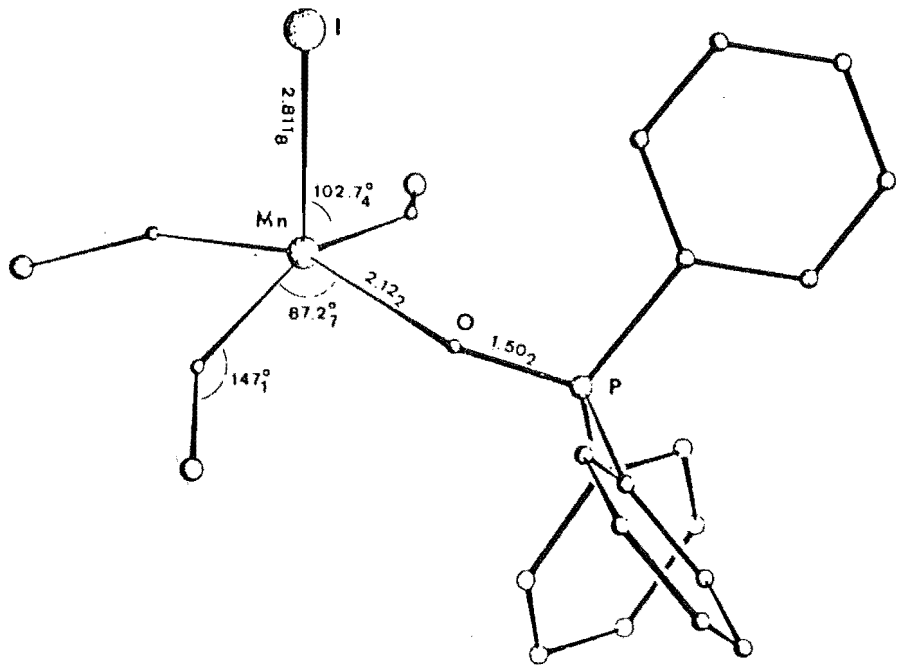

(a)

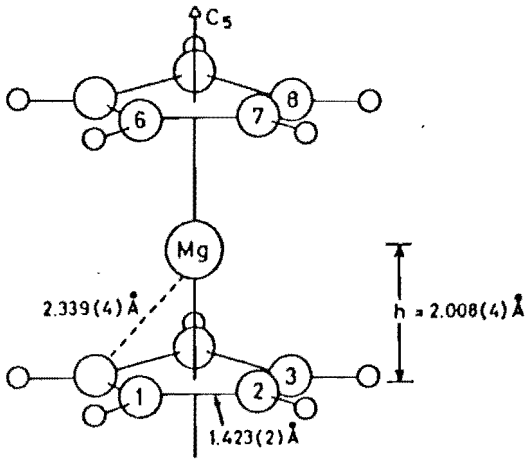

(b)

Figure 3.8 (a) - Perspective view of the $(Mn(Ph_3PO)_4I)^+$ cation.

(b) - Molecular model of $(C_5H_5)_2Mg$ with eclipsed rings.

It is perhaps pertinent at this stage to consider another magnesium compound whose bonding scheme has been extensively discussed [230-234] - that of dicyclopentadienyl magnesium (Cp_2Mg, magnesocene) (Figure 3.8b). Cp_2Mg is isostructural with a whole range of metallocenes. The perpendicular distance from the metal atom to the plane of the ring has been determined by X-ray diffraction [235, 236] to be $\simeq$ 1.65, 1.67, 1.76 and 2.0Å for the iron, cobalt, nickel and magnesium compounds, respectively. The bonding between magnesium and cyclopentadienyl rings is considered to be effected by combination of the $3p_x$ and $3p_y$ orbitals of magnesium and the π orbitals of the Cp rings [234].

In the present case for the $(Mg(Me_3AsO)_5)(ClO_4)_2$ complex, the resemblance between it and the nickel analogue is even more striking than magnesocene and other metallocenes. It then appears that covalent interaction analogous to that of the $(Ni(Me_3AsO)_5)(ClO_4)_2$ complex might be operative for the magnesium compound. Instead of using the 3d orbitals, interaction between the magnesium valence 3s and 3p orbitals and the ligand oxygen $p\pi$ orbitals would be energetically favourable and give a bonding scheme parallel to that of the nickel(II) complex. The axial ligand having two lone pairs in the p orbitals (Mg-O-As axial angle is 163.8°) could combine with the magnesium $3p_x$ and $3p_y$ orbitals. For the basal ligands, π interaction would involve magnesium $3p_z$ and basal ligand oxygen $p\pi$ orbitals.

3.6 CONCLUDING REMARKS

From the above discussions, it appears that M←L axial bonding may be greater for magnesium with empty 3p orbitals ($p\pi \leftarrow p\pi$) compared with nickel having a partially filled 3d shell ($d\pi \leftarrow p\pi$). This would be manifested by the shorter M-O axial bond in the magnesium(II)

complex. By contrast, evidence for stronger basal metal-ligand π bonding for nickel may be understood in terms of M→L π donation. This interaction would be expected to be greater for the ion having the greater number of electrons (nickel $3d^8$ > magnesium $3d^0$) and a more co-planar metal atom with respect to the basal plane.

CHAPTER 4

CRYSTAL STRUCTURES OF THE PENTAKIS(TRIMETHYLPHOSPHINE OXIDE) MAGNESIUM(II) PERCHLORATE AND ITS SIX-COORDINATE MONOAQUO ADDUCT $(Mg(Me_3PO)_5)(ClO_4)_2$ AND $(Mg(Me_3PO)_5H_2O)(ClO_4)_2$

4.1 INTRODUCTION

A wide range of five-coordinate square-pyramidal complexes of compositions $(ML_5)^{2+}$ and $(ML_4(ClO_4))^{+}$ has been isolated where M = Mn, Fe, Co, Ni and Cu(II) and L = Me_3PO and Me_3AsO [40]. More recently, in the course of an investigation [85, 86] of calcium and magnesium perchlorate complexes with Me_3PO and Me_3AsO, it has been found that five-coordinate complexes can be obtained without difficulty with Me_3AsO whereas complexes prepared using Me_3PO are usually six-coordinate. This difference in behaviour was of sufficient interest to warrant detailed study of complexes containing the latter ligand.

One aim was to establish whether or not Me_3PO formed five-coordinate complexes analogous to those formed by Me_3AsO. Crystals of the $(Mg(Me_3PO)_5H_2O)(ClO_4)_2$ complex were prepared at an early stage of this work and eventually a method was devised for preparing the $(Mg(Me_3PO)_5)(ClO_4)_2$ compound. The crystal structures of both $(Mg(Me_3PO)_5)(ClO_4)_2$ and $(Mg(Me_3PO)_5H_2O)(ClO_4)_2$ were subsequently determined. Knowledge of the structures of these complexes provides further information on the nature of metal-ligand interactions. In addition, studies on phosphoryl binding may have relevance in biological systems, particularly the involvement of magnesium(II) ions in the phosphoryl transfer reaction [237],

$$\text{Adenosine triphosphate} \xrightarrow[\text{Enzyme}]{Mg^{2+}} \text{Adenosine diphosphate} + \text{phosphate.}$$

Even phosphine oxide complexes themselves are of interest in biology as indicated by the recent report that complexes of aziridinyl subsitutued phosphine oxides, $Mg(MAPO)_4(ClO_4)_2 \cdot 2H_2O$ and $Ca(MAPO)_3Cl_2$, (MAPO = $(CH_3\overline{CHCH_2N})_3PO$), have anti-cancer properties [238]. The results for the Me_3PO complexes are presented in this chapter and compared with those for Me_3AsO described in the previous chapter. A detailed description of the preparation of the anhydrous $(Mg(Me_3PO)_5)(ClO_4)_2$ compound is also reported in this chapter.

4.2 EXPERIMENTAL

4.2.1 Preparation

(a) $(Mg(Me_3PO)_5H_2O)(ClO_4)_2$ Crystals - Suitable crystals were grown by dissolving the powder samples [85] in acetonitrile-triethyl orthoformate solution and allowing the solution to reduce in volume on standing over dried ether vapour in a closed container. Colourless, plate-shaped, air-stable crystals appeared overnight.

(b) $(Mg(Me_3PO)_5)(ClO_4)_2$ Crystals - Extreme care was taken to exclude moisture during this preparation. The complex was prepared inside a dry box containing phosphorus pentoxide as a dessicant. Steps in the preparation of $(Mg(Me_3PO)_5)(ClO_4)_2$ are outlined below.

To a solution of anhydrous $Mg(ClO_4)_2$ in methanol-triethyl orthoformate was added a five-fold excess of trimethylphosphine oxide dissolved in methanol-triethyl orthoformate. The complex appeared as a fine crystalline powder. Many attempts were made to obtain larger

crystals of suitable size for X-ray analysis from this product. Subsequently the apparatus shown in Figure 4.1 was developed for handling this sensitive compound and proved to be very successful.

A sample of $(Mg(Me_3PO)_5)(ClO_4)_2$ to be recrystallized was introduced into Flask 1. The solvents acetonitrile and ether, both containing triethyl orthoformate, were placed in Flasks 2 and 3. Because the apparatus contained organic solvents, greaseless Taps A, B, C and D were used instead of conventional grease-filled stopcocks. After the sample and the solvents were put into the apparatus, it was removed from the dry box and attached to a vacuum line. Initially the sample was pumped dry. Next the solvents were degassed and then opened to high vacuum through the respective Taps C and D. The third step was to vaporize the acetonitrile into Flask 1. This was done by closing Taps A and D, and slowly cooling Flask 1. After dissolving the sample, with Tap A closed, the apparatus was detached from the vacuum line and placed inside the dry box. Slow growing of crystals was achieved by opening Taps B and D to let the ether vapour diffuse into the acetonitrile solution containing the sample. Plate-shaped crystals appeared in a matter of days.

Since the $(Mg(Me_3PO)_5)(ClO_4)_2$ crystals are considerably more moisture-sensitive than $(Ni(Me_3AsO)_5)(ClO_4)_2$, the technique of sealing the crystals in capillaries under a stream of dry nitrogen was unsuitable. To overcome this problem, a crystal mounting apparatus (Figure 4.2) was developed [239] for selecting and mounting crystals in the absence of moisture.

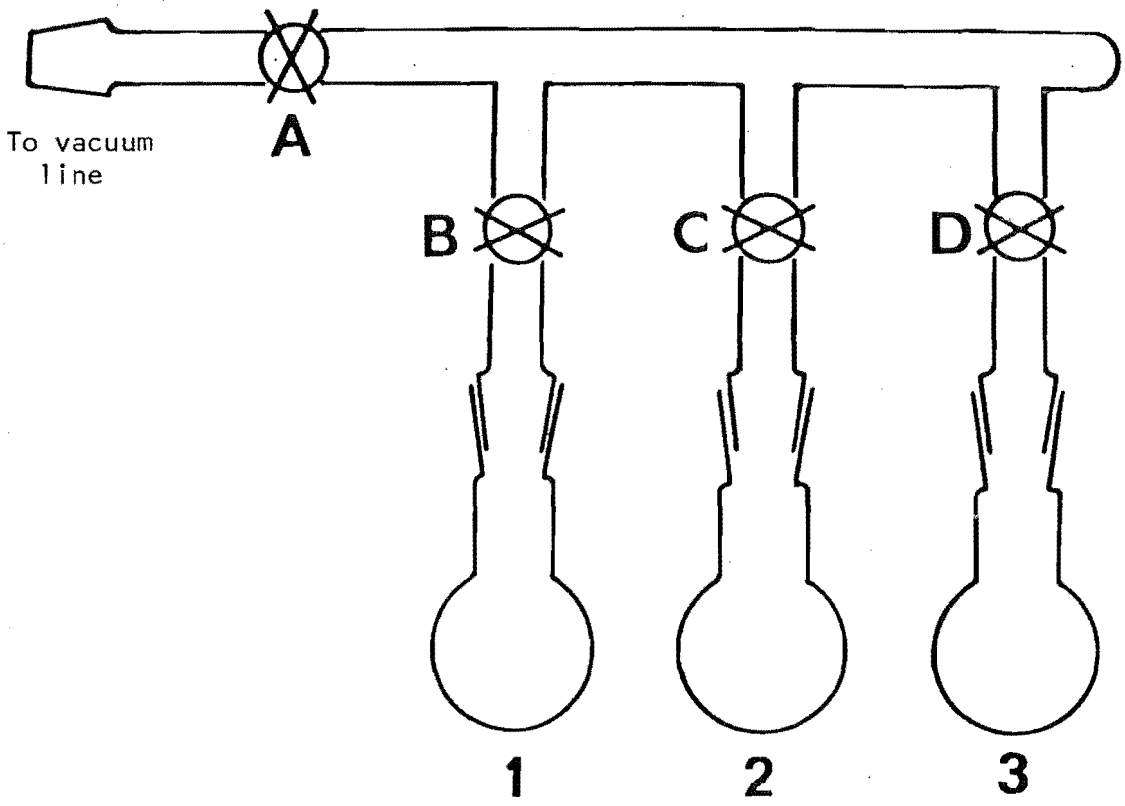

Figure 4.1 - Apparatus for growing crystals in an inert environment. A, B, C and D are greaseless taps. Flask 1 contains the powder sample $(Mg(Me_3PO)_5)(ClO_4)_2$, Flask 2 contains the solvent acetonitrile and Flask 3 contains the solvent ether.

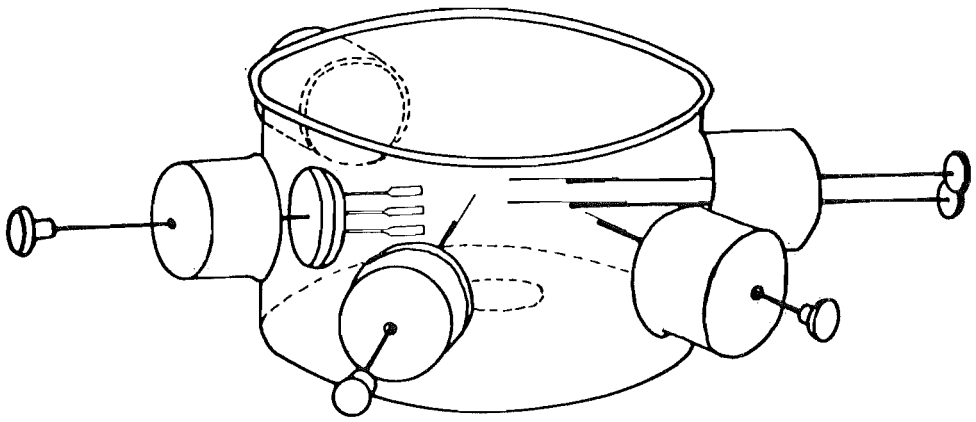

(a)

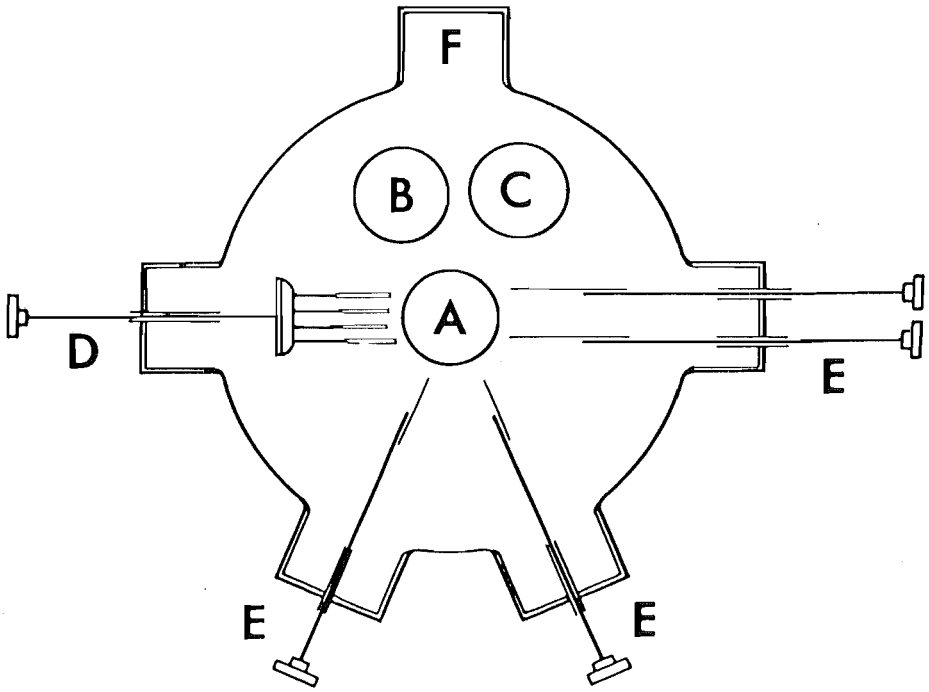

(b)

Figure 4.2 - Apparatus for selecting and mounting air-sensitive crystals.

(a) A perspective view.
(b) A vertical plan view.

(Details of the apparatus are given in the text.)

The apparatus was made from a section of a glass cylinder to which several side arms were attached. The apparatus is 8 cm high and has a diameter of 12 cm. One end of the cylinder was sealed while the other end was covered by a removable plate, which could be made air-tight by using greased ground glass surfaces. Each side arm was stoppered with a 'Suba-Seal' rubber cap. Air-sensitive crystals, for example $(Mg(Me_3PO)_5)(ClO_4)_2$, could be grown inside the apparatus or introduced into it (watch glass A) inside a dry box. Watch glasses B and C contained P_2O_5 and epoxy glue, respectively. To rod D, which was being fitted in a tightly fitting grease-filled cylinder pierced through the rubber seal, was attached a circular plate which carried capillary tubes (Lindemann glass tubes) held by plasticine. Rods E carried glass fibres at one end which were used for selecting and mounting crystals. A spare arm F could be used for other purposes. Crystals were selected under a microscope and delivered into the tubes and sealed with glue before being removed from the apparatus.

4.2.2 Crystal Data

The space groups and preliminary cell dimensions for both compounds were determined from Weissenberg and precession photographs taken with CuK_α X-radiation. For the $(Mg(Me_3PO)_5H_2O)(ClO_4)_2$ complex, systematic extinctions (0kl, k+l odd; hk0, h odd; h00, h odd; 0k0, k odd and 00l, l odd) indicated the space group is either Pnma or $Pn2_1a$ (an alternative setting of the standard space group $Pna2_1$). The $(Mg(Me_3PO)_5)(ClO_4)_2$ complex is isomorphous with $(Mg(Me_2AsO)_5)(ClO_4)_2$ and it was assigned the space group $P2_1/n$.

Data sets on two different hydrated $(Mg(Me_3PO)_5H_2O)(ClO_4)_2$ crystals were collected. The first data set converged at $R_1 = 0.115$ and some of the parameters were not precisely determined; chemically equivalent distances deviated significantly from one another. A second data set was collected using a larger crystal from further recrystallization. However, the same type of deviations were present and despite many attempts it was not possible to resolve these difficulties.

The measured densities of the two crystals, 1.34 and 1.33 g cm^{-3}, indicated Z = 4. The density of the moisture-sensitive anhydrous $(Mg(Me_3PO)_5(ClO_4)_2$ complex was not determined. Although the crystals appeared to be well-formed under the microscope, their mosaicities are high. Good crystals of $(Mg(Me_3PO)_5)(ClO_4)_2$ and $(Mg(Me_3PO)_5H_2O)(ClO_4)_2$ were difficult to obtain. In excess of twenty crystals of $(Mg(Me_3PO)_5)$-$(ClO_4)_2$ were photographically examined but found to be unsuitable for data collection. Finally three different data sets for $(Mg(Me_3PO)_5)$-$(ClO_4)_2$ were collected. But only one such data set was of reasonable quality for structure determination.

During each data collection, the intensities of the three standard reflections showed no significant variation. Lorentz and polarization effects were corrected by the program HILGOUT [240]. No absorption corrections were made. Pertinent information on crystallographic data and data collection details are summarized in Tables 4.1 and 4.2.

4.3 SOLUTION AND REFINEMENT

4.3.1 The Hydrated $(Mg(Me_3PO)_5H_2O)(ClO_4)_2$

Of the two data sets collected, the first data set gave the better

Table 4.1

Crystal Data

	$(Mg(Me_3PO)_5H_2O)(ClO_4)_2$	$(Mg(Me_3PO)_5)(ClO_4)_2$
Formula weight	701.62	683.61
a/Å	21.903(6)	11.271(7)
b/Å	13.999(3)	27.293(19)
c/Å	11.545(3)	11.272(10)
β/deg	90.0	90.246(210)
V_c/Å^3	3539.93	3467.50
d_{measd}/g cm^{-3}	1.34	
d_{calcd}/g cm^{-3}	1.32	1.31
Z	4	4
Max crystal dimension/mm	0.35	0.68
Min crystal dimension/mm	0.04	0.05

Table 4.2

Pertinent Experimental Information

	$(Mg(Me_3PO)_5H_2O)(ClO_4)_2$	$(Mg(Me_3PO)_5)(ClO_4)_2$
Mosaicity/deg	0.15	0.33
θ-Scan range/deg	0.70	0.80
Scan time/sec	70	80, 320, 320
Total background time/sec	17.5	20, 80, 80
θ limit/deg	20	0-15, 15-18, 18-22.5
Total independent reflections	3514	2880
Reflections used in refinement for which $\|F\|^2 \geq 2\sigma(\|F\|^2)$	1596	1596
Weighting parameter p	0.05	0.12
Primary beam collimator diameter/mm	1.0	2.0
Secondary beam collimator diameter/mm	5.0	5.0
X-radiation	Mo K_α	Mo K_α

refined coordinates and thus only the structural solution from this set is described. Efforts to locate positions of the chlorine, phosphorus or magnesium atoms from the three-dimensional Patterson map proved unsuccessful as these atoms have very similar atomic weights. After many fruitless attempts, it was decided to try obtaining the solution using direct methods.

This section describes the determination of the structure achieved by the application of direct methods using the weighted multisolution tangent refinement technique of the well known computer program MULTAN [110]. The observed structure factors were placed on an absolute scale using the results of a Wilson's plot [97] and normalized structure factors $|E|$'s were derived. An analysis of the distribution of $|E|$ statistics did not indicate unambiquously if the space group is centric or non-centric (Table 4.3). Choice of Pnma would require the imposition of a centre of symmetry or a mirror plane upon the cation structure. As this was highly unlikely, the non-centric space group $Pn2_1a$ was chosen and subsequently confirmed by the successful solution of the structure.

A total of 248 normalized reflections were used for phase determination. Their E values range from 3.51 down to an arbitrarily set lower limit of 1.40. The program searched for triplets of reflections satisfying the Σ_2 expression. The maximum number of triplet relationships was set at 2000.

An origin defined by reflections 3 0 6, 3 3 11 and 11 4 3 was selected automatically by the program. In addition, reflection 11 4 3

Table 4.3

Distributions of |E| Statistics for $(Mg(Me_3PO)_5H_2O)(ClO_4)_2$

	Experimental				Theoretical	
	E(1)	E(2)	E(3)	E(4)	centric	non-centric
Av. |E|	0.8280	0.8089	0.9092	0.8711	0.7980	0.8860
Av. $\|E\|^2$	1.0325	0.9873	1.2538	1.1450	1.0000	1.0000
Av. $\|E^2 - 1\|$	0.8638	0.8374	1.0191	0.9385	0.9680	0.7360
Reflections with |E| >1.0	37.66	35.84	42.49	40.61	31.73	36.79
1.2	25.20	24.23	31.17	28.44	23.01	23.69
1.4	15.30	14.11	21.67	19.28	16.15	14.09
1.6	8.65	8.08	14.28	11.66	10.96	7.73
1.8	5.40	4.89	8.48	6.83	7.19	3.92
2.0	2.73	2.62	5.69	4.66	4.55	1.83
2.5	1.02	0.74	1.82	1.02	1.24	0.19
3.0	0.34	0.23	0.46	0.34	0.27	0.01

was also used for fixing the enantiomorph. Two other reflections, 1 0 3 and 8 6 1, their phases having been determined by application of the Σ_1 relationship, were also included in the starting set.

The phase set with the highest absolute figure of merit was used to calculate an E map. The E-Fourier map revealed the magnesium and five phosphorus atoms at chemically reasonable positions. Full-matrix least-squares refinements based on these six atoms gave

$R_1 = 0.412$ and

$R_2 = 0.506$.

The coordinate of the magnesium atom corresponding to the two-fold screw axis direction of the space group was held constant. Subsequent difference Fourier calculations revealed the existence of six oxygen atoms around the central magnesium atom. Two perchlorate chlorine atoms were also located. Refinements of a model using these atomic positions and isotropic thermal parameters yielded

$R_1 = 0.244$ and

$R_2 = 0.311$.

Further difference Fourier syntheses did not reveal other atoms as there were many spurious peaks present around the heavier atoms. A Fourier synthesis using the observed structure factors as coefficients and phases derived from the model with $R_1 = 0.244$ revealed the positions of the remaining 23 atoms (excluding hydrogen atoms). Refinements of this improved model with isotropic thermal parameters resulted in

$R_1 = 0.121$ and

$R_2 = 0.115$.

It was necessary to establish the absolute configuration of the structure because of the polar nature of the space group. Structure factor calculations were carried out for the two enantiomorphous structures. The first set of calculations were based on the model so far established. In the second set, all y coordinates were reversed in sign (space group $Pn2_1a$). The results showed that the second calculations had a lower R factor and thus defined the absolute configuration. These coordinates were used in all further calculations. At this stage, the space group was transformed into the standard setting of $Pna2_1$.

Anisotropic thermal parameters were then assigned to the magnesium, five phosphorus , three axial methyl carbon and the perchlorate anion atoms. Further refinements converged with

$R_1 = 0.107$ and

$R_2 = 0.101$.

However, three atoms: C(53), O(12) and O(21) had non-positive definite temperature factors indicating the thermal ellipsoid representation for these atoms was not physically reasonable. In the final least-squares refinements, only the magnesium, five phosphorus and two chlorine atoms were given anisotropic thermal parameters and yielded the final R factors of

$R_1 = 0.115$ and

$R_2 = 0.109$

for 1596 reflections with $|F_o|^2 \geq 2\sigma(|F_o|^2)$. In the last cycle the ratios of changes in parameters to their estimated standard deviations were all less than 0.6. The final difference Fourier synthesis showed the highest peaks with 0.9 electrons/$\AA^3$ located close to the chlorine atoms. The

weighting scheme appeared to be satisfactory. The final atomic parameters are given in Table 4.4. Observed and calculated structure amplitudes are given in Appendix D.

4.3.2 The Anhydrous $(Mg(Me_3PO)_5)(ClO_4)_2$

Refined coordinates of $(Mg(Me_3AsO)_5)(ClO_4)_2$ were used as starting parameters for $(Mg(Me_3PO)_5)(ClO_4)_2$. Full-matrix least-squares refinements with isotropic thermal parameters for all atoms led to the agreement factors

$$R_1 = 0.139 \text{ and}$$
$$R_2 = 0.164.$$

The perchlorate oxygen atoms appeared extensively disordered or subject to extremely large thermal motions. The perchlorate anions were subsequently treated as tetrahedral rigid groups with Cl-O distance set at 1.44Å [241]. Refinements with anisotropic thermal parameters for the magnesium, five phosphorus and three axial carbon atoms and isotropic thermal parameters for all other atoms yielded the agreement factors

$$R_1 = 0.134 \text{ and}$$
$$R_2 = 0.154.$$

Examination of average values of the minimized functions over ranges of $|F_o|$ and $\sin\theta/\lambda$ showed that the most intense reflections were being overweighted. The empirical p factor was adjusted accordingly.

Table 4.4

Positional and Thermal Parameters for $(Mg(Me_3PO)_5H_2O)(ClO_4)_2$

Atom	x	y	z	B or β_{11}	β_{22}	β_{33}	β_{12}	β_{13}	β_{23}
Mg	0.3399(4)	0.2306(7)	0.1000*	0.0013(2)	0.0044(7)	0.006(1)	-0.0010(3)	-0.0003(5)	-0.0034(9)
P(1)	0.4528(5)	0.3137(8)	-0.066(2)	0.0024(3)	0.0049(7)	0.008(1)	0.0003(4)	-0.0011(5)	-0.0002(9)
P(2)	0.2591(4)	0.1905(8)	-0.150(1)	0.0016(3)	0.0081(9)	0.008(1)	0.0001(4)	0.0003(5)	-0.003(1)
P(3)	0.2190(4)	0.1731(8)	0.258(2)	0.0017(3)	0.0072(8)	0.0050(9)	-0.0013(4)	-0.0006(5)	-0.0006(8)
P(4)	0.4168(5)	0.2842(8)	0.336(1)	0.0028(3)	0.009(1)	0.005(1)	-0.0023(5)	0.0016(6)	0.0017(9)
P(5)	0.3912(4)	-0.0025(7)	0.095(2)	0.0023(3)	0.0049(6)	0.011(1)	0.0012(3)	0.0031(7)	0.002(1)
Cl(1)	0.4121(5)	0.6284(7)	0.093(2)	0.0029(3)	0.0053(7)	0.011(1)	0.0005(4)	-0.0002(6)	0.003(1)
Cl(2)	0.1213(6)	0.459(1)	0.098(2)	0.0029(4)	0.010(1)	0.023(2)	0.0009(5)	-0.001(1)	-0.004(2)
O(1)	0.418(1)	0.298(2)	0.038(2)	3.3(6)					
O(2)	0.313(1)	0.216(1)	-0.074(2)	2.8(5)					
O(3)	0.256(1)	0.183(2)	0.154(2)	3.6(6)					
O(4)	0.367(1)	0.253(2)	0.271(3)	5.0(7)					
O(5)	0.381(1)	0.099(2)	0.107(3)	4.2(6)					
O(6)	0.3004(9)	0.374(2)	0.096(3)	3.6(5)					
C(11)	0.417(1)	0.396(2)	-0.158(4)	2.3(8)					
C(12)	0.526(2)	0.371(3)	0.026(4)	5.0(10)					
C(13)	0.470(1)	0.206(3)	-0.142(4)	3.1(9)					
C(21)	0.195(2)	0.264(3)	-0.118(4)	5.0(10)					
C(22)	0.274(2)	0.205(3)	-0.294(3)	3.6(9)					

* Parameter fixed in all least-squares refinements.

Table 4.4 continued

Atom	x	y	z	B
C(23)	0.240(2)	0.072(3)	-0.134(5)	7.0(10)
C(31)	0.219(2)	0.281(3)	0.348(4)	4.0(10)
C(32)	0.141(2)	0.153(3)	0.224(4)	6.0(10)
C(33)	0.250(2)	0.092(4)	0.342(6)	8.0(10)
C(41)	0.437(2)	0.402(4)	0.306(5)	8.0(20)
C(42)	0.411(2)	0.255(4)	0.474(5)	8.0(10)
C(43)	0.484(2)	0.212(3)	0.295(4)	6.0(10)
C(51)	0.444(3)	-0.041(4)	0.218(6)	13.0(20)
C(52)	0.330(2)	-0.067(3)	0.106(5)	6.0(10)
C(53)	0.423(2)	-0.046(3)	-0.031(4)	5.0(10)
O(11)	0.365(1)	0.566(2)	0.067(3)	8.0(10)
O(12)	0.402(2)	0.703(3)	0.031(5)	14.0(20)
O(13)	0.409(2)	0.662(3)	0.198(5)	13.0(20)
O(14)	0.463(2)	0.596(3)	0.040(4)	13.0(20)
O(21)	0.181(2)	0.450(3)	0.082(5)	12.0(10)
O(22)	0.096(3)	0.526(4)	0.161(6)	20.0(20)
O(23)	0.110(3)	0.490(5)	-0.007(7)	23.0(30)
O(24)	0.100(2)	0.386(4)	0.139(5)	15.0(20)

The converged values are

$R_1 = 0.133$ and

$R_2 = 0.171$

for 1596 reflections with $|F_o|^2 \geq 2\sigma(|F_o|^2)$. In the final cycle of least-squares refinement, no parameter underwent shifts in excess of 0.4 of its estimated standard deviation. Table 4.5 lists the final atomic coordinates and thermal parameters along with their estimated standard deviations. Observed and calculated structure factor amplitudes are available in Appendix E.

4.3.3 Remarks On The Structures

It is worthwhile emphasizing that while the final R factors are rather high and some of the coordinates are slightly less accurate than one would normally expect, the structures are nevertheless of sufficient accuracy for some important features to be discussed. In particular the relative length of axial and basal bonds and the planarity of the basal/equatorial ligands around the central magnesium atom were conclusively established and quantified.

In Tables 4.6 and 4.7 are given the derived root-mean-square amplitudes of vibrations for the anisotropic atoms in $(Mg(Me_3PO)_5H_2O)(ClO_4)_2$ and $(Mg(Me_3PO)_5)(ClO_4)_2$.

4.4 DESCRIPTION OF THE $(Mg(Me_3PO)_5H_2O)(ClO_4)_2$ CRYSTAL STRUCTURE.

The crystal structure consists of an assemblage of $(Mg(Me_3PO)_5H_2O)^{2+}$ cations and two ClO_4^- anions hydrogen-bonded to

Table 4.5

Positional and Thermal Parameters for $(Mg(Me_3PO)_5)(ClO_4)_2$

Atom	x	y	z	B or β_{11}	β_{22}	β_{33}	β_{12}	β_{13}	β_{23}
Non-Group Atoms									
Mg	0.0808(7)	0.1151(2)	0.1447(6)	0.0074(6)	0.0016(1)	0.0064(6)	-0.0004(3)	-0.0004(4)	0.0002(3)
P(1)	0.2468(7)	0.1036(3)	-0.0946(6)	0.0093(8)	0.0020(1)	0.0088(7)	0.0001(3)	0.0007(5)	-0.0002(2)
P(2)	0.3167(7)	0.0927(3)	0.3091(6)	0.0102(8)	0.0023(2)	0.0074(6)	0.0003(3)	-0.0019(5)	0.0003(2)
P(3)	-0.0861(7)	0.1008(3)	0.3807(5)	0.0087(7)	0.0028(2)	0.0072(7)	0.0002(3)	0.0011(6)	0.0003(2)
P(4)	-0.1514(6)	0.0953(3)	-0.0240(6)	0.0083(7)	0.0025(2)	0.0085(6)	-0.0006(3)	-0.0025(5)	0.0000(3)
P(5)	0.0753(9)	0.2399(3)	0.1509(8)	0.0132(8)	0.0013(8)	0.0126(7)	0.0003(3)	-0.0012(6)	0.0001(3)
O(1)	0.136(2)	0.1003(7)	-0.026(2)	4.4(4)					
O(2)	0.242(2)	0.0935(7)	0.198(2)	4.3(4)					
O(3)	0.026(2)	0.1043(7)	0.313(2)	4.4(4)					
O(4)	-0.085(1)	0.0950(6)	0.090(1)	3.8(4)					
O(5)	0.083(2)	0.1862(7)	0.142(2)	5.5(4)					
C(11)	0.342(3)	0.051(1)	-0.064(3)	6.7(8)					
C(12)	0.217(3)	0.110(1)	-0.246(3)	5.5(7)					
C(13)	0.336(3)	0.157(1)	-0.059(3)	6.8(9)					
C(21)	0.266(3)	0.047(1)	0.417(3)	5.0(7)					
C(22)	0.463(3)	0.078(1)	0.278(3)	6.4(8)					
C(23)	0.315(3)	0.150(1)	0.384(3)	6.2(8)					

Table 4.5 continued

Atom	x	y	z	B
C(31)	-0.165(4)	0.047(2)	0.347(4)	8.0(10)
C(32)	-0.047(3)	0.104(1)	0.541(3)	7.3(9)
C(33)	-0.192(4)	0.149(1)	0.341(3)	7.2(9)
C(41)	-0.120(3)	0.043(1)	-0.115(3)	5.1(7)
C(42)	-0.308(3)	0.092(1)	0.002(3)	4.9(6)
C(43)	-0.122(3)	0.150(1)	-0.114(3)	7.1(9)
C(51)	0.128(4)	0.262(2)	0.298(4)	10.0(1)
C(52)	-0.043(7)	0.263(3)	0.102(6)	15.0(20)
C(53)	0.193(5)	0.270(2)	0.065(4)	10.0(10)
Group Atoms				
Cl(1)	0.075(2)	0.4161(5)	0.152(1)	4.3(2)
O(11)	-0.017(7)	0.453(3)	0.152(8)	19.0(20)
O(12)	0.098(8)	0.407(3)	0.031(3)	28.0(30)
O(13)	0.170(6)	0.438(4)	0.213(7)	32.0(30)
O(14)	0.025(7)	0.376(2)	0.211(7)	15.0(10)
Cl(2)	0.071(2)	0.2552(8)	-0.341(2)	8.3(3)
O(21)	0.05(2)	0.222(4)	-0.440(6)	24.0(20)
O(22)	-0.044(6)	0.264(6)	-0.30(1)	42.0(60)
O(23)	0.143(8)	0.229(5)	-0.261(8)	24.0(30)
O(24)	0.13(1)	0.297(3)	-0.390(9)	23.0(20)

Table 4.6

Root-Mean-Square Amplitudes of Vibration (Å) for Selected Atoms

$(Mg(Me_3PO)_5H_2O)(ClO_4)_2$

Atom	Min	Intermed	Max
Mg	0.09(4)	0.19(2)	0.27(2)
P(1)	0.21(2)	0.22(2)	0.27(2)
P(2)	0.18(2)	0.20(2)	0.31(2)
P(3)	0.15(2)	0.20(2)	0.29(2)
P(4)	0.12(3)	0.25(2)	0.34(2)
P(5)	0.16(3)	0.21(2)	0.34(2)
Cl(1)	0.18(3)	0.27(2)	0.30(2)
Cl(2)	0.26(2)	0.29(2)	0.42(2)

Table 4.7

Root-Mean-Square Amplitudes of Vibration (Å) for Selected Atoms

$(Mg(Me_3PO)_5)(ClO_4)_2$

Atom	Min	Intermed	Max
Mg	0.200(8)	0.211(11)	0.250(11)
P(1)	0.231(9)	0.251(9)	0.277(10)
P(2)	0.202(9)	0.267(10)	0.299(10)
P(3)	0.207(11)	0.243(9)	0.324(9)
P(4)	0.192(10)	0.262(10)	0.313(10)
P(5)	0.218(9)	0.275(9)	0.303(9)

the cation via one coordinated water molecule. A stereoscopic packing diagram illustrating the arrangement of the ions in the unit cell is shown in Figure 4.3. Table 4.8 is a compilation of selected inter- and intra-ionic non-bonded contacts. The distances between the oxygen atom O(6) of the coordinated water molecule and the two hydrogen-bonded perchlorate oxygen atoms O(11) and O(21) are 3.06Å and 2.82Å respectively. These values are in good agreement with hydrogen-bonded O...O distance of about 2.7Å given by Hamilton and Ibers [241].

Figure 4.4 is a perspective view of the cation hydrogen-bonded to the perchlorate anions and defines the atomic numbering scheme. Bond distances and bond angles are tabulated in Tables 4.9 and 4.10.

4.4.1 The $(MgL_5H_2O)^{2+}$ Cation

(a) Coordination of the Magnesium Atom - The coordination geometry around the central magnesium atom is octahedral, involving five oxygen atoms of the trimethylphosphine oxide ligands and the oxygen atom of the coordinated water molecule. The average Mg-O bond length with the four equatorial trimethylphosphine oxides of 2.08Å is slightly longer than that found for the trimethylarsine oxide complex (Chapter 3). The Mg-O(6) distance of 2.19Å is also comparatively longer than the average $Mg-OH_2$ distances for six-coordinated magnesium atom in the crystals $Ce_2Mg_3(NO_3)_{12}\cdot 24H_2O$ (2.06 ± 0.01Å) [242], $Mg(NH_4)_2(SO_4)_2\cdot 6H_2O$ (2.07 ± 0.01Å) [243], and $MgSO_4\cdot 6H_2O$ (2.06 ± 0.02Å) [244] (see also Table 3.13).

An interesting feature is the lengthening of the axial Mg-O(5) distance on coordination of the water molecule in the sixth position.

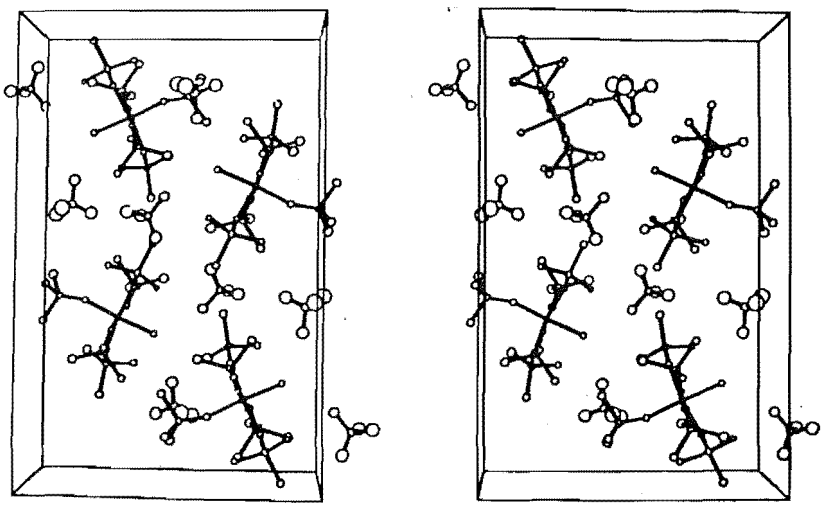

Figure 4.3 - Stereoscopic view showing contents of the unit cell of $(Mg(Me_3PO)_5H_2O)(ClO_4)_2$.

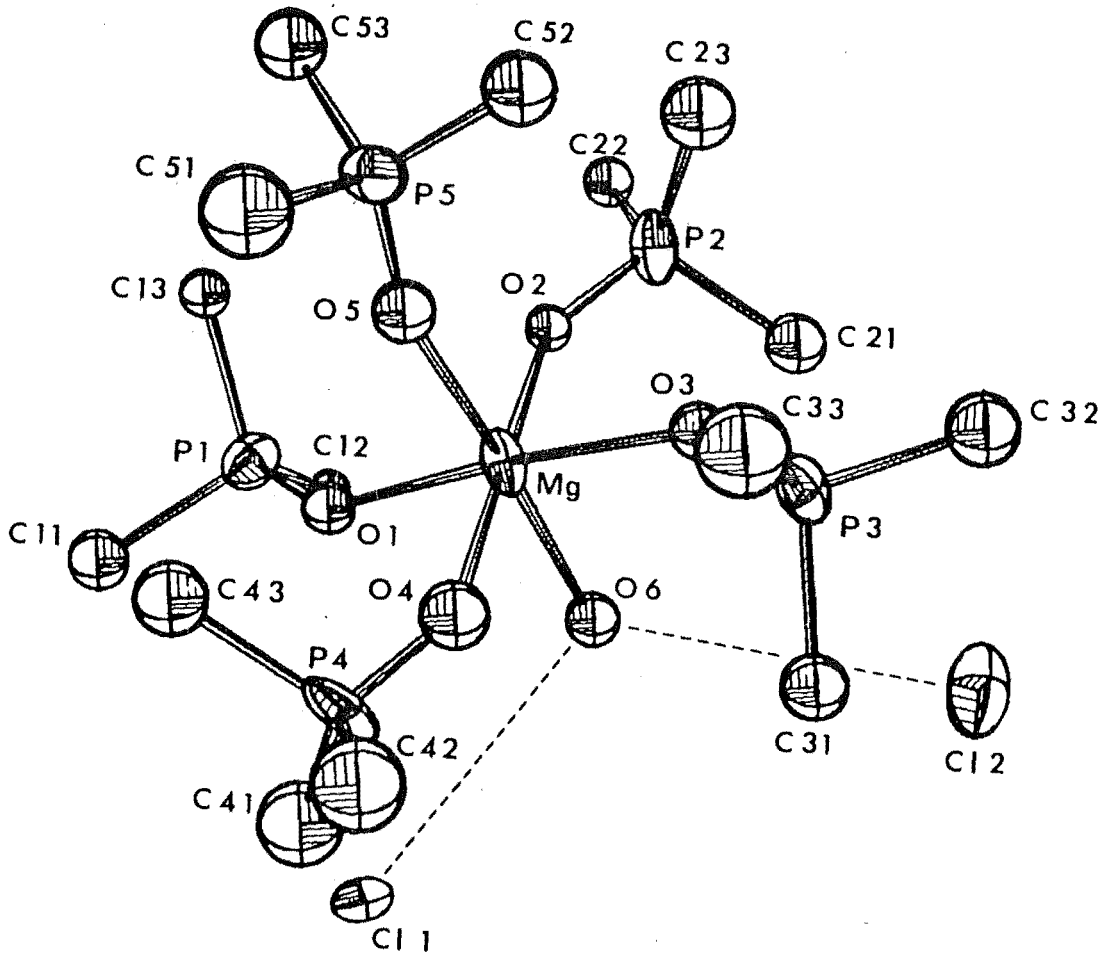

Figure 4.4 - Perspective view of the $(Mg(Me_3PO)_5H_2O)^{2+}$ cation hydrogen bonded to two perchlorate anions.

Table 4.8

Selected Inter- And Intraionic Non-Bonded Contacts (Å)

$(Mg(Me_3PO)_5H_2O)(ClO_4)_2$

Atoms	Distances	Atoms	Distances
Mg ...P(1)	3.34(1)	P(1)...O(2)	3.36(3)
Mg ...P(2)	3.43(2)	P(2)...O(3)	3.50(3)
Mg ...P(3)	3.32(1)	P(3)...O(4)	3.43(3)
Mg ...P(4)	3.29(2)	P(4)...O(1)	3.45(3)
Mg ...P(5)	3.45(1)		
P(1)...P(2)	4.68(1)	P(5)...O(1)	4.29(3)
P(2)...P(3)	4.80(2)	P(5)...O(2)	4.01(2)
P(3)...P(4)	4.69(1)	P(5)...O(3)	4.00(3)
P(4)...P(1)	4.72(2)	P(5)...O(4)	4.16(3)
P(5)...P(1)	4.98(2)	P(1)...O(6)	3.92(3)
P(5)...P(2)	4.86(2)	P(2)...O(6)	3.93(3)
P(5)...P(3)	4.88(2)	P(3)...O(6)	3.83(3)
P(5)...P(4)	4.92(2)	P(4)...O(6)	3.98(3)
O(1)...O(2)	2.87(3)	O(5)...O(1)	3.00(3)
O(2)...O(3)	2.95(3)	O(5)...O(2)	3.04(4)
O(3)...O(4)	2.96(4)	O(5)...O(3)	3.03(3)
O(4)...O(1)	2.98(4)	O(5)...O(4)	2.89(4)
O(6)...O(1)	2.86(3)	O(6)...Cl(1)	4.32(2)
O(6)...O(2)	2.97(3)	O(6)...Cl(2)	4.10(2)
O(6)...O(3)	2.93(3)	O(6)...O(11)	3.06(4)
O(6)...O(4)	3.01(4)	O(6)...O(21)	2.82(5)

Table 4.9

Selected Bond Lengths (Å) In $(Mg(Me_3PO)_5H_2O)(ClO_4)_2$

Atoms	Distances	Atoms	Distances
Mg-O(1)	2.07(3)	P(1)-O(1)	1.44(2)
Mg-O(2)	2.11(3)	P(2)-O(2)	1.51(3)
Mg-O(3)	2.06(3)	P(3)-O(3)	1.46(3)
Mg-O(4)	2.08(3)	P(4)-O(4)	1.39(3)
Av.	2.08(3)	Av.	1.45(5)
Mg-O(5)	2.05(3)	P(5)-O(5)	1.45(3)
Mg-O(6)	2.19(2)		
P(1)-C(11)	1.76(4)	P(2)-C(21)	1.78(4)
P(1)-C(12)	1.85(4)	P(2)-C(22)	1.71(4)
P(1)-C(13)	1.78(4)	P(2)-C(23)	1.73(5)
P(3)-C(31)	1.83(4)	P(4)-C(41)	1.74(5)
P(3)-C(32)	1.78(4)	P(4)-C(42)	1.65(6)
P(3)-C(33)	1.64(6)	P(4)-C(43)	1.85(4)
P(5)-C(51)	1.63(4)		
P(5)-C(52)	1.72(5)		
P(5)-C(53)	1.91(6)		
Cl(1)-O(11)	1.38(3)	Cl(2)-O(21)	1.33(4)
Cl(1)-O(12)	1.28(5)	Cl(2)-O(22)	1.32(6)
Cl(1)-O(13)	1.30(6)	Cl(2)-O(23)	1.31(8)
Cl(1)-O(14)	1.35(4)	Cl(2)-O(24)	1.22(5)

Table 4.10

Selected Bond Angles (deg.) In $(Mg(Me_3PO)_5H_2O)(ClO_4)_2$

Atom	Angles	Atoms	Angles
Cation			
Mg-O(1)-P(1)	143(2)	O(5)-Mg-O(1)	93.6(10)
Mg-O(2)-P(2)	143(2)	O(5)-Mg-O(2)	94.1(12)
Mg-O(3)-P(3)	141(2)	O(5)-Mg-O(3)	94.9(10)
Mg-O(4)-P(4)	141(2)	O(5)-Mg-O(4)	88.6(12)
Mg-O(5)-P(5)	161(2)		
O(1)-Mg-O(2)	86.8(10)	O(6)-Mg-O(1)	84.2(9)
O(2)-Mg-O(3)	90.1(9)	O(6)-Mg-O(2)	87.6(11)
O(3)-Mg-O(4)	91.2(12)	O(6)-Mg-O(3)	87.3(10)
O(4)-Mg-O(1)	91.5(11)	O(6)-Mg-O(4)	89.6(12)
O(1)-Mg-O(3)	171.1(11)	O(1)-P(1)-C(11)	111.4(15)
O(2)-Mg-O(4)	176.9(12)	O(1)-P(1)-C(12)	109.1(17)
O(5)-Mg-O(6)	177.2(11)	O(1)-P(1)-C(13)	111.0(17)
O(2)-P(2)-C(21)	111.3(16)	O(3)-P(3)-C(31)	113.2(18)
O(2)-P(2)-C(22)	112.9(17)	O(3)-P(3)-C(32)	111.0(19)
O(2)-P(2)-C(23)	110.9(19)	O(3)-P(3)-C(33)	108.6(23)
O(4)-P(4)-C(41)	112.4(22)	O(5)-P(5)-C(51)	107.0(23)
O(4)-P(4)-C(42)	112.7(24)	O(5)-P(5)-C(52)	114.1(18)
O(4)-P(4)-C(43)	108.6(18)	O(5)-P(5)-C(53)	119.8(22)
C(11)-P(1)-C(12)	104.4(18)	C(21)-P(2)-C(22)	106.6(19)
C(12)-P(1)-C(13)	107.9(17)	C(22)-P(2)-C(23)	105.0(24)
C(13)-P(1)-C(11)	110.6(18)	C(23)-P(2)-C(21)	109.8(21)
C(31)-P(3)-C(32)	104.8(19)	C(41)-P(4)-C(42)	116.8(27)
C(32)-P(3)-C(33)	115.2(23)	C(42)-P(4)-C(43)	99.7(23)
C(33)-P(3)-C(31)	104.0(25)	C(43)-P(4)-C(41)	105.3(22)
C(51)-P(5)-C(52)	106.4(26)		
C(52)-P(5)-C(53)	102.0(24)		
C(53)-P(5)-C(51)	106.7(22)		

However, the Mg-O(5) distance of 2.05Å is still marginally shorter than other equatorial Mg-O(1-4) distances, even though the effect is not as dramatic as the occurrence of the short bond of 1.92Å in $(Mg(Me_3AsO)_5)^{2+}$. The axial Mg-O(5)-P(5) angle has a similarly large value of 161°, while the average value of the equatorial Mg-O-P angle is 142°. Displacements of the O(5) and P(5) atoms from the normal vector of the equatorial plane defined by the $(OP)_4$ groups are about 0.1 and 0.06Å respectively.

Examination of Table 4.11 shows that the magnesium atom is more coplanar (0.126(9)Å) with the oxygen and phosphorus atoms of its equatorial ligands than is magnesium in $(Mg(Me_3AsO)_5)^{2+}$ (0.454(3)Å). It appears that the effect of a sixth coordinated oxygen atom is to weaken the otherwise strong Mg-O(5) bond. This effect is concomitant with a marked reduction in the displacement of the magnesium atom from the equatorial plane towards the O(5) atom.

(b) Conformation of the Ligands - The relatively poor data sets have resulted in variations in the chemically equivalent geometries amongst the trimethylphosphine oxide ligands. A list of structural parameters of phosphine oxide complexes [71, 245-259] is given in Table 4.12.

The P-O bond lengths are considerably shorter than corresponding As-O distances. This effect is essentially a reflection of the π interaction involving arsenic, phosphorus and oxygen atoms. The larger arsenic d orbitals would be expected to overlap less effectively with the oxygen p orbitals. As-O π interaction in arsine oxides is therefore not as vital as the corresponding P-O π interaction in phosphine oxides.

Table 4.11

Reference Least-Squares Plane For $(Mg(Me_3PO)_5H_2O)(ClO_4)_2$[a]

	Distance Of Atom From Plane/Å
For Atoms Included In Least-Squares Plane	
P(1)	-0.03(1)
P(2)	-0.01(1)
P(3)	-0.12(1)
P(4)	0.05(1)
O(1)	-0.11(2)
O(2)	0.10(2)
O(3)	0.06(3)
O(4)	0.05(3)
For Other Atoms	
Mg	0.126(9)
P(5)	3.57(1)
O(5)	2.17(2)
O(6)	-2.06(2)
Cl(1)	-4.45(1)
Cl(2)	-4.63(1)
C(12)	-0.18(4)
C(22)	-0.07(4)
C(32)	-0.50(4)
C(42)	0.39(5)

[a] Equation of plane referred to orthorhombic crystallographic axes. X, Y, Z are atomic coordinates in Å:

$-0.3733X + 0.9277Y - 0.0021Z = 0.3566.$

Table 4.12

Structural Data for Some Phosphoryl Ligands and Their Complexes

Compound	Bond Lengths (Å)			Bond Angles (deg)			References
	M-O	P-O	P-C	M-O-P	O-P-C	C-P-C	
Me_3PO		1.48	1.81		112.3	106.0	245
Me_3PO*		1.476(2)	1.809(2)		114.4(7)	104.1(8)	246
$Co(Me_3PO)_2(NO_3)_2$	1.94	1.54	1.81	136.4	111.1	107.8	247
$Sb(Me_3PO)Cl_5$	1.99(2)	1.61(2)	1.87	139.0	111.3	106.1	248
$U(Me_3PO)_6Cl.Cl_3$	2.26	1.53	1.79	149.5	110.5	108.4	249
Ph_3PO		1.46(1)	1.76		111.7	107.1	250
Ph_3PO		1.483(2)	1.79		112.3	106.5	251
$Co(Ph_3PO)_2Cl_2$	1.999	1.499	1.80	152.6	111.2	107.8	252
$Cu(Ph_3PO)_2Cl_2$	1.958(4)	1.492(4)	1.80	150.9(3)	111.2	107.7	253
$Cu_4(Ph_3PO)_4O.Cl_6$	1.89(2)	1.51(2)	1.83(4)	180.0			254, 255
$Hg_2(Ph_3PO)_6$	2.34	1.51	1.71	147.7			256
$Ce(Ph_3PO)_2(NO_3)_4$	2.219	1.529	1.82	171.2	109.8	109.2	257
$U(Ph_3PO)_2Cl_4$	2.242(7)	1.524	1.80	165.1	110.0	109.0	258
$(UO_2(AcO)_2Ph_3PO)_2$	2.37(2)	1.48	1.75	143.0	110.6	108.2	74, 259

* Electron diffraction data

It has been suggested that since the phosphorus atom is capable of accepting back donation from the oxygen atom, the phosphine oxide would be a lower σ donor to the metal atom than would the arsine oxide on account of its less electronegative character [39]. Electronic spectra have shown that both phosphine oxide and phosphine sulphide ligands produce lower crystal-field splitting energies, Δ , than do their arsine analogues [39]. The lower Δ values for the phosphine oxide is consistent with its being a weaker donor. Comparison of Tables 3.5 and 4.9 shows that the M-O bond lengths involving arsine and phosphine oxide are not too dissimilar. If phosphine oxide has less σ donor power, then it appears that the similar magnitudes of M-O bond lengths could be a function of some π delocalization.

4.4.2 The Perchlorate Anions

Hydrogen-bonded perchlorate anions have been observed in many structures [260, 261]. Considerable thermal vibrations are observed for the perchlorate anions. Those perchlorate oxygen atoms O(11) and O(21), which are involved in hydrogen-bonding have lower degrees of freedom and show smaller thermal motions. The Cl-O bond distances and O-Cl-O bond angles are in the range of 1.22 to 1.38Å and 95 to 126°.

4.5 DESCRIPTION OF THE $(Mg(Me_3PO)_5)(ClO_4)_2$ CRYSTAL STRUCTURE

Selected interatomic distances and bond angles are given in Tables 4.13 and 4.14. A stereoscopic view of the packing of the ions in the unit cell, looking down the crystallographic b axis is presented in Figure 4.5. The atomic numbering scheme for this structure is the same as that for $(Mg(Me_3AsO)_5)^{2+}$.

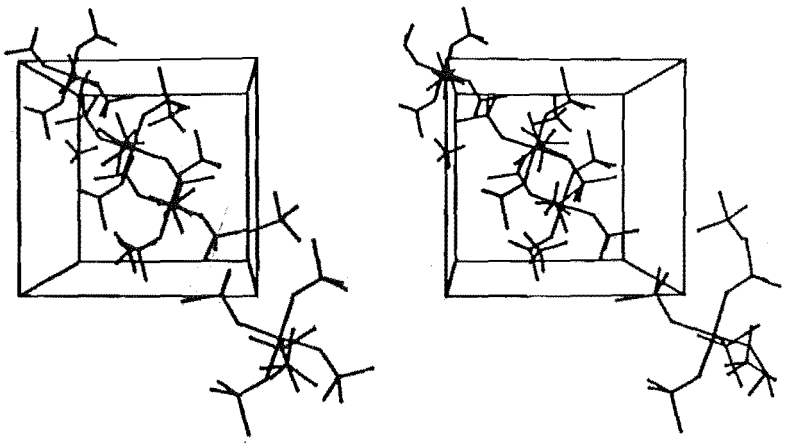

Figure 4.5 - Stereoscopic view showing contents of the unit cell of $(Mg(Me_3PO)_5)(ClO_4)_2$, view is down the crystallographic b axis.

Table 4.13

Selected Interatomic Distances (Å) In $(Mg(Me_3PO)_5)(ClO_4)_2$

Atoms	Distances	Atoms	Distances
Mg-O(1)	2.06(2)	P(1)-O(1)	1.48(2)
Mg-O(2)	2.00(2)	P(2)-O(2)	1.51(2)
Mg-O(3)	2.02(2)	P(3)-O(3)	1.49(2)
Mg-O(4)	2.04(2)	P(4)-O(4)	1.49(2)
Av.	2.03(3)	Av.	1.49(2)
Mg-O(5)	1.94(2)	P(5)-O(5)	1.47(2)
P(1)-C(11)	1.75(3)	P(2)-C(21)	1.73(4)
P(1)-C(12)	1.82(4)	P(2)-C(22)	1.78(4)
P(1)-C(13)	1.82(4)	P(2)-C(23)	1.83(3)
P(3)-C(31)	1.77(4)	P(4)-C(41)	1.79(3)
P(3)-C(32)	1.84(4)	P(4)-C(42)	1.79(3)
P(3)-C(32)	1.86(4)	P(4)-C(43)	1.83(4)
P(5)-C(51)	1.57(8)	Mg...P(1)	3.31(1)
P(5)-C(52)	1.84(5)	Mg...P(2)	3.29(1)
P(5)-C(53)	1.86(5)	Mg...P(3)	3.29(1)
		Mg...P(4)	3.28(1)
		Mg...P(5)	3.41(1)
P(1)...O(2)	3.31(2)	P(1)...P(2)	4.63(1)
P(2)...O(3)	3.29(1)	P(2)...P(3)	4.62(1)
P(3)...O(4)	3.28(2)	P(3)...P(4)	4.62(1)
P(4)...O(1)	3.24(2)	P(4)...P(1)	4.57(1)
P(5)...O(1)	4.36(2)	P(5)...P(1)	5.03(1)
P(5)...O(2)	4.45(2)	P(5)...P(2)	5.17(1)
P(5)...O(3)	4.17(2)	P(5)...P(3)	4.95(1)
P(5)...O(4)	4.40(2)	P(5)...P(4)	5.10(1)
O(1)...O(2)	2.80(3)	O(5)...O(1)	3.07(3)
O(2)...O(3)	2.78(3)	O(5)...O(2)	3.17(3)
O(3)...O(4)	2.82(2)	O(5)...O(3)	3.02(3)
O(4)...O(1)	2.82(3)	O(5)...O(4)	3.17(3)

Table 4.14

Selected Bond Angles (deg.) In $(Mg(Me_3PO)_5)(ClO_4)_2$

Atoms	Angles	Atoms	Angles
Mg-O(1)-P(1)	137.4(12)	O(5)-Mg-O(1)	100.2(9)
Mg-O(2)-P(2)	139.2(12)	O(5)-Mg-O(2)	106.9(9)
Mg-O(3)-P(3)	138.9(12)	O(5)-Mg-O(3)	99.5(9)
Mg-O(4)-P(4)	136.0(11)	O(5)-Mg-O(4)	105.9(9)
Mg-O(5)-P(5)	173.7(16)		
O(1)-Mg-O(2)	86.9(8)	O(1)-Mg-O(3)	160.3(8)
O(2)-Mg-O(3)	87.3(8)	O(2)-Mg-O(4)	147.2(8)
O(3)-Mg-O(4)	87.9(8)		
O(4)-Mg-O(1)	86.8(8)		
O(1)-P(1)-C(11)	110.5(15)	O(2)-P(2)-C(21)	113.0(13)
O(1)-P(1)-C(12)	110.9(13)	O(2)-P(2)-C(22)	111.3(14)
O(1)-P(1)-C(13)	113.7(14)	O(2)-P(2)-C(23)	111.9(14)
O(3)-P(3)-C(31)	112.1(16)	O(4)-P(4)-C(41)	113.0(13)
O(3)-P(3)-C(32)	107.1(14)	O(4)-P(4)-C(42)	110.6(12)
O(3)-P(3)-C(33)	112.7(15)	O(4)-P(4)-C(43)	113.2(14)
O(5)-P(5)-C(51)	111.3(18)	C(11)-P(1)-C(12)	111.9(16)
O(5)-P(5)-C(52)	114.8(28)	C(12)-P(1)-C(13)	104.0(16)
O(5)-P(5)-C(53)	111.4(20)	C(13)-P(1)-C(11)	105.6(16)
C(21)-P(2)-C(22)	106.3(16)	C(31)-P(3)-C(32)	111.4(18)
C(22)-P(2)-C(23)	107.7(17)	C(32)-P(3)-C(33)	110.8(17)
C(23)-P(2)-C(21)	106.2(15)	C(33)-P(3)-C(31)	102.8(19)
C(41)-P(4)-C(42)	104.9(14)	C(51)-P(5)-C(52)	117.1(30)
C(42)-P(4)-C(43)	108.0(16)	C(52)-P(5)-C(53)	104.4(31)
C(43)-P(4)-C(41)	106.7(15)	C(53)-P(5)-C(51)	95.9(22)

Since this structure is isostructural with $(M(Me_3AsO)_5)^{2+}$ (M = Ni, Mg), only the more prominent features are described. The four basal Mg-O distances are in the range of 2.003(20)-2.063(19)Å. This variation is probably just a function of the poor data set. In view of the close similarity of the environment of each basal ligand little significance should be attached to this variation. However, the presence of a considerably shorter axial Mg-O bonds, 1.939(19)Å, again indicates the possibility of multiple bonding in the axial direction. The average basal Mg-O-P bond angles is 137.9° while that for the axial group is extremely large at 173.7°. Displacements of selected atoms from the basal plane are given in Table 4.15. Deviations of O(5) and P(5) atoms from the vector perpendicular to the basal plane are about 0.01 and 0.04Å respectively.

Although the geometry for $(Mg(Me_3PO)_5)^{2+}$ is not as well defined as for $(M(Me_3AsO)_5)^{2+}$ (M = Ni, Mg), all three structures are remarkably similar. The striking aspects of a shorter M-O axial bond and the planarity of the basal ligands are retained on changing from arsenic to phosphorous. Previous discussions [138] on steric effects suggested that the size of the arsenic atoms might be a factor in blocking the entry of a sixth ligand. The present results on the formation of five-coordinate square-pyramidal structure using phosphine oxide (covalent radii: As = 1.21, P = 1.1Å) [226] reveal that size is not such a crucial factor.

4.6 DISCUSSION

4.6.1 General Consideration

As unstable reactive intermediates, five-coordinate arrangements can be achieved by either a dissociative process from six-coordination

Table 4.15

Reference Least-Square Plane For $(Mg(Me_3PO)_5)(ClO_4)_2$[a]

	Distance Of Atom From Plane/Å
For Atoms Included In Least-Squares Plane	
P(1)	0.147(8)
P(2)	-0.123(8)
P(3)	0.073(9)
P(4)	-0.107(9)
O(1)	0.05(2)
O(2)	-0.11(2)
O(3)	0.17(2)
O(4)	-0.10(2)
For Other Atoms	
Mg	0.463(7)
P(5)	3.868(7)
O(5)	2.40(2)
C(12)	0.31(3)
C(22)	-0.50(3)
C(32)	0.17(4)
C(42)	-0.20(3)

[a] Equation of plane referred to orthorhombic crystallographic axes. X, Y, Z are atomic coordinates in Å:

0.0067X + 1.0000Y + 0.0055Z = 2.6949.

or an associative process from four-coordination. The two structures presented in this chapter with five and six-coordination may provide some insight into these intriguing geometrical changes and it is of interest to examine the perturbations caused by the addition of a water molecule to an ML_5 species.

4.6.2 Comparison Of The Hydrated And Anhydrous Structures

(a) Displacement of the Magnesium Atom from the Mean Plane - In the hydrated species, a more coplanar arrangement of the magnesium atom and the ligand atom is observed (Table 4.11). The Mg...Mean Plane of oxygen and phosphorus atoms distance is 0.126(9)Å. In the case of the anhydrous complex, the axial interaction is restricted to only one direction and consequently the magnesium atom is displaced by 0.463(7)Å from the basal plane towards the O(5) atom (Figure 4.6a). A similar situation is found to exist in the haemoglobin molecule. In deoxy haemoglobin the high-spin Fe(II) atom is about 0.6Å above the mean plane of the porphyrin. Upon oxygenation the iron atom becomes low-spin and moves into the mean plane of the porphyrin (Figure 4.6b) [262]. This movement is suggested to trigger a relaxation of the tensed deoxy form. The effect is passed on to the salt bridges and brought about a cooperative interaction in the tetramer haemoglobin molecule [262]. The present results suggest that similar conformational changes about the magnesium atom would also involve reasonably large changes in the position of the metal ion.

(b) Conformational Changes - It is possible to describe the addition of a sixth ligand as having the effect of pulling the metal atom it coordinates to, towards the mean plane of the ligands. The

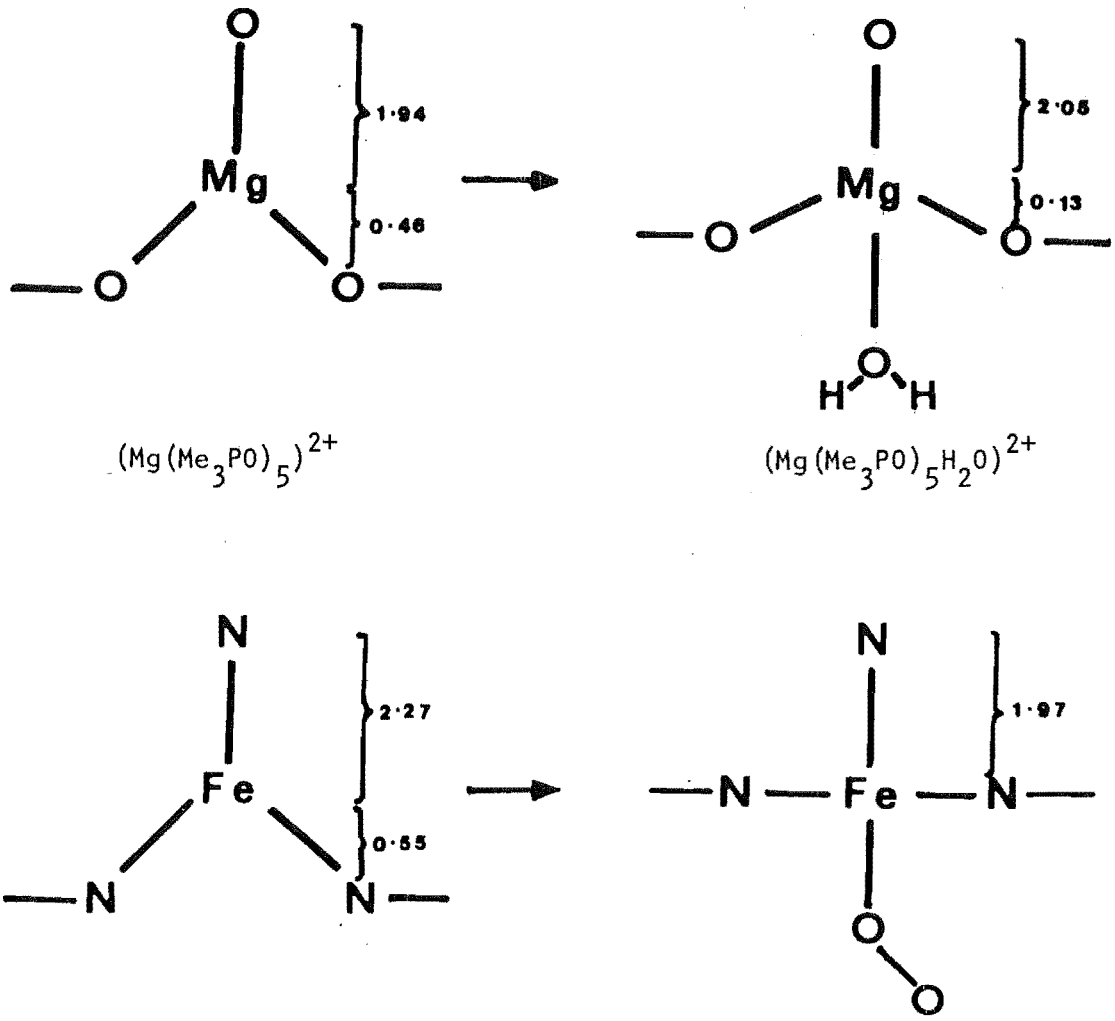

Figure 4.6 - Conformational change from five-coordination to six-coordination.

average axial angles, O(5)-Mg-O (basal) are 92.8° for $(Mg(Me_3PO)_5H_2O)^{2+}$ and 103.1° for $(Mg(Me_3PO)_5)^{2+}$. The interligand axial oxygen-basal oxygen distances are slightly closer for the hydrated cation, the average distances are 2.99Å and 3.13Å for $(Mg(Me_3PO)_5H_2O)^{2+}$ and $(Mg(Me_3PO)_5)^{2+}$ respectively. The oxygen and phosphorus atoms of the equatorial ligands in the hydrated cation are closer to the mean plane than those observed in the anhydrous cation (Tables 4.11 and 4.15).

(c) The Axial Mg-O Bond Length - As expected, the Mg-O(5) bond distance increases for the hydrated complex. The binding of a sixth donor molecule not only pulls the magnesium atom away from the O(5) atom, it also provides more electron density along the axial direction of the magnesium atom. The region of space in the axial direction is thus less susceptible to the binding of the trimethylphosphine oxide ligand (a σ and π donor) and a longer Mg-O(5) bond is observed in the hydrated complex.

(d) The Perchlorate Anions - The perchlorate anions are hydrogen-bonded to the cation in the hydrated compound via the coordinated water molecule. In the anhydrous complex, no hydrogen-bonds are formed in the absence of the water molecule and discrete cations and anions are found in the crystal structure.

4.6.3 Comparison Of Complexes Containing Substituted Phosphine Oxides

On coordinating phosphine oxide around a metal atom, three factors are generally assumed to affect the P-O bond order [263].

(i) The σ bond, P→O, is enhanced by the positively charged metal ion.

(ii) the pπ-dπ back bonding, O→P is decreased by the positive charge of the metal ion, and

(iii) the drift of metal electrons toward oxygen through dπ-pπ overlap, M→O, enhances the O→P back donation.

Normally, the second factor dominates on complex formation and P-O bond order is decreased. In addition to this factor, the nature of hybridization of the oxygen atom, whether it is sp(M-O-P angle = 180°) or sp^2 (M-O-P angle = 120°), would have an effect on the bond order due to the availability of the number of p orbitals capable of π-overlap with the phosphorus orbitals [254]. In all crystal structures involving phosphine oxides to date (Table 4.12), the P-O bonds are found to be slightly longer in metal complexes than those exist in the free ligands. This effect is consistent with a decrease in the electron density at the oxygen atom on coordination and causes a reduction of the σ and/or π bond orders of the P-O linkage [254]. A linear M-O-P angle would provide a maximum pπ-dπ overlap in the P-O bond whereas in the case where the M-O-P angle is bent would require a change in hybridization of oxygen atom from sp to sp^2. This would produce a decrease in P-O π bonding interactions [254].

4.6.4 Influence Of Phosphine And Arsine Oxides On Coordination Geometry

With phosphine oxides, the preferred coordination number appears to be six. Only under well-controlled conditions can a five-coordinate species be obtained. On the other hand, arsine oxides readily produce five-coordinate ions whose crystalline complexes are air-stable.

These results are consistent with other evidence that arsine oxides are generally stronger donors than phosphine oxides [39]. Both

$(Mg(Me_3PO)_5)^{2+}$ and $(Mg(Me_3AsO)_5)^{2+}$ have a large axial Mg-O-X (X = P, As) angle. If steric repulsion between the ligands is dominant, the larger atomic size of the arsenic atom would result in greater interligand steric repulsion. A consequence of this would be a longer axial Mg-O bond and a more linear Mg-O-As angle for the arsine oxide complex. However, the results indicate the reverse effect. The Mg-O-P angle is 173.7° whereas the Mg-O-As angle is 163.8°. Moreover, the Mg-O bond length in the arsine oxide complex of 1.92Å is shorter than that of the phosphine oxide complex, although this small difference may not be significant.

This investigation shows that electronic and electrostatic interactions of the type discussed above and in Chapter 3 are the prime factors stabilizing the formation of five-coordinate cations. Steric effects probably play a minor role in these processes.

4.7 CONCLUDING REMARKS

A consistent and interpretable pattern of phosphine and arsine oxide complex geometry appears through the present work. Where arsine oxides are involved, shorter M-O bond lengths are found as expected for the stronger Lewis basicity of these ligands. The opportunity for M-O π-bonding seems to be present for both ligands but more marked for the phosphine oxide as observed in the more linear M-O-P angle in $(Mg(Me_3PO)_5)^{2+}$ than M-O-As angle in $(Mg(Me_3AsO)_5)^{2+}$. Axial M-O bond elongation on forming the six-coordinate species is related to the greater electron density along the axial direction of the metal atom.

CHAPTER 5

CRYSTAL STRUCTURE OF THE TRI-μ-(TRIMETHYLARSINE OXIDE)-HEXAKIS-(TRIMETHYLARSINE OXIDE)-DICALCIUM(II) TETRAPERCHLORATE $(Ca_2(Me_3AsO)_9)(ClO_4)_4$

5.1 INTRODUCTION

During an attempt to prepare calcium complexes of trimethylarsine oxides, two different calcium perchlorate complexes were isolated [85,86]. One of these two complexes was characterized as $(Ca(Me_3AsO)_4(ClO_4))ClO_4$ while the other was assigned the formula $(Ca(Me_3AsO)_5)(ClO_4)_2$. The X-ray powder photograph of the first compound established isomorphicity with $(Ni(Me_3AsO)_4(ClO_4))ClO_4$ [40], which is known to be square-pyramidal with a structure analogous to $(Co(Ph_2MeAsO)_4(ClO_4))ClO_4$ [34]. Further evidence from infrared and molar conductivity measurements agreed with this assignment. However, the species formulated as $(Ca(Me_3AsO)_5)(ClO_4)_4$ had a markedly different X-ray powder photograph from that of the square-pyramidal compound $(Mg(Me_3AsO)_5)(ClO_4)_2$ (Chapter 3), or other five-coordinate transition metal complexes [40]. Additional information, including infrared and ESR spectra, suggested a square-pyramidal structure, although not conclusively. Since differences in powder photographs can indicate differences in molecular structure, it was decided to carry out a single crystal X-ray analysis of this compound in order to examine how the larger cationic size of the calcium ion influences molecular geometry.

This chapter reports the structure analysis of the calcium arsine oxide complex. The structure determination showed that the five-coordinate formulation of the calcium complex was incorrect. In fact, the coordination geometry of the calcium atom is octahedral, and two such octahedra share a common trigonal face to form a dinuclear

$(Ca_2(Me_3AsO)_9)^{4+}$ cationic unit. Each dinuclear species is stabilized by four perchlorate counter-anions. Results from this analysis indicated that infrared and other physical data per se do not always provide decisive information in favour of one structural geometry over another. This is especially the case for main group metal ions where the lack of appropriate molecular orbital energy levels limit electronic spectroscopy as a valuable structural probe. In hindsight, it is obvious that $(Ca_2(Me_3AsO)_9)(ClO_4)_4$ and $(Mg(Me_3AsO)_5)(ClO_4)_2$ must have different X-ray powder photographs.

Several complexes with bridging substituted phosphine and arsine oxide ligands have been reported. Infrared [46, 264] spectroscopy has provided the bulk of evidence concerning these compounds. The present dinuclear arsine oxide bridged structure appears to be the first of its kind to have been determined by X-ray diffraction. Calcium attains a higher coordination number in this complex through sharing three bridging oxo ligands. This is found in other molecular systems such as the five-coordinate dimers $(Cu(C_9N_2H_{14})OH)_2(ClO_4)_2$ [265] and $(Cu(pyO)(H_2O)Cl_2)_2$ [266].

5.2 EXPERIMENTAL

5.2.1 Preparation

Colourless, hexagonal-shaped crystals of the $(Ca_2(Me_3AsO)_9)(ClO_4)_4$ compound were recrystallized from powder samples [85, 86] in methanol-triethyl orthoformate solution in the presence of an acetonitrile vapour. The crystals are air-stable.

5.2.2 Crystal Data

Precession and Weissenberg photographs showed the compound to be hexagonal. Systematic absences (00l: l = odd) are consistent with space groups $P6_3$ or $P6_3/m$. On the basis of statistical distribution of intensities (Table 5.1), the latter space group was selected. Successful refinement of the structure verified this choice.

The density was measured using the flotation method in a mixture of bromobenzene and 1, 2-dibromoethane. The transparent crystal chosen for data collection had a maximum dimension of about 0.38 mm. 1763 independent reflections were collected in the range of $0^{\circ} < \theta < 57^{\circ}$ using CuK_{α} (Ni-filtered) X-radiation. The data were corrected for Lorentz and polarization effects. However, absorption corrections ($\mu(CuK_{\alpha}) = 91.91\ cm^{-1}$) were not applied because of difficulties in defining the habit of the crystal accurately.

Tables 5.2 and 5.3 give crystal data and relevant information on data collection.

5.3 SOLUTION AND REFINEMENT

5.3.1 Detection Of Wrong Structural Formulation

Initially the compound was formulated as $(Ca(Me_3AsO)_5)(ClO_4)_2$ based on information using infrared, conductometric and micro-analytical data [85]. The first clue to the disparity of the formulation came from space group determination. A hexagonal space group is not compatible with the proposed square-pyramidal geometry. Furthermore, the measured density of 1.71 g cm^{-3} requires the presence of a non-

Table 5.1

Distributions of |E| Statistics for $(Ca_2(Me_3AsO)_9)(ClO_4)_4$

	Experimental				Theoretical	
	E(1)	E(2)	E(3)	E(4)	centric	non-centric
Av. |E|	0.7954	0.7911	0.7817	0.7996	0.7980	0.8860
Av. |E|	1.0256	1.0109	0.9896	1.0327	1.0000	1.0000
Av. $\|E^2 - 1\|$	1.0092	0.9964	0.9855	1.0086	0.9680	0.7360
Reflections with |E| > 1.0	30.69	30.74	30.35	31.59	31.73	36.79
1.2	23.14	22.92	22.29	23.26	23.01	23.69
1.4	16.62	16.11	15.77	16.51	16.15	14.09
1.6	12.08	12.02	11.74	12.08	10.96	7.73
1.8	8.05	8.05	7.94	8.85	7.19	3.92
2.0	5.50	5.39	4.93	4.99	4.55	1.83
2.5	1.59	1.36	1.19	1.30	1.24	0.19
3.0	0.28	0.23	0.23	0.45	0.27	0.01

Table 5.2

Crystal Data

	$(Ca_2(Me_3AsO)_9)(ClO_4)_4$
Formula weight	1702.198
a/Å	11.762(1)
c/Å	27.279(2)
V_c/Å^3	3268.30
d_{measd}/g cm^{-3}	1.71
d_{calcd}/g cm^{-3}	1.73
Z	2
Max crystal dimension/mm	0.38
Min cryatal dimension/mm	0.07

Table 5.3

Experimental Parameters

	$(Ca_2(Me_3AsO)_9(ClO_4)_4$
Mosaicity/deg	0.13
θ-Scan range/deg	0.70
Scan time/sec	70
Total background time/sec	17.5
θ limit/deg	57
Total independent reflections	1763
Reflections used in refinement for which $\|F\|^2 \geq 3\sigma(\|F\|^2)$	1072
Weighting parameter p	0.05
Primary beam collimator diameter/mm	1.0
Secondary beam collimator diameter/mm	5.0
X-radiation	Cu K_α

stoichiometric amount of $(Ca(Me_3AsO)_5)(ClO_4)_2$ in the unit cell.

A three-dimensional Patterson synthesis revealed dominant vectors corresponding to two triangular arrangements of atoms. One triangle is slightly larger than the other and they are staggered with respect to each other. Protracted attempts to fit preconceived heavy atom arrangements to these vector maps all failed and ultimately the empirical formulation $(Ca(Me_3AsO)_5)(ClO_4)_2$ became suspect.

5.3.2 Resolution Of The Formulation

The next stage in the investigation was to derive a possible geometry that could account for the density and the Patterson vectors. Closer scrutiny of all spectral and micro-analytical data led to the conclusion that a dinuclear $(Ca_2(Me_3AsO)_9)(ClO_4)_4$ * structure could explain both the experimental density and the vector maps.

* Analytical data are:

	% Carbon		% Hydrogen	
	Found	Calc.	Found	Calc.
$(Ca(Me_3AsO)_5)(ClO_4)_2$	18.5	19.6	4.76	4.90
$(Ca_2(Me_3AsO)_9)(ClO_4)_4$	18.5	19.0	4.76	4.76

In the original proposed formulation of the $(Ca(Me_3AsO)_5)(ClO_4)_2$ complex [85] errors were made in the calculated % of carbon and hydrogen which were reported as 18.1 and 4.6% respectively [86].

5.3.3 Structural Solution And Refinement

From density consideration, the unit cell contains two $(Ca_2(Me_3AsO)_9)^{4+}$ cations and eight ClO_4^- anions, in accordance with conductometric results of 1:2 electrolytes [139]. In the space group $P6_3/m$, the four calcium atoms must necessarily fill either of the two sets of four equivalent special positions:

4f : 1/3, 2/3, z; 2/3, 1/3, $\bar{z}$; 2/3, 1/3, $\frac{1}{2}$+z; 1/3, 2/3, $\frac{1}{2}$-z.

4e : 0, 0, z; 0, 0, $\bar{z}$; 0, 0, $\frac{1}{2}$+z; 0, 0, $\frac{1}{2}$-z.

Conductometric and density measurements are consistent with the unit cell containing two $(Ca_2(Me_3AsO)_9)^{4+}$ cationic formula units and eight ClO_4^-. The Patterson synthesis was not consistent with an infinite stack of cations along the z-axis. However, peaks in the vector map were consistent with the calcium atoms occupying the 4f positions.

(a) Plane Projection Analysis - Because of fortunate coincidences between high molecular and space group symmetry , it was found not only possible but also very convenient to solve the structure in projection down the very long z-axis [267]. It was apparent that the two staggered triangles of vectors were due to the arsenic atoms. An arrangement with six arsenic atoms forming two staggered triangles enclosing a calcium atom at the centre (1/3, 2/3, z) was recognized from the Patterson projection map. Subsequent two-dimensional structure factor calculations and difference Fourier syntheses revealed all atoms except the perchlorate oxygen atoms. Refinement in two dimensions with atoms assigned isotropic thermal parameters converged with

$R_1 = 0.117$ and

$R_2 = 0.149$

for 64 hk0 reflections with $|F_o|^2 \geq 3\sigma(|F_o|^2)$.

(b) Three-Dimensional Analysis - The z coordinates of the calcium and arsenic atoms only were then deduced from strong Patterson vectors of the type 00w. Subsequent structure factor calculations and difference Fourier syntheses returned the x and y coordinates of all atoms discovered in projection as well as their z coordinates. Refinements using isotropic thermal parameters for all atoms in this model gave values

$$R_1 = 0.149 \text{ and}$$
$$R_2 = 0.201$$

for 1072 reflections with $|F_o|^2 \geq 3\sigma(|F_o|^2)$. Difficulties were encountered in attempting to locate the perchlorate oxygen atoms. It was decided to leave this matter until a better model was established since substantial anisotropic thermal vibrations were found in most atoms. Refinements with atoms assigned anisotropic thermal parameters led to

$$R_1 = 0.088 \text{ and}$$
$$R_2 = 0.144.$$

The restrictions on anisotropic temperature factor coefficients for atoms in special positions were accounted for by using Levy's rule [268,269]. It was necessary to write a subroutine to handle these transformations. For example, the anisotropic atomic temperature factor for the calcium atoms was restricted to $\beta_{11} = \beta_{22} = 2\beta_{12}$ and $\beta_{23} = \beta_{13} = 0$. Therefore only β_{11} and β_{33} were needed to be varied and the β_{22} and β_{12} temperature factors were adjusted accordingly at the end of each refinement cycle. The multiplicities for atoms occupying special positions were treated in the same manner.

Only one of the three crystallographically distinct perchlorate groups was well-ordered. The other two chlorine atoms occupied special positions at $0,0,\frac{1}{4}$ (type a, point symmetry $\bar{6}$) and 0,0,0 (type b, point symmetry $\bar{3}$). Thus neither of these chlorine atoms could be surrounded by an ordered set of four oxygen atoms. A synopsis of the various models examined for these perchlorate anions is given below:

(i) Detailed difference Fourier syntheses calculated around these two chlorine atoms necessarily yielded peaks showing disordered oxygen atoms. The chlorine atom at the origin had eight peaks around it, six of them at $x_1,y_1,0$ and two at $0,0,z_1$ and $0,0,\bar{z}_1$ (Figure 5.1). The chlorine atom at $0,0,\frac{1}{4}$ was surrounded by five peaks, three of them at $x_2,y_2,\frac{1}{4}$ and two at $0,0,z_2$ and $0,0,\bar{z}_2$ (Figure 5.2). Full-matrix least-squares positional and anisotropic refinements of all atoms converged at

$$R_1 = 0.057 \text{ and}$$
$$R_2 = 0.067.$$

However, these two perchlorate anions had unreasonable stereochemistries. To resolve these problems, several other models were investigated.

(ii) The structure was refined in the non-centrosymmetric space group $P6_3$ to relieve some of the symmetry constraints on the perchlorate anions. Atoms related by a mirror plane in $P6_3/m$ were given slightly different positional coordinates in $P6_3$. The parameters for the cationic atoms and the chlorine atoms were included in the refinements. A difference Fourier calculation that followed did not show electron densities for the oxygen atoms at chemically reasonable positions around the chlorine atoms. This procedure was abandoned.

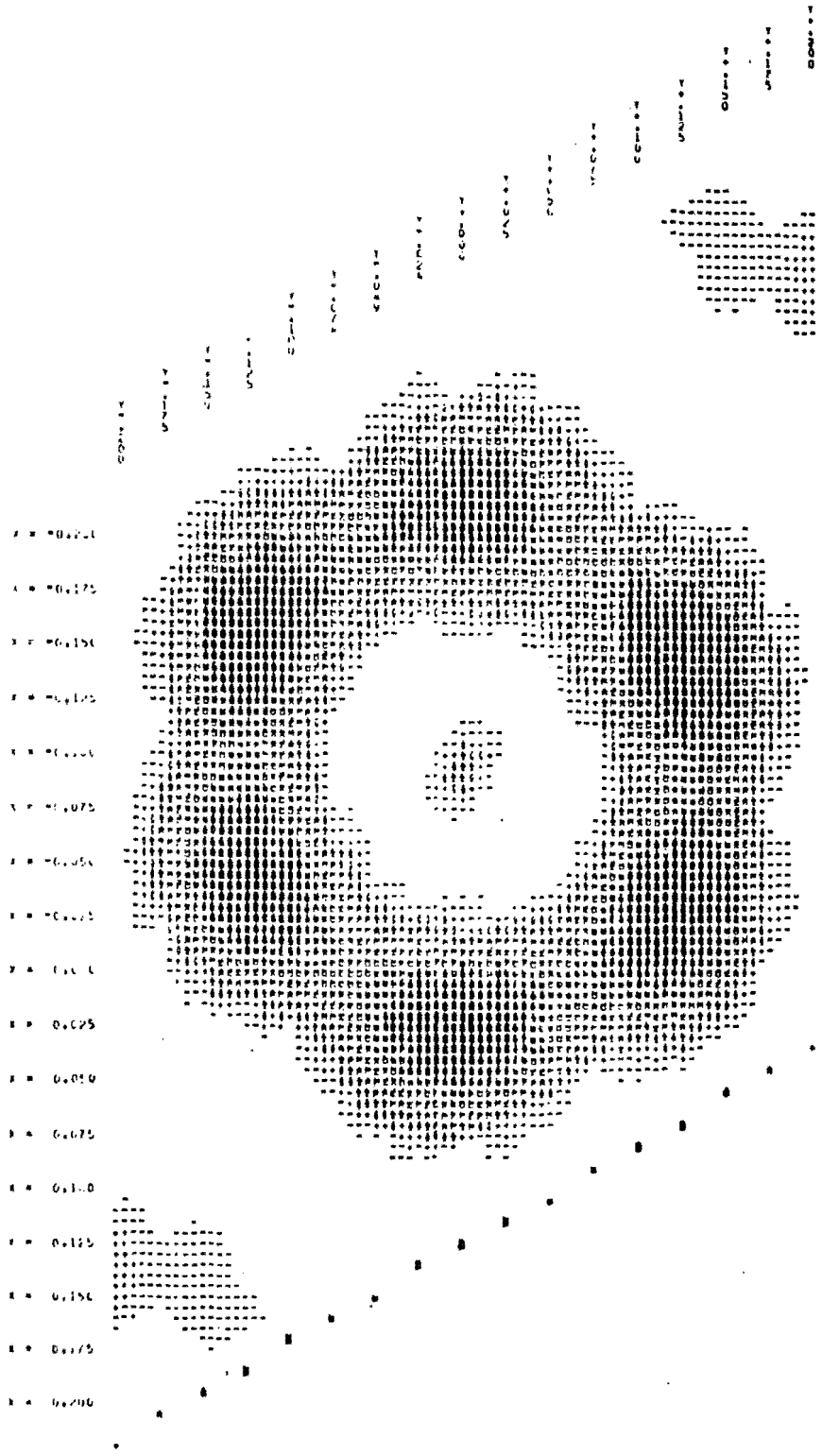

Figure 5.1 - Difference Fourier map calculated around the chlorine atom at the origin. The z-coordinate = 0.

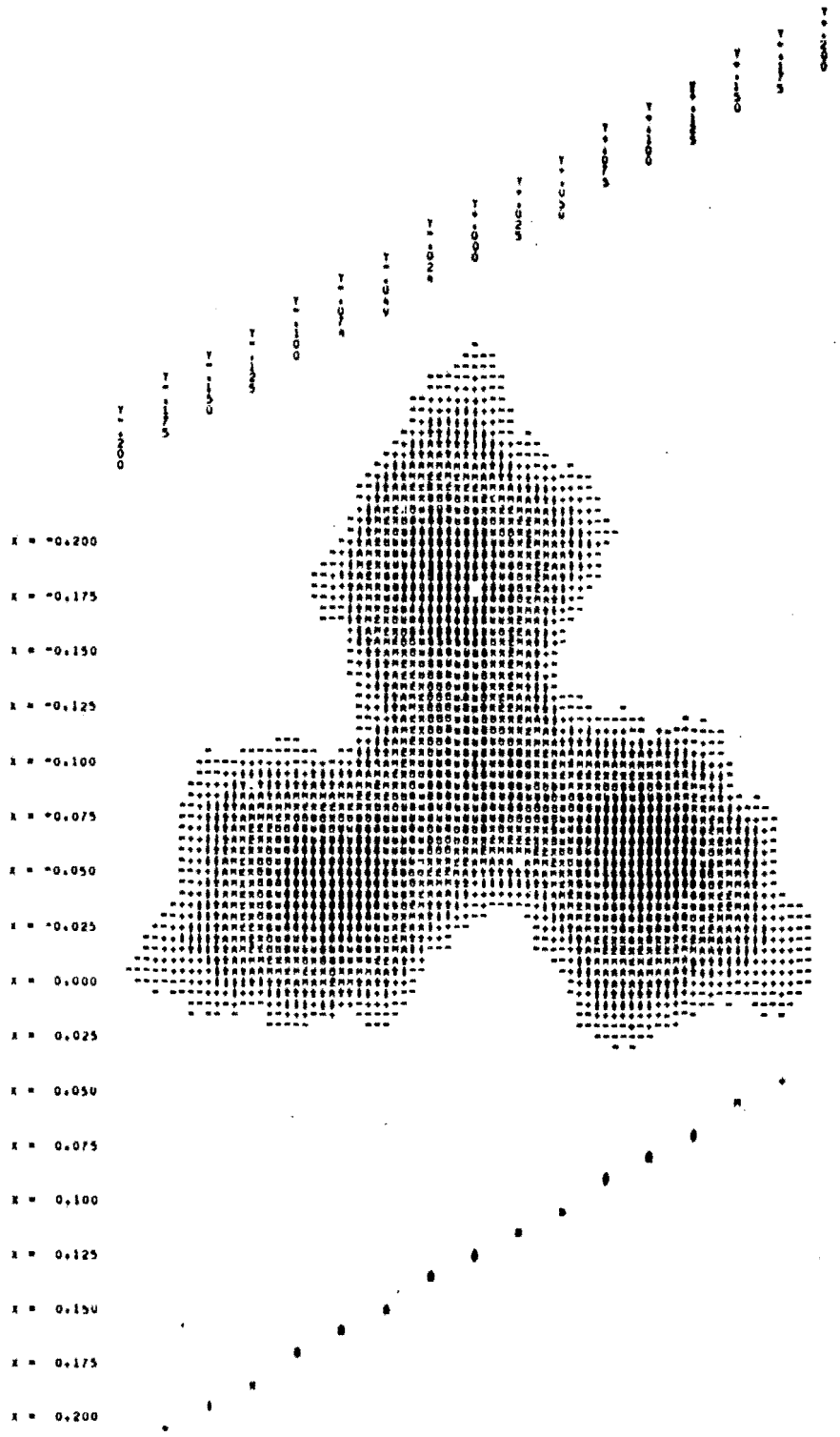

Figure 5.2 - Difference Fourier map calculated around the chlorine atom at 0, 0, ¼.
The z-coordinate = ¼.

(iii) The final model used described the perchlorate oxygen atoms as tetrahedral rigid groups with Cl-O distances set at 1.44Å in space group $P6_3/m$. The final refinement, containing two appropriately weighted rigid groups for each perchlorate anion, converged with

$$R_1 = 0.061 \text{ and}$$

$$R_2 = 0.072$$

for 1072 reflections with $|F_o|^2 \geq 3\sigma(|F_o|^2)$. Figure 5.3 illustrates these disordered arrangements.

There were only negligible changes (in the order of 0.01Å) in the cation geometry using different models for the perchlorate anions. The largest shift in the final cycle of refinement was 0.27σ. The highest peak from the final difference Fourier was about one half the electron density of the most disordered perchlorate oxygen atoms. The error in an observation of unit weight was 1.886.

Atomic coordinates and temperature factors of all non-hydrogen atoms are listed in Tables 5.4 and 5.5. Table 5.6 lists the root-mean-squares amplitudes of vibration. Structure factors calculated using the parameters in Tables 5.4 and 5.5 are listed in Appendix F.

5.4 DESCRIPTION OF THE CRYSTAL STRUCTURE

This is a particularly interesting structure since the unit cell contains separate dinuclear cations and perchlorate counter-anions. Each cation consists of two octahedrally coordinated Ca(II) ions with both terminal and bridging trimethylarsine oxide ligands. In the crystal lattice, the dinuclear inter-calcium vectors run parallel to the crystallographic z-axis. The discrete perchlorate counter-anions occupy holes in the cationic arrangement with apparently normal interionic

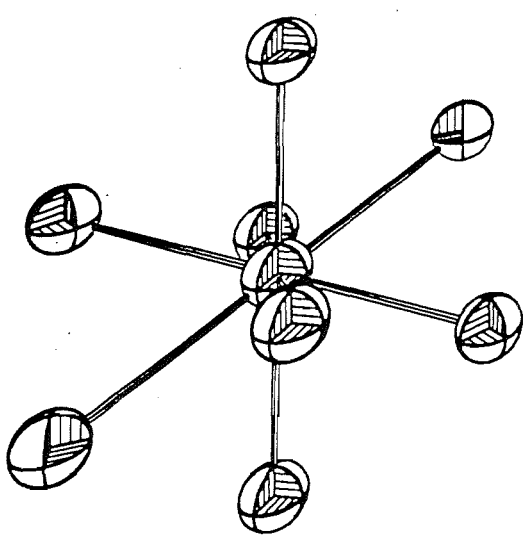

(a)

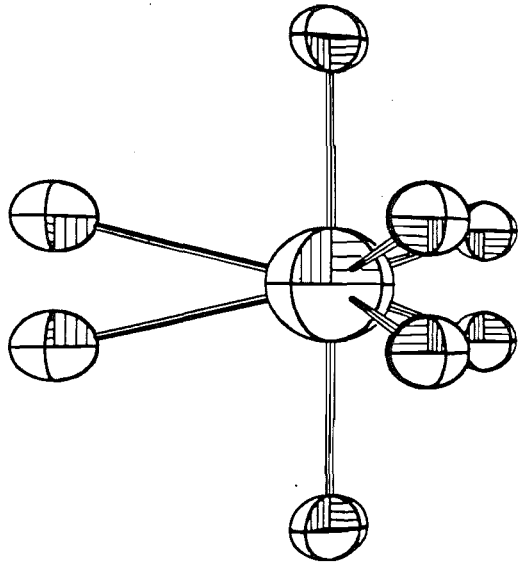

(b)

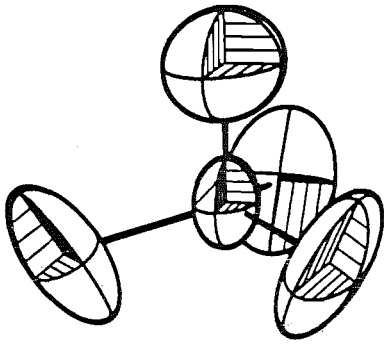

(c)

Figure 5.3 - Three crystallographically distinct perchlorate anions in $(Ca_2(Me_3AsO)_9)(ClO_4)_4$.

(a) Perchlorate anion with chlorine atom at the origin.

(b) Perchlorate anion with chlorine atom at 0, 0, ¼.

(c) Perchlorate anion with chlorine atom at 2/3, 1/3, z.

Table 5.4

Positional and Thermal Parameters for Non-group Atoms

$(Ca_2(Me_3AsO)_9)(ClO_4)_4$

Variable parameters have been multiplied by 10^4. Parameters without standard deviations are fixed by symmetry.

Atom	x	y	z	β_{11}	β_{22}	β_{33}	β_{12}	β_{13}	β_{23}
Ca	1/3	2/3	1860(1)	61(2)	$\beta_{22} = \beta_{11}$	7(0)	$2\beta_{12} = \beta_{11}$	0	0
As(1)	1205(1)	3806(1)	1018(1)	112(2)	106(2)	14(0)	37(2)	-9(1)	-15(1)
As(2)	4677(3)	4861(3)	1/4	214(4)	188(4)	12(0)	172(3)	0	0
O(1)	1673(8)	4984(8)	1434(3)	110(10)	110(10)	16(1)	39(9)	-7(3)	-19(3)
O(2)	3630(10)	5409(9)	1/4	110(10)	60(10)	7(1)	50(10)	0	0
C(11)	-230(30)	2230(20)	1224(8)	470(50)	150(30)	36(5)	10(30)	40(10)	-30(10)
C(12)	2590(20)	3510(20)	850(10)	200(30)	390(50)	100(10)	170(30)	-10(10)	-120(20)
C(13)	750(30)	4250(30)	430(7)	720(80)	430(50)	24(4)	390(60)	-70(10)	-40(10)
C(21)	6460(20)	6370(30)	1/4	90(30)	470(60)	24(5)	170(40)	0	0
C(22)	4410(20)	2790(20)	1929(5)	490(50)	300(40)	18(3)	320(40)	0(10)	-23(8)
Cl(1)	0	0	0	132(7)	$\beta_{22} = \beta_{11}$	17(1)	$2\beta_{12} = \beta_{11}$	0	0
Cl(2)	0	0	1/4	350(20)	$\beta_{22} = \beta_{11}$	49(4)	$2\beta_{12} = \beta_{11}$	0	0
Cl(3)	2/3	1/3	783(7)	230(10)	$\beta_{22} = \beta_{11}$	58(4)	$2\beta_{12} = \beta_{11}$	0	0
O(31)	6640(40)	2220(30)	700(10)	780(80)	680(90)	160(20)	470(80)	30(30)	-150(30)
O(32)	2/3	1/3	1210(20)	800(100)	$\beta_{22} = \beta_{11}$	100(20)	$2\beta_{12} = \beta_{11}$	0	0

Table 5.5

Positional and Thermal Parameters for Group Atoms

$(Ca_2(Me_3AsO)_9)(ClO_4)_4$

Atom	x	y	z	B
Perchlorate group 1				
O(11)	-1320(10)	-810(80)	-132(0)	15(1)
O(12)	0	0	528(0)	17(2)
Perchlorate group 2				
O(21)	-1110(30)	80(60)	2368(0)	19(1)
O(22)	0	0	3028(0)	33(6)

Positional parameters have been multiplied by 10^4.

Table 5.6

Root-Mean-Square Amplitudes of Vibration (Å) for Selected Atoms

$(Ca_2(Me_3AsO)_9)(ClO_4)_4$

Atom	Min	Intermed	Max
Ca	0.167(6)	0.179(5)	0.179(5)
As(1)	0.178(3)	0.264(2)	0.283(2)
As(2)	0.172(4)	0.213(3)	0.363(3)
O(1)	0.18(1)	0.25(1)	0.30(1)
O(2)	0.16(2)	0.17(2)	0.24(2)
C(11)	0.23(3)	0.34(3)	0.64(3)
C(12)	0.22(3)	0.34(3)	0.70(4)
C(13)	0.24(3)	0.39(3)	0.64(3)
C(21)	0.15(4)	0.30(3)	0.50(3)
C(22)	0.15(3)	0.32(2)	0.52(3)
Cl(1)	0.250(9)	0.263(9)	0.263(9)
Cl(2)	0.43(2)	0.43(2)	0.43(2)
Cl(3)	0.35(1)	0.35(1)	0.47(2)
O(31)	0.34(3)	0.65(3)	0.86(4)
O(32)	0.61(7)	0.65(7)	0.65(7)

contact distances. The arrangements of the ions in the unit cell is depicted in Figure 5.4. Figure 5.5 is a view of the structure projected down the z-axis. Three adjacent unit cells are shown and in addition the symmetry elements of the space group are given.

Selected interatomic distances and bond angles are given in Tables 5.7 and 5.8 respectively.

5.4.1 The $(Ca_2L_9)^{4+}$ Cation

Figure 5.6 shows an edge-on view of the dinuclear calcium cationic unit and defines the atom labelling system used. The view presented is perpendicular to the three-fold axis which passes through the two calcium atoms.

(a) Coordination of the Calcium Atom - The calcium atoms sit on the three-fold rotational symmetry axis. The coordination geometry around each calcium atom is best described as a trigonally distorted octahedron. Each calcium atom is surrounded by six oxygen atoms of the trimethylarsine oxide ligands. Three of the ligands form terminal groups while the other three bridge to the adjacent calcium atom to form the confacial bi-octahedral complex. Thus the dinuclear species possesses D_{3h} symmetry having two face-sharing CaL_6 units. The two triangles formed by the terminal oxygen atoms are staggered with respect to the triangle of the central oxygen atoms. The two calcium atoms are separated by a distance of 3.491(6)Å.

The unique Ca-O(2) bond length (2.474(7)Å) for the bridging ligands is long compared with the unique Ca-O(1) terminal bond distance of 2.284(7)Å. The axial angles around the calcium atom are 96.4° for those involving the terminal ligands, O(1)-Ca-O(1) and 73.9° for the bridging

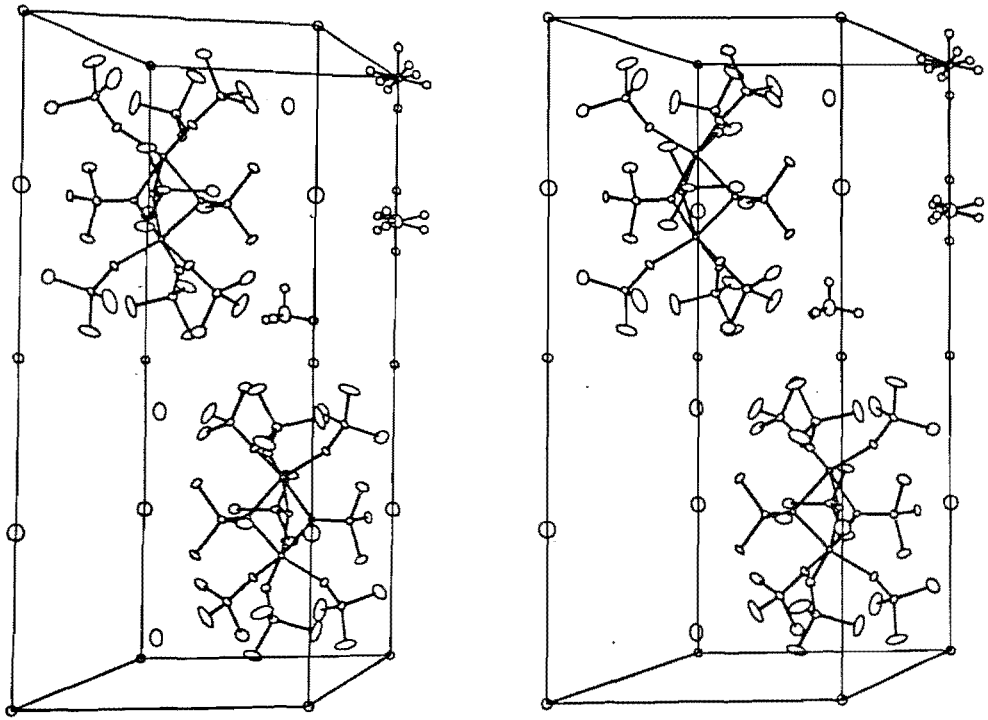

Figure 5.4 - Stereoscopic view showing contents of the unit cell of $(Ca_2(Me_3AsO)_9)(ClO_4)_4$. For clarity only three perchlorate anions are shown with their oxygen atoms attached.

Figure 5.5 - View of three adjacent unit cells of $(Ca_2(Me_3AsO)_9)(ClO_4)_4$ projected down the z-axis.

(a) The z-coordinates are from 0 to $\frac{1}{2}$.

(b) The z-coordinates are from $\frac{1}{2}$ to 1.

(c) Symmetry elements of space group $P6_3/m$.

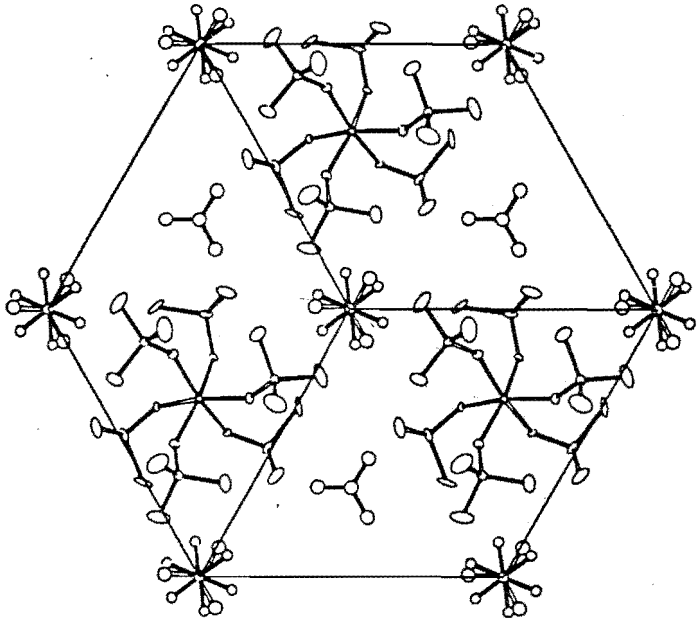

(a)

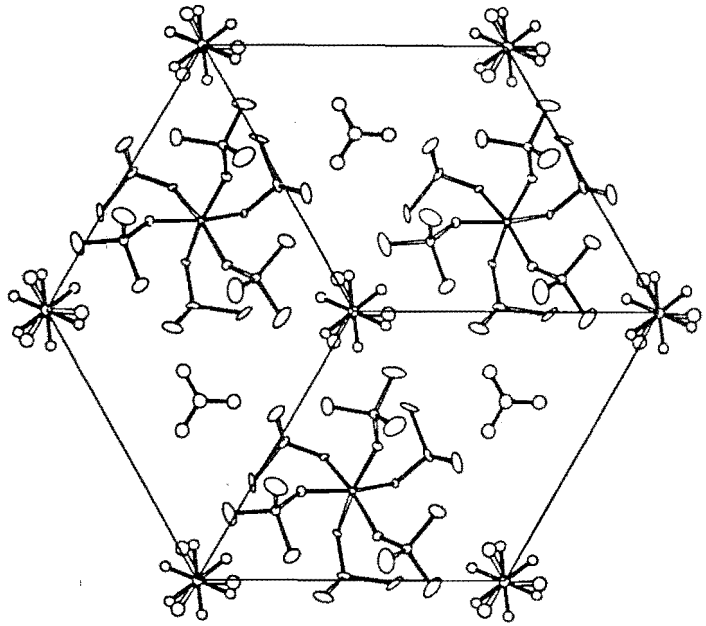

(b)

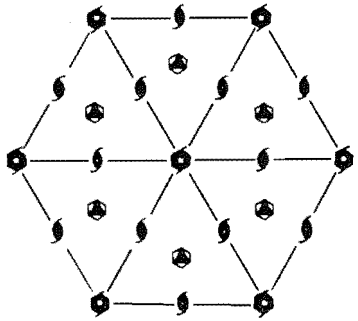

(c)

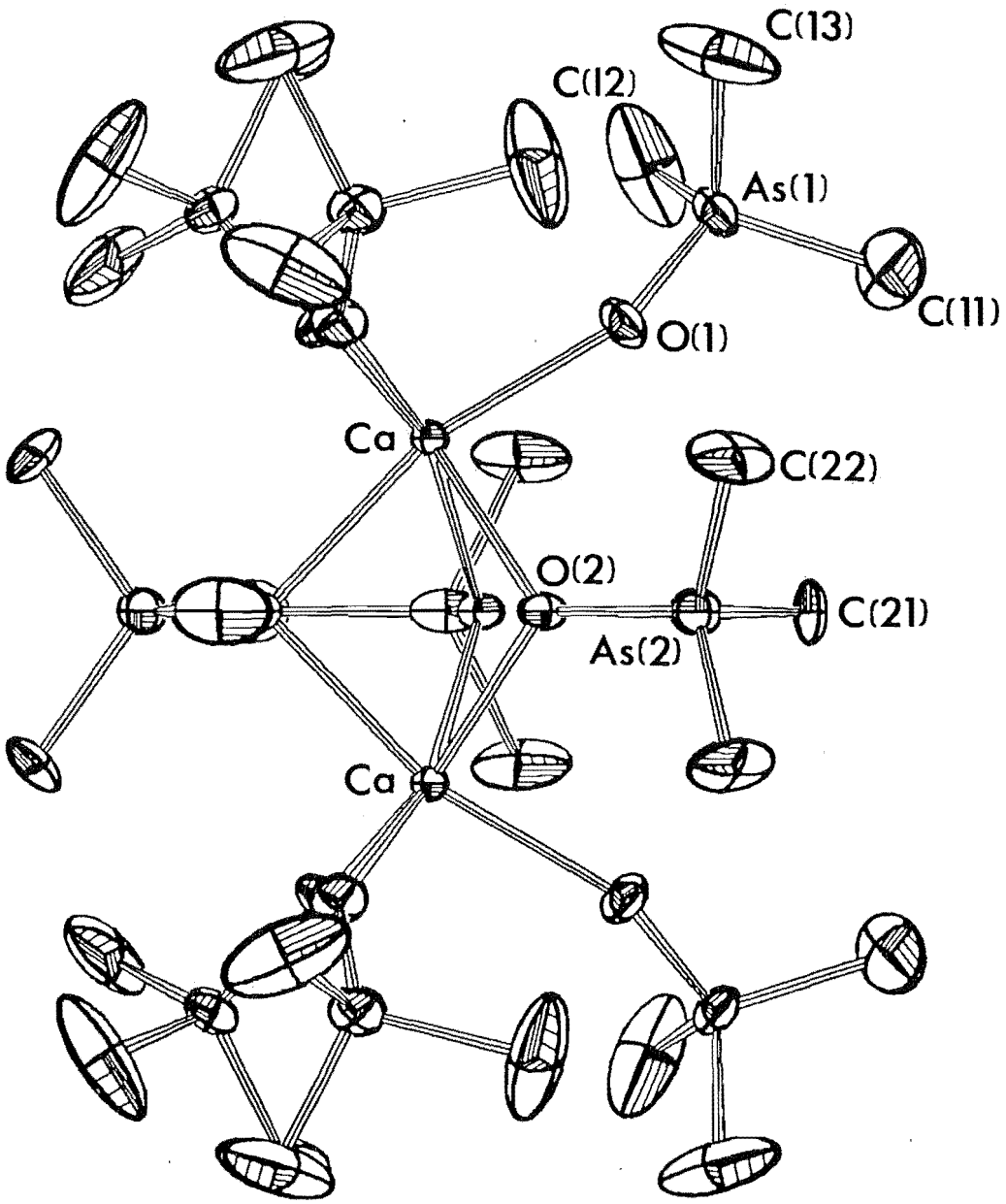

Figure 5.6 - Perspective view of the $(Ca_2(Me_3AsO)_9)^{4+}$ cation.

Table 5.7

Selected Interatomic Distances (Å) In $(Ca_2(Me_3AsO)_9)(ClO_4)_4$

Atoms	Distances	Atoms	Distances
Cation			
Ca-O(1)	2.284(7)	Ca...Ca^{iv}	3.491(6)
Ca-O(2)	2.424(7)	Ca...As(1)	3.800(2)
		Ca...As(2)	3.661(2)
As(1)-O(1)	1.657(7)	As(2)-O(2)	1.649(10)
As(1)-C(11)	1.865(20)	As(2)-C(21)	1.957(26)
As(1)-C(12)	1.886(19)	As(2)-C(22)	1.926(14)
As(1)-C(13)	1.845(20)		
Anion			
Cl(3)-O(31)	1.32(3)	Cl(3)-O(32)	1.16(6)

The Roman numeral superscripts represent the symmetry transformations given below. Where there is no further qualification, symmetry(i) is implied.

(i) x, y, z

(ii) -y, x-y, z

(iii) y-x, -x, z

(iv) x, y, $\frac{1}{2}$-z

Table 5.8

Selected Bond Angles (deg.) In $(Ca_2(Me_3AsO)_9)(ClO_4)_4$

Atoms	Angles	Atoms	Angles
O(1)-Ca-O(1)^{ii}	96.4(3)	Ca-O(1)-As(1)	148.8(5)
O(1)-Ca-O(2)	99.2(3)	Ca-O(2)-Ca^{iv}	92.1(4)
O(1)-Ca-O(2)^{ii}	162.8(3)	Ca-O(2)-As(2)	127.0(3)
O(1)-Ca-O(2)^{iii}	89.1(3)		
O(2)-Ca-O(2)^{ii}	73.9(3)		
O(1)-As(1)-C(11)	112.4(7)	O(2)-As(2)-C(21)	108.4(9)
O(1)-As(1)-C(12)	111.2(7)	O(2)-As(2)-C(22)	110.2(6)
O(1)-As(1)-C(13)	112.5(8)	C(21)-As(2)-C(22)	110.2(8)
C(11)-As(1)-C(12)	109.2(12)	C(22)-As(2)-C(22)^{iv}	107.9(11)
C(12)-As(1)-C(13)	103.9(14)		
C(13)-As(1)-C(11)	107.2(13)		
O(31)-Cl(3)-O(32)	100.3(20)		
O(31)-Cl(3)-O(31)^{ii}	116.9(12)		

groups, O(2)-Ca-O(2). The Ca-O(2)-Ca^{iv} angle bridging the two CaL_6 units is 92.1°. Another pertinent structural parameter is the displacement of the calcium atom from the centroid of its own octahedron. The distance (d') between the mid-point of the plane of bridging oxygen atoms and the calcium atom is 1.746Å. The corresponding distance (d'') to the mid-point of the plane of the peripheral oxygen atom is 1.162Å (Figure 5.7).

The Ca-O distances found here are longer than the Ni-O and Mg-O distances in $(M(Me_3AsO)_5)^{2+}$ (M = Ni, Mg), but close to the sum of the crystal radii of calcium and oxygen of 2.39Å [286]. A survey of Ca-O distances showed that those found for this structure are in the range of other reported results (Table 5.9) [270-275].

(b) Conformation of the Ligands - There are two types of trimethylarsine oxide ligand in the cations. Six crystallographically equivalent ligands form terminal groups while the other three symmetry related ligands bridge to the calcium centres. The As-O bond length for the terminal group is slightly longer than that of the bridging group, 1.657(7)Å and 1.649(10)Å respectively. The Ca-O(1)-As(1) angle is 148.8°; while that for the bridging ligand, the Ca-O(2)-As(2) angle is 127.0°. These parameters are comparable to those observed in other arsine oxide structures (Table 3.14).

5.4.2 The Perchlorate Anions

Two of the three crystallographically independent perchlorate anions exhibit disorder. The chlorine atom at 0,0,0 is in an environment of $\bar{3}$ symmetry while that at 0,0,¼ has $\bar{6}$ symmetry imposed on it. Each chlorine atom may be considered to be at the centroid of two possible

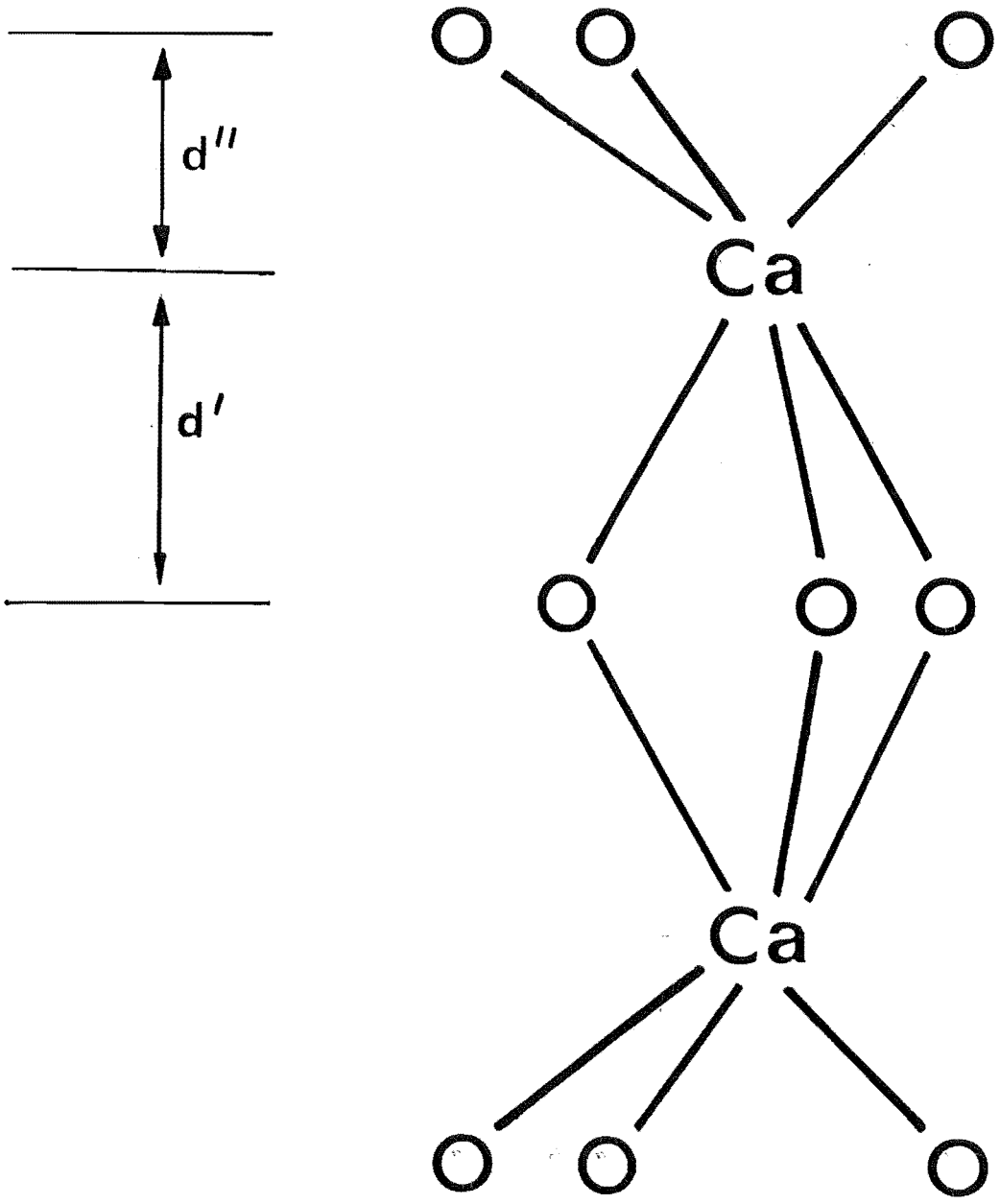

Figure 5.7 - Arrangements of the terminal and bridging ligands in dinuclear complex. For $(Ca_2(Me_3AsO)_9)^{4+}$, d' = 1.746Å and d'' = 1.162Å. For a perfect bi-octahedron, d' = d''.

Table 5.9

Comparison Of Calcium-Oxygen Bond Distances (Å)

Compound	Coord. No.	Av. Ca-O	Max	Min	References
$Ca(C_{10}H_{13}O_8N_2P)\cdot 6H_2O$ [a]	7	2.42	2.65	2.29	270
$CaBr_2(C_6H_{12}N_4)_2\cdot 10H_2O$ [b]	6	2.33	2.34	2.32	271
$Ca(C_{11}H_{10}O_6N)_2\cdot 3H_2O$ [c]	7	2.38	2.43	2.34	272
$CaCl_2(C_6H_{11}O_4N_3)\cdot 3H_2O$ [d]	7	2.39	2.50	2.30	273
$CaBr_2(C_{12}H_{22}O_{11})\cdot 7H_2O$ [e]	8	2.45	2.45	2.38	274
$Ca(C_5H_7O_4N)\cdot 3H_2O$ [f]	8	2.48	2.60	2.38	275

a = Thymidylate, b = Hexamethylenetetramine, c = Blepharisma, d = Glycylglycylglycine, e = Lactose, f = Glutamate.

orientations for its bonded tetrahedrally arranged oxygen atoms. In the first case, the overlapped arrangement is necessarily staggered. Each such site may be occupied by one anion in either of the two orientations (a) and (b) shown below.

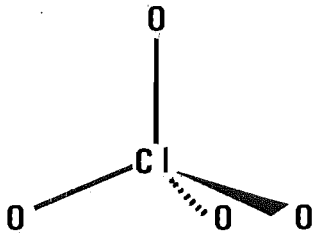

(a)

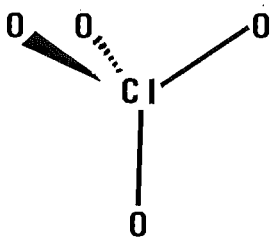

(b)

In the second case, the arrangement is necessarily eclipsed and each site may be occupied by one anion in either of the two orientations (c) and (d) shown below.

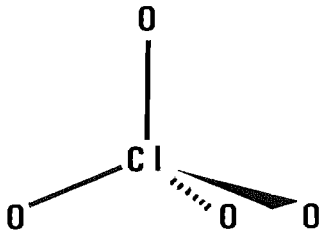

(c)

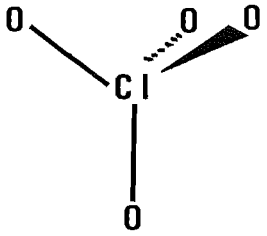

(d)

Oxygen atoms of the third perchlorate anion could be resolved, since it lies on the crystallographic three-fold axis and showed no evidence of disorder. Diagrams of these three perchlorate anions are presented in Figure 5.3 (page 126).

The phenomenon of oxygen disorder in perchlorate anions is well documented in the literature [276-279]. Models ranging from spheres of electron clouds around the chlorine atoms [280,281] to the isolation of equal occupation of the ion in two sites [282-285] have been used to describe the disorder.

5.5 DISCUSSION

5.5.1 General Consideration

The structure of $(Ca_2(Me_3AsO)_9)(ClO_4)_4$ is of interest even though it does not fit into the pattern under investigation through the five and six-coordinate compounds discussed in earlier chapters. Studies of metal complexes with phosphine and arsine oxide ligands are prevalent in the literature [15, 38-41]. However, only a few examples of bridged oxo ligands of this type have been reported [46, 264]. The bridging properties of these ligands appear restricted to a few systems, perhaps because chemistry in this area is still relatively unexplored. Although this work demonstrates that the square-pyramidal analogue of $(Mg(Me_3AsO)_5)^{2+}$ is not achieved for calcium, five-coordinate $(CaL_4ClO_4)^{2+}$ complexes have been reported where L = Ph_3AsO and Me_3AsO [85, 86]. Calcium ions (ionic radius Ca^{2+} = 0.99Å) [286], can achieve the higher coordination number, but in appropriate circumstances, five-coordinate complexes can be synthesized.

Other polynuclear complexes of calcium exhibit a variety of stereochemistries and even higher coordination numbers [287-290]. For example both seven and eight coordination are found for crystallographically independent Ca(II) ions in $Ca_2C_{12}H_2O_{12}\cdot 9H_2O$ [291]. The dinuclear structure of $(Ca_2(Me_3AsO)_9)^{4+}$ is similar to a number of compounds of the form $A_n(M_2X_9)$ where A^{m+} = univalent cations; M = Cr, Mo, W, Ti, V, Zr, Rh, Bi, Re; X = Cl and Br; and m and n = 1 - 3 [3-5, 292-298]. The principal concern with these complexes has been to determine the extent of metal-metal bonding [292]. Since there is no such interaction in the present complex cation (Ca...Ca = 3.491Å) comparisons are not justified.

5.5.2 Comparison With Other Phosphine And Arsine Metal Complexes

A series of coordination compounds has been prepared containing antimony or bismuth trihalide and triphenylphosphine oxide or triphenylarsine oxide ligand and examined using vibrational spectra [299, 300]. The complete structure analyses of two such compounds have been completed. The $I_3BiI_3Bi(Ph_3AsO)_3$ complexes consists of two distorted octahedra sharing a face through iodide ions and with all the triphenylarsine oxide ligands linked to one of the Bi atoms [301, 302]. In contrast, the dimeric symmetrical molecules of $(BiI_3(Ph_3PO)_2)_2$ are built of two octahedra sharing an edge through two iodine atoms with the triphenylphosphine oxide ligands in cis positions [303]. Another related structure is the dimeric species $(Zn(C_6H_4(Me_2AsO)_2)_2)^{4+}$ where the two zinc atoms are linked by arsine oxides (Figure 5.8) [304]. Karayannis et al [46] have reported the polymeric organophosphoryl magnesium complex $(Mg(Ph_3PO)_4)_n(ClO_4)_{2n}$ (n = 1, 2 .....) on the basis of infrared, X-ray powder and molar conductivity evidence. In the same report, a trinuclear cation $(Cr_3(Ph_3PO)_8(ClO_4)_3)^{6+}$ having bridging phosphine oxides as shown in Figure 5.9a was also formulated. More pertinent to the present structure is the octahedral polymer of the general formula $M(Me_3AsO)_2X_2$ where M = Co, Ni; X = Cl, Br [264] reported by Brodie et al. In Figure 5.9b is shown this proposed structure containing oxo rather than halogen bridges.

The dimensions in the current structure are in close agreement with reported data (Table 3.14). The dimeric species $(Zn(C_6H_4(Me_2AsO)_2)_2)^{4+}$ has a crystallographic centre of symmetry. The Zn-O(4') bond distance of 2.3Å is significantly longer, as might be expected, for the bridging ligand. The non-bridging equatorial Zn-O distances (Zn-O(2) = 1.88Å and Zn-O(3) = 1.77Å) are comparatively short. These results are in favourable agreement with $(Ca_2(Me_3AsO)_9)^{4+}$ which also exhibits a longer bridging Ca-O distance.

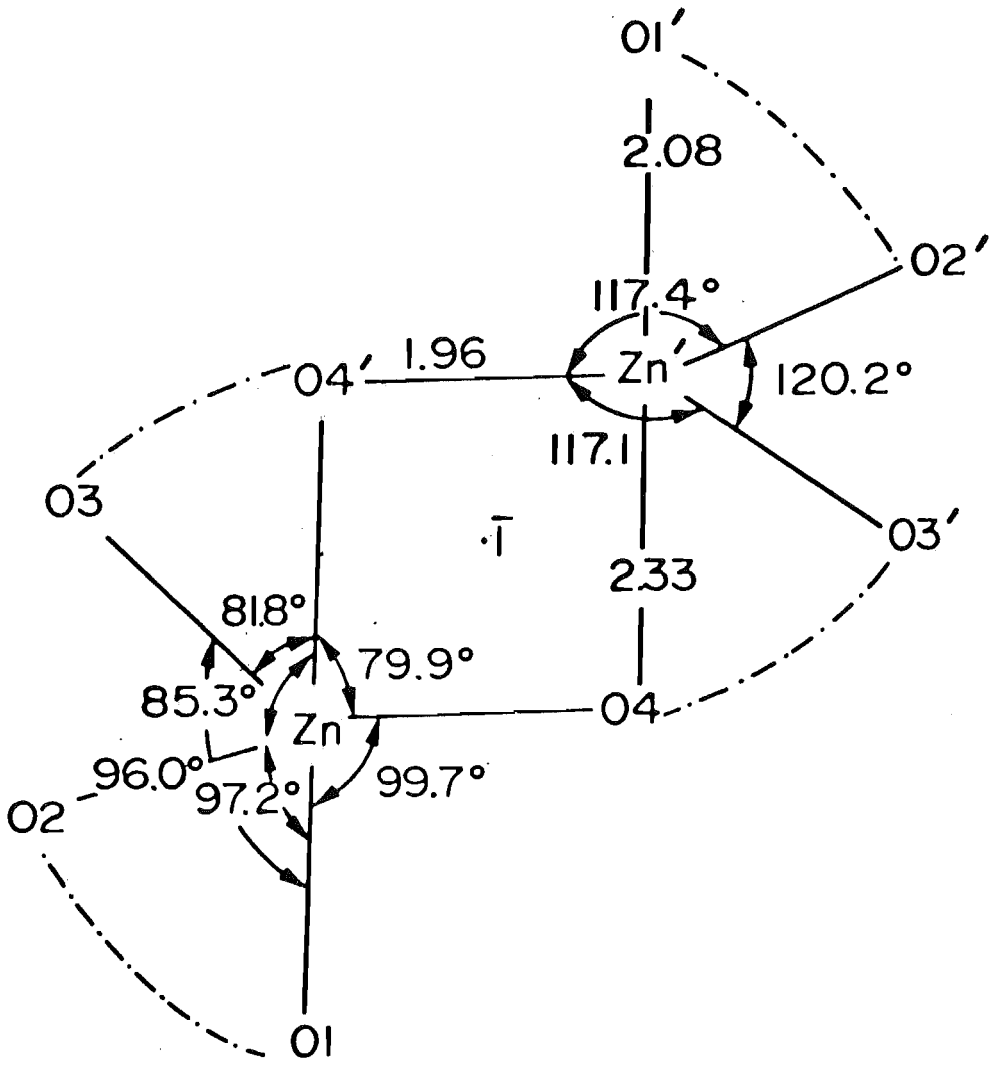

Figure 5.8 - The dimeric species $(Zn(C_6H_4(Me_2AsO)_2)_2)^{4+}$ where the two zinc atoms are linked by arsine oxides.

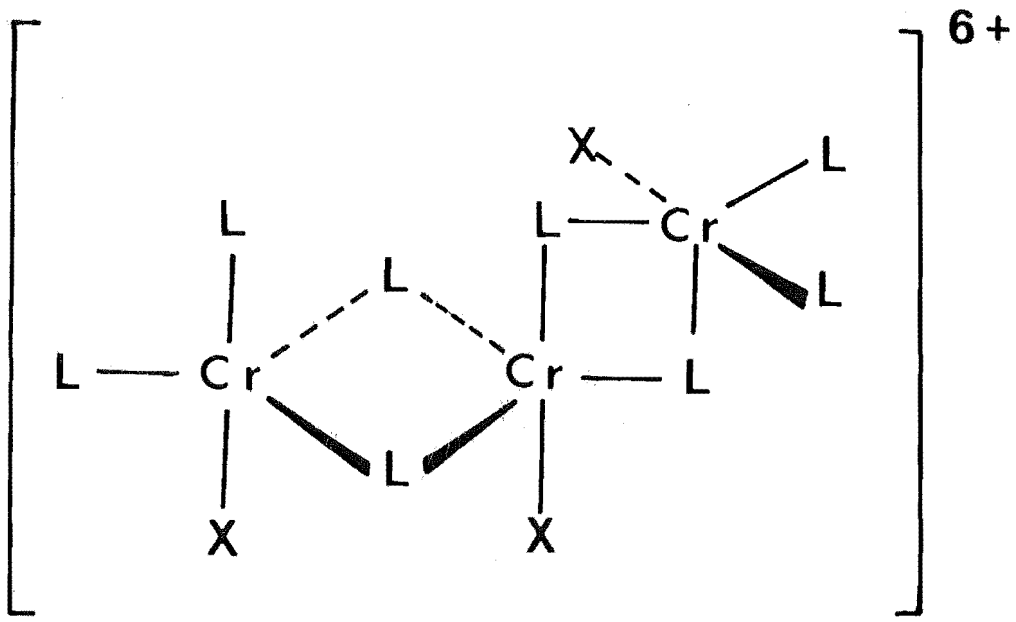

(a)

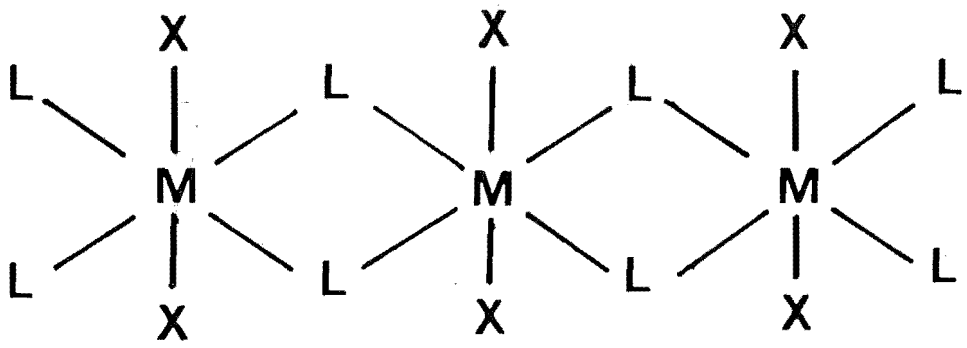

(b)

Figures 5.9 - Compounds containing phosphine oxides or arsine oxides as bridging ligands.

(a) A trinuclear cation $(Cr_3(Ph_3PO)_8(ClO_4)_3)^{6+}$; L = Ph_3PO and X = ClO_4.

(b) Octahedral polymer $M(Me_3AsO)_2X_2$; M = Co, Ni; L = Me_3AsO and X = Cl, Br.

5.6 CONCLUDING REMARKS

An interesting feature observed in this structure is that the As-O bonds for the bridging and terminal ligands are very similar. One would normally expect the As-O bond for the bridging groups to be weaker as a result of a greater electron involvement in σ-bonds from the oxygen atom to two metal centres. There appears, then, to be a compensating electron donation effect by the methyl groups of the bridging arsine oxide ligands. A shift in electron density, as illustrated in Figure 5.10, could explain the strengthening effect in the As-O bond and a concomitant weakening of the As-C bonds (the As-C bond lengths for the bridging ligands are longer than those of the terminal ligands, Table 5.7). Since the methyl groups are incapable of π donation, the increased As-O bond strength must be restricted to the σ-interaction.

Further discussions of this effect using infrared and nmr results are given in Sections 6.3.2(b) and 6.4.2.

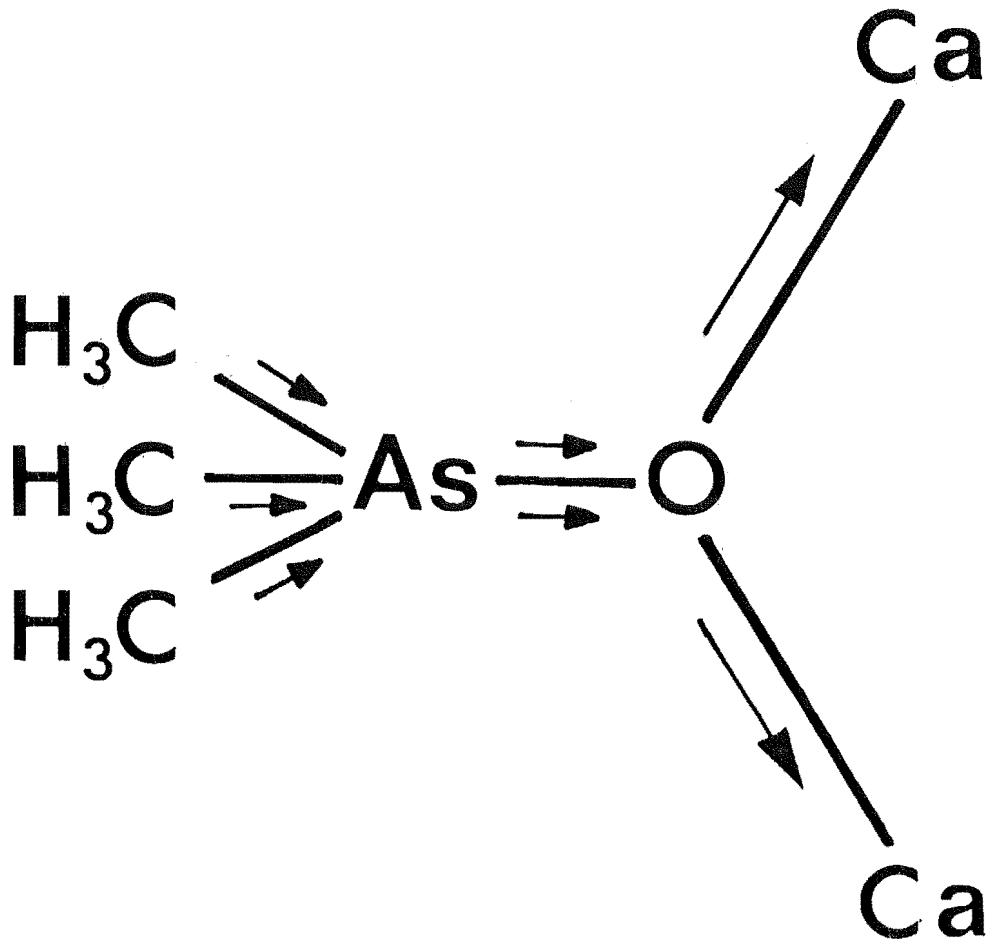

Figure 5.10 - Proposed shift in electron density for a bridging Me_3AsO ligand in $(Ca_2(Me_3AsO)_9)^{4+}$.

CHAPTER 6

GENERAL DISCUSSIONS

6.1 INTRODUCTION

This chapter summarizes some other physical studies that are particularly relevant to the present work. The following sections deal with:

(i) a brief survey of five-coordination chemistry, with reference to the different approaches that have been used in describing bonding in trigonal-bipyramidal and square-pyramidal species,

(ii) infrared results for the present series of complexes and discussion of the vibrational modes involved,

(iii) nmr data of some related phosphine and arsine oxide complexes and a detailed discussion of the spectra of $(Ca_2(Me_3AsO)_9)(ClO_4)_4$,

(iv) strain-energy minimization calculations for $(Mg(Me_3AsO)_5)^{2+}$ to determine the relative stabilities of the observed square-pyramidal stereochemistry and other hypothetical stereochemistries, and

(v) one proposal for a bonding scheme for these five-coordinate square-pyramidal complexes.

6.2 A BRIEF REVIEW OF FIVE-COORDINATION CHEMISTRY

No attempt will be made in this section to discuss five-coordination exhaustively. Comprehensive reviews on various aspects of the subject have been written by Muetterties and Schunn [305], Sacconi [306], Furlani [307] and Wood [308]. The main aim here is to make general remarks on the

stereochemistry and nature of bonding in five-coordination chemistry in relation to the structures studied here. In particular some examples of complexes containing five equivalent monodentate ligands are presented and their structural parameters discussed.

6.2.1 Stereochemistry

Ideally five-coordinate structures confront us with a choice between two central atom site symmetries: square-pyramidal (C_{4v}) and trigonal-bipyramidal (D_{3h}). However these two idealized geometries are rarely found in practice and compounds with the so-called trigonal-bipyramidal or square-pyramidal geometries may often be distorted from their idealized forms. A mechanism relating to the interconversion pathway between the idealized two geometries has been proposed by Berry (Figure 6.1) [309].

There are a number of factors that affect the stereochemistry. Foremost amongst these are the size and disposition of the coordinating ligand. Many five-coordinate complexes have been prepared using ligands that inhibit six-coordination. Some ligands have been tailored to promote essentially trigonal-bipyramidal or square-pyramidal complex formation due to their steric constraints. Next, the size and electronic configuration of the metal ion are of importance. A larger metal ion can make possible higher coordination numbers while the electronic configuration of a particular metal ion may be stabilized energetically in either the C_{4v} or alternatively, the D_{3h} symmetry situation. Crystal packing forces and the size of counter-ions may play a role in determining overall conformations. Electronic effects in chemical bonds also affect the stability of various five-coordination geometries.

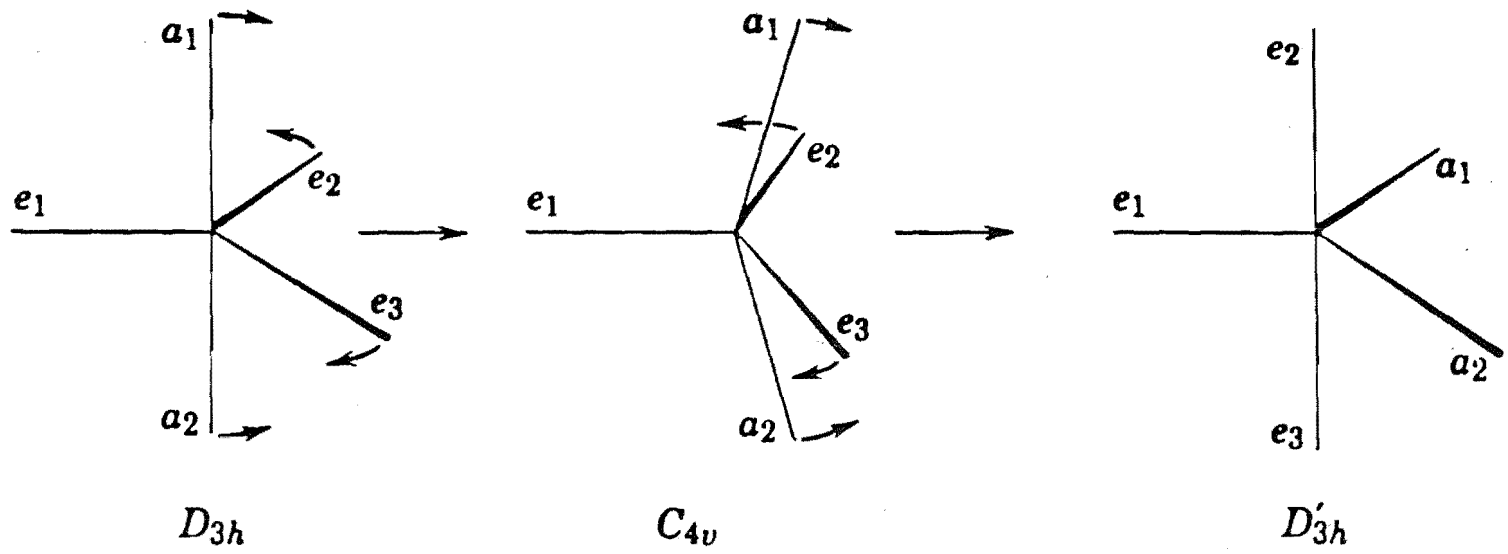

Figure 6.1 - Schematic representation of the Berry intramolecular rearrangement for the trigonal-bipyramid involving a square-pyramid intermediate.

6.2.2 The Nature Of Bonding

(a) Charge Repulsion Approach - On the basis of purely coulombic charge repulsion calculations, Zemann [310] demonstrated that the trigonal-bipyramidal arrangement is more stable by 24.94 kJ/mole than the square-pyramidal structure. His calculations showed that an optimum square-pyramid is one with an axial L_{axial}-M-L_{basal} angle of 104.1°.

Analogous results were obtained by Gillespie [118, 119] who used the electron-pair repulsion (VSEPR) approach. He predicted that the trigonal-bipyramid, having fewer interactions at 90° than the square-pyramid, would be the more stable entity. For both geometrical arrangements, the axial electron pairs would be subjected to a greater repulsion than the equatorial pairs, hence the equilibrium arrangement would be one in which the axial pairs are at slightly greater distance from the nucleus than the equatorial pairs. For transition metal complexes, interactions between bonding pairs and non-bonding d electrons need to be considered. When interactions between bonding electron pairs are more important, as in complexes of 'covalent' character, the trigonal-bipyramidal structures are favoured. If the predominant interaction is between the bonding electron pairs and the non-bonding d electrons, as in complexes with 'ionic' character, the square-pyramidal geometry is expected. This classification of 'covalent' and 'ionic' bond types appears to be somewhat arbitrary as many square-pyramidal complexes undoubtedly have considerable π bonding involving the basal ligands.

In an extension of Gillespie's idea, Kepert [311] calculated the potential energy surfaces of five-coordinate complexes. Minima were found in the total ligand-ligand repulsion energy U which was obtained by summing over all donor atom-donor atom repulsions.

For complexes with five equivalent ligands, there is no potential energy barrier between the square-pyramidal and trigonal-bipyramidal geometries. For compounds of stoichiometry M(monodentate')(monodentate)$_4$ the idealized geometry preferred depends on relative M-L bond lengths. With M(monodentate')$_2$(monodentate)$_3$ type of complexes, these calculations show a preference for trigonal-bipyramidal stereochemistry with two longer axial bonds (Figure 6.2).

(b) Crystal Field Models - The relative energies of d orbitals in trigonal-bipyramidal and square-pyramidal crystal fields are indicated in Figure 6.3a. Crystal field stabilization energy calculations indicated there is a slight preference for square-pyramid over the trigonal-bipyramid stereochemistry for all d^n configurations. However, an examination of structural data shows that although in general square-pyramidal is the preferred geometry for nickel and cobalt, other complexes such as $(Fe(N_3)_5)^{2-}$, $(CuCl_5)^{3-}$, and $(Pt(SnCl_3)_5)^{3-}$ are trigonal-bipyramidal [308].

The structural features of a series of high spin five-coordinate complexes (M(Me$_6$tren)Br)Br (M = Mn, Fe, Cu, Ni, Co, Zn) (Figure 6.3b) have been explained reasonably successfully in terms of d orbital populations in the crystal field model [312]. Figure 6.3c shows a plot of M-N and M-Br distances against the metal atomic number. The equatorial M-N distances increase for nickel and copper (d^8 and d^9) complexes when the $d_{x^2-y^2}$ and d_{xy} orbitals in the equatorial plane are filled. The M-Br distances and the apical M-N distances behave similarly, though the Mn-N axial distance is shorter while the Ni-Br distance is longer than expected.

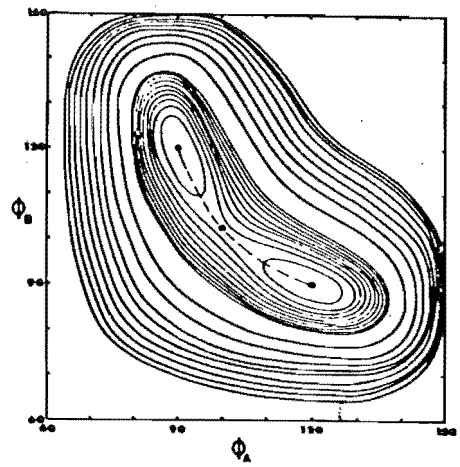

(a)

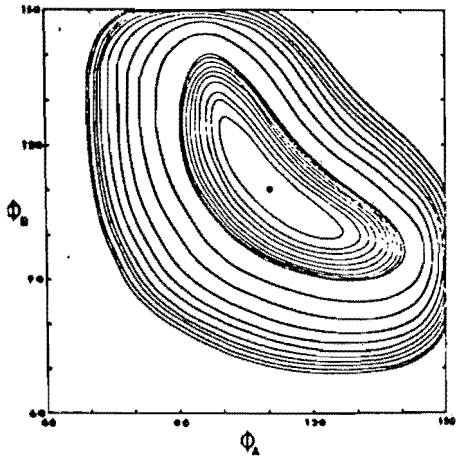

(b)

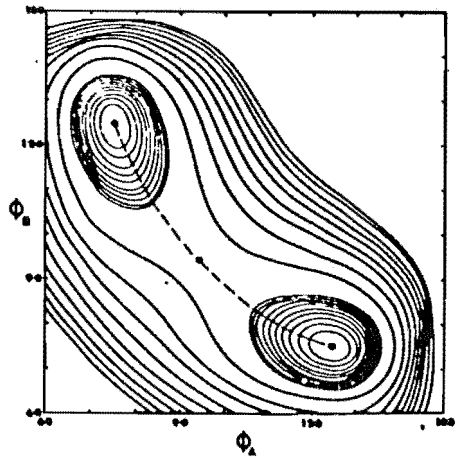

(b)

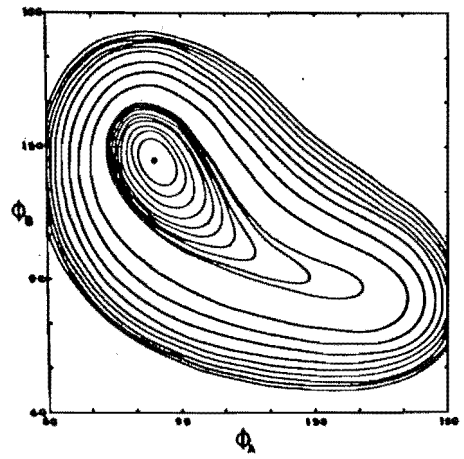

(c)

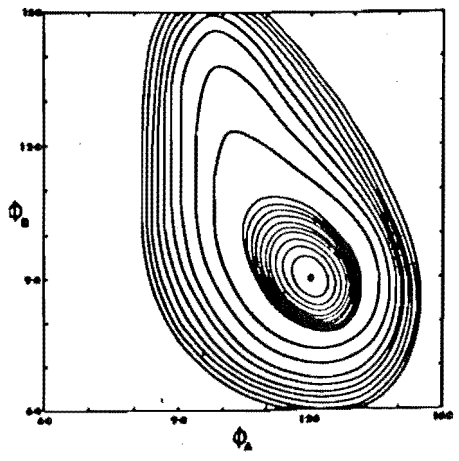

(c)

Figure 6.2 - Potential energy surfaces for five-coordinate compounds.

(a) No potential energy barrier between the square-pyramidal (SP) and trigonal-bipyramidal (TBP) geometries for ML_5.

(b) Idealized geometry for $ML'L_4$ depends on relative metal-ligand bond lengths.

(c) Potential energy favours TBP for ML'_2L_3

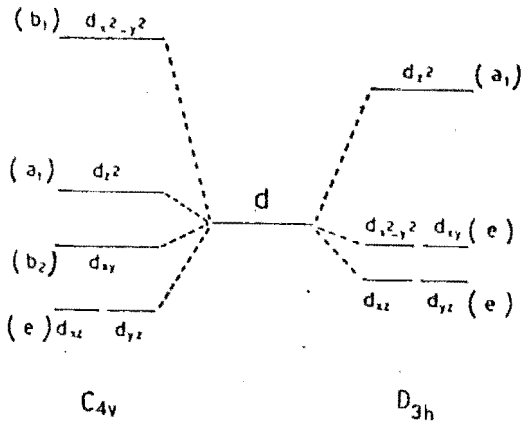

(a)

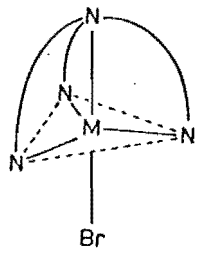

(b)

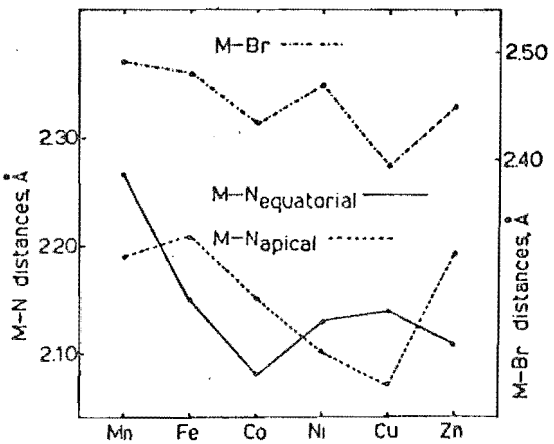

(c)

Figure 6.3 (a) Splitting of 3d orbitals in trigonal-bipyramidal and square-pyramidal crystal fields.

(b) The trigonal-bipyramidal $(M(Me_6tren)Br)^+$ cation.

(c) Plot of M-N and M-Br distances against the atomic number for a series of $(M(Me_6tren)Br)^+$ cations.

In a recent attempt to rationalize the electronic spectra of penta-coordinate complexes using crystal field theory, the effect of π bonding was thoroughly discussed by Furlani [307]. For square-pyramidal complexes more efficient π bonding can occur than for the trigonal-bipyramidal. Of the five d orbitals in fields of C_{4v} symmetry, $d_{x^2-y^2}$ is σ antibonding, d_{z^2} is slightly σ antibonding, while d_{xy}, d_{xz} and d_{yz} are available for π bonding. In fields of D_{3h} symmetry, only d_{xz} and d_{yz} are capable of π overlap, and d_{xy} and $d_{x^2-y^2}$ can be partly σ and partly π bonding. Their overall π interaction is expected to be small. Since π bonding tends to stabilize the square-pyramidal stereochemistry, the results appear to contradict Gillespie's generalization. The VSEPR model [118, 119] favours square-pyramidal arrangements for complexes with 'ionic' character. However, crystal field theory predicts that π bonding, which might be considered to produce bonds that are more covalent, is more important for these complexes [313].

The nature of polarizability and/or nephelauxetic effects of the donor groups has also been considered [121]. In general, the ability of ligands to stabilize five-coordination decreases in the order $CN^- >> I^- > Br^- > Cl^- > NO_2^- > NCS^-$. On the whole, crystal field models have been used with reasonable success as a working rule for explaining many structural features, especially in the field of electronic spectroscopy [314].

(c) Molecular Orbital Treatment - Extended Huckel calculations were performed on phosphorous chlorofluorides ($PCl_{5-n}F_n$, n = 0 - 5) as examples of trigonal-bipyramidal molecules [315]. The results showed that axial bonds are longer than equatorial bonds and that fluorine preferentially occupies the axial sites. The phosphorous 3s orbital character is greater in the equatorial direction giving rise to stronger bonds.

Berry et al [316] determined the electronic and geometric structures of PF_5, AsF_5 and BrF_5 by computing their orbital energies. For both PF_5 and AsF_5, the trigonal-bipyramidal geometry is the more stable, while for BrF_5, the square-pyramidal geometry is preferred. In essence, these molecular orbital calculations seem to agree with predictions by the VSEPR method.

More recently, Rossi and Hoffmann [317] presented a detailed molecular orbital treatment on five-coordinate transition metal complexes. In the absence of π bonding, complexes with D_{3h} symmetry have the interaction scheme illustrated in Figure 6.4a. The e'' orbital is mainly metal d_{xz} and d_{yz}, the e' set is due primarily to mixing of d_{xy} and $d_{x^2-y^2}$ with equatorial ligand σ orbitals. The a_1' set is derived from strong d_{z^2}-axial ligand and weaker d_{z^2}-equatorial ligand interactions. Within the C_{4v} framework, the L_{basal}-M-L_{basal} angle θ has to be considered (Figure 6.4b). As θ decreases, the d_{xy} orbital remains purely metal in character but d_{xz} and d_{yz} begin to mix with basal ligand orbitals and become less stable. Both d_{z^2} and $d_{x^2-y^2}$ orbitals decrease in energy due to their reduced interactions with axial and equatorial ligand orbitals respectively.

From this scheme, the axial bond is predicted to be weaker for d^0-d^4 and d^{10}, and stronger for d^8, low-spin complexes with trigonal-bipyramidal geometry. The apical bond, for a square-pyramidal complex with $\theta<165^\circ$, is stronger for d^0-d^6 and d^{10} and weaker for d^8. The preferred position for a π bonding ligand is equatorial in trigonal-bipyramidal complexes while for square-pyramidal complexes such overlap is greater for basal positions only for these high θ values.

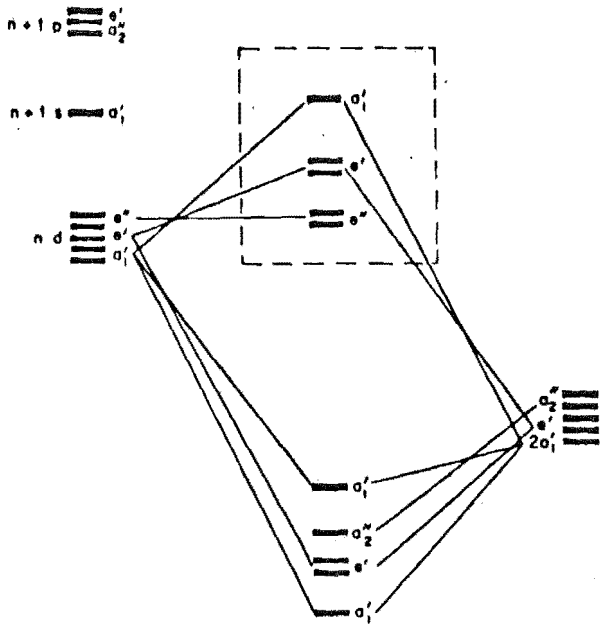

(a)

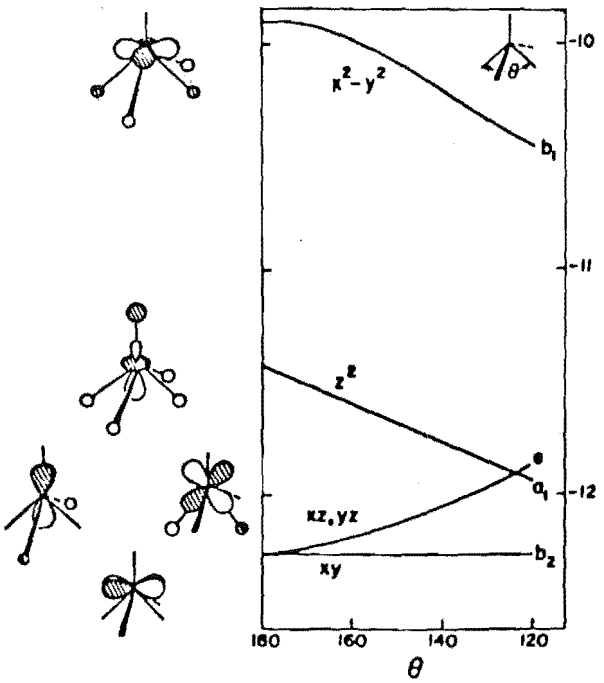

(b)

Figure 6.4 (a) Interaction diagram for a D_{3h} ML_5 complex.

(b) Calculated energy levels of ML_5 as a function of L_{basal}-M-L_{basal} angle θ. The vertical energy scale is in electron volts.

The scheme was successfully used to explain the stereochemistry of the trigonal-bipyramidal $(Ir(CNMe)(diphos)_2)(ClO_4)_2$ complex which has a short equatorial Ir-C bond due to Ir→CNMe π stabilization [318]. However, a structure contradicting this prediction has recently been published. In the compound $(Cr(NH_3)_6)(HgCl_5)$, $Hg(d^{10})$ is trigonal-bipyramidal and the axial Hg-Cl bonds are shorter than equatorial bonds [319].

6.2.3 Crystal Structures Of Some ML_5 Systems

A major influence on the stereochemistry of five-coordination is the steric bulk of ligands. The use of monodentate ligands, particularly when they are all equivalent, would eliminate constraints imposed by chelating ligands and provide a better understanding of the relative stabilities of trigonal-bipyramidal and square-pyramidal structures. Table 6.1 contains a list of structural data for several ML_5 species. Some of these ML_5 species [216, 218, 320-333] are discussed below in examining different factors which might govern their stereochemistries.

(a) Pentachloro-Metal Complexes - Both $(CuCl_5)^{3-}$ [328, 329] and $(CdCl_5)^{3-}$ [330] ions have trigonal-bipyramidal geometry. The axial bond distances of 2.30Å in $(CuCl_5)^{3-}$ are considerably shorter than the corresponding equatorial bond distances of 2.39Å. This difference has been ascribed to the greater repulsion between the ligands and the fully occupied metal $d_{x^2-y^2}$ orbital in the equatorial plane. The d_{z^2} orbital is only half-filled for Cu(II) d^9 and the axial direction thus experiences a smaller repulsion. For the d^{10} system, in $(CdCl_5)^{3-}$, this filled axial orbital should experience enhanced repulsion. This effect is indeed observed but the axial Cd-Cl bond length is still shorter (0.03Å) than the equatorial distance of 2.56Å. This is contrary to the predictions of both VSEPR and molecular orbital models.

Table 6.1

M-L Bond Lengths For Some ML_5 Structures

Compound	Geometry	Configuration	M-L (Å) Axial/ Apical	M-L (Å) Equatorial/ Basal	References
$Nb(NMe_2)_5$	C_{4v}	d^0	1.98	2.04	320
$(MnCl_5)^{2-}$	C_{4v}	d^4(hs)[a]	2.58	2.30	321
$(Fe(N_3)_5)^{2-}$	D_{3h}	d^5(hs)	2.04	2.00	322
$(Co(C_6H_7NO)_5)^{2+}$	D_{3h}	d^7(hs)	2.10	1.98	218
$Ni(CN)_5$	D_{3h}	d^8	1.84	1.99	216
$Ni(CN)_5$	C_{4v}	d^8	2.17	1.86	216
$Ni(P(OCHCH_2)_3)_5^{2+}$	D_{3h}	d^8	2.14	2.19	323
$Fe(CO)_5$	D_{3h}	d^8	1.81	1.83	324
$Co(CNCH_3)_5^{+}$	D_{3h}	d^8	1.84	1.88	325
$(Pt(SnCl_3)_5)^{3-}$	D_{3h}	d^8	2.54	2.54	326
$(Mn(CO)_5)^{-}$	D_{3h}	d^8	1.82	1.80	327
$(CuCl_5)^{3-}$	D_{3h}	d^9	2.30	2.39	328
$(CuBr_5)^{3-}$	D_{3h}	d^9	2.45	2.52	329
$(CdCl_5)^{3-}$	D_{3h}	d^{10}	2.53	2.56	330
$(InCl_5)^{2-}$	C_{4v}	d^{10}	2.42	2.46	331
AsF_5	D_{3h}	d^{10}	1.71	1.66	332
$Sb(C_6H_5)_5$	C_{4v}	d^{10}	2.12	2.22	333

[a](hs) = high-spin

The pentachloroindate (III), $(InCl_5)^{2-}$ ion [331], is square-pyramidal with a shorter In-Cl axial bond. No explanation has been offered for this effect. This is another example that does not agree with the results of the VSEPR calculations. The $(MnCl_5)^{2-}$ ion [321] exhibits quite large angular deviations from idealized C_{4v} symmetry. For a high-spin square-pyramidal d^4 species, using the simple electron repulsion arguments, a longer axial bond length would be predicted and this is indeed observed.

(b) $(Co(CNCH_3)_5)^+$ and $Ni(P(OCHCH_2)_3)_5^{2+}$ Ions - $(Co(CNCH_3)_5)^+$ [325] assumes a trigonal-bipyramidal geometry, slightly distorted due to intermolecular contacts. For this ion, the axial bond distances follow the trend for d^8 configurations in being shorter than the equatorial distances. The shortness of the Co-C bonds, with a bond order of >1.5, was considered to arise from metal to ligand $d\pi \rightarrow p\pi$ back bonding.

Another d^8 species, $Ni(P(OCHCH_2)_3)_5^{2+}$ [323] also is a trigonal-bipyramidal complex where compression of the Ni-P bond distance is observed in the axial direction. The average Ni-P axial bond distance is 2.14Å while the average Ni-P equatorial bond distance is 2.19Å. This contraction has also been explained in terms of electron pair repulsion model. The adoption of D_{3h}, rather than the C_{4v}, symmetry could arise from the steric requirements of the phosphine ligands.

(c) The Pentaphenylantimony Structure - The structure of pentaphenylantimony $Sb(C_6H_5)_5$ [333] has square-pyramidal geometry. The axial Sb-C bond is significantly different (~2.12Å) from the other four basal bonds (2.20 - 2.23Å). A strain-energy minimization calculation has shown that intermolecular forces favour the square-pyramidal configuration by 4.6 kJ/mole but that intramolecular forces favour the trigonal-bipyramid

by 30.5 kJ/mole [334]. The authors suggested that the failure to predict the observed structural geometry may be due to the neglect of coulombic interactions.

(d) Penta(dimethylamido) and Penta(piperide) Niobium(V) Complexes - X-ray analyses show the coordination geometry of $(Nb(NMe_2)_5)$ [320] and $(Nb(NC_5H_{10})_5)$ [320] to be very similar and best described as distorted square-pyramid. Both structures have shorter Nb-N axial bonds. Nb(V) is a d^0 system and on the basis of VSEPR arguments, NbL_5 would be expected to have trigonal-bipyramidal geometry. No conclusive remarks were presented on the preference for square-pyramidal arrangement except that π bonding was advanced as an explanation for the short Nb-N axial interaction.

6.3 INFRARED ANALYSES

6.3.1 The Trimethylphosphine Oxide And Trimethylarsine Oxide Ligands

In order to determine the coordination of trimethylphosphine and trimethylarsine oxides in the complexes under study, it is appropriate to begin by considering the classification of the ligand vibrational modes. Several detailed infrared and Raman analyses on trimethylphosphine and trimethylarsine oxides have been reported in the literature [335-339]. Since electron diffraction results on trimethylamine oxide [340], trimethylphosphine and trimethylarsine [341, 342] (including microwave data for the latter two compounds [343, 344]) are generally consistent with a C_{3v} model, assignments of vibrational frequencies of oxides of trimethylphosphine and trimethylarsine were based on the assumption that the molecules possessed C_{3v} symmetry. Under the C_{3v} point group, a molecule has 36 normal modes of vibration of the type $8A_1 + 4A_2 + 12E$; of which only the A_2 modes are infrared and Raman inactive.

The assignment of vibrational frequencies is facilitated by the relative simplicity of the ligand spectra. Listed in Table 6.2 are the fundamental vibrations for both trimethylphosphine and trimethylarsine oxides derived from infrared and Raman results [335-338]. A closer examination of Table 6.2 reveals slight differences between frequencies obtained from different studies. This may conceivably be due to a variation in the dryness of the samples. Trimethylphosphine and trimethylarsine oxides are hygroscopic and consequently it is difficult to exclude moisture in the sampling process. The infrared spectra of trimethylphosphine and trimethylarsine oxides obtained in the present study are given in Figure 6.5; these data are generally in good agreement with published values.

The fundamental P-O and As-O stretching frequencies have been unequivocally established to lie in the regions of 1170 and 870 cm^{-1} respectively [263, 345-348]. It is now well recognized that shifts of ν(P-O) and, to a lesser extent, ν(As-O) are taken as indications of complex formation since these ligands coordinate via the oxygen atom [263]. The effect of complex formation on the P-O stretching frequency of trimethylphosphine oxide has been reported, and extensively discussed in terms of π interactions in the P-O bond (arising from overlap between filled oxygen $2p_x$ and $2p_y$ orbitals and vacant phosphorous $3d_{xz}$ and $3d_{yz}$ orbitals [339]). Merianian and Zingaro [349] calculated the force constants of As-O bond for both single and double bond characters. By substituting the values into the equation for a harmonic oscillator, they obtained ν(As-O) of 960 and 776 cm^{-1} respectively for a single and double bond. Since the As-O stretching frequency in arsine oxides is normally observed to lie close to 870 cm^{-1}, this would suggest a bond order in As-O

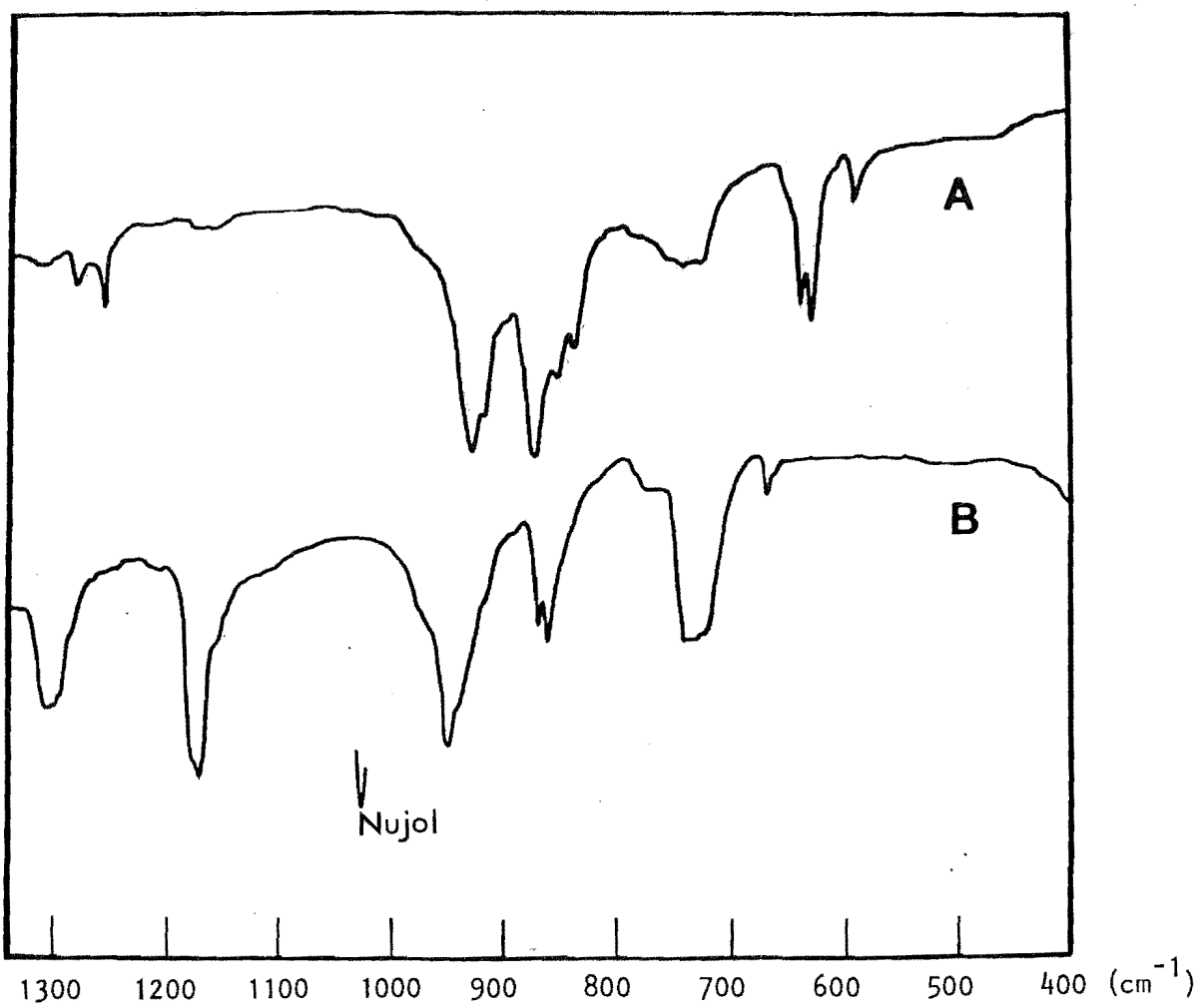

Figure 6.5 - Infrared spectra of the ligands.

(a) Trimethylarsine oxide.

(b) Trimethylphosphine oxide.

Table 6.2

Fundamental Vibrations For Me_3PO And Me_3AsO
(above 400 cm^{-1}.)

Me_3PO			Me_3AsO		
Raman[335]	Assignment	Infrared[336]	Raman[337]	Assignment	Infrared[338]
2948 vs	ν_{as} CH_3	2985 m	3012 m	ν_{as} $CH_3(E)$	3001 w
			3004 m	and	2992 m
			2990 m	ν_{as} $CH_3(A_1)$	2984 s
2913 vs	ν_s CH_3	2916 s	2936 m,sh	ν_s $CH_3(E)$	2919 w
			2926 m	and	2910 m
			2900 w,sh	ν_s $CH_3(A_1)$	
2890 w	overtones			δ_{as} $CH_3(E)$	2840 vw
2879 w	and			δ_{as} $CH_3(E)$	2800 vw
2802 vw	combinations			ρ $CH_3(A_1+E)$	1846 vw
				ν As-O(A_1+A_1)	1720 vw
1460 w	δ_{as} CH_3	1456 m	1457 vw	δ_{as} $CH_3(E)$	1431 m
1440 w		1434 m	1444 w	and	1415 m
1411 w		1417 m	1437 vw,sh	δ_{as} $CH_3(E)$	1402 w
1405 w			1410 w		
			1404 vw		
1319 vw	δ_s CH_3	1302 m	1295 vw	δ_s $CH_3(E)$	1275 m
1292 vw		1290 m	1262 vw	δ_s $CH_3(A_1)$	1257 m
1146 m	ν PO	1160 s	866 s	ν AsO	870 s
958 vw	ρ CH_3	955 m	940 vw	ρ $CH_3(E)$	938 sh
952 vw		937 s	928 vw	ρ $CH_3(A_1)$	932 s
941 vw		867 m	918 vw		917 s
883 vw			835 m		851 s
855 vw					837 s
745 m	ν_{as} PC(E)	743 m	641 m	ν_{as} AsC(E)	642 s
672 s	ν_s PC(A_1)	669 s	630 s	ν_s AsC(A_1)	594 s

vs = very strong, s = strong, m = medium, w = weak, vw = very weak, sh = shoulder, as = antisymmetric,. s = symmetric, A = non-degenerate E = doubly-degenerate

somewhat higher than one. Choplin et al [339] have performed calculations on the bond orders of As-O and P-O and found they lie in the range of 1.43 - 1.60 and 1.80 - 1.96 respectively.

6.3.2 The Metal Complexes

Shifts in P-O and As-O stretching frequencies are observed for all the compounds in the present study. In addition, infrared spectroscopy can be used to detect anion coordination from splitting of infrared bands, although the absence of such splitting does not necessarily preclude anion coordination [50]. By comparing spectra of the metal complexes with spectra of the free ligand, bands associated with M-O deformation may be identified.

All complexes in this study contain perchlorate counter-anions. For a regular tetrahedral perchlorate anion in T_d symmetry, there are nine vibrational degrees of freedom, some of which are degenerate. As a result, they are distributed between four modes of vibrations (Table 6.3) [350]. This degeneracy may be removed when the symmetry is lowered either through hydrogen-bonding to the anion or coordination of the anion to the metal ion. Isolated tetrahedral perchlorate ions show only two absorptions in the infrared due to ν_3 (at $\simeq$1100 cm^{-1}) and ν_4 (at $\simeq$620 cm^{-1}). When the T_d symmetry is lowered to C_{3v}, for example when perchlorate binds as a ligand through one oxygen atom, the triple degeneracy for ν_3 and ν_4 is removed producing bands at 1150 - 1170 and 630 cm^{-1} and the ν_1 (at $\simeq$930 cm^{-1}) and ν_2 (at $\simeq$460 cm^{-1}) modes become infrared active. Lowering the anionic symmetry as in the case for bidentate coordination produces more splitting of the absorption bands.

Table 6.3

Vibrations Of The Perchlorate Group As A Function Of Symmetry [350]

State of ClO_4	Symmetry								
$-O^*-ClO_3$	C_{3v}	ν_2 $A_1(I,R)$ ClO_4str	ν_6 $E(I,R)$ rocking	ν_1 $A(I,R)$ s.str ClO_3		ν_4 $E(I,R)$ a.str ClO*	ν_3 $A(I,R)$ s.bend ClO_3		ν_5 $E(I,R)$ a.bend ClO_3
ClO_4	T_d	ν_1 $A(R)$ s.str 932	ν_2 $E(R)$ s.bend 460	ν_3 $F_2(I,R)$ a.str 1110			ν_4 $F_2(I,R)$ a.bend 626		
$-O^*$ $-O^*$ ClO_2	C_{2v}	ν_2 $A_1(I,R)$ $Cl-O_2{}^*$ s.str	ν_4 $A_1(I,R)$ $ClO_2{}^*$ s.bend	ν_5 $A_2(R)$ torsion	ν_1 $A_1(I,R)$ ClO_2 s.str	ν_6 $B_1(I,R)$ $Cl-O_2{}^*$ a.str	ν_8 $B_2(I,R)$ $Cl-O_2{}^*$ a.str	ν_3 $A_1(I,R)$ ClO_2 s.bend	ν_7 $B_1(I,R)$ rocking	ν_9 $B_2(I,R)$ rocking

A and B = non-degenerate, E = doubly-degenerate, F = triply-degenerate, I = infrared active, R = Raman active,

s = symmetric, a = antisymmetric, O^* = oxygen coordinated to metal

(a) Trimethylphosphine Oxide Metal Complexes - An obvious difference between the two spectra of $(Mg(Me_3PO)_5)(ClO_4)_2$ and $(Mg(Me_3PO)_5H_2O)(ClO_4)_2$ is the presence of several vibrations characteristic of water in the latter compound (Figure 6.6). The bands at 3600 cm^{-1} and 3545 cm^{-1} can be assigned as the antisymmetric and symmetric O-H stretching modes while the band at 1624 cm^{-1} is due to the H-O-H bending mode [351]. The $(ClO_4)^-$ vibrations in both complexes show little shift from those observed for tetrahedral symmetry which is consistent with the presence of non-coordinated $(ClO_4)^-$ ions. The easily distinguished ν(P-O) absorption bands move to lower frequencies on coordination. This has been discussed in other systems. For example Cotton et al [263] had analysed this shifting in terms of kinematic coupling and bonding effects (σ and π donation and π back donation) and concluded from the observed shift to lower energy that the decrease of oxygen $p\pi \rightarrow$ phosphorus $d\pi$ back bonding should be dominant. The ν(P-O) bands are at 1151 and 1160 cm^{-1} for $(Mg(Me_3PO)_5)(ClO_4)_2$ and $(Mg(Me_3PO)_5H_2O)(ClO_4)_2$, respectively. The larger shift in the ν(P-O) band for the anhydrous species ($\simeq$20 cm^{-1}) may be considered to result from weaker P-O bonds and thereby indicates stronger Mg-O interactions in the five-coordinate square-pyramidal $(Mg(Me_3PO)_5)^{2+}$ cation. Results from X-ray analyses (Chapter 4) show that the average P-O bond length for the $(Mg(Me_3PO)_5)^{2+}$ cation of 1.49Å is slightly longer than that of 1.45Å for the $(Mg(Me_3PO)_5H_2O)^{2+}$ cation. The metal-ligand stretching vibrations can be assigned to the new bands which occur between 450 - 400 cm^{-1}, which are in good agreement with previous values [352]. The slightly lower frequency of the Mg-O band for the hydrated compound (Table 6.4) may again reflect weaker M-O bonds. This is consistent with the M-O bond length of 2.03Å and 2.08Å for the anhydrous and hydrated complexes respectively.

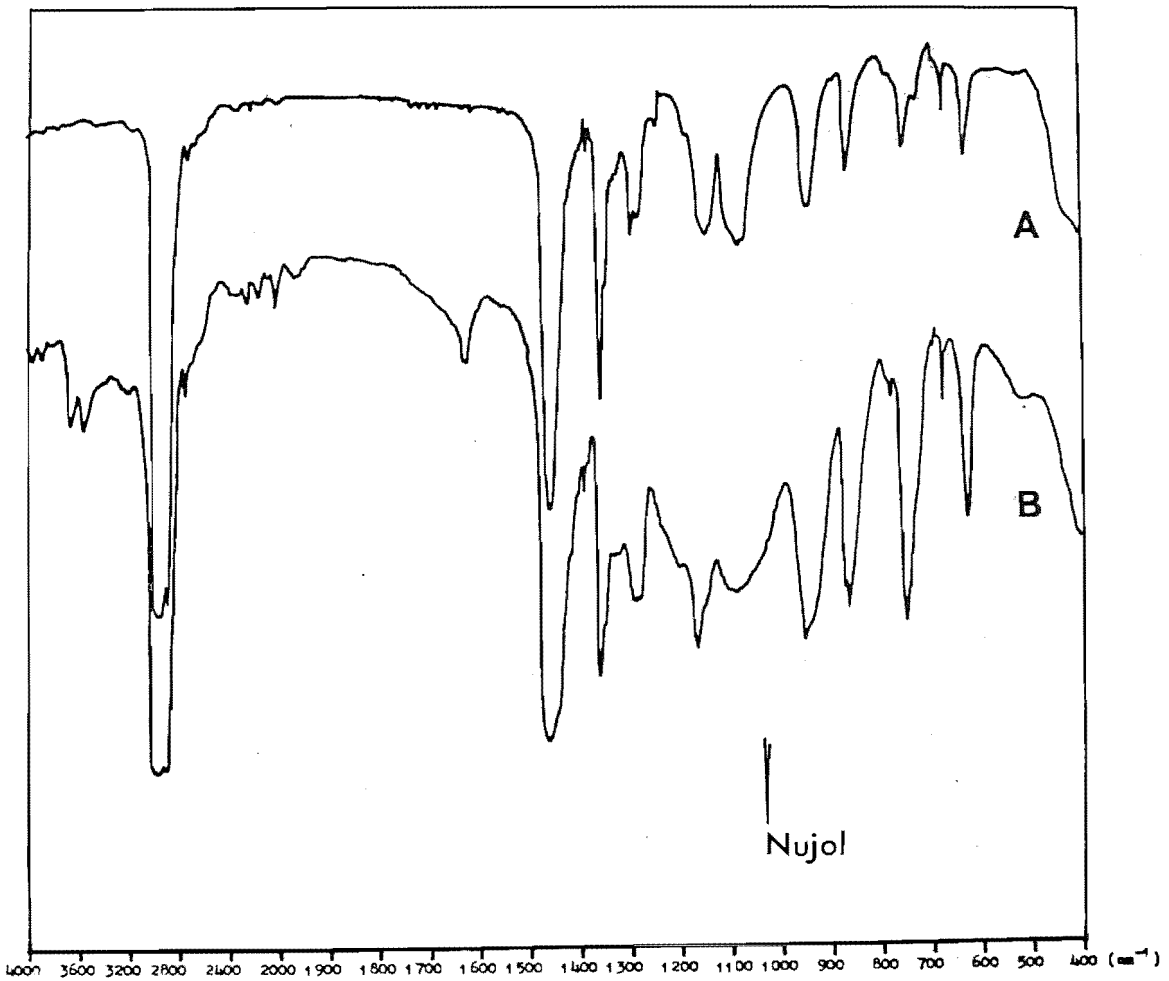

Figure 6.6 - Infrared spectra of phosphine oxide complexes.

(a) $(Mg(Me_3PO)_5)(ClO_4)_2$ (b) $(Mg(Me_3PO)_5H_2O)(ClO_4)_2$.

Table 6.4

Infrared Data (cm^{-1})

Compound	ν(X-O) X = P, As	$\Delta\nu$(X-O)	ν(M-O)
Me_3PO	1170s		
$(Mg(Me_3PO)_5)(ClO_4)_2$	1151vs	-10	409m
$(Mg(Me_3PO)_5H_2O)(ClO_4)_2$	1160vs	-19	430-420m, br.
Me_3AsO	870s		
$(Mg(Me_3AsO)_5)(ClO_4)_2$	956m, 887vs	+17	420s, br.
$(Ni(Me_3AsO)_5)(ClO_4)_2$	866vs	- 4	407m, br.
$(Ca_2(Me_3AsO)_9)(ClO_4)_4$	883vs, 862s	+13, -8	354br

vs = very strong

s = strong

m = medium

br = broad

(b) Trimethylarsine Oxide Metal Complexes - The infrared spectra of $(Mg(Me_3AsO)_5)(ClO_4)_2$, $(Ni(Me_3AsO)_5)(ClO_4)_2$ and $(Ca_2(Me_3AsO)_9)(ClO_4)_4$ show the absence of coordinated $(ClO_4)^-$ anion (Figure 6.7). The compounds have strong bonds at ≈1095 cm^{-1} and 625 cm^{-1}, consistent with the T_d site symmetry. Absorption near 870 cm^{-1} has been well established as arising from the As-O stretching mode. While for the trimethylphosphine oxide complexes, coordination invariably lowers the ν(P-O) stretching band, the trends in trimethylarsine oxide complexes are less systematic. This has been attributed to greater coupling between As-O and M-O oscillators which would tend to raise ν(As-O) by ≈50 cm^{-1} more than the corresponding increase in ν(P-O) [35, 263]. On average, then, ν(As-O) in these complexes would be expected to differ only to a small degree observed from ν(As-O) in the free ligand. An examination of the ν(M-O) values shows that the dinuclear calcium complex has a ν(M-O) band at ≈354 cm^{-1}, compared with bands at 420 cm^{-1} and 407 cm^{-1} for the Mg(II) and Ni(II) complexes. From X-ray data, both the M-O bond distances in the dinuclear octahedrally-coordinated calcium complex are longer than in the square-pyramidal Mg(II) and Ni(II) complexes. This is consistent with stronger bonding in the latter two complexes.

In the Mg(II) complex, the ν(As-O) band at 887 cm^{-1} is shifted to a higher frequency than that of the free ligand. There is also an extra new band at 956 cm^{-1} whose origin has not been explained. Correspondingly, the ν(As-O) band for the Ni(II) complex is found at a slightly lower frequency of 866 cm^{-1} than that of the Mg(II) complex. This effect may have been a function of the higher mass of the nickel atom. In five-coordinate complexes, lower ν(As-O) band energies have been observed (855 - 866 cm^{-1}) [352]. An interesting feature is the multiplet splitting of the ν(As-O) band at 800 - 900 cm^{-1} for the $(Ca_2(Me_3AsO)_9)(ClO_4)_4$ complex. There appear to be two absorption components at 862 and

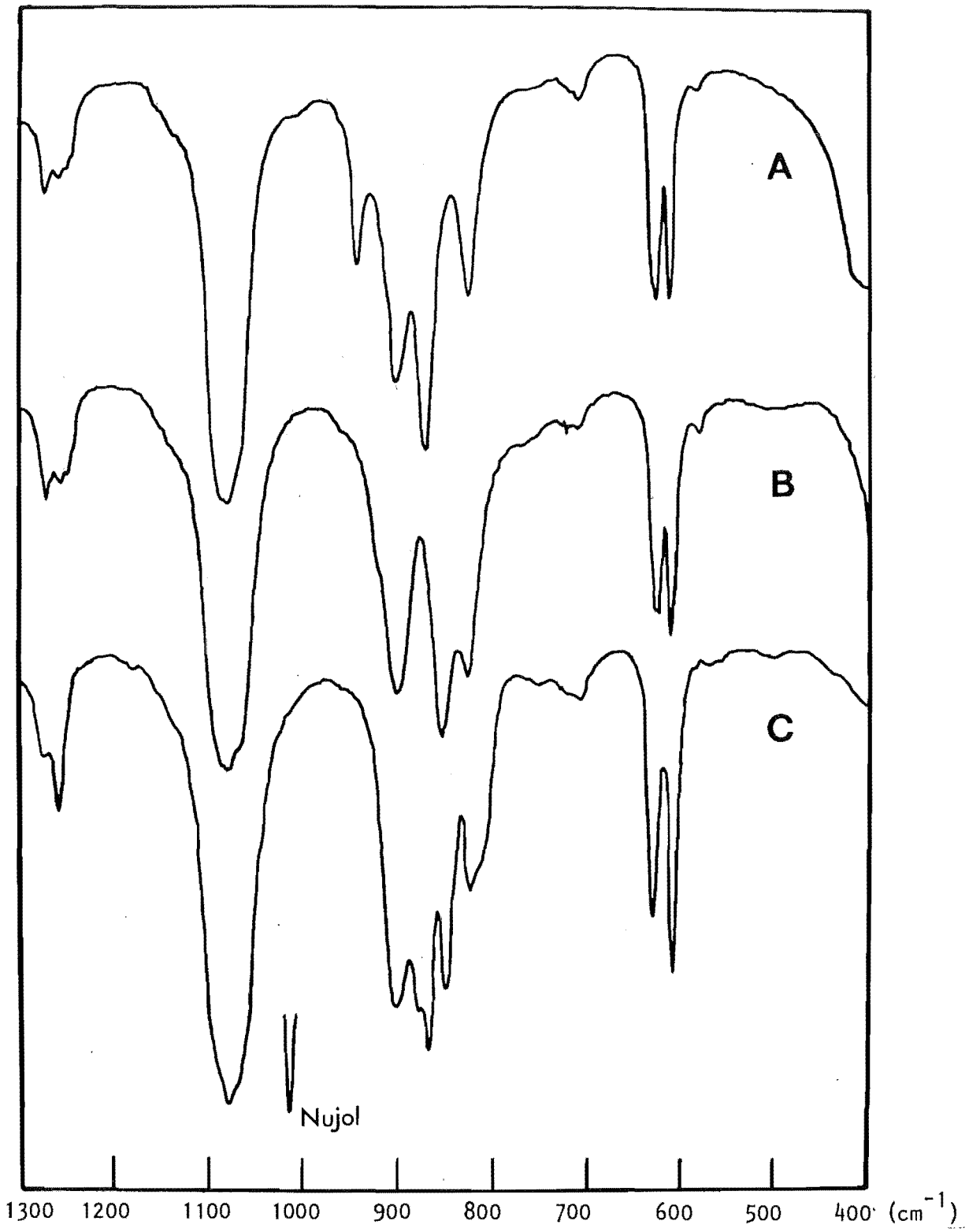

Figure 6.7 - Infrared spectra of arsine oxide complexes.

(a) $(Mg(Me_3AsO)_5)(ClO_4)_2$

(b) $(Ni(Me_3AsO)_5)(ClO_4)_2$

(c) $(Ca_2(Me_3AsO)_9)(ClO_4)_4$

883 cm^{-1} corresponding to ν(As-O) stretching modes. Since X-ray structure determination of $(Ca_2(Me_3AsO)_9)(ClO_4)_4$ (Chapter 5) [2] shows that the arsine oxide ligands are in two different environments and the As-O bond for the terminal group is marginally longer, it is then possible to assign the band at 862 cm^{-1} to the terminal ligands and the absorption at 883 cm^{-1} to the bridging ligands. The band at 891 cm^{-1} is difficult to interpret. Since X-ray results show that both the terminal and bridging ligands have different As-C bond lengths, the bands at 891 cm^{-1} and 915 cm^{-1} could be assigned to the rocking modes of the slightly different methyl groups on the bridging and terminal groups (see also Section 6.4.2 on nmr results).

6.4 NUCLEAR MAGNETIC RESONANCE DATA

Another useful tool for investigating the influences of coordination on the elctronic structure of inorganic compounds is the nmr technique [353]. In atoms and molecules, the electrons shield the nuclei from the external magnetic field. The magnitude of this shielding effect is sensitive to the nature of the environment of the nucleus in question. Upon complex formation, the circulation of electrons in the ligands would be expected to be perturbed by the metal ions. Depending on the nature of interaction, the ligand resonances can occur at higher or lower fields than for the free ligands. The shielding, δ, of a nucleus in a molecule is usually written in the form

$$\delta = \delta_d + \delta_p .$$

The diamagnetic contribution, δ_d, corresponds to uniform circulation of electrons as if they were free. The paramagnetic deshielding term, δ_p, is a correction term to rectify the excess circulation implicit in δ_d.

In the majority of cases, variation of δ_p rather than δ_d from system to system is the major component contributing to the observed trends in chemical shifts. Another parameter in nmr is the intramolecular spin-spin coupling which is due to some tendency for a bonding electron to pair its spin with that of the next atom.

Not many phosphoryl complexes have been studied by the nmr technique [354-356]. Table 6.5 is a list of coordination shift, Δ, of the ^{31}P chemical shift (that is, the change in chemical shift upon coordination) for a number of phosphoryl complexes reported in the literature. In all cases, the shifts are towards low fields, which suggests the phosphorous atoms become less shielded on coordination. A dependence on the metal ions is established. However, the observed order of shift does not appear to fall into any systematic pattern.

A cautionary note must be inserted here. The X-ray analyses (Chapters 3 - 5), establish the hybridization of oxygen orbitals changes on coordination. In addition, bond angles around ligand molecules may show considerable variations. Because nmr measurements are normally performed in solution, exact geometries are unknown. Besides, disproportion of phosphoryl complexes in solution is always a possibility. Interpretation of nmr results should therefore be treated with care.

6.4.1 NMR Results Of Phosphine And Arsine Oxide Metal Complexes

Recently, an investigation of phosphoryl and arsenyl complexes using nmr technique was undertaken by Quah [357]. Some of his results are summarized below:

(a) ^1H nmr - Proton nmr study was carried out on some trimethyl-

Table 6.5

^{31}P nmr Of Some Phosphoryl Complexes

Ligand	Complex	-Δ(ppm)	References
$OP(OCH_3)_2H$	$B(L)F_3$	5.0	354
$OP(OC_2H_5)_2H$	$B(L)F_3$	4.0	354
$OPCl_3$	$Ti(L)_2Cl_4$	14.4	355
$OP(C_6H_5)Cl_2$	$Ti(L)_2Cl_4$	15.2	355
$OP(C_6H_5)_2Cl$	$Ti(L)_2Cl_4$	13.2	355
$(C_6H_5)_2P(O)N(CH_3)P(O)(C_6H_5)_2$	$Ti(L)Cl_4$	16.0	355
HMPA	$Mo(L)(CO)_5$	4.8	356
HMPA	$W(L)(CO)_5$	3.6	356

phosphine oxide complexes. The results are shown in Table 6.6. All the proton nuclei are deshielded on coordination. The deshielding effect is expected since coordination will result in the donation of electrons from the ligand to the metal ion. A drift of electron density in the direction H→C→P→O, would lead to the observed deshielding. The order of chemical shift, $Th^{4+}>La^{3+}>Mg^{2+}>Ca^{2+}$, appears to parallel charges on the metal ion. Only slight differences are observed in the coupling constants. A possible explanation is that the metal-ligand interaction is too far removed from the coupling nuclei for the effect to be very significant.

(b) ^{13}C nmr - Results from ^{13}C nmr studies are summarized in Tables 6.7, 6.8 and 6.9. Contrary to the situation for protons, the carbon atoms do become shielded on coordination. Two factors might be considered to alter the magnitude of shielding:

(i) to compensate for a build up of positive charge on the arsenic or phosphorus atom on coordination, there will be a shift of electron density from the carbon atom to the phosphorus atom; hence deshielding occurs, and

(ii) similarly, there will be an inflow of electron from the proton to the carbon atom; hence shielding occurs.

From the nmr results, the second factor seems to be more important and a net shifting to higher field of $\delta(C_1)$ on coordination is observed.

For the trimethylphosphine oxide complexes, the chemical shifts follow the order $Th^{4+}>La^{3+}>Mg^{2+}>Ca^{2+}$. In the case of the triphenylphosphine oxide complexes, the order is $Th^{4+}>La^{3+}>Ca^{2+}>Mg^{2+}>Li^{+}>Na^{+}$. However, a quite different result was obtained for the triphenylarsine

Table 6.6

^1H nmr Of Some Me_3PO Complexes [a] (ppm From TMS)

Compound	$\delta(^1H)$	av $\delta(^1H)$	J(P-H)(cps)	$\Delta\delta(^1H)$
Me_3PO	1.50 1.27	1.39	13.5	
$(Mg(Me_3PO)_5)(ClO_4)_2$	1.62 1.39	1.50	13.75	0.11
$(Ca(Me_3PO)_5)(ClO_4)_2$	1.61 1.38	1.49	13.75	0.10
$(La(Me_3PO)_6)(ClO_4)_3$	1.69 1.46	1.58	13.75	0.19
$(Th(Me_3PO)_6ClO_4)(ClO_4)_3$	1.89 1.66	1.77	14.00	0.38

[a] In deuterated acetonitrile solution

av = average

Table 6.7

^{13}C nmr Of Some Me_3PO Complexes [a] (ppm From TMS)

Compound	$\delta(C_1)$	$\Delta\delta(C_1)$	av $\Delta\delta(C_1)$	$J(C_1)$ (cps)
Me_3PO	19.92 16.44			69.6
$(Mg(Me_3PO)_5)(ClO_4)_2$	19.11 15.50	-0.81 -0.94	-0.88	72.2
$(Ca(Me_3PO)_5)(ClO_4)_2$	19.35 15.78	-0.57 -0.66	-0.62	71.4
$(La(Me_3PO)_6)(ClO_4)_3$	19.04 15.51	-0.88 -0.93	-0.91	70.6
$(Th(Me_3PO)_6ClO_4)(ClO_4)_3$	18.41 14.86	-1.51 -1.58	-1.55	71.0
$(Zn(Me_3PO)_4)(ClO_4)_2$	18.70 15.16	-1.22 -1.28	-1.25	70.80

[a] In deuterated acetonitrile solution

av = average

Table 6.8

^{13}C nmr Of Some Ph_3PO Complexes [a] (ppm From TMS)

Compound	$\delta(C_1)$	$\delta(C_p)$	$\delta(C_{ortho/meta})$		$\Delta\delta(C_1)$	av $\Delta\delta(C_1)$	$J(C_1)$
Ph_3PO	137.06 131.93	132.66 132.53	132.85 132.38	129.64 129.05			102.6
$(Li(Ph_3PO)_4)(ClO_4)$	136.23 131.04	133.00	133.00 132.52	129.87 129.21	-0.83 -0.89	-0.86	103.8
$(Na(Ph_3PO)_5)(ClO_4)$	136.41	132.89	132.42	129.78 129.19	-0.65	-0.65	
$(Mg(Ph_3PO)_4)(ClO_4)_2$	134.78 129.11	133.58 133.44	133.31 132.78	129.96 129.36	-2.28 -2.82	-2.55	113.4
$(Ca(Ph_3PO)_4ClO_4)(ClO_4)$	133.96 128.61	133.71	133.18 132.63	130.08 129.47	-3.10 -3.32	-3.21	107.0
$(La(Ph_3PO)_4ClO_4)(ClO_4)_2$	132.68	134.06 133.96	133.49 132.95	130.08 129.44	-4.38	-4.38	
$(Th(Ph_3PO)_5ClO_4)(ClO_4)_3$	131.42 125.96	134.73	133.84 133.28	130.45 129.85	-5.64 -5.97	-5.31	109.2

[a] In deuterated acetone

C_1 = carbon atom bonded to phosphorous atom

Table 6.9

^{13}C nmr Of Some Ph_3AsO Complexes [a] (ppm From TMS)

Compound	$\delta(C_1)$	$\delta(C_p)$	$\delta(C_{ortho/meta})$		$\Delta\delta(C_1)$
Ph_3AsO	134.86	132.91	132.12	130.36	
$(Li(Ph_3AsO)_2)(ClO_4)$	129.12	134.73	132.49	131.14	-5.74
$(Mg(Ph_3AsO)_4)(ClO_4)_2$	130.56	134.47	132.17	131.00	-4.30
$(Ca(Ph_3AsO)_5ClO_4)(ClO_4)$	131.14	133.38	132.25	130.34	-3.72
$(La(Ph_3AsO)_5ClO_4)(ClO_4)_2$	129.18	134.48	132.51	131.23	-5.68
$(Th(Ph_3AsO)_6ClO_4)(ClO_4)_3$	124.93	136.17	133.00	131.75	-9.93
$(zn(Ph_3AsO)_4)(ClO_4)_2$	129.83	134.75	132.47	131.11	-5.03

[a] In deuterated acetone

Table 6.10

^{31}P nmr Of Some Ph_3PO Complexes (ppm From Ph_3PO)

Compound	(^{31}P) Downfield
$(Li(Ph_3PO)_4)(ClO_4)$	4.5
$(Mg(Ph_3PO)_4)(ClO_4)_2$	6.7
$(Ca(Ph_3PO)_4ClO_4)(ClO_4)$	7.0
$(La(Ph_3PO)_4ClO_4)(ClO_4)_2$	12.0
$(Th(Ph_3PO)_5ClO_5)(ClO_4)_3$	20.7

oxide series where the order is $Th^{4+}>Li^{+}>La^{3+}>Zn^{2+}>Mg^{2+}>Ca^{2+}$. Deshielding of the ortho, para and meta carbon nuclei in the triphenyl substituted ligands probably takes place through the π system of the phenyl rings. No systematic trends are observed for the coupling constants.

(c) ^{31}P nmr - The experimental ^{31}P chemical shift data on triphenylphosphine oxide complexes are summarized in Table 6.10. The order of downfield (^{31}P) shifts follows the pattern $Th^{4+}>La^{3+}>Ca^{2+}>Mg^{2+}>Li^{+}$.

6.4.2 ^{1}H And ^{13}C nmr Spectra Of $(Ca_2(Me_3AsO)_9)(ClO_4)_4$

The ^{1}H nmr spectrum of the trimethylarsine oxide ligand is shown in Figure 6.8a. There is one peak due to the methyl proton and it is situated at 1.52 ppm downfield from tetramethylsilane (TMS). For the $(Ca_2(Me_3AsO)_9)(ClO_4)_4$ complex, the spectrum shows the presence of two peaks located at 1.85 and 2.26 ppm (Figure 6.8b). This downfield shift of the proton absorption peak of the ligand on coordination is consistent with the trend established for various oxo complexes discussed in the previous section.

The integration showed the two peaks for $(Ca_2(Me_3AsO)_9)(ClO_4)_4$ to be in a ratio of 3 : 1. From the formulation of the dinuclear complex, a ratio of 2 : 1 is expected since there are twice the number of protons in the terminal groups compared with those in the bridging groups. However, deuterated acetonitrile which was used as the solvent has an absorption peak at 1.95 ppm. Exactly how much contribution there is from the acetonitrile to the peak at 1.85 ppm is unknown, but it has undoubtedly affected the ratio. Confirmation of the ^{1}H nmr evidence for two different environments of the methyl groups came from ^{13}C nmr, which

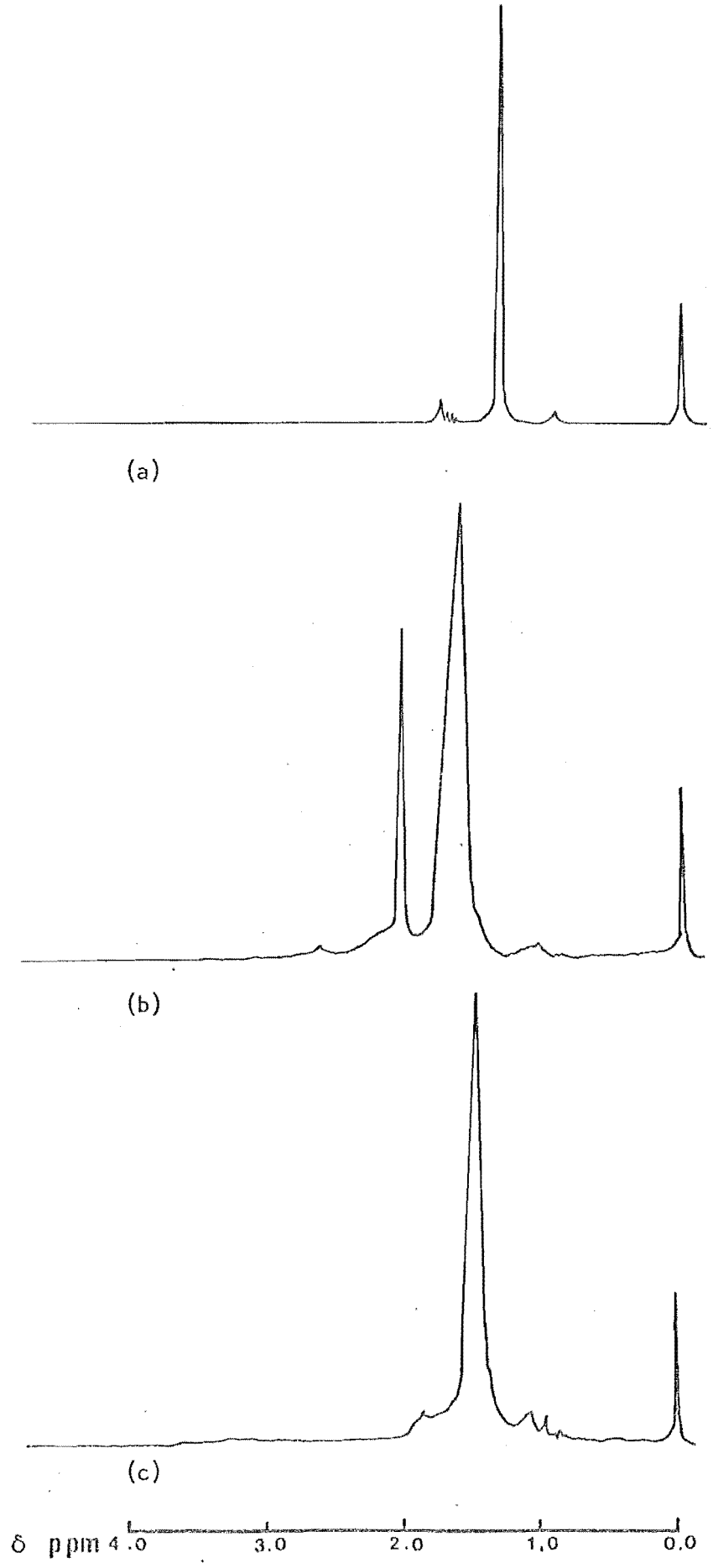

Figure 6.8 - ^{1}H nmr spectra.

(a) Me_3AsO

(b) $(Ca_2(Me_3AsO)_9)(ClO_4)_4$

(c) $(Ca_2(Me_3AsO)_9)(ClO_4)_4$ and excess Me_3AsO.

shows two peaks at 30.70 and 49.38 ppm (the solvent used was 0.5 ml CD_3CN and 0.1 ml D_2O) [359]. In addition, the ^1H nmr spectrum of $(Ca_2(Me_3AsO)_9)(ClO_4)_4$ in the presence of excess Me_3AsO ligand was recorded. Only one peak at 1.66 ppm is present in the spectrum. This result shows that the dinuclear complex can dissociate into monomeric species. Therefore the relative intensities of the peaks in the spectrum shown in Figure 6.8b may also be affected by partial dissociation of the dinuclear complex.

The most significant result from this nmr work is that the bridging ligand protons are more deshielded than the terminal ligand protons. This correlates well with the evidence for differences in the As-C bond strength for the terminal and bridging ligands alluded to in Section 5.6. The X-ray results showed that the bridging As-C bonds are significantly longer (about 2.4σ) than the terminal As-C bonds. This is consistent with indications from the nmr spectra that there is a greater drain of electron density from the bridging ligands than for the terminal ones.

6.5 Strain-Energy Minimization And Coulombic Interaction Calculations

Strain-energy calculations were carried out on three different conformations of the $(Mg(Me_3AsO)_5)^{2+}$ cation in an attempt to analyse their relative stabilities. The three conformations are:

(i) the square-pyramidal geometry determined from X-ray analysis (XSP).

(ii) a hypothetical trigonal-bipyramidal geometry (HTB), and

(iii) a hypothetical distorted square-pyramidal geometry (HSP).

The coordinates for the latter two arrangements were generated by performing symmetry operations on appropriate atoms of the square-pyramidal structure as shown below:

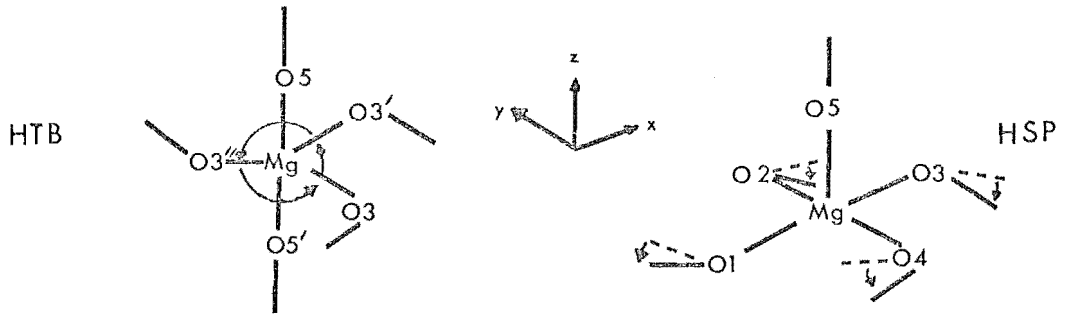

O3 basal group of XSP rotated 120° and 240° to generate O3' and O3'' groups for HTB (about z-axis); O5' group of HTB obtained from inverting the z-coordinates of O5 group.

All basal Me_3As groups of XSP rotated by 20° about the M-O bonds away from the axial group to give the HSP geometry.

Hydrogen atoms for the three conformations were placed at calculated positions by assuming the C-H bond length as 1.0Å and that the C-H bond and As-O bond are staggered.

The strain-energy, E_s, of a compound is a summation of a number of energy terms. These are the energies associated with bond stretching (E_r), bond angle deformation (E_θ), bond torsion (E_ϕ) and non-bonded interaction (E_{nb}). The stability of a conformation would depend on a fine balance of these energy terms. The interaction energies between atoms in the structures were kindly provided by Dr. R.G.A.R. Maclagan.

After several iterative cycles of the strain-energy calculations [358], it was observed that there were no significant differences in energy between the (XSP) geometry and that of the (HTB) geometry. A higher energy was obtained for the (HSP) geometry, due mainly to greater non-bonded interactions between adjacent hydrogen and oxygen atoms of the

basal ligands. The order of stability is (XSP) ≃(HTB) > (HSP). The maximum difference in energy is less than 5.0 kJ/mole.

The next step was to investigate the influence of coulombic interactions in the various conformations. The distribution of electron densities in the square-pyramid was obtained from a molecular orbital calculation with the assistance of Dr. R.G.A.R. Maclagan. Partial negative characters were found for the oxygen and carbon atoms of the ligands, while the arsenic and hydrogen atoms were found to possess partial positive characters*. These values were used in coulombic interaction calculations.

The calculations showed decisively that the (XSP) geometry is the most stable. THe order of stability is (XSP) > (HSP) > (HTB). The difference in energy is ≃34 kJ/mole between the (XSP) and the (HTB) geometries and ≃25 kJ/mole between the (XSP) and the (HSP) geometries.

A major stabilizing influence for the square-pyramidal geometry came from the electrostatic interaction between adjacent oxygen and arsenic atoms of the basal ligands. This provides confirmation of the bonding scheme proposed earlier for the square-pyramidal complex [1].

* These observations are in good agreement with nmr results which showed the carbon atoms became shielded and the hydrogen atoms deshielded on metal complex formation.

6.6 BONDING IN PHOSPHORYL AND ARSENYL METAL COMPLEXES

Some details of the geometries of the four related compounds: $(Mg(Me_3AsO)_5)(ClO_4)_2$, $(Ni(Me_3AsO)_5)(ClO_4)_2$, $(Mg(Me_3PO)_5H_2O)(ClO_4)_2$ and $(Mg(Me_3PO)_5)(ClO_4)_2$ are presented in Figure 6.9. One of the most conspicuous common features of these structures is the shorter axial M-O bond lengths, compared with the basal/equatorial M-O bond lengths. Another common and unexpected feature is the near coplanarity of the phosphorus /arsenic atoms of the ligands with their coordinated basal plane atoms. These aspects of the structures have been considered in Chapters 3 and 4.

In a complex the positively charged metal ion bonded to an electronegative ligand must interact with electrons in the ligand orbitals. Different types of bonding have been described between metal ions and the ligands in phosphoryl and arsenyl complexes. Cotton et al [263] described the bonding in terms of σ- and π- donation from the oxygen atom to the metal ion and π-back donation from metal ions to ligand π orbitals. Joesten and co-workers [360], however, considered that the metal ions simply play the role of orientating the ligands. Their reasoning was based on the iso-structural complexes $M(OMPA)_3(ClO_4)_2$ (M = Mg, Co and Cu); since the magnesium atom does not possess available 3d electrons for π-back donation, they concluded that the metal ions affect the ligands predominantly through electrostatic interactions.

If the complexes contain basically electrostatic M-L bonding as suggested, the M-O distance and M-O-X (X = P, As) angle are expected to be sensitive to intra- and inter-molecular packing forces. Applying the electrovalent model to the present structures, it is difficult to rationalize how a shorter axial M-O bond could arise for an axial ligand that experiences a greater repulsion from four basal neighbours. From

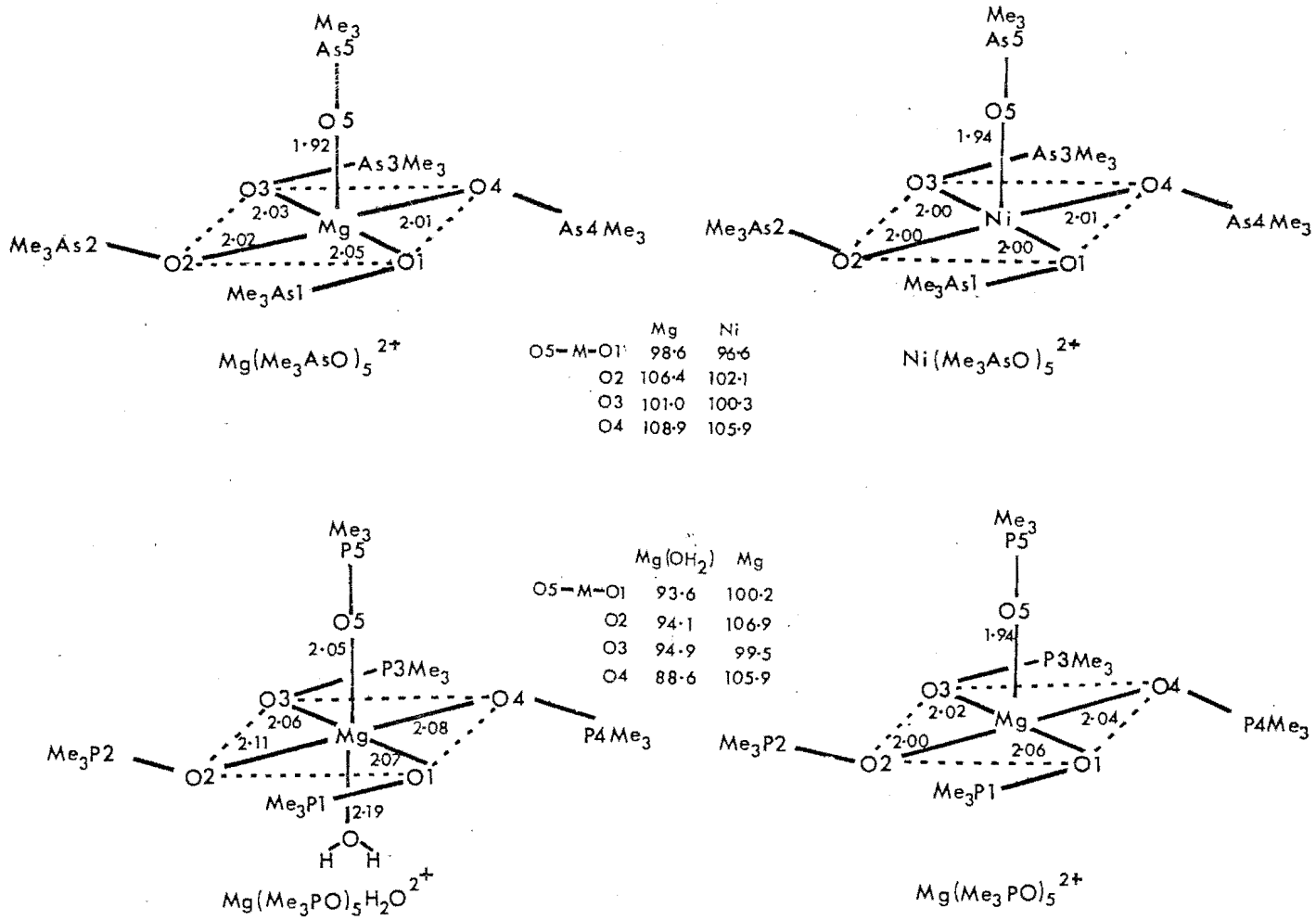

Figure 6.9 - A summary of pertinent geometrical parameters for $(Mg(Me_3AsO)_5)^{2+}$, $(Ni(Me_3AsO)_5)^{2+}$, $(Mg(Me_3PO)_5H_2O)^{2+}$ and $(Mg(Me_3PO)_5)^{2+}$.

electronic spectra of the compounds CoL_2X_2 and $CoL_4(ClO_4)_2$ ($L = Me_3PO$, Me_3AsO; $X = Cl$, Br, I) the Racah parameters, B', are of the order of 75 to 83% of the free ion values [38]. This suggests that there is, in fact, appreciable orbital overlap involving σ as well as π bonding. As discussed in Chapters 3 and 4, the present structures are best described by considering the bonding between the ligands and the metal ion as covalent.

Inspection of Tables 3.14 and 4.12 shows that there is a great variation in the M-O-X angles in this type of complexes. In view of the proposed type of π interaction, it would be expected that maximum overlap between metal and ligand orbitals would occur when the M-O-X angle is 180°. This is indeed the case in $Cu_4(Ph_3PO)_4OCl_6$ where the Cu-O-P angle is linear and the Cu-O bond distance is short, 1.89(2)Å [254].

Simple CNDO/2 Molecular Orbital calculations [361] were carried out for both the axial and basal arsine oxide ligands as oriented in $(Mg(Me_3AsO)_5)^{2+}$. The results of these calculations show that the energies of the metal ion and the ligand orbitals are of comparable magnitude, favouring σ and π bonding [362]. In constructing the MO diagrams, the oxygen atoms of the basal ligands were considered to be involved in $p_z(\pi)$ electron donation (Figure 6.10). The axial ligand was treated as a donor with two p orbitals involved in π overlap (Figure 6.11). Bonding in magnesium compounds is usually considered to be mainly electrostatic in nature. It is of interest that metal-metal covalent bonding has been suggested for complexes containing both magnesium and transition metals [363-365].

Possible interaction diagrams for both $(Ni(Me_3AsO)_5)^{2+}$ and $(Mg(Me_3AsO)_5)^{2+}$ are given in Figures 6.12 and 6.13 respectively. For

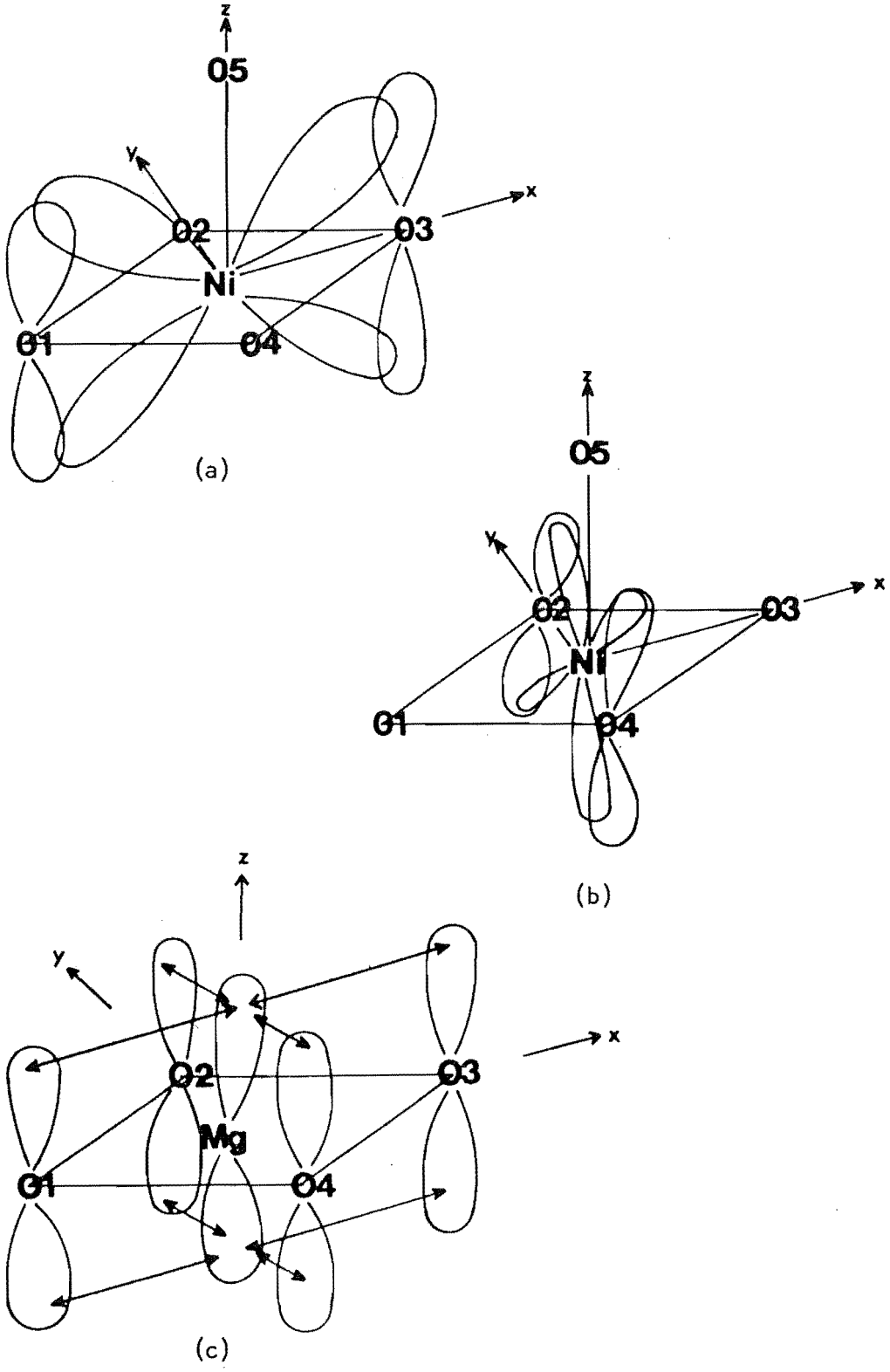

Figure 6.10 - Interactions between orbitals of basal oxygen atoms and metal atom.

(a) Nickel d_{xz} with p_z of O(1) and O(3).

(b) Nickel d_{yz} with p_z of O(2) and O(4).

(c) Magnesium p_z with oxygen p_z.

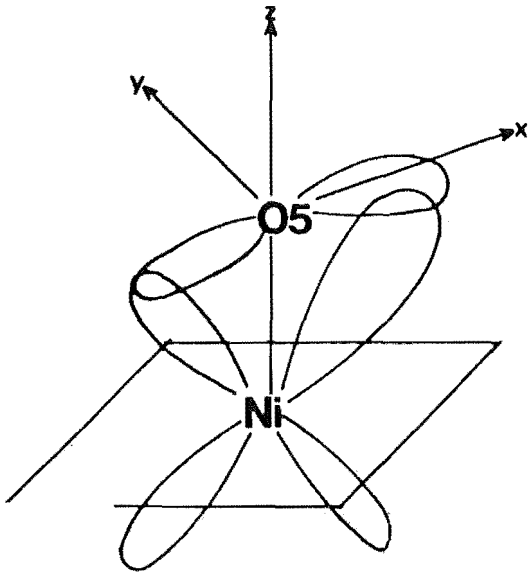

(a)

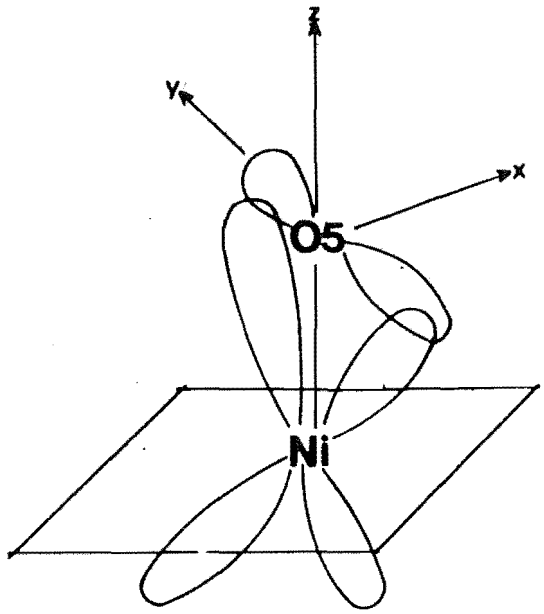

(b)

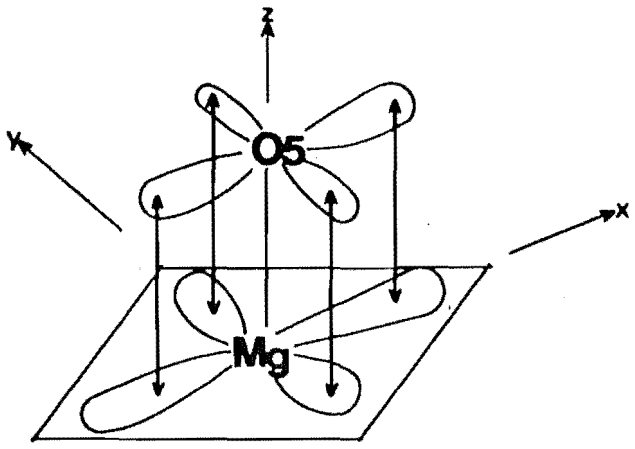

(c)

Figure 6.11 - Interactions between orbitals of axial oxygen atom and metal atom.

(a) Nickel d_{xz} with O(5) p_x

(b) Nickel d_{yz} with O(5) p_y

(c) Magnesium p_x and p_y with O(5) p_x and p_y.

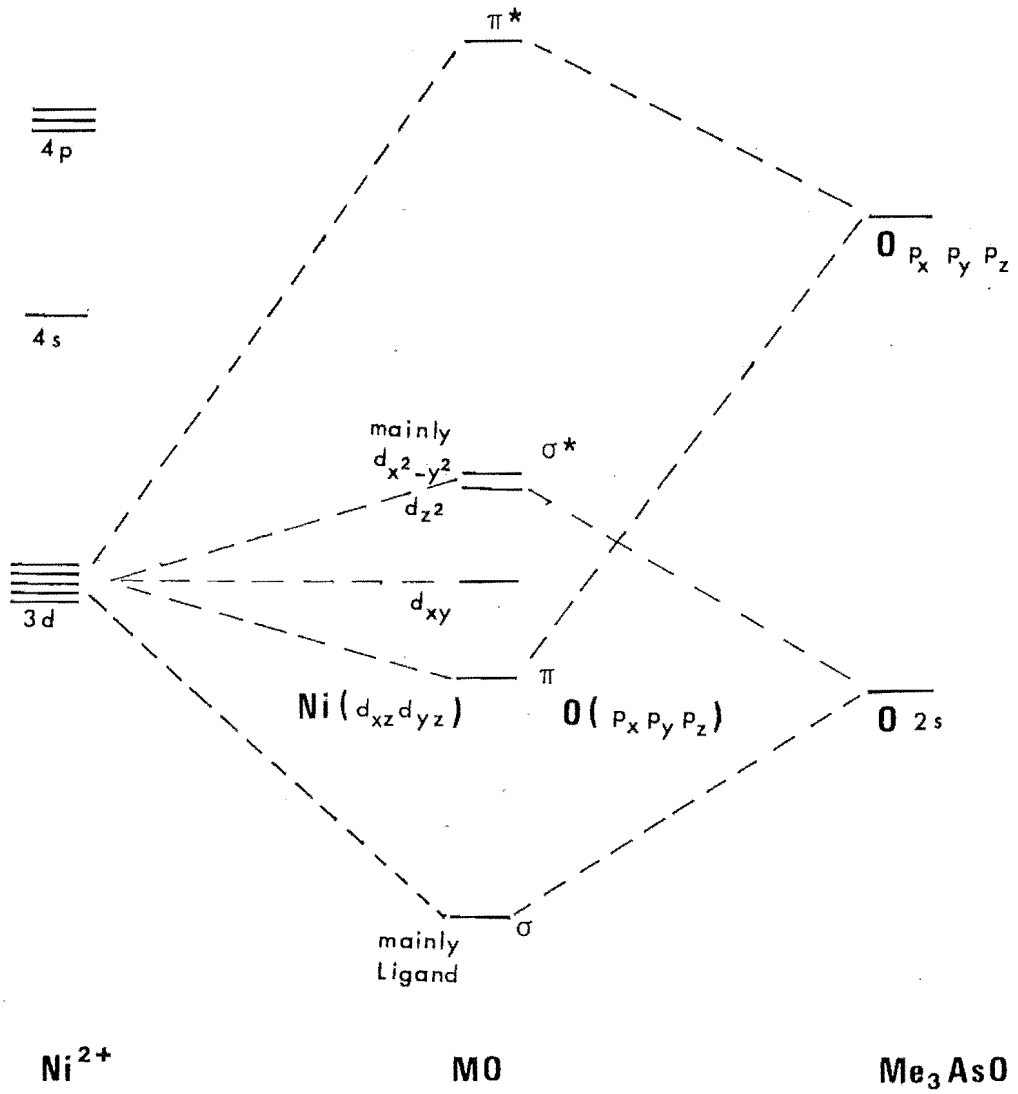

Figure 6.12 - Proposed molecular orbitals for $(Ni(Me_3AsO)_5)^{2+}$.

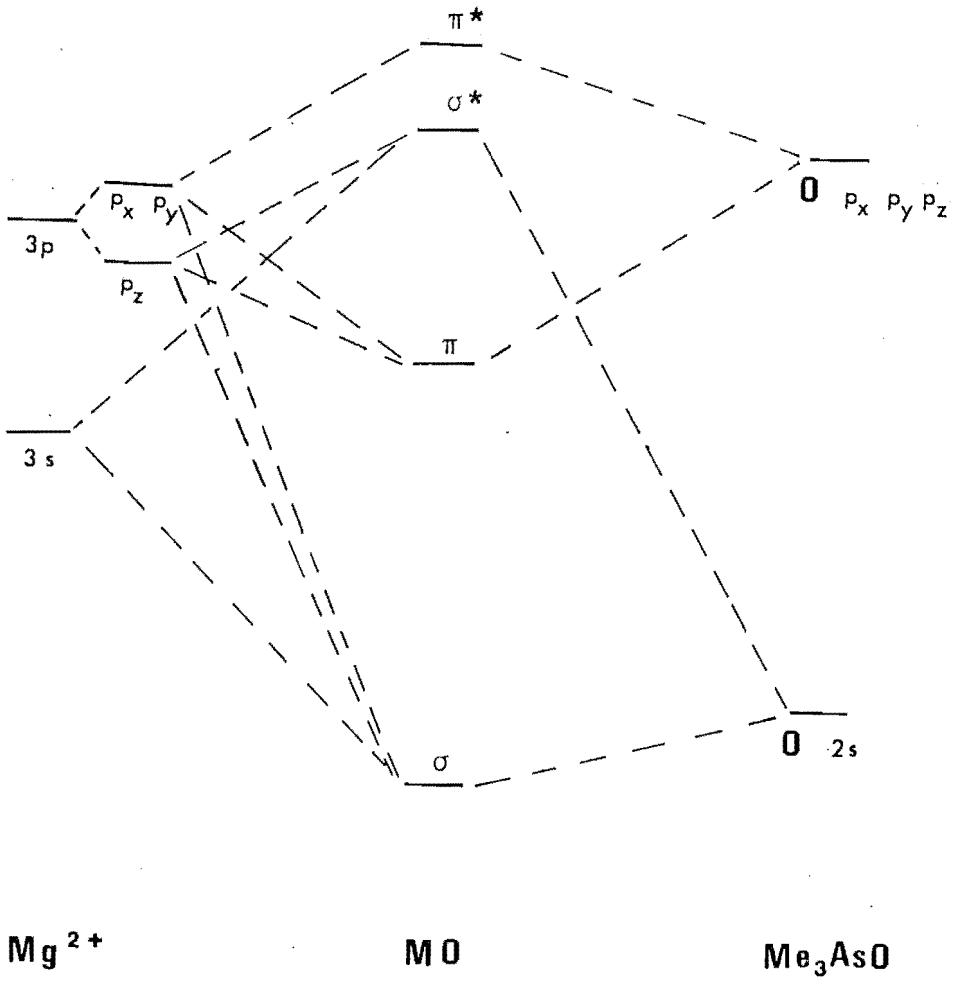

Figure 6.13 - Proposed molecular orbitals for $(Mg(Me_3AsO)_5)^{2+}$.

the $(Ni(Me_3AsO)_5)^{2+}$ cation, the metal $d_{x^2-y^2}$ and d_{z^2} orbitals point towards the ligands and would combine with the sp^2 (basal ligand) and sp(axial ligand) hybrid orbitals of the oxygen atom respectively to form σ bonding and antibonding MO's. The metal d_{xz} and d_{yz} compounds possess the right π symmetry to interact with the basal oxygen p_z and axial oxygen p_x and p_y orbitals. The metal d_{xy} orbital has lobes lying in-between the metal-ligand bond directions and thus remain essentially non-bonding. For the $(Mg(Me_3AsO)_5)^{2+}$ cation, σ bonding may be considered as arising from combination between the 3s, 3p orbitals of Mg(II) and the sp^2 and sp hybrid orbital of the oxygen atom. The p_x, p_y and p_z orbitals of Mg(II) and p_x, p_y and p_z orbitals on the oxygen have the correct symmetry to overlap and form π bonding and antibonding MO's. A similar type of π bonding has been suggested for the interaction between the filled $p\pi$ orbital of oxygen of tertiary butoxide and empty $p\pi$ orbital of lithium [366].

CHAPTER 7

SIGNIFICANCE OF GEOMETRICAL AND ELECTRONIC PROPERTIES OF CALCIUM AND MAGNESIUM IONS IN RELATION TO THEIR BIOLOGICAL ACTIVITIES

7.1 INTRODUCTION

Metal ions play an important role in a large number of biological processes. Some of these complexes are quite specific in their metal ion requirements. Others are less so although replacement of one metal ion by another, usually alters the metal ion activity [367]. Of the metal ions in the human body, Na(I), K(I), Mg(II) and Ca(II) ions account for more than 99% of the total metal ion content. The importance of these four metal ions in biochemical processes has been recently reviewed by Williams [368].

Calcium and magnesium ions are associated with a number of control and trigger mechanisms, e.g. the role of calcium in controlling the permeability of semipermeable membranes and that of magnesium in effecting the phosphate group transfer reactions [367]. In this chapter, two biochemical systems are considered with a view to understanding the coordination geometries of the metal ions and their possible effects on activities. These are the photosynthetic and muscle contraction systems which involve magnesium and calcium ions for activation, respectively. In photosynthesis, solar energy is utilized by plants to manufacture carbohydrates from carbon dioxide and water via a series of complex chemical reactions [369]. The photochemical reactions are made possible by the presence in plants of certain pigments; in particular the chlorophyll molecules. These are cyclic tetrapyrroles of magnesium [370]. On the other hand, regulation of muscle contraction is thought to involve calcium ions binding to muscle fibre components [371, 372]. The bound

fibre component then undergoes some sort of conformational changes which eventually brings about contraction.

It is generally believed that, in biological systems, metal ions provide appropriate stereochemical and electronic environments for biological action. Unfortunately biological systems are usually complex and it is difficult to obtain definite information on detailed molecular mechanisms. Because of their relative simplicity, model systems can provide detailed data which may illuminate modes of biological action [373]. This is especially true for the metal containing systems since very accurate information regarding the molecular conformation can be obtained from a wide range of physical techniques. The complexes studied in this work are obviously not related in molecular composition to the natural systems mentioned. However, this study reveals some interesting aspects of the coordination behaviour of calcium and magnesium ions which may be used to analyse the possible roles of these cations in biological systems. These aspects are:

(i) the strong axial M-L bond, and

(ii) the formation of five-coordinate complexes with monodentate ligands in the absence of water and the subsequent conformational change when a water molecule is added.

These two key points are discussed in the following sections with reference to the biological mechanisms in photosynthesis and muscle contraction.

7.2 THE PHOTOSYNTHETIC SYSTEM

Photosynthetic organisms consist of aggregates of pigment molecules associated with photochemical reaction centres. The pigment molecules absorb light quanta and deliver the energy to the reaction centre, where an oxidation-reduction photochemical reaction is initiated. The overall photosynthetic process can be represented as:

$$CO_2 + H_2O \xrightarrow[\text{pigment molecules}]{h\nu} 1/6(C_6H_{12}O_6) + O_2 \qquad \Delta H = 468 \text{ kJ/mole}$$

where $C_6H_{12}O_6$ denotes a monomeric unit of carbohydrate [369].

7.2.1 Chlorophylls - Chelate Compounds Of Magnesium

Chlorophylls are cyclic tetrapyrroles forming an aromatic π system. Important features in chlorophylls are the presence of a five-membered alicyclic cyclopentanone ring, a phytol group on ring IV and a magnesium atom at the centre of the tetrapyrrole ring (Figure 7.1) [374]. These characteristics are believed to have fundamental roles in many aspects of the photosynthetic process.

The coordination properties of the magnesium atom in chlorophyll have for some time now been recognized to play a decisive role in photosynthesis [375-377]. In vitro studies by infrared and nmr spectroscopic techniques show that the magnesium atom, with a coordination number of four in the pyrrole ring, is coordinatively unsaturated. As a consequence, the axial positions of the magnesium atom are susceptible to attack by electron donor groups [378]. In polar solvents, such as acetone, pyridine and the like, the unsaturation of the magnesium is alleviated by electron donation by coordination of the solvent molecules. Monomeric species of the type chlorophyll-ligand and chlorophyll-$(\text{ligand})_2$ are formed. In nonpolar solvents, such as benzene, CCl_4, etc., no suitable solvent

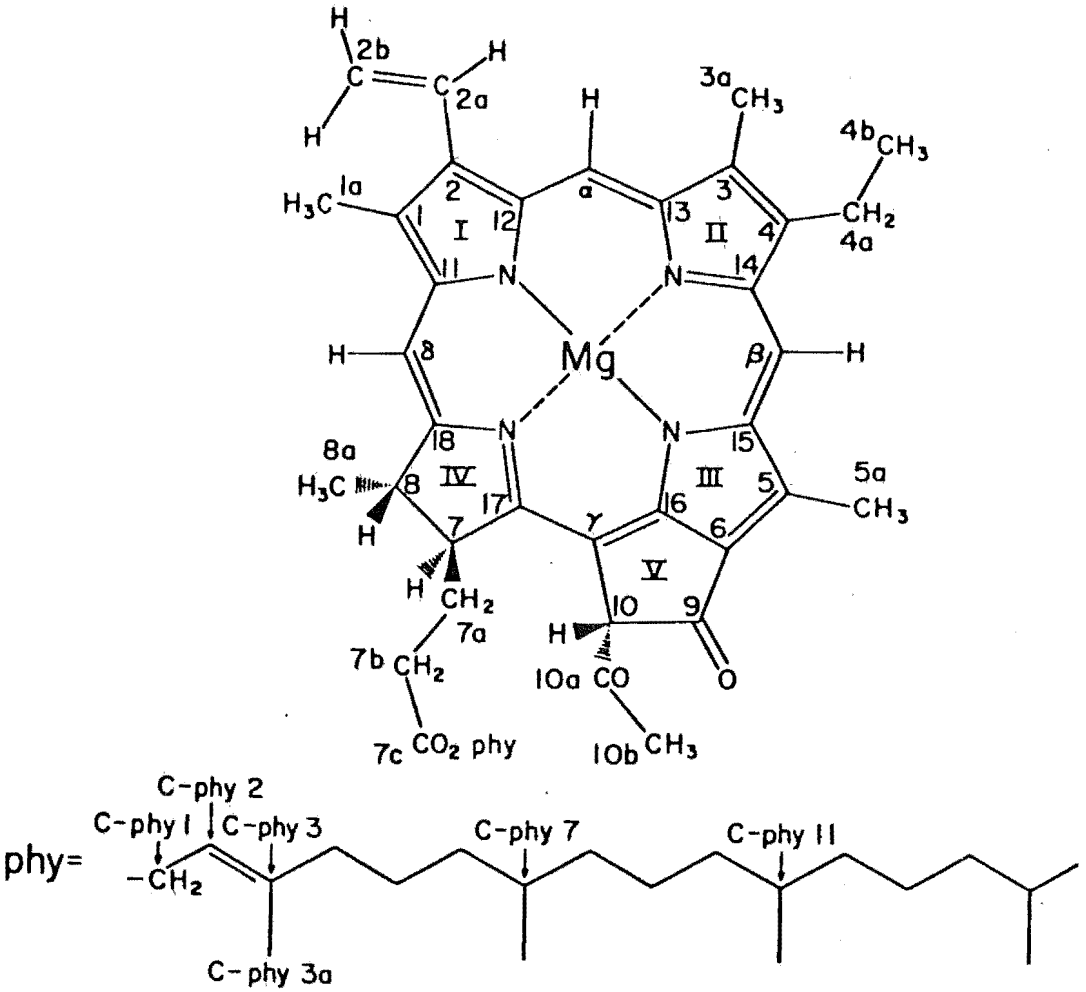

Figure 7.1 - Structural formula of chlorophyll a.

nucleophiles are available. As a result, the unsaturation of the magnesium is satisfied by intermolecular interactions between the keto C=O group of one chlorophyll molecule and the magnesium atom of another chlorophyll molecule. The keto C=O...Mg interaction produces a dimer, $(\text{chlorophyll})_2$, in CCl_4 and benzene (Figure 7.2a). In aliphatic hydrocarbon solvents, additional keto C=O...Mg interactions are formed and oligomers ($(\text{chlorophyll}_2)_n$, n=10) with a molecular weight greater than 20,000 have been observed (Figure 7.2b). While nucleophiles which cannot cross link molecules give monomeric chlorophyll species, polar ligands such as water with suitable hydrogen bonds can link together several chlorophyll molecules to form polynuclear entities (Figure 7.2c) [374].

7.2.2 Chlorophyll Model For Light Conversion

In order to formulate a model for photoreactive chlorophyll, use is made of knowledge on the mode of interactions involving the magnesium atom. The bulk of the pigments in plants is the antenna chlorophyll for light harvesting purposes. Only about 1% of the total pigment are the photoreactive chlorophyll molecules. The photoreactive chlorophylls are a pair of chlorophylls linked by a water molecule. They absorb light at lower frequency (about 690 cm^{-1}) compared with the antenna chlorophyll and thus serve as an energy sink for the transfer of energy.

From the close similarities of the optical spectra of chlorophyll in vivo and that of the oligomers in nonpolar solvents, it is suggested that the antenna chlorophylls basically involve chlorophyll-chlorophyll interactions [378]. The type of keto C=O...Mg interaction between chlorophyll molecules would form $(\text{chlorophyll}_2)_n$ aggregates (Figure 7.2a).

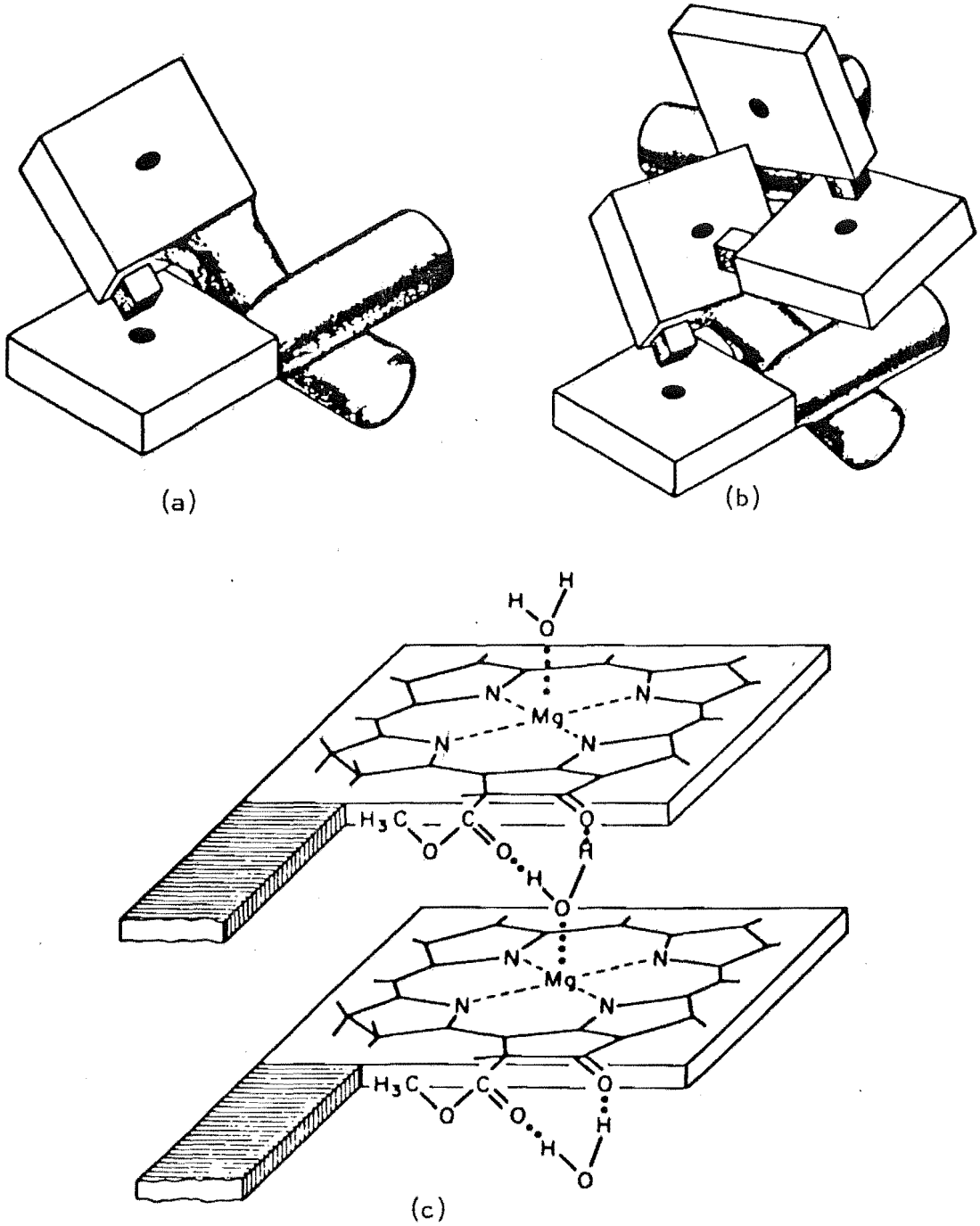

Figure 7.2 - Mg-O interactions in chlorophyll molecules.

(a) Chlorophyll dimer formed by keto C=O...Mg interactions.

(b) Chlorophyll oligomers formed by additional keto C=O...Mg interactions.

(c) Chlorophylls bridged by a water molecule.

Excitation energy absorbed by pigments is transferred to the reaction centre, where it is converted into chemical energy.

The nature of the reaction centres has been a subject of much interest [379]. Evidence, mainly from ESR studies [380] suggests the existence of chlorophyll-H_2O interactions in the reaction centre. This led to the conclusion that the reaction centre is most likely an adduct of two chlorophyll molecules cross-linked by one water molecule. The two water protons are hydrogen bonded to the keto group and the carbonyl of the ester group on the cyclopentanone ring of the first chlorophyll molecule and the water oxygen atom is coordinated to the magnesium atom of the second chlorophyll molecule (Figure 7.2c). Other studies, especially that from endor (electron nuclear double resonance) experiments, provide strong evidence to support the dimeric model [381].

The following scheme for the photo activities of the chlorophyll molecules has been suggested [380]:

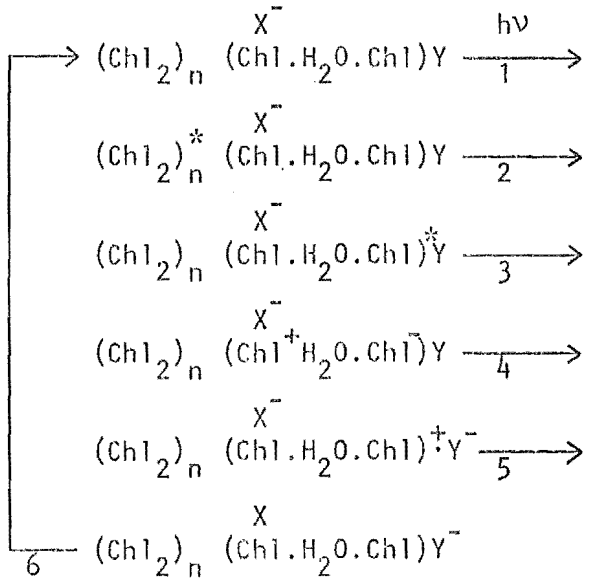

Step 1 denotes the absorption of light quanta by the antenna chlorophyll. In step 2, excitation energy is transferred to the reaction centre dimer molecule, which undergoes in step 3 the primary electron transfer from

one chlorophyll to the other to give a triplet radical pair. In step 4, the acceptor Y is reduced to Y^{-}. The initial chlorophyll state is restored in step 5 by the reduction of the oxidized dimer by X^{-}, using an electron that comes from water.

It can be seen that the crux of chlorophyll activity in photosynthesis is the coordination properties of the magnesium atom. Firstly, it is involved in interacting with keto C=O group, forming aggregates of antenna chlorophyll to facilitate transfer of excitation energy. Secondly, it is involved in the charge separation process in the reaction centre. Thirdly, the presence of the lightest cation, Mg(II), in chlorophyll suggests the minimization of the so-called "heavy atom" effect which tends to shorten the life-time of the excited state via spin-orbit coupling [382].

7.2.3 Significance Of The Coordination Geometry Of Magnesium Ion In Chlorophyll

The above section discusses the recent findings [374] that the reaction centre of photosynthetic systems contains a special pair of chlorophyll molecules linked by a water molecule (Figure 7.2c). More recent studies based on mathematical calculations on the distribution of spin-density favours the reaction centre as a $(Chl\text{-}H_2O)_2$ adduct (Figure 7.3a) [383]. This controversy has yet to be settled. Regardless of the formulations of the dimer molecule, the magnsium atom is in a five-coordinate environment. Upon light excitation, the primary photochemical reaction at the reaction centre is to produce a charge transfer-state (Section 7.2.2). Charge separation in the special reaction centre chlorophyll pair can occur by a process of hydride transfer from the coordinated water molecule to the other chlorophyll molecule as shown in Figure 7.3b [374]. From the study of five-coordinate magnesium phosphine and arsine oxide complexes, it is observed

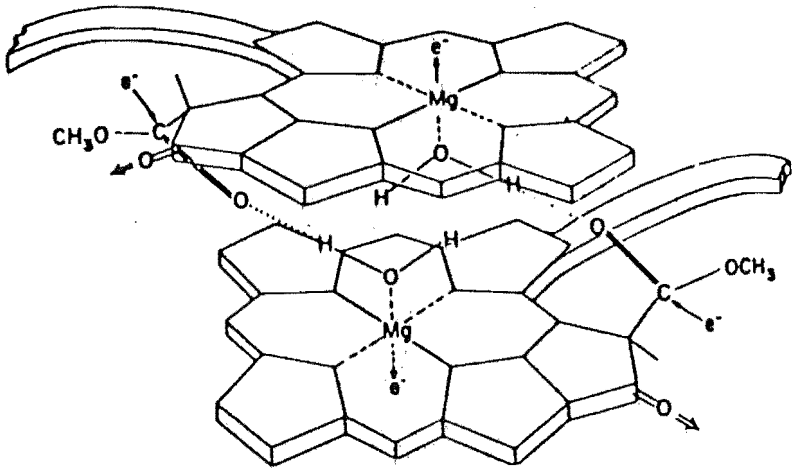

(a)

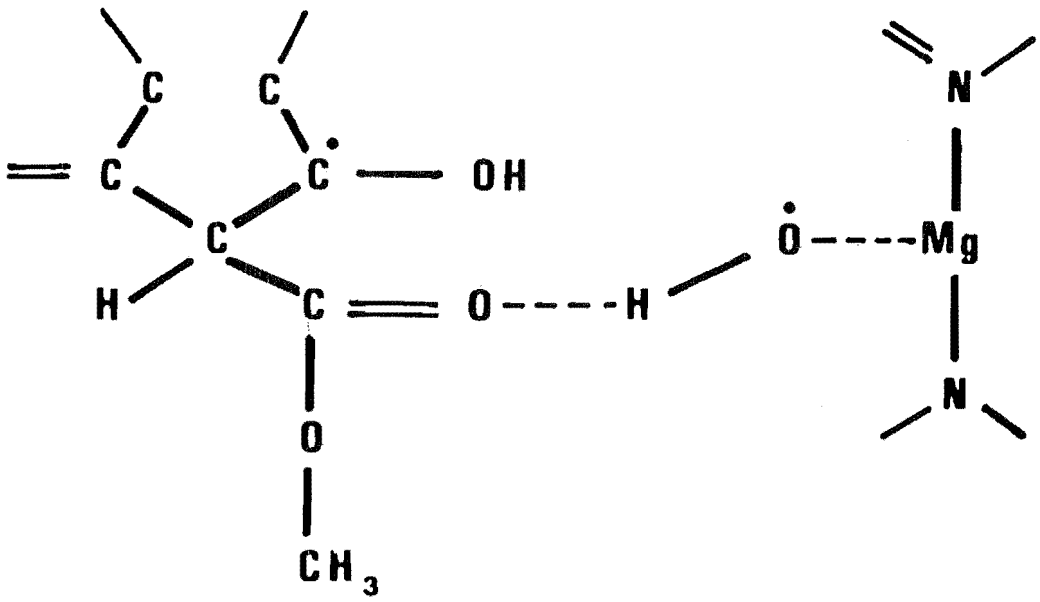

(b)

Figure 7.3 (a) Reaction centre chlorophyll molecules proposed by Fong.

(b) Charge separation in the reaction centre chlorophyll molecules proposed by Katz.

that there is a greater strength in bonding to the axial group. If this effect is present in the chlorophyll reaction centre molecules, a strong magnesium-water axial bond would enhance the charge separation by weakening the OH bond.

A recent crystal structure determination of ethyl chlorophyllide a [134] shows that the magnesium atom is five-coordinated. A second water molecule is hydrogen bonded to the coordinated water molecule. Extensive hydrogen bonds are formed between adjacent chlorophyllide molecules and a layered structure is obtained (Figure 7.4). It is suggested [384] that this layered structure could be structurally similar to the arrangement of the antenna chlorophyll molecules. It appears that five-coordinate magnesium is readily formed in these chlorophyll systems. This may be due to the possibility that magnesium can interact strongly in the axial direction and promote five-coordination readily. Thus five-coordinate magnesium complexes may yield information on the role of strong water coordination in a biological system like chlorophyll.

7.3 MUSCLE CONTRACTION

Before considering the control of muscles contraction, it is necessary to outline the generally accepted sliding filament model for muscle contraction [372]. Muscle contraction occurs when a force is generated between two types of muscle filament: one containing the protein myosin and the other the proteins actin, tropomyosin and troponin. The force causes the two types of filaments to interact and slide past each other. This interaction results in an overall shortening and thus contraction of the muscle as a whole.

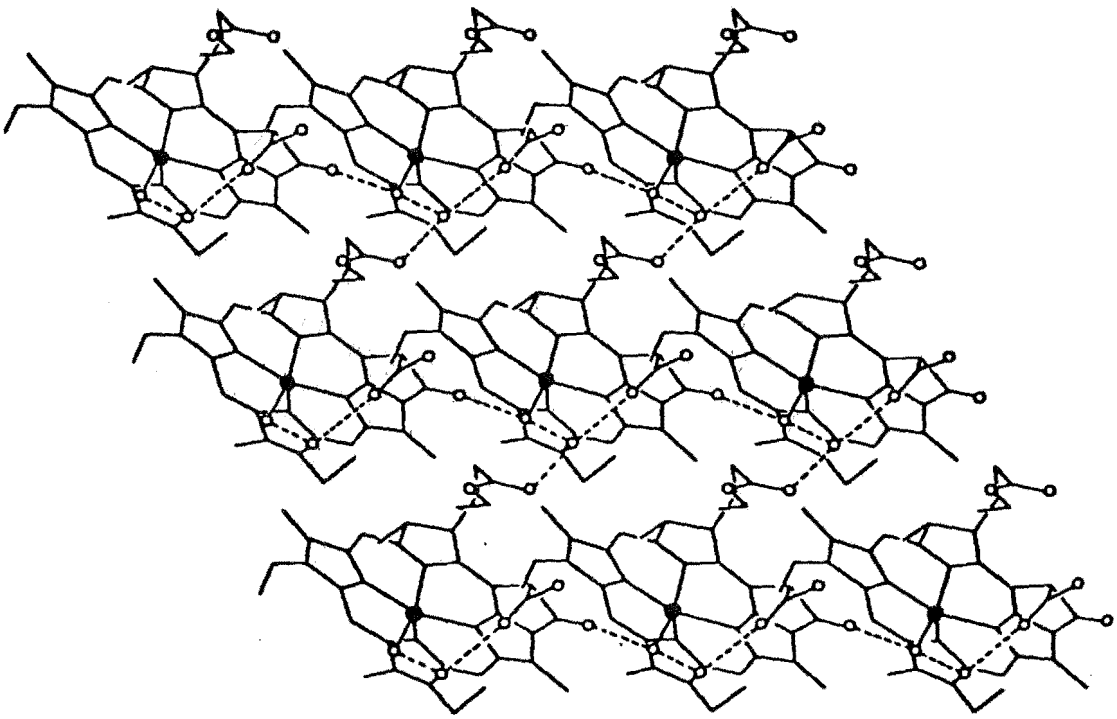

Figure 7.4 - One layer in the crystal structure of ethyl chlorophyllide a·$2H_2O$.

------- hydrogen bonds.

• magnesium atom.

7.3.1 The Muscle Structure

A schematic diagram of the arrangements of filaments is given in Figure 7.5 [385, 386]. The protein myosin is the major constituent of the thick filament. Myosin is a long (1500Å) and thin (diameter 20 to 40Å) molecule with two globular heads attached to one end of a long tail (Figure 7.6a). The other end of the tail is almost completely α-helical and can be cleaved by enzymes into two parts. One part is called the light meromyosin (LMM) which is about 900Å long. The other part of the rod, called the heavy meromyosin subfragment 2 (HMM S-2), is about 500Å long. It is this portion which may bend outward from the thick filament and form cross bridges thus interacting with the thin filament. The globular heads, called the HMM S-1, has a shape approximately like a long thin ellipsoid and is about 100 - 150Å long and about 30 - 40Å in diameter. It is suggested that the globular heads can bind to the actin molecules and bring about muscle contraction [371, 372, 387].

There are three major proteins incorporated in the thin filament. Of the three, actin is present in the largest amount. The actin molecule is spherical with a diameter of 40 - 50Å. These molecules polymerize to form long, thin, double helical arrangements (Figure 7.6b). Tropomyosins are long, thin molecules (420Å long) that attached end to end, being located near to the groove between the paired actin strands (Figure 7.6c). Troponin is a protein bound to tropomyosin and actin. It is built up of an assemblage of three globular sub-units. Troponin-T (TN-T) which binds to tropomyosin; troponin-C (TN-C) which binds to calcium ions and troponin-I (TN-I) which on its own can inhibit the interactions between actin and myosin (Figure 7.6d) [388].

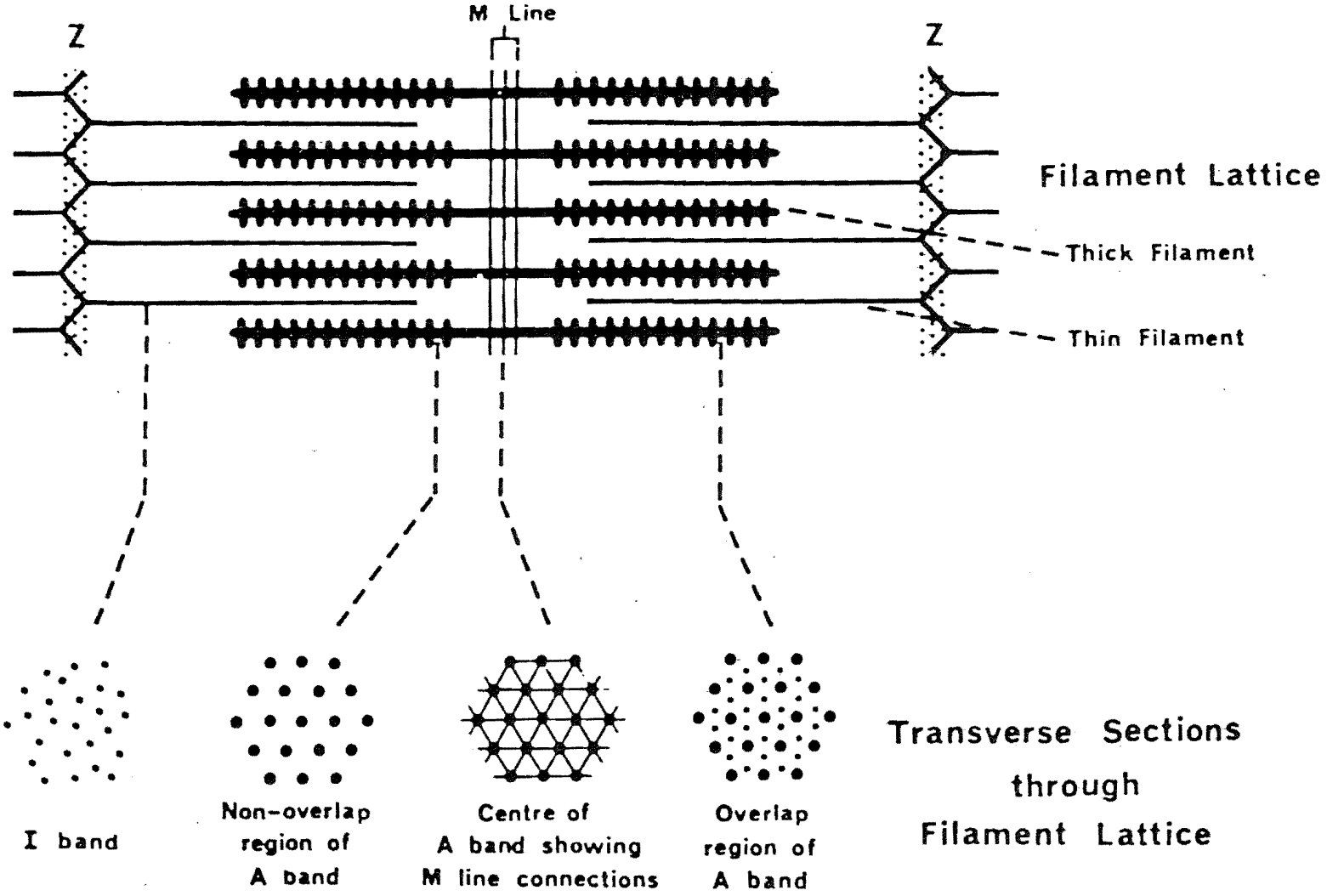

Figure 7.5 - Schematic diagram of muscle filaments.

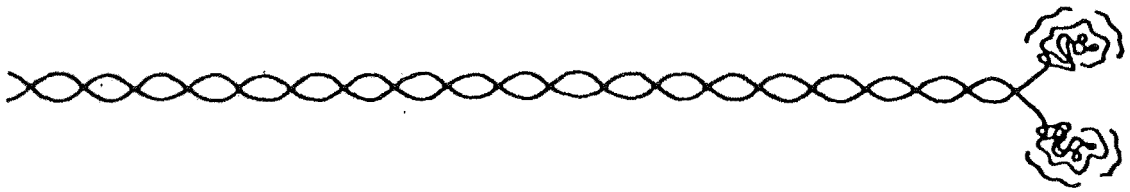

(a)

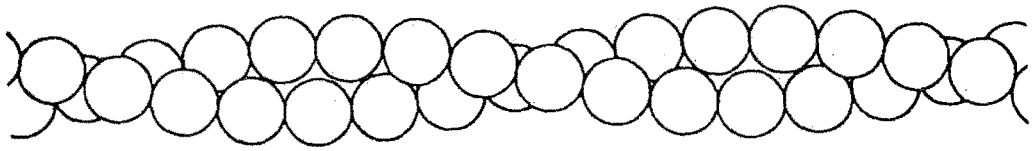

(b)

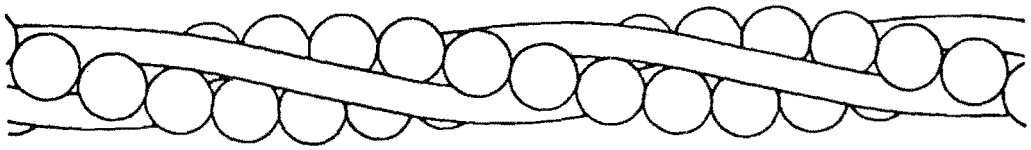

(c)

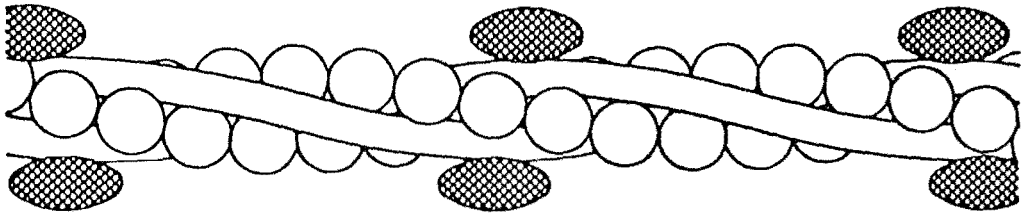

(d)

Figure 7.6 - The muscle filaments.

(a) Myosin
(b) Actin
(c) Actin and tropomyosin
(d) Actin, tropomyosin and troponin.

7.3.2 The Mechanism Of Muscle Contraction

The chemical species responsible for triggering contraction are calcium ions [389]. The globular heads of myosin have sites for adenosine triphosphate (ATP) hydrolysis which is activated by calcium ions. The addition of ATP and magnesium ions to filament systems in the absence of calcium ions does not lead to hydrolysis of ATP. If calcium ions are added into the system, the sites on the myosin heads are activated and ATP is hydrolysed. Interactions can then occur between the filaments and result in the sliding of one filament against another to cause contraction.

At the molecular level, the action of the calcium ions is to bind to troponin molecules, which leads to a conformational change in the filaments [390]. In the absence of calcium ions, TN-I binds strongly to the actin molecule, tropomyosin is located in an inhibitory position and prevents the attachment of the myosin head to the actin. When the contraction machinery is switched on by the addition of calcium ions, the calcium ions bind to TN-C. This causes the TN-I to actin linkage to weaken. TN-I then moves away from the actin molecule. The tropomyosin can now move away from its blocking position to one nearer the groove (Figure 7.7) [391]. This is the 'on' position and myosin head can bind to actin. Relaxation occurs by the inverse process, that is, calcium ions are taken by the membrane at the expense of those bound by TN-C, the latter returning to its initial state which in turn allows tropomyosin to block the myosin head interaction site on actin.

7.3.3 Significance Of The Coordination Geometry Of Calcium Ions In Muscle

The work on the detailed structure analyses of $(Mg(Me_3PO)_5)(ClO_4)_2$ and $(Mg(Me_3PO)_5H_2O)(ClO_4)_2$ indicates that a similar type of conformation

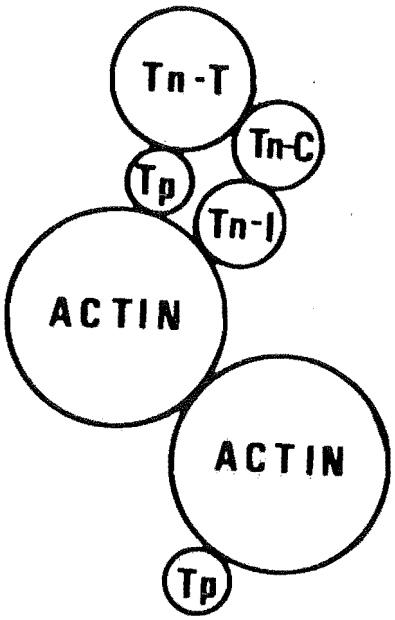

(a)

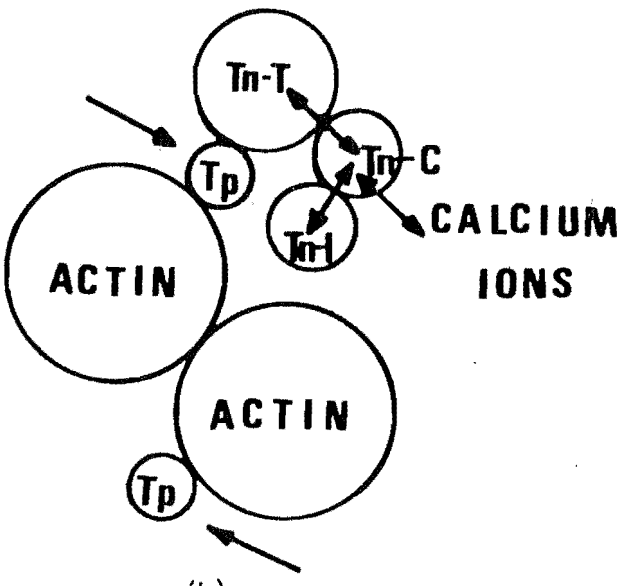

(b)

Figure 7.7 - Diagram of a transverse section of thin filament, Tp = tropomyosin, Tn = troponin.

(a) In the absence of Ca^{2+}, the Tn-T subunit binds to Tp and Tn-I binds to actin.

(b) In the presence of Ca^{2+}, linkages between troponin subunits are tightened and linkages between Tn-I and actin are weakened; tropomyosin moves deeper into the actin groove, exposing the site at which myosin can bind.

change comparable to that of deoxy- and oxy- forms of haemoglobin could also exist for biologically important non-transition metal ions. There is evidence that the coordination of water to particular metal systems is a key step in a number of biological processes. It has been observed that muscle contraction is associated with a high degree of dehydration-hydration [392]. The coordination of water to metal ion systems to give six-coordinate metal geometry and its subsequent elimination to give five-coordinate metal geometry may have important consequences for muscle action.

The crystal structure of a muscle calcium binding protein has been determined [393]. There are two calcium ions coordinating to two different loops in the amino acid chain (Figure 7.8). The calcium ion in the CD loop is coordinated by six oxygen atoms in an octahedral arrangement. Although the calcium ion in the EF loop is also six-coordinated, the octahedron is distorted. The -X direction (Figure 7.8) of the calcium coordination sphere is devoid of any ligand. In small organic and inorganic compounds, the calcium ions usually have a range of coordination numbers; seven or eight coordinated calcium complexes have been observed. It may be that this vacant site of the muscle-calcium complex is significant. What could possibly happen is that through alteration of the hydrophobic protein environment (perhaps triggered by the nerve electrical impulse) a water molecule may be able to bind to the vacant site. This could ultimately lead to a release of the calcium atom from the EF loop (through weakening of the coordination to the protein). Conformational changes in the protein would follow. This could result in a change in the affinity of one protein for another, such as in the case of TN-C and TN-I interaction, and give rise to muscle contraction.

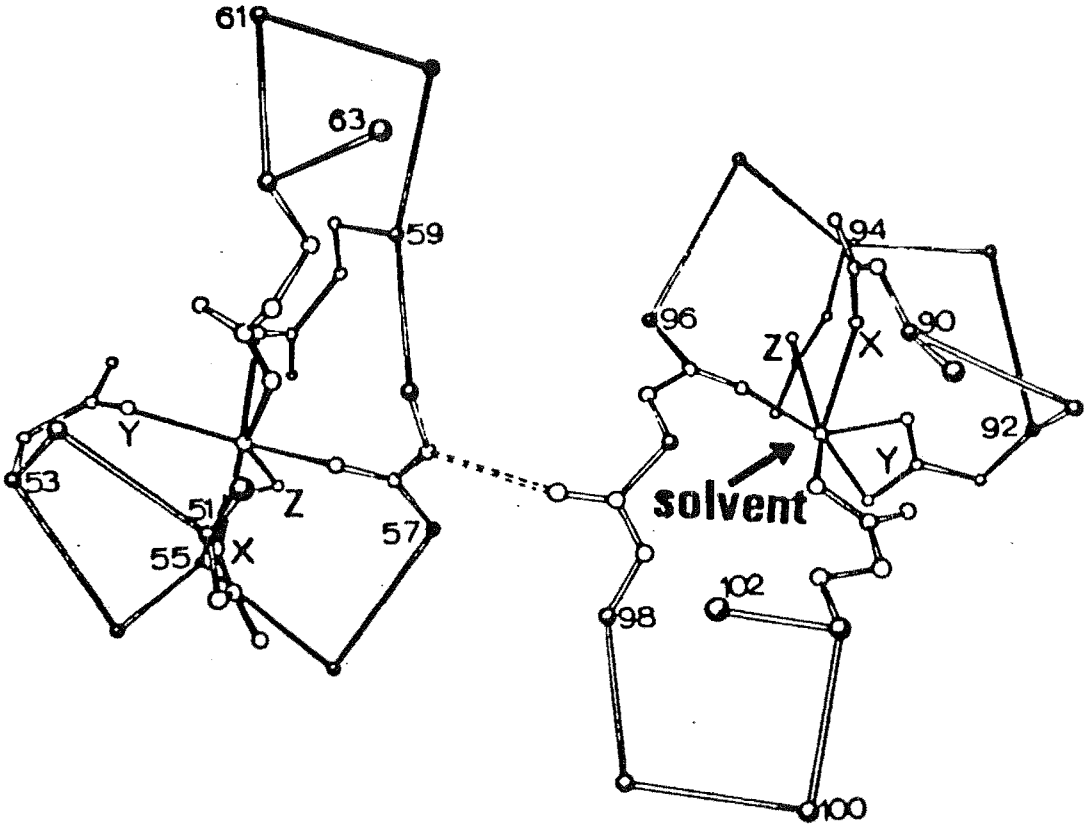

Figure 7.8 - Possible binding of solvent to calcium centre.

APPENDIX A

Crystallographic Computing System

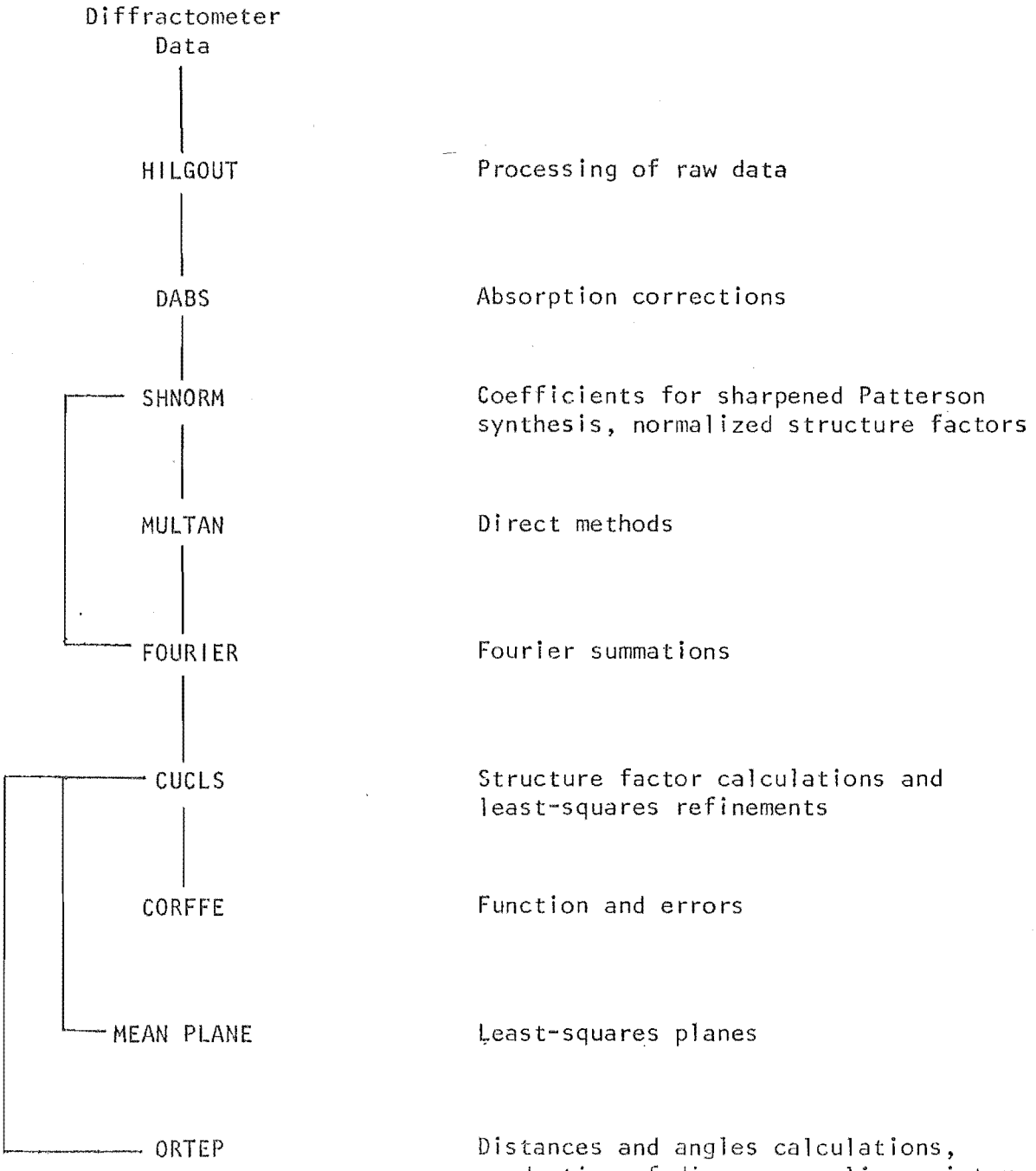

APPENDIX B

OBSERVED AND CALCULATED STRUCTURE AMPLITUDES FOR $(Mg(Me_3AsO)_5)(ClO_4)_2$

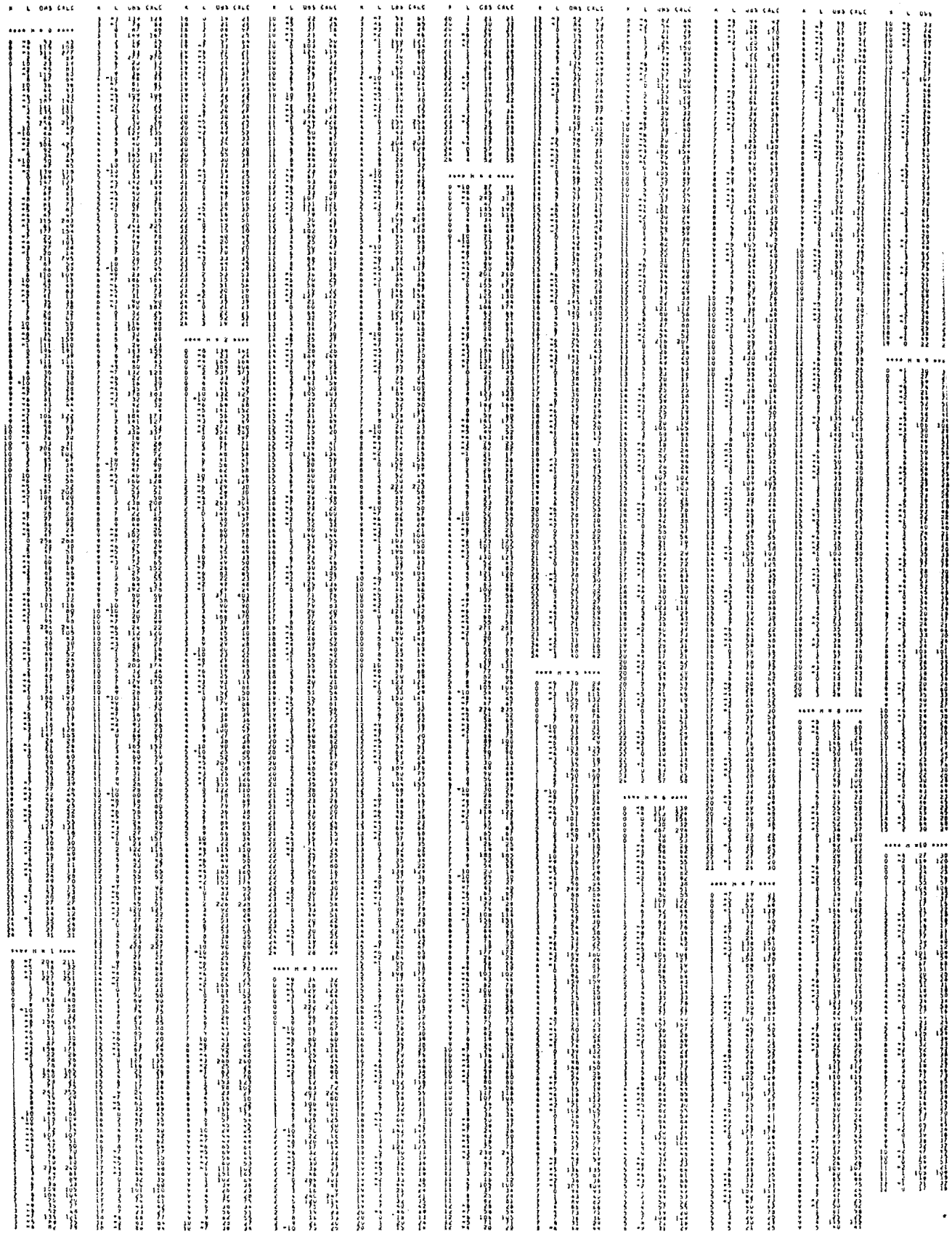

APPENDIX C

OBSERVED AND CALCULATED STRUCTURE AMPLITUDES FOR $(Ni(Me_3AsO)_5)(ClO_4)_2$

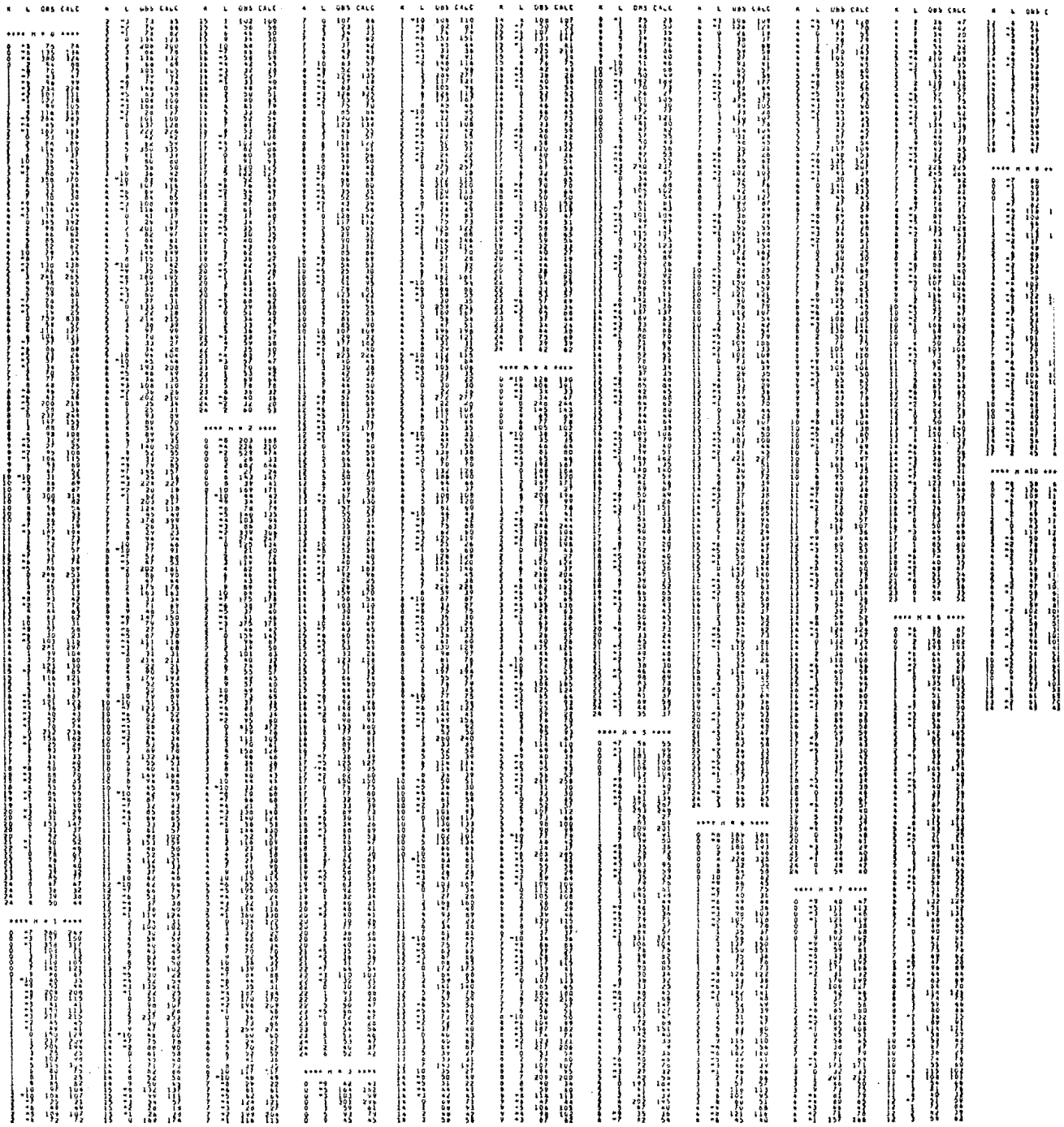

APPENDIX D

OBSERVED AND CALCULATED STRUCTURE AMPLITUDES FOR $(Mg(Me_3PO)_5H_2O)(ClO_4)_2$

APPENDIX E

OBSERVED AND CALCULATED STRUCTURE AMPLITUDES FOR $(Mg(Me_3PO)_5)(ClO_4)_2$

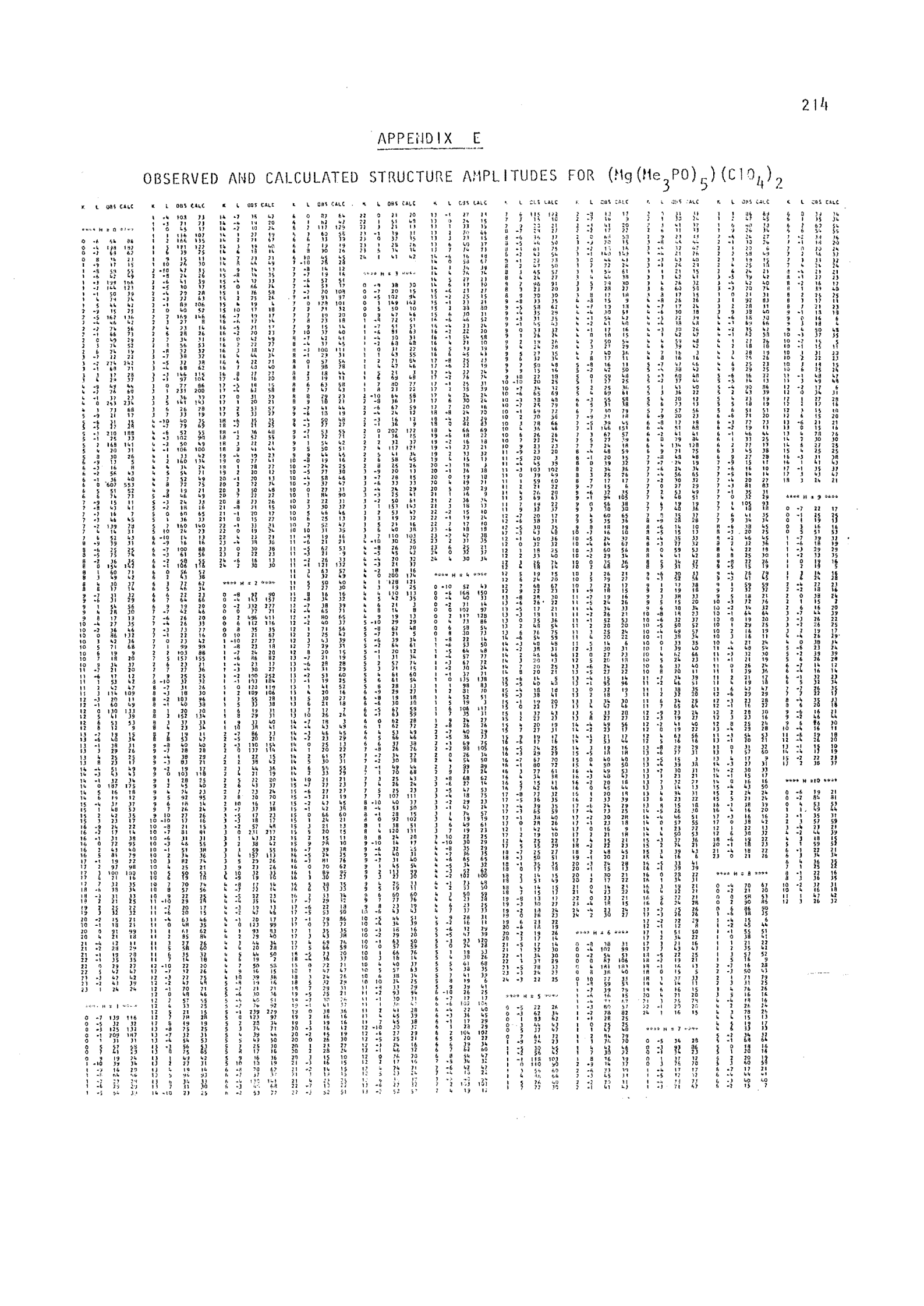

APPENDIX F

OBSERVED AND CALCULATED STRUCTURE AMPLITUDES FOR $(Ca_2Me_3AsO)_9)(ClO_4)_4$

K	L	OBS	CALC
**** H = 0 ****			
0	2	103	100
0	4	102	92
0	6	391	493
0	8	269	304
0	10	88	84
0	12	195	207
0	14	307	331
0	16	76	76
0	18	87	83
0	20	237	246
0	22	30	27
0	24	45	46
0	26	77	75
0	28	91	94
1	0	67	71
1	1	131	143
1	2	70	70
1	3	15	20
1	4	65	75
1	5	59	65
1	6	70	72
1	7	61	61
1	8	65	67
1	9	25	18
1	10	58	55
1	11	33	36
1	12	35	26
1	13	91	95
1	14	58	58
1	15	56	53
1	16	28	27
1	17	18	14
1	18	66	67
1	19	58	58
1	21	27	26
1	23	53	48
1	27	32	33
1	29	17	14
2	0	101	100
2	1	118	111
2	2	198	203
2	3	297	326
2	4	322	361
2	5	61	59
2	6	52	55
2	7	215	222
2	8	143	152
2	9	67	70
2	10	200	203
2	11	74	67
2	12	111	116
2	13	95	91
2	14	34	34
2	15	28	27
2	16	125	123
2	17	130	128
2	18	81	84
2	19	25	26
2	20	60	54
2	21	64	64
2	22	50	57
2	23	27	28
2	24	90	86
2	26	31	28
2	27	42	41
2	28	19	22
2	29	18	17
3	0	190	180
3	1	32	34
3	2	30	31
3	3	127	131
3	5	34	34
3	7	28	27
3	8	81	78
3	9	91	83
3	10	96	91
3	11	75	78
3	13	32	33
3	14	31	29
3	15	22	23
3	16	41	38
3	17	61	62
3	22	30	33
3	23	44	41
3	24	29	29
3	26	26	28
4	1	30	32
4	2	105	105
4	3	39	35
4	4	163	163
4	5	30	25
4	6	27	25
4	7	24	20
4	8	119	121
4	9	46	42
4	10	164	150
4	11	28	28
4	12	61	62
4	13	34	34
4	15	26	20
4	16	89	90
4	17	22	20
4	18	49	49
4	22	44	44
4	23	36	34
4	24	73	71
4	25	21	13
5	0	41	36
5	1	16	21
5	3	50	48
5	4	54	53
5	5	64	59
5	7	137	138
5	8	24	26
5	10	28	23
5	13	51	48
5	14	20	21
5	16	19	12
5	17	36	37
5	21	50	49
5	23	24	23
5	24	20	23
6	0	93	88
6	1	85	81
6	2	113	108
6	3	147	140
6	4	111	104
6	5	22	20
6	6	32	30
6	7	105	101
6	8	26	29
6	9	78	76
6	10	113	109
6	11	92	87
6	12	63	56
6	13	75	76
6	16	101	96
6	17	77	74
6	18	74	72
6	19	20	20
6	21	36	35
6	23	45	46
6	24	24	22
7	1	40	42
7	2	24	25
7	3	90	84
7	4	24	17
7	6	26	26
7	7	25	29
7	8	21	20
7	9	40	35
7	11	42	42
7	12	31	28
7	15	28	30
7	16	21	25
7	17	57	56
7	19	33	29
8	0	118	113
8	2	24	20
8	4	47	48
8	5	28	25
8	6	99	96
8	7	36	36
8	8	82	79
8	9	34	34
8	10	61	56
8	11	34	23
8	12	34	33
8	14	61	64
8	16	31	31
8	18	29	28
8	20	59	60
9	0	25	24
9	1	29	30
9	4	25	24
9	5	28	25
9	7	29	33
9	11	20	11
9	13	30	28
9	16	38	37
10	1	44	45
10	7	24	21
**** H = 1 ****			
0	0	77	71
0	1	147	143
0	2	77	70
0	3	15	20
0	4	72	75
0	5	64	65
0	6	77	72
0	7	66	61
0	8	71	67
0	9	24	18
0	10	62	55
0	11	34	36
0	12	35	26
0	13	96	95
0	14	64	58
0	15	58	53
0	16	28	27
0	17	19	14
0	18	69	67
0	19	58	58
0	20	19	26
0	21	30	26
0	23	53	40
0	26	20	18
0	27	36	33
1	0	77	87
1	1	94	83
1	2	34	30
1	3	215	215
1	4	98	94
1	5	38	40
1	6	143	136
1	7	133	126
1	8	98	100
1	10	16	13
1	11	97	95
1	13	61	57
1	14	89	92
1	16	64	62
1	17	107	108
1	18	24	22
1	19	19	15
1	20	58	61
1	21	30	32
1	22	46	47
1	23	50	50
1	26	38	37
1	27	25	27
1	28	18	11
2	0	237	264
2	1	50	51
2	2	142	147
2	3	40	37
2	4	188	209
2	5	70	75
2	6	70	77
2	7	111	116
2	8	70	80
2	9	87	82
2	10	194	199
2	11	55	54
2	13	17	14
2	14	63	59
2	16	146	150
2	18	81	83
2	20	107	103
2	21	30	33
2	22	38	36
2	23	46	45
2	24	68	73
2	25	30	31
2	26	25	19
2	28	21	17
3	1	66	58
3	2	45	53
3	3	15	14
3	4	41	41
3	6	64	61
3	7	92	90
3	8	87	86
3	9	60	52
3	10	92	97
3	11	29	25
3	14	46	43
3	15	24	24
3	16	41	42
3	18	74	73
3	19	32	34
3	20	39	38
3	21	32	32
3	24	20	18
3	25	23	16
3	27	23	19
4	0	35	23
4	1	57	55
4	3	192	193
4	4	22	23
4	5	47	46
4	6	165	159
4	7	113	113
4	8	137	133
4	9	127	125
4	11	129	127
4	12	42	41
4	13	76	76
4	14	88	84
4	16	55	49
4	17	114	114
4	20	62	61
4	21	29	29
4	22	40	46
4	23	59	59
4	25	22	25
4	26	46	47
4	27	23	24
5	0	32	25
5	1	59	55
5	2	59	57
5	3	61	56
5	5	31	28
5	7	31	33
5	9	19	26
5	10	30	31
5	14	21	26
5	15	46	48
5	16	19	21
5	17	36	36
5	18	31	33
5	25	20	19
6	0	116	110
6	1	111	111
6	2	33	31
6	3	30	27
6	4	33	33
6	6	77	76
6	7	60	57
6	8	22	25
6	9	36	31
6	12	31	32
6	13	58	55
6	14	66	66
6	15	64	62
6	17	26	29
6	18	24	24
6	19	38	34
6	20	32	35
6	21	28	30
7	0	34	29
7	1	29	23
7	3	53	52
7	6	44	40
7	7	52	47
7	8	53	54
7	10	27	26
7	11	39	36
7	13	36	33
7	16	26	21
7	17	32	35
7	21	19	18
8	0	32	28
8	1	46	45
8	2	24	24
8	3	27	24
8	5	47	43
8	6	31	35
8	7	89	92
8	13	54	52
8	14	38	37
8	17	24	23
9	0	21	27
9	1	36	30
9	4	22	20
9	9	21	19
9	11	29	27
9	13	29	33
9	14	20	21
9	15	28	36
10	0	51	55
10	3	13	16
10	4	45	50
**** H = 2 ****			
0	0	112	100
0	1	123	111
0	2	212	203
0	3	323	326
0	4	347	361
0	5	64	59
0	6	56	55
0	7	228	222
0	8	148	152
0	9	70	70
0	10	210	203
0	11	75	67
0	12	115	116
0	13	99	91
0	14	38	34
0	15	28	27
0	16	125	123
0	17	130	128
0	18	84	84
0	19	26	26
0	20	57	54
0	21	65	64
0	22	58	57
0	23	27	28
0	24	86	86
0	26	24	28
0	27	38	41
0	28	22	22
0	29	20	17
1	0	122	126
1	1	14	7
1	2	47	41
1	3	134	122
1	4	105	102
1	5	72	64
1	7	69	61
1	9	74	67
1	10	24	20
1	11	40	46
1	12	16	16
1	14	61	64
1	15	63	68
1	17	43	48
1	18	26	30
1	19	23	19
1	20	24	24
1	24	26	25
2	0	227	244
2	2	84	86
2	3	66	62
2	4	82	83
2	5	107	99
2	6	123	125
2	7	29	35
2	8	51	48
2	9	17	12
2	10	24	28
2	12	110	118
2	13	32	36
2	14	128	128
2	15	41	43
2	16	86	90
2	18	35	35
2	20	62	61
2	26	21	18
2	28	38	37
3	0	103	101
3	1	53	55
3	3	152	165
3	4	55	62
3	5	24	27
3	6	81	88
3	7	149	156
3	8	21	15
3	9	31	37
3	10	98	99
3	11	53	51
3	13	78	78
3	14	98	103
3	15	20	15
3	16	25	19
3	17	89	93
3	19	24	27
3	20	32	31
3	21	49	53
3	24	31	29
3	27	34	34
4	0	147	156
4	1	18	22
4	2	28	23
4	3	24	26
4	4	23	29
4	5	29	30
4	6	148	148
4	7	47	45
4	8	130	130
4	9	38	32
4	11	21	19
4	12	100	100
4	13	22	18
4	14	79	80
4	15	25	29
4	20	85	87
4	24	21	21
4	25	19	20
4	26	44	47
5	0	211	212
5	1	38	39
5	2	24	21
5	3	27	24
5	4	110	105
5	5	19	18
5	6	80	80
5	7	22	18
5	8	51	45
5	10	119	126
5	11	26	28
5	12	34	33
5	14	93	96
5	17	23	20
5	18	27	30
5	20	56	55
5	21	13	12
5	24	51	52
6	1	76	76
6	2	44	45
6	3	47	50
6	4	101	107
6	7	56	53
6	8	58	56
6	9	57	58
6	10	87	89
6	11	46	42
6	12	29	26
6	13	71	73
6	15	29	26
6	16	47	46
6	17	27	25
6	19	32	33
6	22	27	32
7	1	45	41
7	3	25	24
7	4	39	35
7	7	81	73
7	8	31	25
7	9	33	32
7	12	21	15
7	13	27	26
7	17	21	18
8	0	26	24
8	2	27	28
8	3	50	53
8	4	31	36
8	5	22	21
8	11	28	23
8	16	40	41
9	1	34	39
9	4	25	26
9	8	20	18
9	11	17	8
**** H = 3 ****			
0	0	212	190
0	1	35	34
0	2	33	31
0	3	136	131
0	5	34	34
0	7	28	27
0	8	86	78
0	9	96	83
0	10	96	91
0	11	77	78
0	13	33	33
0	14	30	29
0	15	20	23
0	16	41	38
0	17	62	62
0	22	28	33
0	23	43	41
0	24	24	29
0	26	27	28
1	0	97	100
1	1	194	200
1	2	48	47
1	3	93	95
1	4	15	16
1	6	117	125
1	7	171	163
1	8	25	17
1	9	87	73
1	10	76	69
1	11	107	104
1	12	49	49
1	13	102	102
1	14	138	141
1	15	87	85
1	17	68	65
1	19	60	59
1	20	48	55
1	21	70	69
1	23	56	60
1	24	27	28
1	25	22	24
1	26	25	28
1	27	53	53
1	28	20	22
2	0	80	82
2	1	103	98
2	4	79	88
2	5	38	34
2	6	55	59
2	7	80	79
2	8	19	19
2	9	59	56
2	10	25	28
2	11	28	28
2	12	28	23
2	13	124	125
2	14	38	41
2	15	70	73
2	16	19	15
2	19	51	50
2	21	37	37
2	23	36	29
2	24	20	27
2	27	29	31
3	0	52	50
3	1	37	36
3	3	83	85
3	4	39	46
3	5	71	74
3	6	100	103
3	8	98	100
3	9	57	66
3	11	86	88
3	14	51	49
3	16	37	40
3	17	56	61
3	19	29	28
3	20	41	46
3	22	35	39
3	23	31	30
3	25	31	31
3	26	30	31
4	1	17	22
4	2	60	65
4	3	42	45
4	4	47	45
4	5	62	64
4	7	30	38
4	9	74	77
4	10	75	78
4	11	83	86
4	16	37	40
4	17	40	38
4	18	43	44
4	19	27	26
4	20	21	16
4	23	43	42
5	0	35	36
5	1	36	37
5	2	31	33
5	3	78	79
5	5	49	50
5	6	54	61
5	9	76	79
5	11	75	76
5	12	30	35
5	13	33	33
5	14	52	51
5	17	39	41
5	18	23	24
5	23	51	50
6	1	55	54
6	3	35	38
6	5	29	35
6	6	35	42
6	7	45	47
6	8	58	61
6	9	33	34
6	10	44	46
6	11	22	24
6	13	30	34
6	15	34	37
6	17	25	24
7	0	63	65
7	2	40	42
7	4	66	69
7	6	40	41
7	7	24	16
7	8	42	42
7	10	60	67
7	14	31	29
7	16	44	44
8	0	33	38
8	3	46	48
8	6	26	22
9	1	18	15
9	3	33	35
9	6	22	22
**** H = 4 ****			
0	0	15	13
0	1	32	32
0	2	105	105
0	3	41	35
0	4	161	163
0	5	29	25
0	6	26	25
0	7	26	20
0	8	115	121
0	9	44	42
0	10	157	150
0	11	24	28
0	12	62	62
0	13	34	34
0	15	27	28
0	16	87	90
0	18	47	49
0	19	24	16
0	22	41	44
0	23	34	34
0	24	72	71
1	0	216	215
1	1	16	13
1	2	49	46
1	3	20	23
1	4	137	131
1	6	48	46
1	10	138	142
1	11	23	27
1	12	34	32
1	14	68	65
1	16	33	38
1	17	22	22
1	20	48	48
1	22	45	45
1	24	52	50
2	0	116	123
2	1	45	45
2	3	27	22
2	4	16	15
2	6	120	120
2	7	39	39
2	8	112	117
2	9	38	35
2	12	58	54
2	14	71	73
2	20	68	68
2	22	37	34
2	23	27	27
2	26	30	29
3	0	79	81
3	1	68	68
3	2	17	17
3	3	126	138
3	4	76	83
3	6	59	67
3	7	153	160
3	8	27	22
3	9	41	41
3	10	92	95
3	11	58	60
3	13	82	84
3	14	67	73
3	16	29	26
3	17	33	84
3	19	25	30
3	20	23	20
3	21	53	53
3	23	22	25
3	24	34	35
4	0	52	59
4	2	44	48
4	4	71	77
4	5	37	42
4	9	19	18
4	10	21	18
4	12	38	37
4	13	31	35
4	14	30	26
4	16	64	64
4	18	30	33
5	0	30	28
5	2	29	22
5	3	104	106
5	4	78	79
5	5	25	19
5	7	74	75
5	8	32	29
5	10	63	60
5	11	47	43
5	12	23	18
5	15	24	23
5	16	40	34
5	17	66	65
5	21	28	28
6	0	27	29
6	3	29	28
6	6	33	33
6	7	44	44
6	8	34	32
6	12	26	24
6	17	21	18
7	0	56	58
7	2	24	22
7	3	31	34
7	7	23	16
7	11	23	18
7	14	27	28
8	3	20	25
8	4	26	28
**** H = 5 ****			
0	0	43	36
0	1	18	21
0	3	48	48
0	4	52	53
0	5	66	59
0	7	135	138
0	8	22	26
0	10	25	23
0	13	48	48
0	14	20	21
0	17	36	37
0	21	45	49
0	23	24	23
0	24	22	23
0	25	18	12
1	0	42	44
1	2	93	91
1	3	20	15
1	4	120	114
1	5	90	89
1	6	49	49
1	7	85	90
1	8	38	37
1	9	62	56
1	10	137	137
1	11	38	35
1	13	32	33
1	14	35	31
1	15	20	17
1	16	71	72
1	18	75	79
1	20	35	34
1	21	33	31
1	23	36	36
1	24	32	39
1	25	27	30
2	0	42	42
2	1	43	48
2	2	19	20
2	4	31	25
2	5	30	33
2	6	56	54
2	7	57	63
2	8	40	46
2	13	49	52
2	15	32	30
2	16	52	53
2	19	22	21
2	21	23	24
3	0	35	30
3	1	65	65
3	2	54	55
3	3	41	42
3	4	13	13
3	5	34	41
3	7	34	35
3	10	34	36
3	13	63	64
3	14	22	25
3	15	58	59
3	16	41	42
3	18	24	23
3	19	20	22
3	21	20	21
4	0	50	53
4	1	48	53
4	2	50	56
4	3	27	36
4	4	77	86
4	6	23	24
4	8	44	43
4	10	70	72
4	13	39	40
4	14	20	14
4	15	44	42
4	16	45	48
4	17	22	22
4	18	39	42
4	19	24	22
4	20	31	28
5	1	45	46
5	3	33	32
5	6	59	64
5	7	64	62
5	8	40	42
5	13	49	47
5	16	22	24
5	17	21	18
6	0	31	40
6	2	21	23
6	3	36	42
6	5	36	40
6	9	33	33
6	11	40	43
6	14	24	27
7	0	40	43
7	1	34	38
7	3	33	33
7	6	27	21
7	7	19	18
7	9	29	25
**** H = 6 ****			
0	0	96	88
0	1	85	81
0	2	115	108
0	3	152	140
0	4	110	104
0	5	25	20
0	6	33	30
0	7	109	101
0	8	30	29
0	9	80	76
0	10	114	109
0	11	88	87
0	12	63	56
0	13	74	76
0	16	101	96
0	17	76	74
0	18	71	72
0	21	37	35
0	23	46	46
0	24	25	22
1	0	81	78
1	2	21	18
1	3	96	90
1	4	60	54
1	5	26	22
1	6	42	42
1	7	77	75
1	9	40	42
1	10	26	24
1	11	25	30
1	13	32	32
1	14	44	43
1	15	27	27
1	17	60	59
2	0	29	27
2	1	96	96
2	2	22	23
2	3	33	31
2	4	77	75
2	7	78	78
2	8	30	29
2	10	59	59
2	11	36	35
2	12	24	21
2	13	72	72
2	14	24	24
2	15	60	60
2	16	33	28
2	21	35	36
3	0	124	127
3	1	19	20
3	4	27	25
3	6	52	51
3	7	24	27
3	10	67	67
3	12	37	36
3	13	20	19
3	14	67	67
3	20	40	41
4	0	21	21
4	5	26	29
4	7	49	52
4	8	40	42
5	4	47	44
5	5	24	25
5	7	40	40
5	10	31	29
5	12	25	20
5	13	19	15
6	0	73	61
6	4	26	27
6	10	36	34
**** H = 7 ****			
0	1	44	42
0	2	28	25
0	3	93	84
0	6	27	26
0	7	25	29
0	8	27	20
0	9	35	35
0	11	40	42
0	12	28	28
0	15	33	30
0	16	28	25
0	17	57	56
0	19	28	29
1	0	80	71
1	3	68	69
1	4	42	42
1	5	50	48
1	8	19	19
1	9	45	40
1	10	68	64
1	11	51	50
1	15	21	16
1	17	35	36
2	0	43	48
2	1	44	42
2	3	61	61
2	4	25	23
2	5	26	29
2	6	42	43
2	7	27	23
2	9	68	65
2	10	36	39
2	11	51	55
2	13	46	46
2	14	45	47
2	17	39	35
2	19	19	17
3	0	42	42
3	1	22	20
3	2	27	24
3	6	24	17
3	7	53	52
3	9	46	47
3	14	26	28
4	0	22	19
4	1	46	48
4	3	40	40
4	6	54	54
4	7	63	63
4	8	35	40
4	11	22	20
4	13	44	45
4	14	28	25
5	1	33	28
5	2	25	26
5	4	19	17
**** H = 8 ****			
0	0	121	113
0	2	23	20
0	4	45	48
0	5	26	25
0	6	100	96
0	7	37	36
0	8	84	79
0	9	35	34
0	10	60	56
0	11	24	23
0	12	38	33
0	14	66	64
0	16	27	31
0	18	30	28
0	20	63	60
1	3	26	18
1	4	21	11
1	7	35	34
1	8	26	21
1	9	25	23
1	17	18	14
1	18	25	19
2	0	28	21
2	2	26	21
2	3	51	46
2	4	37	34
2	8	21	24
2	9	32	33
2	11	43	41
2	12	27	25
2	16	27	29
3	0	35	35
3	3	35	29
3	6	24	28
3	7	25	25
3	8	36	31
3	12	20	15
4	0	20	14
4	1	25	17
4	3	30	33
4	4	23	27
**** H = 9 ****			
0	0	28	24
0	1	34	30
0	4	30	24
0	5	29	25
0	7	32	33
0	13	29	28
0	16	38	37
1	0	43	42
1	3	80	75
1	5	22	20
1	6	34	34
1	7	34	34
1	9	24	26
1	10	27	25
1	11	42	41
1	14	43	42
1	15	22	24
2	0	29	30
2	2	22	24
2	3	21	23
2	4	27	27
2	6	38	36
2	8	27	23
2	10	39	37
3	0	36	33
3	3	24	22
3	4	21	20
**** H =10 ****			
0	1	50	45
0	7	20	21
1	6	27	25
1	7	19	18
1	8	24	21

REFERENCES

1. Y.S. Ng, G.A. Rodley and W.T. Robinson, Inorg. Chem., 15, 303 (1976).
2. Y.S. Ng, G.A. Rodley and W.T. Robinson, Acta Crystallogr., Sect. B, In Press.
3. R. Saillant, R.B. Jackson, W.E. Streib, K. Folting and R.A.D. Wentworth, Inorg. Chem., 10, 1453 (1971).
4. G.J. Wessel and D.J.W. Ijdo, Acta Crystallogr., 10, 466 (1957).
5. W.H. Watson and J. Waser, ibid., 11, 689 (1958).
6. A.W. Hoffmann, Ann. Chem. Pharm., Suppl. 1, 1 (1861).
7. R.H. Pickard and J. Kenyon, J. Chem. Soc., 89, 262 (1906).
8. A.B. Burg and W.E. McKee, J. Am. Chem. Soc., 73, 4590 (1951).
9. K. Issleib and A. Brack, Z. Anorg. Allg. Chem., 277, 258 (1954).
10. J.C. Sheldon and S.Y. Tyree, J. Am. Chem. Soc., 80, 4775 (1958).
11. F.A. Cotton, E. Bannister, R. Barnes and R.H. Holm, Proc. Chem. Soc., 158 (1959).
12. K. Issleib, A. Tzschach and H.O. Frohlich, Z. Anorg. Allg. Chem., 298, 164 (1958).
13. I. Lindqvist and G. Olofsson, Acta Chem. Scand., 13, 1753 (1959).
14. W. Hieber and A. Lipp, Chem. Ber., 92, 2085 (1959).
15. N.M. Karayannis, C.M. Mikulski and L.L. Pytlewski, Inorg. Chim. Acta Rev., 5, 69 (1971).
16. Proceedings of the International Conference on Coordination Compounds, Amsterdam, p. 46, 55 and 61 (1955).
17. I. Lindqvist and C.I. Branden, Acta Crystallogr., 12, 642 (1959).
18. P.W.N.M. van Leeuwen and W.L. Groenveld, Inorg. Nucl. Chem. Lett., 3, 145 (1967).
19. N.M. Karayannis, C. Owens, L.L. Pytlewski and M.M. Labes, J. Inorg. Nucl. Chem., 31, 2059 (1969).
20. F.A. Cotton and E. Bannister, J. Chem. Soc., 1873 (1960).
21. E. Bannister and F.A. Cotton, ibid., 1878 (1960).
22. E. Bannister and F.A. Cotton, ibid., 2276 (1960).
23. F.A. Cotton and D.M.L. Goodgame, J. Am. Chem. Soc., 82, 5771 (1960).
24. F.A. Cotton and D.M.L. Goodgame, ibid., 82, 5774 (1960).
25. K. Issleib and B. Mitscherling, Z. Anorg. Allg. Chem., 304, 73 (1960).

26. D.M.L. Goodgame and F.A. Cotton, J. Chem. Soc., 3735 (1961).

27. D.J. Phillips and S.Y. Tyree, J. Am. Chem. Soc., 83, 1806 (1961).

28. D.M.L. Goodgame, M. Goodgame and F.A. Cotton, Inorg. Chem., 1 , 239 (1962).

29. J.T. Donoghue and R.S. Drago, ibid., 1, 866 (1962).

30. J.T. Donoghue and R.S. Drago, ibid., 2, 572 (1963).

31. F.A. Cotton, D.M.L. Goodgame and R.H. Soderberg, ibid., 2, 1162 (1963).

32. M.D. Joesten and K.M. Nykerk, ibid., 3, 548 (1964).

33. J. Lewis, R.S. Nyholm and G.A. Rodley, Nature (London), 207, 72 (1965).

34. P. Pauling, G.B. Robertson and G.A. Rodley, ibid., 207, 73 (1965).

35. G.A. Rodley, D.M.L. Goodgame and F.A. Cotton, J. Chem. Soc., 1499 (1965).

36. M.D. Joeston and J.F. Forbes, J. Am. Chem. Soc., 88, 5465 (1966).

37. K.P. Lannert and M.D. Joesten, Inorg. Chem., 7, 2048 (1968).

38. A.M. Brodie, S.H. Hunter, G.A. Rodley and C.J. Wilkins, J. Chem. Soc., (A), 987 (1968).

39. A.M. Brodie, S.H. Hunter, G.A. Rodley and C.J. Wilkins, ibid., (A), 2039 (1968).

40. A.M. Brodie, S.H. Hunter, G.A. Rodley and C.J. Wilkins, Inorg. Chim. Acta, 2, 195 (1968).

41. S.H. Hunter, R.S. Nyholm and G.A. Rodley, ibid., 3, 631 (1969).

42. N.M. Karayannis, C. Owens, L.L. Pytlewski and M.M. Labes, J. Inorg. Nucl. Chem., 31, 2767 (1969).

43. N.M. Karayannis, C.M. Mikulski, L.L. Pytlewski and M.M. Labes, Inorg. Chem., 9, 582 (1970).

44. D.M.L. Goodgame, M. Goodgame and P.J. Haywood, J. Chem. Soc., (A), 1352 (1970).

45. G.E. Parris and G.G. Long, J. Inorg. Nucl. Chem., 32, 1585 (1970).

46, N.M. Karayannis, C.M. Mikulski, M.J. Strocko, L.L. Pytlewski and M.M. Labes, ibid., 32, 2629 (1970).

47. H.A. Tayim, A. Bouldoukian and F. Awad, ibid., 32, 3799 (1970).

48. O.A. Serra and A.C. Massabni, Inorg. Nucl. Chem. Lett., 7, 275 (1971).

49. F. Mani, ibid., 7, 447 (1971).

50. N.M. Karayannis and C.M. Mikulski, J. Inorg. Nucl. Chem., 33, 2691 (1971).

51. B.J. Brisdon, J. Chem. Soc., (Dalton), 2247 (1972).

52. D.W. Johnson and D. Sutton, Can. J. Chem., 50, 3326 (1972).

53. S.S. Sandhu and R.S. Sandhu, Inorg. Chim. Acta., 6, 383 (1972).

54. F. Mani and M. Bacci, ibid., 6, 487 (1972).

55. M.W.B. de Bolster, I.E. Kortram and W.L. Groenveld, Inorg. Nucl. Chem. Lett., 8, 751 (1972).

56. H.A. Tayim, S.K. Thabet and M.U. Karkanawi, ibid., 8, 235 (1972).

57. M.W.G. de Bolster, I.E. Kortram and W.L. Groenveld, J. Inorg. Nucl. Chem., 34, 575 (1972).

58. M.W.G. de Bolster, I.E. Kortram and W.L. Groenveld, ibid., 35 1843 (1973).

59. N.M. Karayannis, C.M. Mikulski, L.L. Pytlewski and M.M. Labes, Inorg. Chim. Acta, 10, 97 (1974).

60. B.J. Brisdon and D. Cocker, Inorg. Nucl. Chem. Lett., 10, 179 (1974).

61. S.S. Sandhu and R.S. Sandhu, J. Inorg. Nucl. Chem., 37, 597 (1975).

62. J.T. Donoghue and R.S. Drago, Inorg. Chem., 2, 1158 (1965).

63. F.A. Hart and J.E. Newbery, J. Inorg. Nucl. Chem., 30, 318 (1968).

64. D.R. Cousins and F.A. Hart, ibid., 29, 1745 (1967).

65. D.R. Cousins and F.A. Hart, ibid., 29, 2965 (1967).

66. O.A. Serra, M.L.R.Gibran and A.M.B. Galindo, Inorg. Nucl. Chem. Lett., 8, 673 (1972).

67. S.S. Sandhu and G.S. Aulakh, J. Inorg. Nucl. Chem., 37, 581 (1975).

68. G. Bandoli, G. Bortolozzo and D.A. Clemente, Inorg. Nucl. Chem. Lett., 7, 401 (1971).

69. Z.M.S. Al-Kazzaz and K.W. Bagnall, J. Inorg. Nucl. Chem., 36, 1493 (1973).

70. K.W. Bagnall and M.W. Wakerley, J. Chem. Soc., (Dalton), 889 (1974).

71. S.S. Sandhu and G.S. Aulakh, J. Indian Chem. Soc., 51, 717 (1974).

72. K. Bagnall and M.W. Wakerley, J. Less. Com. Metals, 35, 267 (1974).

73. J.G.H. du Preez and C.P.J. van Vuuran, J. Chem. Soc., (Dalton), 1548 (1975).

74. C. Pannattoni, R. Graziani, G. Bandoli, B. Zarli and G. Bombieri, Inorg. Chem., 8, 320 (1969).

75. R. Graziani, B. Zarli, A. Cassol, G. Bombieri, E. Forsellini and E. Tondello, ibid., 9, 2116 (1970).

76. C.J. Wilkins, H.M. Haendler, J. Chem. Soc., 3174 (1965).

77. J.P. Clark, V.M. Langford and C.J. Wilkins, ibid., (A), 792 (1967).

78. D.M. Adams, A.J. Carty, P. Carty and D.G. Tuck, ibid., (A), 162 (1968).

79. S.S. Sandhu and S.S. Sandhu, J. Inorg. Nucl. Chem., 31, 1363 (1969).

80. G.B. Deacon and J.C. Parrott, Aust. J. Chem., 25, 1169 (1972).

81. R.E. Beaumont, R.G. Goel and H.S. Prasad, Inorg. Chem., 12, 944 (1973).

82. S.S. Sandhu and H. Singh, J. Indian Chem. Soc., 50, 373 (1973).

83. A.R. Hands and A.J.H. Mercer, J. Chem. Soc., (A), 449 (1968).

84. Y.M.G. Yasin, O.J.R. Hodder and H.M. Powell, Chem. Commun., 705 (1966).

85. G.B. Jameson and G.A. Rodley, Inorg. Nucl. Chem. Lett., 11, 547 (1975).

86. G.B. Jameson and G.A. Rodley, ibid., 12, 519 (1976).

87. 'International Tables For X-Ray Crystallography', Vol. III, Kynoch Press, Birmingham, England (1962).

88. M. Renniger, Z. Krist, 97, 107 (1937).

89. W.R. Busing and H.A. Levy, ORNL-4054, Oak Ridge National Laboratory, U.S.A. (1967).

90. T.C. Furnas, 'Single Crystal Orienter Instruction Manual', General Electric Company, Milwaukee, U.S.A. (1966).

91. P.W.R. Corfield, R.J. Doedens and J.A. Ibers, Inorg. Chem. 6, 197 (1967).

92. D.F. Grant, R.C.G. Killean and J.L. Lawrence, Acta Crystallogr., B25, 374 (1969).

93. W.T. Robinson and J.A. Ibers, Inorg. Chem., 6, 1208 (1967).

94. D.W.J. Cruickshank, 'Computing Methods in Crystallography', Ed., J.S. Rollett,Pergamon, Oxford, p. 114 (1965).

95. A. Modified version of DATAPH by P. Coppens.

96. A.L. Patterson, Z. Krist, A90, 517 (1935).

97. S.R. Hall, NRC-4, National Research Council, Ottawa, Canada (1968).

98. G.H. Stout and L.H. Jensen, 'X-ray Structure Determination', Macmillan, p. 270 (1968).

99. M.J. Buerger, 'Vector Space', Wiley, New York, N.Y., p. 66 (1959).

100. M.J. Buerger, 'Crystal Structure Analysis', Wiley, New York, N.Y. (1960).

101. J. Karle and I.L. Karle, Acta Crystallogr., 16, 969 (1963).

102. M.M. Woolfson, 'Direct Methods In Crystallography', Oxford University Press, New York (1961).

103. D. Harker and J.S. Kasper, Acta Crystallogr., 1, 70 (1948).

104. D. Sayre, ibid., 5, 60 (1952).

105. W. Cochran and M.M. Woolfson, ibid., 8, 1 (1955).

106. W.N. Zachariasen, ibid., 5, 68 (1952).

107. J. Karle and H. Hauptman, ibid., 9, 635 (1956).

108. J. Karle, ibid., B27, 2063 (1971).

109. P. Main, M.M. Woolfson and G. Germain, Acta Crystallogr., B26, 274 (1970).

110. P. Main, M.M. Woolfson and G. Germain, MULTAN. A Computer Program For The Automatic Solution Of Crystal Structures, University of Louvain, Belgium (1971).

111. G. Germain, P. Main and W.W. Woolfson, Acta Crystallogr., A27, 368 (1971).

112. A. Zalkin, FORDAP. A Fortran Program For Fourier Calculation, University of California, Berkeley (1965).

113. W.R. Busing, K.O. Martin and H.A. Levy, ORFLS. Oak Ridge National Laboratory Report ORNL-TM-305 (1963).

114. D.T. Cromer and J.B. Mann, Acta Crystallogr., A24, 321 (1968).

115. R.F. Stewart, E.R. Davidson and W.T. Simpson, J. Chem. Phys., 42, 3175 (1965).

116. D.T. Cromer, Acta Crystallogr., 18, 17 (1965).

117. S.H. Hunter, K. Emerson and G.A. Rodley, Chem. Commun., 1398 (1969).

118. R.J. Gillespie, J. Chem. Soc., 4672 (1963).

119. R.J. Gillespie, ibid., 4679 (1963).

120. E.L. Muetterties, Acct. Chem. Res., 3, 266 (1970).

121. R. Morassi, I. Bertini and L. Sacconi, Coord. Chem. Rev., 11, 343 (1973)

122. J.K. Burdett, Inorg. Chem., 15, 212 (1976).

123. W.J. Mortier, J.J. Pluth and J.V. Smith, Nature, 256, 718 (1975).

124. B. Reuter and E. Riedel, Z. Anorg. Allg. Chem., 369, 306 (1969).

125. H. Brusset, H. Gillier-Pandraud and S.M. Delcroix, Bull. Soc. Chim. France, 3364 (1966).

126. G.E. Bacon, Acta Crystallogr., 5, 684 (1952).

127. C. Kratky and J.D. Dunitz, ibid., 31, S49 (1975).

128. C. Kratky and J.D. Dunitz, ibid., 31, 1586 (1975).

129. M. Vallino, J. Organomet. Chem., 20, 1 (1969).

130. G. Stucky and R.E. Rundle, J. Am. Chem. Soc., 86, 4821 (1964).

131. A. Zemann and J. Zemann, Acta Crystallogr., 14, 835 (1961).

132. R. Timkovich and A. Tulinsky, J. Am. Chem. Soc., 91, 4430 (1969).

133. M.S. Fischer, D.H. Templeton, A. Zalkin and M. Calvin, ibid., 93, 2622 (1971).

134. H.C. Chow, R. Serlin and C.E. Strouse, ibid., 97, 7230 (1975).

135. K. Ballschmiter and J.J. Katz, ibid., 91, 2661 (1969).

136. R.S. Rosenberg, C.A. Root and H.B. Gray, ibid., 97, 21 (1975).

137. M.H. West and J.I. Legg, ibid., 98, 6945 (1976).

138. S.H. Hunter, Ph.D. Thesis, University of Canterbury, N.Z. (1969).

139. G.B. Jameson, B.Sc.(Hons) Report, University of Canterbury, N.Z. (1973).

140. L. Sacconi, P.L. Orioli and M. Di Vaira, J. Am. Chem. Soc., 87, 2059 (1965).

141. P.L. Orioli, M. Di Vaira and L. Sacconi, ibid., 88, 4383 (1966).

142. E.B. Fleischer and S.W. Hawkinson, Inorg. Chem., 7, 2312 (1968).

143. H.S. Preston and C.H.L. Kennard, Chem. Commun. 819 (1968).

144. H.S. Preston and C.H.L. Kennard, J. Chem. Soc., (A), 2682 (1969).

145. J.I. Legg, D.O. Nielson and D.L. Smith, J. Am. Chem. Soc., 90, 5030 (1968).

146. M. Di Vaira and L. Sacconi, Chem. Commun., 10 (1969).

147. N.A. Bailey, J.G. Gibson and E.D. McKenzie, ibid., 741 (1969).

148. P.S. Shetty, R.E. Ballard and Q. Fernando, ibid., 717 (1969).

149. W. Mazurek, A.T. Philip, B.E. Hoskins and F.D. Whillians, ibid., 184 (1970).

150. B.F. Hoskins and F.D. Whillians, J. Chem. Soc., (Dalton), 657 (1975).

151. R. Serlin, H.C. Chow and C.E. Strouse, J. Am. Chem. Soc., 97, 7237 (1975)

152. D.F. Koenig, Acta Crystallogr., 18, 663 (1965).

153. J.L. Hoard, M.J. Hamor, T.A. Hamor and W.S. Caughey, J. Am. Chem. Soc., 87, 2312 (1965).

154. R.C. Pettersen and L.E. Alexander, ibid., 90, 3873 (1968).

155. J.L. Hoard, G.H.Cohen and M.D. Glick, ibid., 89, 1992 (1967).

156. G.B. Jameson, private communication (1976).

157. E. Frasson, C. Panattoni and L. Sacconi, J. Phys. Chem., 63, 1908 (1959

158. M.R. Fox, P.L. Orioli, E.C. Lingafelter and L. Sacconi, Acta Crystallogr., 17, 1159 (1964).

159. P.L. Orioli, M. Di Vaira and L. Sacconi, Chem. Commun., 300 (1966).

160. F.K. Ross, G.D. Stucky, Inorg. Chem., 8, 2734 (1969).

161. M. Seleborg, S.L. Holt and B. Post, ibid., 10, 1501 (1971).

162. P. Dapporto and L. Sacconi, J. Chem. Soc., (A), 618 (1970).

163. P.L. Orioli and M. Di Vaira, ibid., (A), 2078 (1968).

164. L. Sacconi, P.L. Orioli and M. Di Vaira, Chem. Commun., 849 (1967).

165. P. Jose, L.M. Pant and A.B. Biswas, Acta Crystallogr., 17, 24 (1964).

166. H.C. Freeman, J.M. Guss and R.L. Sinclair, Chem. Commun., 485 (1968).

167. C.W. Reimann and M. Zocchi, Acta Crystallogr., B27, 683 (1971).

168. L.F. Power and A.M. Tait, Inorg. Nucl. Chem. Lett., 7, 337 (1971).

169. T.C. Downie, W. Harrison and E.S. Raper, Acta Crystallogr., B27, 706 (1971).

170. H. Loiseleur, ibid., B28, 816 (1972).

171. J. Podlahova and J. Loub, ibid., B28, 1623 (1972).

172. A.F. Cameron, D.W. Taylor and R.H. Nuttal, J. Chem. Soc., (Dalton), 422 (1972).

173. M.E. Stone, B.E. Robertson and E. Stanley, ibid., (A), 3632 (1971).

174. J. Drew, M.B. Hursthouse and P. Thornton, ibid., (Dalton), 1658 (1972).

175. R.J. Irving, M.L. Post and D.C. Povey, ibid., (Dalton), 697 (1973).

176. N.F. Curtis, I.R.N. McCormick and T.N. Waters, ibid., (Dalton), 1537 (1973).

177. S. Guha, Acta Crystallogr., B29, 2167 (1973).

178. S. Ray, A. Zalkin and D.H. Templeton, ibid., B29, 2741 (1973).

179. R. Louis, B. Metz and R. Weiss, ibid., B30, 774 (1974).

180. R.L. Lintvedt, L.L. Borer, D.P. Murtha, J.M. Kuszaj and M.D. Glick, Inorg. Chem., 13, 18 (1974).

181. G.R. Clark and J.D. Orbell, Chem. Commun., 139 (1974).

182. E.C. Alyea, G. Ferguson and R.J. Restivo, Inorg. Chem., 14, 2491 (1975).

183. F.S. Ezra and R.L. Collin, Acta Crystallogr., B29, 1398 (1973).

184. F. Dahan, ibid., B30, 22 (1974).

185. M.O. Julian, V.W. Day and J.L. Hoard, Inorg. Chem., 12, 1754 (1973).

186. C. Calvo, Acta Crystallogr., 23, 289 (1967).

187. J. Toney and G.D. Stucky, J. Organomet. Chem., 28, 5 (1971).

188. A.G. Nord and P. Kierkegaard, Acta Chem. Scand., 22, 1466 (1968).

189. C.K. Johnson, Acta Crystallogr., 18 , 1004 (1965).

190. B. Morosin, ibid., 22, 315 (1967).

191. M. Vijayan and M.A. Viswamitra, ibid., 23, 1000 (1967).

192. M.C. Percaud and M.T. Le Bihan, ibid., B24, 1502 (1968).

193. M.R. Truter and B.L. Vickery, J. Chem. Soc., (Dalton), 395 (1972).

194. A.A. Khan and W.H. Baur, Acta Crystallogr., B28, 683 (1972).

195. W.H. Baur and J.L. Rolin, ibid., B28, 1448 (1972).

196. H. Flack, ibid., B29, 656 (1973).

197. F.J. Hollander, D.H. Templeton and A. Zalkin, ibid., B29, 1289 (1973).

198. G. Blank, ibid., B29, 1677 (1973).

199. A.G. Nord and K.B. Lindberg, Acta Chem. Scand., A29, 1 (1975).

200. C.I. Branden, ibid., 17, 1363 (1963).

201. W.A. Cullen and J. Trotter, Can. J. Chem., 41, 2983 (1963).

202. G.S. Harris, F. inglis, H.J. McKechnie, K.K. Cheung and G. Fegruson, Chem. Commun., 442 (1967).

203. C. Panattoni, R. Graziani, U. Croatto, B. Zarli and G. Bombieri, Inorg. Chim. Acta, 2, 43 (1968).

204. G. Ferguson and E.W. Macaulay, J. Chem. Soc., (A), 1 (1969).

205. F.F. Farris and W.R. Robinson, J. Organomet. Chem., 31, 375 (1971).

206. P.J.M.W.L. Birker, P. Prick and P.T. Beurskens, Cryst. Struct. Commun., 5, 135 (1976).

207. B. Birknes, Acta Chem. Scand., B30, 450 (1976).

208. W.H. Baur and A.A. Khan, Acta Crystallogr., B26, 1584 (1970).

209. A.A. Khan, M.E. Straumanis and W.J. James, ibid., B26, 1889 (1970).

210. D.W.J. Cruickshank, J. Chem. Soc., 5486 (1961).

211. F.M. Aubry and G.M. Brown, Acta Crystallogr., B24, 745 (1968).

212. L.J. Nassimbeni and M.M. Thackeray, ibid., B30, 1072 (1974).

213. G. Raper, W.S. McDonald, ibid., B29, 2013 (1973).

214. M. Sekizaki, ibid., B29, 327 (1973).

215. J.R. Fritch, G.G. Christoph and W.P. Schaefer, Inorg. Chem., 12, 2170 (1973).

216. K.N. Raymond, P.W.R. Corfield and J.A. Ibers, ibid., 7, 1362 (1968).

217. T.G. Spiro, K.N. Raymond and A. Terzis, ibid., 9, 2415 (1970).

218. B.A. Coyle and J.A. Ibers, ibid., 9, 767 (1970).

219. F.C. March, G. Ferguson and D. Lloyd, J. Chem. Soc., (Dalton), 1377 (1975).

220. E.I. Stiefel, R. Eisenberg, R.C. Rosenberg and H.B. Gray, J. Am. Chem. Soc., 88, 2956 (1966).

221. G.N. Schrauzer and V.P. Mayweg, ibid., 88, 3235 (1966).

222. C.G. Pierpont and R. Eisenberg, J. Chem. Soc., (A), 2285 (1971).

223. J.L. Martin and J. Takats, Inorg. Chem., 14, 1358 (1975).

224. E.I. Stiefel, Z. Dori and H.B. Gray, J. Am. Chem. Soc., 89, 3353 (1967).

225. M. Cowie and M.J. Bennett, Inorg. Chem., 15, 1595 (1976).

226. F.A. Cotton and G. Wilkinson, 'Advanced Inorganic Chemistry', Wiley, New York, N.Y., p. 52 (1972).

227. G. Ciani, M. Manassero and M. Sansoni, J. Inorg. Nucl. Chem., 34, 1760 (1972).

228. J.R. Preer and H.B. Gray, J. Am. Chem. Soc., 92, 7306 (1970).

229. W.R. Cullen and J. Trotter, Can. J. Chem., 40, 1113 (1962).

230. E.R. Lippincott, J. Xavier and D. Steele, J. Am. Chem. Soc., 83, 2262 (1961).

231. F.A. Cotton and L.T. Reynolds, ibid., 80, 269 (1958).

232. G.M. Begun and R.N. Compton, J. Chem. Phys., 58, 2271 (1973).

233. S. Evans, M.L.H. Green, B. Jewitt, A.F. Orchard and C.F. Pygall, J. Chem. Soc., (Faraday II), 68, 1847 (1972).

234. A. Haaland, J. Lusztyk, J. Brunvoll and K.B. Starowieyski, J. Organomet. Chem., 85, 279 (1975).

235. P.J. Wheatley, 'Perspectives in Structural Chemistry', Ed. J.D. Dunitz and J.A. Ibers, Wiley, New York, N.Y., Vol. II, p. 1 (1967).

236. E. Weiss and E.O. Fischer, Z. Anorg. Allg. Chem., 278, 219 (1955).

237. R.M. Izatt, J.L. Christensen and J.H. Rytting, Chem. Rev., 71, 439 (1971).

238. R.O. Inlow and M.D. Joesten, J. Inorg. Nucl. Chem., 37, 2353 (1975).

239. G.A. Rodley and Y.S. Ng, J. Appl.Crystallogr., In Press.

240. The data processing program HILGOUT is based on programs (DRED) by J.F. Blount and (PICKOUT) by R.J. Doedens.

241. W.C. Hamilton and J.A. Ibers, 'Hydrogen Bonding In Solids', Benjamin, New York, N.Y., p. 16 (1968).

242. A. Zalkin, J.D. Forrester and D.H. Templeton, J. Chem. Phys., 39, 2881 (1963).

243. T.N. Margulis and D.H. Templeton, Z. Kristallogr., Kristallogeometrie., Kristall-phys., Kristall-chem., 117, 344 (1962).

244. A. Zalkin, H. Ruben and D.H. Templeton, Acta Crystallogr., 17, 235 (1964).

245. H.K. Wang, Acta Chem. Scand., 19, 879 (1965).

246. C.J. Wilkins, K. Hagen, L. Hedberg, Q. Shen and K. Hedberg, J. Am. Chem. Soc., 97, 6352 (1975).

247. F.A. Cotton and R.H. Soderberg, ibid., 85, 2402 (1963).

248. C.I. Branden and I. Lindqvist, Acta Chem. Scand., 15, 167 (1961).

249. G. Bombieri, E. Forsellini, D. Brown and B. Whittaker, J. Chem. Soc., (Dalton), 735 (1976).

250. G. Bandoli, G. Bortolozzo, D.A. Clemente, U. Croato and C. Panattoni, ibid., (A), 2778 (1970).

251. G. Ruban and V. Zabel, Cryst. Struct. Commun., 5, 493 (1976).

252. M.M. Mangion, R. Smith and S.G. Shore, Cryst. Struct. Commun., 5, 493 (1976).

253. J.A. Bertrand and A.R. Kalyanaraman, Inorg. Chim. Acta, 5, 341 (1971).

254. J.A. Bertrand, Inorg. Chem., 6, 495 (1967).

255. J.A. Bertrand and J.A. Kelley, J. Am. Chem. Soc., 88, 4746 (1966).

256. D.L. Kepert, D. Taylor and A.H. White, J. Chem. Soc., (Dalton), 1658 (1973).

257. M.U. Haque, C.N. Caughlan, F.A. Hart and R. van Nice, Inorg. Chem., 10, 115 (1971).

258. G. Bombieri, D. Brown and R. Graziani, J. Chem. Soc., (Dalton), 1873 (1975).

259. C. Panattoni, G. Bandoli, R. Graziani and U. Croatto, Chem. Commun., 278 (1968).

260. L.L. Koh and K. Eriks, Acta Crystallogr., B27, 1405 (1971).

261. E.D. Estes, W.E. Hatfield and D.J. Hodgson, Inorg. Chem., 13, 1654 (1974)

262. M.F. Perutz, Nature, (London), 228, 726 (1970).

263. F.A. Cotton, R.D. Barnes and E. Bannister, J. Chem. Soc., 2199 (1960).

264. A.M. Brodie, J.E. Douglas and C.J. Wilkins, ibid., (A), 1931 (1969).

265. D.L. Lewis, W.E. Hatfield and D.J. Hodgson, Inorg. Chem., 11, 2216 (1972)

266. E.D. Estes and D.J. Hodgson, ibid., 15, 348 (1976).

267. H. Lipson and W. Cochran, 'The Determination Of Crystal Structures', G. Bell Ltd., p. 79 (1966).

268. W.J.A.M. Peterse and J.H. Palm, Acta Crystallogr., 20, 147 (1966).

269. H. Levy, ibid., 9, 679 (1956).

270. K.N. Trueblood, P. Horn and V. Luzzati, ibid., 14, 965 (1961).

271. L. Mazzarela, A.L. Kovacs, P. De Santis and A.M. Liquori, ibid., 22, 65 (1967).

272. T. Kubota, T. Tokoroyama, Y. Tsukuda, H. Koyama and A. Miyake, Science, 179, 400 (1973).

273. Van der Helm and T.V. Willoughby, Acta Crystallogr., B25, 2317 (1969).

274. C.E. Bugg, J. Am. Chem., Soc., 95, 908 (1973).

275. H. Einspahr and C.E. Bugg, Acta Crystallogr., B30, 1037 (1974).

276. J.M. Epstein, B.N. Figgis, A.H. White and A.C. Willis, J. Chem. Soc., (Dalton), 1954 (1974).

277. J.L. De Boer and A. Vos, Acta Crystallogr., B28, 835 (1972).

278. A. Camerman, L.H. Jensen and A.T. Balaban, ibid., B25, 2623 (1969).

279. R. Norrestam and O. Tillberg, ibid., B28, 1704 (1972).

280. O.P. Anderson, J. Chem. Soc., (Dalton), 1237 (1973).

281. R.J. Prosen and K.N. Trueblood, Acta Crystallogr., 9, 741 (1956).

282. M. Ito, F. Marumo and Y. Saito, ibid., B28, 463 (1972).

283. F.M. Aubry, ibid., B24, 754 (1968).

284. M. Przybylska, ibid., B30, 2455 (1974).

285. R. Jungst and G. Stucky, Inorg. Chem., 13, 2404 (1974).

286. L. Pauling, 'The Nature Of The Chemical Bond', Cornell University Press, p. 514 (1960).

287. F. Hollander, D.H. Templeton and A. Zalkin, Acta Crystallogr., B29, 1295 (1973).

288. V.A. Uchtman, J. Phys. Chem., 76, 1298 (1972).

289. H. Einspahr and C.E. Bugg, Acta Crystallogr., B30, 1037 (1974).

290. R.H. Kretsinger, D.J. Nelson, Coord. Chem. Rev., 18, 29 (1976).

291. V.A. Uchtman and R.J. Jandecek, private communication, (1975).

292. F.A. Cotton and D.A. Ucko, Inorg. Chem. Acta, 6, 161 (1972).

293. H.M. Powell and A.F. Wells, J. Chem. Soc., 1008 (1935).

294. J.L. Hoard and L. Goldstein, J. Chem. Phys., 3, 199 (1935).

295. O. Lindqvist, Acta Chem. Scand., 22, 2943, (1963).

296. H.M. Powell and R.V.G. Ewens, J. Chem. Soc., 286 (1939).

297. P. Andersen, Acta Chem. Scand., 21, 243 (1967).

298. A.M. Greenaway, Ph.D. Thesis, University of Canterbury, N.Z. (1976).

299. S. Milicev and D. Hadzi, Inorg. Nucl. Chem. Lett., 7, 745 (1971).

300. S. Milicev and D. Hadzi, Inorg. Chem. Acta, (1976).

301. F. Lazarini and L. Golic, Acta Crystallogr., A31, S140 (1975).

302. F. Lazarini and L. Golic, J. Cryst. Mol. Struct., 6, 113 (1976).

303. F. Lazarini and S. Milicev, Acta Crystallogr., B32, 2873 (1976).

304. S.H. Hunter, G.A. Rodley and K. Emerson, Inorg. Nucl. Chem. Lett., 12, 113 (1976).

305. E.L. Muetterties and Schunn, Quart. Rev., 20, 245 (1966).

306. L. Sacconi, Pure Appl. Chem. 17, 95 (1968).

307. C. Furlani, Coord. Chem. Rev., 3, 141 (1968).

308. J.S. Wood, 'Progress In Inorganic Chemistry', Ed. S.J. Lippard, 16, 227 (1972).

309. R.S. Berry, J. Chem. Phys., 32, 933 (1960).

310. J. Zemann, Z. Anorg. Allg. Chem., 324, 241 (1963).

311. D.L. Kepert, Inorg. Chem., 12, 1938 (1973).

312. P.L. Orioli, Coord. Chem. Rev., 6, 285 (1971).

313. B.F. Hoskins and F.D. Whillans, Coord. Chem. Rev., 9, 365 (1973).

314. M. Ciampolini, Structure and Bonding, 6, 52 (1969).

315. P.C. Van Der Voorn and R.S. Drago, J. Am. Chem. Soc., 88, 3255 (1966).

316. C.J. Ballhausen, R.S. Berry, H. Johnsen and M. Tamres, Acta Chem. Scand., 22, 231 (1968).

317. A. Rossi and R. Hoffmann, Inorg. Chem., 14, 365 (1975).

318. S.Z. Goldberg and R. Eisenberg, Inorg. Chem., 15, 58 (1976).

319. W. Clegg, D.A. Greenhalgh and B.P. Straughan, J. Chem. Soc., (Dalton), 2591 (1975).

320. C. Heath and M.B. Hursthouse, Chem. Commun. 143 (1971).

321. I. Bernal, N. Elliot and R. Lalancette, ibid, 803 (1971).

322. J.S. Wood and J. Drummond, ibid., 1373 (1969).

323. E.R. Riedel and R.A. Jacobson, Inorg. Chim. Acta, 4, 407 (1970).

324. B. Beagley and D.G. Schmidling, J. Mol. Struct., 22, 466 (1974).

325. F.A. Cotton, T.G. Dunne and J.S. Wood, Inorg. Chem., 4, 318 (1965).

326. R.D. Cramer, R.V. Lindsey, C.T. Prewiittand U.G.Stolberg, J.Am. Chem. Soc., 87, 658 (1965).

327. B.A. Frenz and J.A. Ibers, Inorg. Chem., 11, 1109 (1972).

328. K.N. Raymond, D.W. Meek and J.A. Ibers, ibid., 7, 1111 (1968).

329. S.A. Goldfield and K.N. Raymond, ibid., 10, 2604 (1971).

330. E.F. Epstein and I. Bernal, J. Chem. Soc., (A), 3628 (1971).

331. D.S. Brown, F.W.B. Einstein and D.G. Tuck, Inorg. Chem., 8, 14 (1969).

332. F.B. Clippard and L.S. Bartell, ibid., 9, 805 (1970).

333. A.L. Beauchamp, M.J. Bennett and F.A. Cotton, J. Am. Chem. Soc., 90, 6675 (1968).

334. C.P. Brock and J.A. Ibers, Acta Crystallogr., A32, 38 (1976).

335. H. Rojhantalab and J.W. Nibler, Spectrochim. Acta, A32, 519 (1976).

336. R. Pantzer, W. Schmidt and J. Goubeau, Z. Anorg. Allg. Chem., 395, 262 (1973).

337. H. Rojhantalab and J.W. Nibler, Spectrochim. Acta, A32, 947 (1976).

338. F. Watari, ibid., A31, 1143 (1975).

339. F. Choplin and G. Kaufmann, ibid., A26, 2113 (1970).

340. M.W. Lister and L.E. Sutton, Trans. Faraday Soc., 35, 495 (1939).

341. H.D. Springall and L.O. Brockway, J. Am. Chem. Soc., 60, 996 (1938).

342. L.S. Bartell and L.O. Brockway, J. Chem. Phys., 32, 512 (1960).

343. D.R. Lide and D.E. Mann, ibid., 29, 914 (1958).

344. D.R. Lide, Spectrochim. Acta, 15, 473 (1959).

345. L.C. Thomas and R.A. Chittenden, ibid., 20, 467 (1964).

346. G.B. Deacon and J.H.S. Green, ibid., A24, 845 (1968).

347. M.J. Frazer, W. Gerrard and R. Twaits, J. Inorg. Nucl. Chem., 25, 637 (1963).

348. G.B. Deacon and J.H.S. Green, Spectrochim. Acta, A25, 355 (1969).

349. A. Merijanian and R.A. Zingaro, Inorg. Chem., 5, 187 (1966).

350. B.J. Hathaway and A.E. Underhill, J. Chem. Soc., 3091 (1961).

351. I. Nakagawa and T. Shimanouchi, Spectrochim. Acta, 20, 429 (1964).

352. A.M. Brodie, Ph.D. Thesis, University of Canterbury, N.Z. (1968).

353. A. Chakravorty, 'Spectroscopy In Inorganic Chemistry', Ed., C.R. Rao and J.R. Ferraro, p. 247 (1970).

354. L. Elegant, R. Wolf and M. Azzaro, Bull. Soc. Chim. France, 4269 (1969

355. M. Becke-Goehring and A. Slawisch, Z. Anorg. Allg. Chem., 346, 295 (1966).

356. O. Rougues and R. Poilblanc, J. Organomet. Chem., 24, C47 (1970).

357. K.E. Quah, M.Sc. Thesis, University of Canterbury, N.Z. (1975).

358. R.H. Boyd, J. Chem. Phys., 49, 2574 (1968).

359. I thank Dr. M.H.G. Munro for running the ^{13}C nmr.

360. M.D. Joesten, M.S. Hussain and P.G. Lenhert, Inorg. Chem., 9, 151 (1970).

361. J.A. Pople and G.A. Segal, J. Chem. Phys., 44, 3289 (1966).

362. S.P. McGlynn, L.G. Vanquickborne, M. Kinoshita and D.G. Carroll, 'Introduction To Applied Quantum Chemistry', Holt, Rinehart and Winston, p. 426 (1972).

363. G.B. McVicker, Inorg. Chem., 14, 2087 (1975).

364. G.B. McVicker and R.S. Matyas, Chem. Commun., 972 (1972).

365. S.W. Ulmer, P.M. Skarstad, J.M. Burlitch and R.E. Hughes, J. Am. Chem. Soc., 95, 4469 (1973).

366. M.S. Bains, Can. J. Chem., 42, 945 (1964).

367. M.N. Hughes, 'The Inorganic Chemistry Of Biological Processes', Wiley, London, (1972).

368. R.J.P. Williams, Quart. Rev., 24, 331 (1970).

369. Govinjee, 'Bioenergetics Of Photosynthesis', Academic Press, New York, p. 1 (1975).

370. J.J. Katz, 'Inorganic Biochemistry', Ed., G.L. Eichhorn, Elsevier, Vol. II, Chap. 29, p.1022 (1974).

371. Y. Tonomura and F. Oosawa, Ann. Rev. Biophys. Bioengin., 1, 159 (1972).

372. H.E. Huxley, Scientific American, 213(6), 18 (1965).

373. J.H. Wang, Acct. Chem. Res., 3, 90 (1970).

374. J.J. Katz and J.R. Norris, 'Current Topics Of Bioenergetics', Ed., D.R. Sanadi and L. Packer, 5, p. 41 (1973).

375. T.A. Evans and J.J. Katz, Biochim. Biophys. Acta, 396, 414 (1975).

376. T.M. Cotton, A.D. Trifunac, K. Ballschmiter and J.J. Katz, Biochim. Biophys. Acta, 368, 181 (1974).

377. K. Ballschmiter and J.J. Katz, Biochim. Biophys. Acta, 256, 306 (1972)

378. J.R. Norris, H. Schaer and J.J. Katz, Ann. N.Y. Acad. Sci., 244, 260 (1975).

379. G. Beddard, Nature, (London), 263, 459 (1976).

380. J.R. Norris, R.A. Uphaus, H.L. Crespi and J.J. Katz, Pro. Nat. Acad. Sci., 68, 625 (1971).

381. G. Feher, A.J. Hoff, R.A. Issacson and L.C. Ackerson, Ann. N.Y. Acad. Sci., 244, 238 (1975).

382. F.K. Fong, Pro. Nat. Acad. Sci., 71, 3692 (1974).

383. F.K. Fong, J. Theor. Biol., 46, 407 (1974).

384. C.E. Strouse, 'Progress In Inorganic Chemistry', Ed., S.J. Lippard, 21, p. 159 (1976).

385. G. Offer, 'Companion To Biochemistry', Ed., A.T. Bull, Longman, London, p.623 (1974).

386. J.M. Squire, Ann. Rev. Biophys. Bioengin., 4, 137 (1975).

387. H.E. Huxley, Science, 164, 1356 (1969).

388. A. Waber and J.M. Murray, Physiol. Rev., 53, 612 (1973).

389. G. Hoyle, Scientific American, 222(4), 84 (1970).

390. D.A.D. Parry and J.M. Squire, J. Mol. Biol., 75, 33 (1973).

391. C. Cohen, Scientific American, 233(5), 36 (1975).

392. A. Szent-Gyorgyi, Pro. Nat. Acad. Sci., 71, 3343 (1974).

393. R.H. Kretsinger and C.E. Nockolds, J. Biol. Chem., 248, 3313 (1973).

(13) J. M. Haschke and H. A. Eick, *J. Am. Chem. Soc.*, 92, 1526 (1970).
(14) J. M. Haschke, *Inorg. Chem.*, 14, 779 (1975).
(15) K.-F. Seifert, *Fortschr. Mineral.*, 45, 214 (1968).
(16) H. Baernighausen, H. P. Beck, and H.-W. Grueninger, *Proc. Rare Earth Res. Conf., 9th*, 1, 74 (1971).
(17) H. Baernighausen, *Rev. Chim. Miner.*, 10, 77 (1973).
(18) M. J. Buerger, *J. Chem. Phys.*, 15, 1 (1947).
(19) J. Neubueser and H. Wondratschek, *Krist. Tech.*, 1, 529 (1966).
(20) J. Neubueser and H. Wondratschek "Maximal Subgroups and Minimal Supergroups of the Space Groups", private communication with H. Wondratschek, University of Karlsruhe, Karlsruhe, West Germany, 1974.
(21) D. Brown, "Halides of the Lanthanides and Actinides", Wiley, New York, N.Y., 1968.
(22) J. D. Corbett, *Rev. Chim. Miner.*, 10, 239 (1973).
(23) L. F. Druding, J. D. Corbett, and N. B. Ramsey, *Inorg. Chem.*, 2, 869 (1963).
(24) G. I. Novikov and O. G. Polyachenok, *Zh. Neorg. Khim.*, 8, 1053 (1963); *Russ. J. Inorg. Chem.*, 8, 545 (1963).
(25) L. F. Druding and J. D. Corbett, *J. Am. Chem. Soc.*, 83, 2462 (1961).
(26) N. A. Fishel and H. A. Eick, *J. Inorg. Nucl. Chem.*, 33, 1201 (1971).
(27) O. G. Polyachenok and G. I. Novikov, *Zh. Neorg. Khim.*, 8, 2818 (1963); *Russ. J. Inorg. Chem.*, 8, 1478 (1963).
(28) U. Loechner and J. D. Corbett, *Inorg. Chem.*, 14, 426 (1975).
(29) J. D. Corbett and B. C. McCollum, *Inorg. Chem.*, 5, 938 (1966).
(30) P. E. Caro and J. D. Corbett, *J. Less-Common Met.*, 18, 1 (1969).
(31) J. D. Corbett, L. F. Druding, W. J. Burkhard, and C. B. Lindahl, *Discuss. Faraday Soc.*, 32, 79 (1961).
(32) R. A. Sallach and J. D. Corbett, *Inorg. Chem.*, 2, 457 (1963).
(33) J. D. M. Bevan in "Comprehensive Inorganic Chemistry", Vol. 4, J. C. Bailar, Jr., H. J. Emeleus, R. Nyholm, and A. F. Trotman-Dickenson Ed., Pergamon Press, Oxford, 1973, Chapter 49.
(34) J. M. Haschke, *J. Solid State Chem.*, 14, 238 (1975).
(35) A. N. Christensen, *Acta Chem. Scand.*, 19, 1391 (1965).
(36) A. F. Wells, "Structural Inorganic Chemistry", 3rd ed, Oxford University Press, London, 1962, Chapter XXVI.
(37) B. G. Hyde, A. N. Bagshaw, S. Anderson, and M. O'Keeffe, *Annu. Rev. Mater. Sci.*, 4, 43–92 (1974).
(38) P. E. Caro, *Natl. Bur. Stand. (U.S.), Spec. Publ.*, No. 364, 367 (1972).

Contribution from the Department of Chemistry, University of Canterbury, Christchurch, New Zealand

Crystal Structures of the Pentakis(trimethylarsine oxide)metal(II) Perchlorates [Ni(Me3AsO)5](ClO4)2 and [Mg(Me3AsO)5](ClO4)2

Y. S. NG, G. A. RODLEY,* and WARD T. ROBINSON

Received March 13, 1975 AIC50189H

The crystal structures of two isomorphous compounds, pentakis(trimethylarsine oxide)nickel(II) perchlorate, [Ni(Me3AsO)5](ClO4)2, and its magnesium analogue, have been determined by x-ray analyses. The compounds crystallize in the centrosymmetric space group $P2_1/n$, with four molecules in unit cells of dimensions a = 11.301 (3), 11.330 (5) Å, b = 27.256 (6), 27.562 (6) Å, c = 11.294 (5), 11.328 (6) Å, and β = 90.41 (3), 90.58 (5)° for the nickel and magnesium complexes, respectively. The structures were solved using diffractometer data and difference Patterson techniques. Least-squares refinements converged with final conventional R values of 0.064 (3975 data) and 0.068 (3552 data) for the nickel and magnesium complexes, respectively. The structures consist of discrete $[M(Me_3AsO)_5]^{2+}$ (M = Ni, Mg) cations well separated from perchlorate anions. The coordination geometry around the metal atoms is approximately square pyramidal, with nickel and magnesium atoms 0.359 (3) and 0.454 (3) Å above the least-squares plane of the basal oxygen and arsenic atoms, respectively. The arrangements of atoms around the central metal atoms are discussed in terms of the different electronic properties of magnesium and nickel. Small but significant differences between the two structures indicate the binding of the Me3AsO ligands is more than simple σ donation. Other structural features, notably a large cavity in the coordination sphere, also indicate that electronic rather than steric factors govern the structures of the cations.

Introduction

It is now apparent that monodentate oxo ligands of the type R_3XO (X = P, As) readily form five-coordinate complexes with metal(II) perchlorates.[1-7] Two basic types are obtained: $[M(R_3XO)_4ClO_4](ClO_4)$[2] and $[M(R_3XO)_5](ClO_4)_2$.[8] Preliminary x-ray photographic studies of $[Co(Ph_2MeAsO)_4ClO_4]ClO_4$ and $[Ni(Me_3AsO)_5](ClO_4)_2$ have shown the cations have essentially the same square-pyramidal structures.[2,8] We have now completed detailed analyses of the latter complex and its magnesium analogue using accurate diffractometer data sets.

The present results enable us to reassess the reasons for the formation of the square-pyramidal geometry in such systems. Previously attention was focused on steric factors. We now believe electronic binding properties of the oxo ligands are of prime importance. Also small but significant differences between the nickel and magnesium structures give further insight into the bonding of oxo ligands to metal ions.

Formation of five-coordinate complexes by non transition metal ions such as calcium and magnesium has not been studied extensively. However this geometry could be of considerable importance in biological systems.

While octahedral coordination may be the most common geometry for these ions, ligand systems with appropriate properties (electronic as well as steric) readily produce five-coordinate Ca^{2+} and Mg^{2+} complexes. The magnesium structure reported here provides detailed information on a magnesium complex, representative of a range of five-coordinate complexes of Ca^{2+} and Mg^{2+} recently prepared with oxo ligands.[9] A basically similar square-pyramidal structure has been found from an x-ray analysis of a chlorophyll-like aquomagnesium tetraphenylporphyrin.[10] Also a five-coordinate structure for certain chlorophyll systems has been indicated from infrared and NMR studies.[11] In other biological systems hydrophobic regions of protein structures may facilitate coordination numbers less than 6 through the elimination of water from the coordination sphere.

Experimental Section

Orange, plate-shaped crystals of $[Ni(Me_3AsO)_5](ClO_4)_2$ were grown from an acetonitrile solution in the presence of an ether vapor.[12] Colorless, transparent, plate-shaped crystals of $[Mg(Me_3AsO)_5](ClO_4)_2$ were provided by Mr. G. B. Jameson.[9] The nickel crystals, being sensitive to moisture, were sealed in capillary tubes under a stream of nitrogen. The crystals were assigned to the monoclinic system after examination by Weissenberg and precession photography, using Cu Kα radiation. Conditions limiting possible reflections were uniquely consistent with the monoclinic space group $P2_1/c$ but it was found convenient to solve both structures using the unconventional setting $P2_1/n$ (equivalent positions: x, y, z; $-x, -y, -z$; $1/2 + x, 1/2 - y, 1/2 + z$; $1/2 - x, 1/2 + y, 1/2 - z$). All data in this paper refer to this latter space group setting.

Unit cell parameters were obtained by least-squares analysis of the setting angles of 12 reflections accurately centered in a 5.0-mm

Table I. Crystal Data

	$[Ni(Me_3AsO)_5](ClO_4)_2$	$[Mg(Me_3AsO)_5](ClO_4)_2$
Formula wt	937.74	903.34
a/Å	11.301 (3)	11.330 (5)
b/Å	27.256 (6)	27.562 (6)
c/Å	11.294 (5)	11.328 (6)
β/deg	90.41 (3)	90.58 (5)
V_c/Å^3	3478.8	3537.5
d_{measd}/g cm^{-3}		1.73
d_{calcd}/g cm^{-3}	1.79	1.70
Z	4	4
Max crystal dimension/mm	0.5	0.43
Min crystal dimension/mm	0.13	0.18

diameter collimator with its circular receiving aperture set at 230 mm from the crystal on a Hilger and Watts four-circle computer-controlled diffractometer (24°). Important crystal data are summarized in Table I. The figures in parentheses in Table I and elsewhere in this paper are estimated standard deviations in the least significant figures quoted and were usually derived from the inverse matrix in the course of normal least-squares refinement calculations.

The density of the nickel complex was not measured because of its sensitivity to moisture. However, the density of the magnesium complex was determined by flotation in a mixture of bromobenzene and dibromoethane.[13] This value agrees satisfactorily with the calculated density for 4 molecules in the unit cell. No crystallographic symmetry is imposed on individual molecules.

Collection and Reduction of Intensity Data

Data were collected using well-formed plate-shaped crystals. The boundary faces were identified and their distances from arbitrary origins in the crystals measured using a binocular microscope.

The mosaicity of each crystal was examined by means of open-counter ω scans at a takeoff angle of 3°. Intensities were collected using Zr-filtered Mo Kα x radiation for the Ni^{2+} complex whereas Ni-filtered Cu Kα x radiation was used for the Mg^{2+} complex. The intensities of all reflections were recorded using the θ–2θ scan techniques. Calibrated attenuators were used to bring strong reflections within the linear response range of the scintillation counter whenever counting rates exceeded 8000 counts/sec.

Throughout the data collection, three standard reflections were referred to regularly. These reflections dropped to 63% of their initial values in the case of the nickel complex. All reflections were adjusted to the same relative scale. No great fluctuations in the standard reflections occurred for the magnesium complex.

The standard deviation for each measured intensity was

$$\sigma(I) = [C + 0.25(t_c/t_b)^2(B_1 + B_2) + (pI)^2]^{1/2}$$

where C is the scan count, t_c and t_b are scan and background times, B_1 and B_2 are the background counts, p is assigned a value of 0.05 and is a factor used to avoid overweighting more intense reflections, and I was obtained from

$$I = C - 0.5(t_c/t_b)(B_1 + B_2)$$

Data were corrected for Lorentz–polarization effects and then for absorption[14] in the two compounds. Data collection and processing details are summarized in Table II.

Solution and Refinement of the Structures

In all least-squares refinements, the function minimized[15] was $\sum w(|F_o| - |F_c|)^2$, where w is assigned as $4F_o^2/\sigma(F_o^2)^2$, and $|F_o|$ and $|F_c|$ are the observed and calculated structure factor amplitudes respectively. Atomic scattering factors for nonhydrogen atoms were obtained from Cromer and Mann[16] and those for hydrogen atoms were from Stewart et al.[17] The real and imaginary contributions of anomalous scattering, $\Delta f'$ and $\Delta f''$, for As, Ni, Cl, and Mg were from Cromer's tabulation.[18] The conventional R factors are defined as

$$R_1 = \Sigma||F_o| - |F_c||/\Sigma|F_o|$$

$$R_2 = (\Sigma w(|F_o| - |F_c|)^2/\Sigma w|F_o|^2)^{1/2}$$

The original structure analysis, using film data and symbolic addition procedures, had converged with an R factor of 0.13 (1171 data).[8] However, these atom parameters did not lead to satisfactory refinements with the new diffractometer data sets and were abandoned. The positions of the central metal atom and the five arsenic atoms were then obtained from the difference between Patterson syntheses calculated using the diffractometer data sets.[19] Both of the unsharpened Patterson maps for the Ni^{2+} and Mg^{2+} complexes were placed on the same relative scale by equating average, dominant, equivalent As–As vector peak densities. The map for the magnesium complex was subtracted from that of the nickel. An image of a square-pyramidal arrangement of five arsenic atoms about one metal atom was located with the metal atom centered at the origin. A similar arrangement, presumed related by a twofold screw axis, was also discerned and served to position these atoms absolutely in real space. Full-matrix least-squares refinements of positional and isotropic thermal parameters for these six atoms, using data from the magnesium complex, led to values of 0.366 and 0.445 for R_1 and R_2, respectively. A difference Fourier synthesis showed the locations of all the nonhydrogen atoms in the structure except the apical methyl carbon atoms of the cation and the oxygen atoms of the perchlorate anions. The remaining atoms were found from successive structure factor calculations and difference Fourier syntheses. Refinements were carried out using isotropic temperature factors and this model gave $R_1 = 0.120$ and $R_2 = 0.160$. The same positional parameters and isotropic temperature factors were transferred to the nickel complex and refined to convergence with $R_1 = 0.120$ and $R_2 = 0.137$, respectively. A difference Fourier synthesis at this stage showed considerable anisotropic thermal motion for most atoms in the structure. Core storage limitations of our computer permitted only 176 parameters to be varied simultaneously. Therefore, least-squares refinements using anisotropic temperature factors were carried out in two separate blocks for each structure. The scale factor and all parameters for the nickel and axial arsenic atoms were varied in both blocks. The parameters for the perchlorate anions, the four basal arsenic atoms, and the axial ligand carbon atoms were varied in the first block. The parameters for all of the arsine oxide oxygen and basal methyl carbon atoms were varied in the second block. These refinements converged with $R_1 = 0.064$ and $R_2 = 0.076$ for the nickel structure and $R_1 = 0.068$ and $R_2 = 0.083$ for the magnesium structure. These low R factors and the extremely close similarity of the two structures are taken to indicate that both refined models are correct. However two of the methyl carbons, in the Ni^{2+} complex only, C(22) and C(42) had non-positive-definite temperature factors indicating that the thermal ellipsoid representation for these two atoms was not physically reasonable. Shifts in the last cycles of refinements were all less than 1.1 and 0.8 of the estimated standard deviations for the nickel and magnesium complex parameters, respectively.

Final difference Fourier syntheses showed no peaks higher than those assigned to highly anisotropic methyl carbon atoms in earlier such calculations. Examinations of average values of the minimized function over ranges of $|F_o|$ and $\lambda^{-1}\sin\theta$ showed the weighting schemes chosen were satisfactory. The standard errors in observations of unit weight are 1.99 and 2.33 for the nickel and magnesium complexes, respectively.

Final positional and anisotropic thermal parameters are listed in Tables III and IV. Comparison of these values with those obtained in the earlier analysis[8] showed that, although the published cationic

Table II. Experimental Parameters

	$[Ni(Me_3AsO)_5](ClO_4)_2$	$[Mg(Me_3AsO)_5](ClO_4)_2$
Mosaicity/deg	0.19	0.18
θ-Scan range/deg	0.72	0.90
Scan time/sec	72	90
Total background time/sec	18	22.5
θ limit/deg	22	50
Total independent reflections	3975	3552
Reflections used in refinement for which $\|F\|^2 \geq 3\sigma(\|F\|^2)$	1890	2413
Range of transmission factors	0.31–0.50	0.04–0.03
Weighting parameter p	0.05	0.05
Primary beam collimator diameter/mm	2.0	2.0
Secondary beam collimator diameter/mm	5.0	5.0

Table III. Positional and Thermal Parameters for $[Ni(Me_3AsO)_5](ClO_4)_2$

Atom	x	y	z	U_{11}[a]	U_{22}	U_{33}	U_{12}	U_{13}	U_{23}
Ni	0.0920 (3)	0.1085 (1)	0.1382 (2)	0.031 (2)	0.055 (2)	0.029 (2)	−0.001 (2)	0.004 (2)	−0.002 (2)
As(1)	0.2558 (2)	0.0999 (1)	−0.0977 (2)	0.034 (2)	0.075 (2)	0.035 (2)	−0.002 (2)	0.009 (2)	−0.004 (2)
As(2)	0.3268 (2)	0.0894 (1)	0.3056 (2)	0.038 (2)	0.087 (3)	0.036 (2)	0.002 (2)	−0.004 (2)	0.002 (2)
As(3)	−0.0777 (2)	0.1008 (1)	0.3732 (2)	0.040 (2)	0.089 (2)	0.035 (2)	0.001 (2)	0.006 (2)	0.002 (2)
As(4)	−0.1443 (2)	0.0958 (1)	−0.0288 (2)	0.035 (2)	0.083 (2)	0.032 (2)	−0.003 (2)	−0.002 (2)	−0.002 (2)
As(5)	0.0897 (3)	0.2366 (1)	0.1484 (2)	0.079 (3)	0.056 (2)	0.069 (2)	0.000 (2)	0.009 (2)	0.003 (2)
O(1)	0.125 (1)	0.0914 (5)	−0.031 (1)	0.04 (2)	0.11 (2)	0.038 (9)	0.01 (1)	0.005 (8)	−0.001 (9)
O(2)	0.257 (1)	0.0865 (5)	0.175 (1)	0.008 (9)	0.09 (2)	0.047 (9)	0.010 (8)	0.003 (7)	0.012 (8)
O(3)	0.054 (1)	0.1042 (6)	0.311 (1)	0.04 (2)	0.13 (2)	0.035 (9)	0.02 (2)	0.016 (8)	0.010 (9)
O(4)	−0.079 (1)	0.0950 (6)	0.103 (1)	0.03 (2)	0.10 (2)	0.06 (1)	0.007 (9)	−0.004 (9)	0.002 (9)
O(5)	0.112 (2)	0.1787 (6)	0.121 (1)	0.16 (3)	0.08 (2)	0.09 (2)	0.02 (2)	0.01 (2)	−0.00 (2)
C(11)	0.352 (2)	0.0418 (9)	−0.076 (2)	0.08 (3)	0.09 (3)	0.08 (2)	0.02 (2)	0.01 (2)	−0.00 (2)
C(12)	0.227 (2)	0.1052 (9)	−0.265 (2)	0.06 (2)	0.13 (3)	0.02 (2)	0.02 (2)	−0.01 (2)	0.00 (2)
C(13)	0.338 (2)	0.1572 (9)	−0.055 (2)	0.06 (2)	0.08 (2)	0.09 (2)	−0.03 (2)	0.04 (2)	−0.00 (2)
C(21)	0.265 (2)	0.0394 (8)	0.412 (2)	0.08 (3)	0.06 (2)	0.07 (2)	0.01 (2)	−0.01 (2)	0.03 (2)
C(22)	0.491 (2)	0.074 (1)	0.271 (2)	0.00 (2)	0.27 (4)	0.08 (2)	0.02 (2)	−0.00 (2)	−0.03 (3)
C(23)	0.314 (3)	0.1514 (9)	0.378 (2)	0.11 (3)	0.07 (3)	0.10 (3)	−0.02 (2)	−0.03 (2)	0.00 (2)
C(31)	−0.156 (2)	0.0383 (9)	0.336 (2)	0.10 (3)	0.07 (3)	0.10 (3)	0.00 (2)	0.02 (2)	−0.04 (2)
C(32)	−0.054 (2)	0.103 (1)	0.541 (2)	0.10 (3)	0.15 (3)	0.02 (2)	−0.00 (2)	−0.00 (2)	0.01 (2)
C(33)	−0.186 (3)	0.154 (1)	0.330 (2)	0.09 (3)	0.09 (3)	0.10 (3)	−0.04 (2)	0.02 (2)	0.02 (2)
C(41)	−0.113 (2)	0.0367 (8)	−0.116 (2)	0.06 (3)	0.06 (2)	0.08 (2)	−0.01 (2)	0.00 (2)	0.03 (2)
C(42)	−0.315 (2)	0.0996 (9)	0.004 (2)	−0.00 (2)	0.15 (3)	0.07 (2)	−0.01 (2)	−0.01 (2)	−0.01 (2)
C(43)	−0.104 (2)	0.1532 (9)	−0.125 (2)	0.10 (3)	0.09 (2)	0.05 (2)	−0.01 (2)	0.00 (2)	−0.03 (2)
C(51)	0.084 (4)	0.251 (1)	0.315 (2)	0.31 (6)	0.13 (4)	0.08 (3)	0.05 (4)	0.01 (3)	−0.04 (3)
C(52)	−0.056 (3)	0.261 (1)	0.086 (3)	0.12 (4)	0.15 (4)	0.24 (5)	−0.10 (3)	−0.07 (4)	0.01 (4)
C(53)	0.198 (3)	0.274 (1)	0.062 (4)	0.13 (4)	0.05 (3)	0.33 (6)	−0.02 (3)	0.08 (4)	0.02 (3)
Cl(1)	0.0792 (8)	0.4108 (3)	0.1499 (7)	0.058 (6)	0.083 (6)	0.067 (5)	−0.001 (6)	0.003 (5)	0.006 (5)
Cl(2)	0.085 (1)	0.2537 (4)	−0.3255 (9)	0.114 (9)	0.089 (8)	0.121 (9)	−0.008 (7)	−0.005 (8)	0.002 (6)
O(11)	0.025 (3)	0.3749 (8)	0.206 (2)	0.23 (4)	0.08 (2)	0.25 (3)	−0.05 (2)	0.12 (3)	−0.01 (2)
O(12)	0.131 (3)	0.405 (1)	0.047 (2)	0.20 (4)	0.29 (4)	0.14 (3)	0.07 (3)	0.09 (3)	−0.01 (3)
O(13)	0.161 (3)	0.428 (1)	0.210 (2)	0.30 (5)	0.45 (6)	0.15 (3)	−0.25 (5)	−0.18 (3)	0.14 (3)
O(14)	0.000 (3)	0.446 (1)	0.138 (3)	0.17 (4)	0.18 (3)	0.32 (4)	0.07 (3)	0.14 (3)	0.11 (3)
O(21)	0.046 (4)	0.220 (1)	−0.396 (3)	0.34 (6)	0.14 (3)	0.31 (5)	−0.08 (3)	0.02 (4)	−0.09 (3)
O(22)	0.158 (3)	0.236 (1)	−0.237 (3)	0.20 (4)	0.22 (3)	0.21 (3)	0.02 (3)	−0.10 (3)	0.07 (3)
O(23)	−0.000 (4)	0.274 (2)	−0.270 (4)	0.24 (6)	0.48 (8)	0.39 (7)	0.20 (6)	0.05 (5)	−0.11 (6)
O(24)	0.141 (3)	0.287 (1)	−0.385 (3)	0.26 (5)	0.24 (5)	0.30 (5)	−0.13 (4)	−0.12 (4)	0.14 (4)

[a] The form of the thermal ellipsoid expression is $\exp[-(\beta_{11}h^2 + \beta_{22}k^2 + \beta_{33}l^2 + 2\beta_{12}hk + 2\beta_{13}hl + 2\beta_{23}kl)]$; $U_{ij} = \beta_{ij}/2\pi^2 a_i^* a_j^*$ (Å).

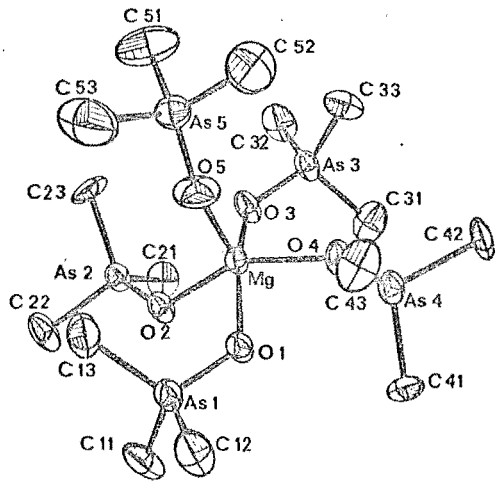

Figure 1. Perspective view of the $[Mg(Me_3AsO)_5]^{2+}$ cation showing 30% probability thermal ellipsoids.

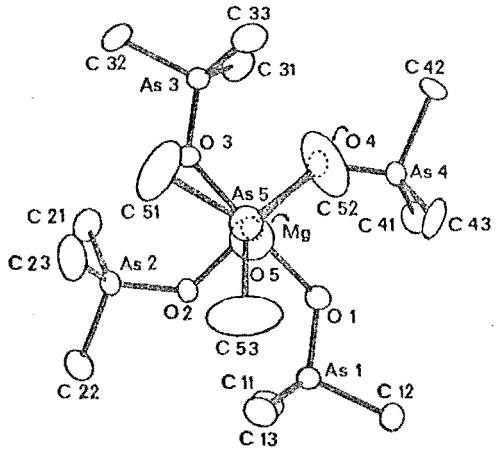

Figure 2. View of the $[Mg(Me_3AsO)_5]^{2+}$ cation looking down the crystallographic b axis.

structure was correct, the ions were incorrectly located in the unit cell.

Root-mean-square amplitudes of vibrations are given in Table V. Listings of final values of $|F_o|$ and $|F_c|$ (in electrons) for the reflections used in the refinements of both structures will appear following these pages in the microfilm edition of this journal (see paragraph at end of paper regarding supplementary material).

Description of the Crystal Structures

In the crystalline state, the two isomorphous compounds $[M(Me_3AsO)_5](ClO_4)_2$ (M = Ni, Mg) consist of well-separated ions, all interionic distances not involving hydrogen atoms being greater than 3.3 Å. Figure 1 is a perspective view of the $[Mg(Me_3AsO)_5]^{2+}$ cation and defines the atomic numbering scheme used throughout this paper for both complexes. Another view of the same ion is presented in Figure 2. Important interatomic distances and bond angles are collected in Tables VI and VII, respectively.

The perchlorate anions are well removed from the square-pyramidal cation. Although the anions have relatively high thermal motions, they exhibit no chemically significant deviations from normal tetrahedral geometry. The bond lengths and angles in the perchlorate anions range from 1.23 to 1.38 Å and from 101 to 123°. Their positions with respect to the cations are illustrated in the stereoscopic lattice packing diagram (Figure 3). The square base of the pyramid is parallel to the B face of the unit cell. Intercationic distances not involving hydrogen atoms are all greater than 3.5 Å in both structures. Disregarding the axial ligand methyl groups, the $[M(Me_3AsO)_5]^{2+}$ cation has approximate C_4 geometry. The

Table IV. Positional and Thermal Parameters for $[Mg(Me_3AsO)_5](ClO_4)_2$

Atom	x	y	z	U_{11}	U_{22}	U_{33}	U_{12}	U_{13}	U_{23}
Mg	0.0908 (3)	0.1112 (1)	0.1381 (4)	0.032 (3)	0.052 (3)	0.039 (3)	−0.000 (3)	−0.001 (2)	−0.000 (3)
As(1)	0.2552 (1)	0.1014 (1)	−0.1009 (1)	0.0418 (9)	0.077 (2)	0.042 (1)	−0.0037 (9)	0.0045 (8)	−0.0049 (9)
As(2)	0.3261 (1)	0.0876 (1)	0.3051 (1)	0.042 (1)	0.078 (2)	0.043 (2)	0.0043 (9)	−0.0043 (8)	−0.0003 (9)
As(3)	−0.0794 (1)	0.1001 (1)	0.3744 (1)	0.042 (1)	0.093 (2)	0.041 (2)	0.0007 (9)	0.0050 (8)	0.0036 (9)
As(4)	−0.1461 (1)	0.0934 (1)	−0.0299 (1)	0.0396 (9)	0.078 (2)	0.041 (1)	−0.0031 (9)	−0.0052 (8)	−0.0009 (9)
As(5)	0.0890 (2)	0.2394 (1)	0.1503 (2)	0.075 (2)	0.053 (1)	0.068 (2)	0.001 (1)	0.0021 (9)	0.0035 (9)
O(1)	0.1255 (7)	0.0947 (4)	−0.0345 (7)	0.039 (6)	0.095 (8)	0.043 (6)	−0.003 (6)	0.004 (5)	−0.018 (6)
O(2)	0.2539 (7)	0.0859 (3)	0.1759 (7)	0.038 (6)	0.090 (8)	0.041 (6)	0.008 (5)	−0.005 (5)	0.002 (6)
O(3)	0.0502 (8)	0.1025 (4)	0.3113 (8)	0.043 (6)	0.116 (9)	0.049 (7)	0.007 (6)	0.010 (5)	−0.001 (6)
O(4)	−0.0773 (7)	0.0923 (4)	0.1030 (7)	0.044 (6)	0.093 (8)	0.036 (6)	0.011 (6)	−0.011 (5)	−0.002 (5)
O(5)	0.105 (1)	0.1804 (4)	0.128 (1)	0.13 (2)	0.047 (7)	0.14 (2)	0.022 (8)	0.013 (9)	−0.007 (7)
C(11)	0.351 (1)	0.0458 (7)	−0.076 (2)	0.06 (2)	0.13 (2)	0.09 (2)	0.04 (2)	0.017 (9)	−0.00 (2)
C(12)	0.224 (1)	0.1080 (7)	−0.267 (1)	0.06 (2)	0.15 (2)	0.05 (2)	0.00 (2)	−0.000 (9)	0.01 (2)
C(13)	0.343 (1)	0.1574 (7)	−0.052 (1)	0.06 (2)	0.12 (2)	0.08 (2)	−0.02 (2)	0.007 (9)	−0.00 (2)
C(21)	0.270 (1)	0.0387 (6)	0.413 (1)	0.09 (2)	0.10 (2)	0.05 (1)	−0.01 (2)	−0.006 (9)	0.029 (9)
C(22)	0.490 (1)	0.0748 (8)	0.271 (1)	0.04 (1)	0.18 (3)	0.07 (2)	0.02 (2)	−0.011 (9)	−0.00 (2)
C(23)	0.313 (2)	0.1512 (5)	0.377 (1)	0.11 (2)	0.06 (2)	0.09 (2)	−0.00 (2)	−0.04 (2)	−0.04 (1)
C(31)	−0.157 (2)	0.0391 (7)	0.338 (2)	0.12 (2)	0.12 (2)	0.08 (2)	0.04 (2)	0.01 (2)	−0.01 (2)
C(32)	−0.056 (2)	0.1026 (9)	0.544 (1)	0.09 (2)	0.19 (3)	0.05 (2)	−0.00 (2)	0.019 (9)	0.01 (2)
C(33)	−0.182 (1)	0.1501 (6)	0.327 (1)	0.09 (2)	0.10 (2)	0.08 (2)	−0.03 (2)	0.02 (1)	0.01 (2)
C(41)	−0.110 (1)	0.0366 (6)	−0.117 (1)	0.08 (2)	0.09 (2)	0.07 (2)	−0.02 (1)	−0.014 (9)	0.05 (1)
C(42)	−0.315 (1)	0.0948 (7)	0.000 (1)	0.023 (8)	0.15 (2)	0.07 (2)	−0.000 (9)	0.001 (8)	0.01 (2)
C(43)	−0.108 (2)	0.1510 (6)	−0.121 (1)	0.12 (2)	0.09 (2)	0.04 (1)	0.02 (2)	−0.021 (9)	−0.040 (9)
C(51)	0.100 (2)	0.2586 (8)	0.311 (2)	0.25 (3)	0.11 (2)	0.07 (2)	0.02 (2)	−0.01 (2)	−0.02 (2)
C(52)	−0.057 (2)	0.2611 (9)	0.099 (3)	0.12 (2)	0.11 (2)	0.24 (3)	−0.05 (2)	−0.08 (2)	0.00 (2)
C(53)	0.207 (2)	0.2734 (8)	0.073 (3)	0.18 (3)	0.10 (2)	0.25 (4)	−0.00 (2)	0.13 (3)	0.01 (2)
Cl(1)	0.0783 (4)	0.4108 (2)	0.1484 (4)	0.061 (3)	0.078 (3)	0.074 (4)	−0.007 (3)	−0.000 (3)	0.003 (3)
Cl(2)	0.0787 (6)	0.2556 (2)	−0.3256 (6)	0.116 (5)	0.097 (4)	0.110 (5)	−0.003 (4)	−0.014 (4)	0.009 (4)
O(11)	0.033 (2)	0.3731 (6)	0.210 (2)	0.22 (2)	0.10 (2)	0.27 (3)	−0.07 (2)	0.12 (2)	−0.02 (2)
O(12)	0.121 (2)	0.403 (1)	0.041 (2)	0.38 (4)	0.34 (4)	0.09 (2)	0.13 (3)	0.07 (2)	0.01 (2)
O(13)	0.159 (2)	0.429 (1)	0.206 (2)	0.35 (4)	0.45 (5)	0.25 (3)	−0.29 (4)	−0.23 (3)	0.21 (3)
O(14)	−0.003 (2)	0.4463 (7)	0.139 (2)	0.15 (2)	0.18 (2)	0.38 (4)	0.08 (2)	0.12 (2)	0.12 (3)
O(21)	0.038 (3)	0.222 (1)	−0.398 (2)	0.36 (4)	0.21 (3)	0.23 (3)	−0.11 (3)	−0.03 (3)	−0.03 (3)
O(22)	0.153 (2)	0.2359 (8)	−0.244 (2)	0.26 (3)	0.20 (3)	0.25 (3)	0.02 (2)	−0.14 (3)	0.06 (2)
O(23)	−0.006 (3)	0.276 (2)	−0.266 (3)	0.33 (4)	0.55 (7)	0.25 (4)	0.26 (5)	0.06 (3)	−0.11 (4)
O(24)	0.132 (3)	0.290 (1)	−0.388 (2)	0.41 (5)	0.25 (3)	0.19 (3)	−0.16 (3)	−0.05 (3)	0.04 (3)

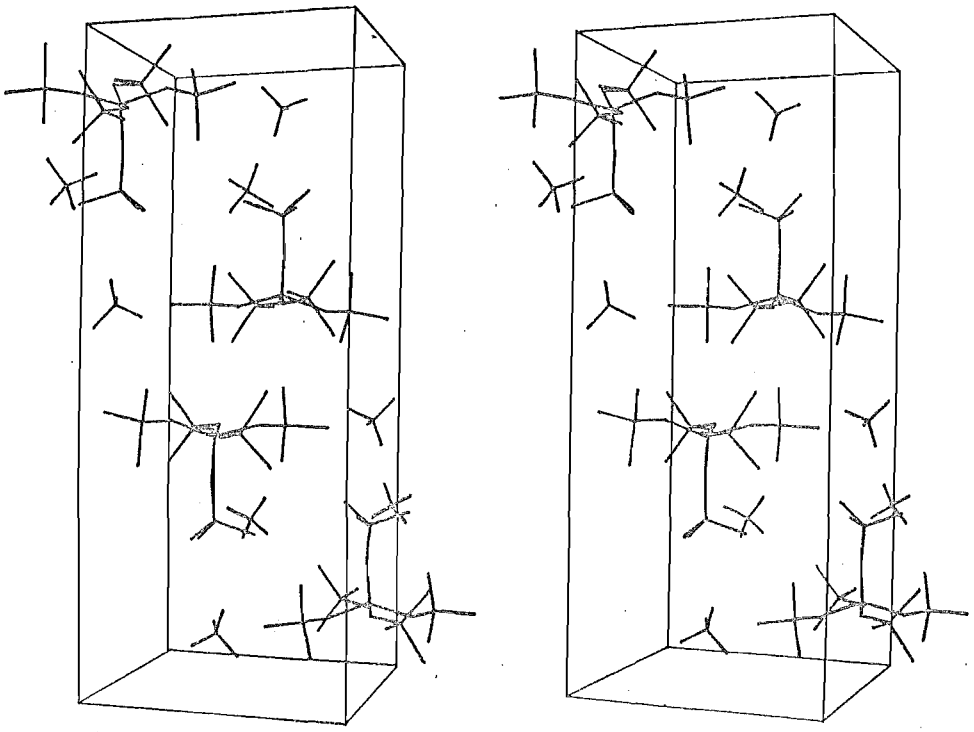

Figure 3. Stereogram showing contents of the unit cell of $[Mg(Me_3AsO)_5](ClO_4)_2$.

oxygen atoms O(1) to O(4), together with the arsenic atoms As(1) to As(4), though not statistically coplanar, are close to their best least-squares plane which is taken as the basal plane for a square pyramid. Table VIII defines these planes together with the displacements of selected atoms from them. The fifth axial oxygen atom does not lie directly above the central metal atom, being displaced approximately 0.1 Å from the normal vector of the basal plane in both complexes. However the apical arsenic atom is closely collinear with this normal vector; thus the arrangement of the arsenic atoms is also square pyramidal.

The M–O distances in the square pyramid range from 1.94 (2) to 2.01 (1) Å for M = Ni and from 1.92 (1) to 2.05 (1) Å for M = Mg. An interesting feature of the two complexes

Table V. Root-Mean-Square Amplitudes of Vibration (Å) for Selected Atoms

$[Ni(Me_3AsO)_5](ClO_4)_2$				$[Mg(Me_3AsO)_5](ClO_4)_2$			
Atom	Min	Intermed	Max	Atom	Min	Intermed	Max
Ni	0.162 (5)	0.182 (5)	0.234 (4)	Mg	0.178 (6)	0.200 (6)	0.229 (6)
As(1)	0.162 (4)	0.206 (4)	0.276 (3)	As(1)	0.194 (2)	0.212 (2)	0.279 (2)
As(2)	0.182 (4)	0.203 (4)	0.294 (4)	As(2)	0.194 (2)	0.217 (2)	0.280 (2)
As(3)	0.176 (4)	0.208 (4)	0.299 (3)	As(3)	0.192 (2)	0.214 (2)	0.305 (2)
As(4)	0.176 (4)	0.191 (4)	0.288 (3)	As(4)	0.186 (2)	0.215 (2)	0.279 (2)
As(5)	0.235 (4)	0.254 (4)	0.289 (4)	As(5)	0.229 (2)	0.261 (2)	0.274 (2)
O(1)	0.18 (3)	0.21 (2)	0.33 (2)	O(1)	0.19 (1)	0.20 (1)	0.32 (1)
O(2)	0.08 (5)	0.21 (2)	0.30 (2)	O(2)	0.18 (1)	0.21 (1)	0.30 (1)
O(3)	0.15 (3)	0.22 (2)	0.38 (2)	O(3)	0.19 (1)	0.24 (1)	0.34 (1)
O(4)	0.16 (3)	0.24 (2)	0.32 (2)	O(4)	0.17 (2)	0.22 (1)	0.31 (1)
O(5)	0.26 (3)	0.30 (2)	0.41 (3)	O(5)	0.20 (2)	0.36 (2)	0.38 (2)
C(51)	0.22 (5)	0.38 (4)	0.57 (5)	C(51)	0.24 (3)	0.34 (3)	0.51 (3)
C(52)	0.15 (7)	0.44 (5)	0.55 (5)	C(52)	0.23 (3)	0.37 (3)	0.53 (3)
C(53)	0.19 (5)	0.34 (5)	0.60 (4)	C(53)	0.28 (3)	0.32 (3)	0.58 (3)
Cl(1)	0.24 (1)	0.26 (1)	0.29 (1)	Cl(1)	0.241 (6)	0.270 (5)	0.286 (5)
Cl(2)	0.29 (1)	0.34 (1)	0.35 (1)	Cl(2)	0.303 (7)	0.318 (7)	0.362 (7)

is the significantly shorter axial, compared to basal, M–O bond. Comparisons between analogous bond angles reveal consistency to within 7.2° between cations in the two structures.

Discussion

The basically square-pyramidal structure adopted by the nickel– and magnesium–trimethylarsine oxide complexes is closely similar to that reported for $[Co(Ph_2MeAsO)_4ClO_4]ClO_4$.[2] In addition other studies[1,3] have indicated the existence of the same basic geometry in other arsine oxide– and phosphine oxide–metal systems. The availability of data for both a transition metal ion complex and a regular element complex having closely similar structures provides some insight as to why the square-pyramidal structure is favored. Also, these data highlight differences in the axial and basal plane binding of the ligands.

(1) Stabilization of the Square Pyramidal Structure. A striking feature of the observed structure is the closeness of the basal arsenic atoms to the mean plane of the $(OAs)_4$ grouping (Table VIII). This produces a square-pyramidal structure which has a large cavity opposite the axial group. Although there is a reasonably close intercationic contact between the metal atom and a methyl group from a neighboring cation (M···C ≥ 3.8 Å), it is unlikely that the particular square-pyramidal structure observed results from crystal-packing forces. Indeed electronic spectra show that square-pyramidal $[Ni(Me_3AsO)_5]^{2+}$ can exist as a stable entity in solution.[3] A similar but not so pronounced effect has been observed for the structure of $[Mn(Ph_3PO)_4I]^+$.[20] Similarly in the structure of $[Co(Ph_2MeAsO)_4ClO_4]ClO_4$[2] the same essentially planar $(OAs)_4$ geometry is found even though the steric requirements of the Ph_2MeAsO ligand are quite different from those of Me_3AsO.

It has usually been assumed that for high-spin complexes (such as this nickel complex) five-coordination is stabilized primarily by particular steric properties of the ligands.[8,21,22] However, if this was the case for R_3XO oxo complexes, a different molecular structure from that observed might have been expected. Steric interactions would possibly favor the trigonal-bipyramidal structure as found for the high-spin ML_5 complex $[Co(2\text{-picO})_5]^{2+}$ [23] (2-picO = 2-picoline *N*-oxide). Also, in these cations, rotation of Me_3As groups of the basal ligands (about M–O bonds) away from the axial group would appear to give a more sterically favorable structure.

It is apparent that these structures are stabilized by some factor(s) in addition to M–O σ bonding. To a first approximation this effect must be independent of the stabilizing effect of a partially filled d shell of the central metal atom as essentially the same geometrical arrangement is adopted by Mg^{2+} and Ni^{2+}. The M–O–As bond angles for the basal plane

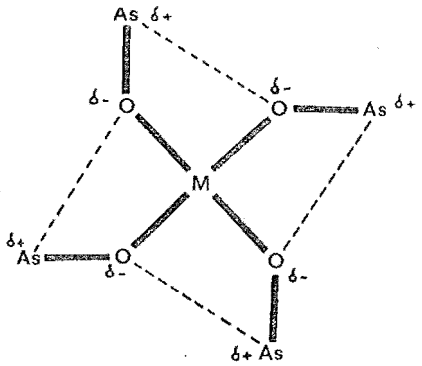

Figure 4. Interactions of oxygen atoms with arsenic atoms of adjacent ligands.

are significantly smaller than for the less hindered axial ligand and smaller than found for other arsine oxide complexes.[24,25] The observed basal M–O–As angle (~127°) produces a relatively close approach between arsenic and oxygen atoms of adjacent ligands (~3.1 Å). In addition the value indicates close to sp^2 hybridization for the oxygen atom and favorable disposition of the oxygen lone pair toward an arsenic atom of a neighboring ligand. We suggest one stabilizing influence could be an electrostatic-type interaction between neighboring oxygen and arsenic atoms as illustrated in Figure 4. This type of interaction could prevent free rotation of the Me_3As groups about the M–O bond. However the basically planar ML_4 structure may be stabilized by several interligand interactions including favorable steric packing of the arsenic methyl groupings.

(2) Comparison of the Nickel and Magnesium Structures. The ionic radii of Ni^{2+} and Mg^{2+} are closely similar (0.69 and 0.65 Å, respectively).[26] A comparison of structural parameters, for the two molecules should therefore give a good indication of the influence of the partially filled d shell in the case of Ni^{2+}.

From Tables VI–VIII it can be seen that differences between the two structures are generally small and in only a few instances greater than the standard deviation values. However there are general and consistent trends indicating (a) marginally stronger "basal" metal–ligand bonding for nickel and (b) marginally stronger "axial" bonding for magnesium.

(a) Although the ionic radius of nickel is slightly greater than that for magnesium, Ni–O "basal" distances are not longer than those for Mg–O and possibly marginally shorter. Also the nickel atom is more closely coplanar with the $(OAs)_4$ grouping than magnesium, indicating greater metal–ligand π bonding[20] (Table VIII). This difference is also indicated by the O(1)–M–O(3) and O(2)–M–O(4) angles which differ significantly for the two structures (in both cases they are greater for M = Ni).

Table VI. Selected Interatomic Distances (Å) in $[M(Me_3AsO)_5](ClO_4)_2$

	M = Ni	M = Mg
	Cation	
M–O(1)	2.00 (1)	2.049 (9)
M–O(2)	2.00 (1)	2.017 (9)
M–O(3)	2.00 (1)	2.03 (1)
M–O(4)	2.01 (1)	2.010 (9)
Av	2.00 (1)[a]	2.03 (2)
M–O(5)	1.94 (2)	1.92 (1)
As(1)–O(1)	1.68 (1)	1.668 (8)
As(2)–O(2)	1.67 (1)	1.670 (8)
As(3)–O(3)	1.65 (1)	1.641 (9)
As(4)–O(4)	1.66 (1)	1.688 (8)
Av	1.67 (1)	1.67 (2)
As(5)–O(5)	1.63 (2)	1.65 (1)
M···As(1)	3.263 (4)	3.313 (4)
M···As(2)	3.289 (4)	3.318 (4)
M···As(3)	3.292 (4)	3.329 (4)
M···As(4)	3.276 (4)	3.311 (4)
M···As(5)	3.492 (4)	3.536 (4)
As(1)···O(2)	3.11 (1)	3.166 (8)
As(2)···O(3)	3.11 (1)	3.155 (9)
As(3)···O(4)	3.05 (1)	3.082 (8)
As(4)···O(1)	3.05 (1)	3.078 (8)
As(1)–C(11)	1.94 (2)	1.90 (2)
As(1)–C(12)	1.92 (2)	1.92 (2)
As(1)–C(13)	1.88 (2)	1.91 (2)
As(2)–C(21)	1.95 (2)	1.93 (2)
As(2)–C(22)	1.94 (2)	1.93 (1)
As(2)–C(23)	1.88 (3)	1.94 (1)
As(3)–C(31)	1.96 (3)	1.94 (2)
As(3)–C(32)	1.91 (2)	1.94 (2)
As(3)–C(33)	1.95 (3)	1.90 (2)
As(4)–C(41)	1.92 (2)	1.90 (1)
As(4)–C(42)	1.97 (2)	1.95 (1)
As(4)–C(43)	1.96 (2)	1.94 (1)
As(5)–C(51)	1.93 (3)	1.90 (2)
As(5)–C(52)	1.90 (3)	1.85 (2)
As(5)–C(53)	1.87 (3)	1.86 (2)
	Anion	
Cl(1)–O(11)	1.32 (2)	1.35 (2)
Cl(1)–O(12)	1.31 (2)	1.33 (2)
Cl(1)–O(13)	1.23 (2)	1.23 (2)
Cl(1)–O(14)	1.31 (3)	1.35 (2)
Cl(2)–O(21)	1.29 (3)	1.31 (2)
Cl(2)–O(22)	1.38 (2)	1.36 (2)
Cl(2)–O(23)	1.28 (2)	1.32 (2)
Cl(2)–O(24)	1.29 (3)	1.33 (3)

[a] Esd's for average bond lengths were calculated from the expression $\sigma = \Sigma_{i=1}^{i=N}[(l_i - \bar{l})^2/(N-1)]^{1/2}$, where l_i is the ith bond length and $\bar{l}$ is the averaged bond length.

(b) While there is no significant difference in the M–O "axial" values, the M–O(5)–As(5) angle associated with this grouping is about 7° greater for the magnesium complex. This may indicate stronger bonding for magnesium, resulting from enhanced M←L (axial) π bonding. For both complexes the M–O–As (axial) angle is considerably larger than that for the basal ligands (~160° compared with ~127°). This together with the shorter axial M–O bond lengths (~1.9 Å compared with ~2.0 Å) indicates greater s character for the axial oxygen hybrid orbitals and the possibility that M←L (axial) π bonding may be important. Any π bonding involving metal dπ and *two* oxygen pπ orbitals would produce larger M–O–As bond angles.

The differences summarized in paragraphs (a) and (b) may be rationalized in terms of the electronic configurations of nickel and magnesium. While the involvement of empty 3d orbitals in bonding to magnesium would not normally be considered, the energy-lowering effect of the electronegative oxygen environment could enable dπ←pπ (axial) bonding to occur. Such bonding would be expected to be greater for a metal ion with *empty* 3d orbitals (like magnesium) compared with one like nickel having a partially filled 3d shell. The observations mentioned in paragraph (b) appear to support this conclusion. By contrast the evidence for stronger metal–ligand basal π bonding for nickel may be understood in terms of metal→ligand π donation which would be expected to be greater for the ion having the greater number of d electrons (nickel ($3d^8$) > magnesium ($3d^0$)).

Table VII. Selected Bond Angles (deg) in $[M(Me_3AsO)_5](ClO_4)_2$ (Cation)

	M = Ni	M = Mg
M–O(1)–As(1)	124.6 (8)	125.8 (5)
M–O(2)–As(2)	127.4 (7)	128.0 (5)
M–O(3)–As(3)	128.2 (8)	129.6 (5)
M–O(4)–As(4)	126.6 (8)	126.9 (5)
M–O(5)–As(5)	157 (1)	163.8 (8)
O(5)–M–O(1)	96.6 (7)	98.6 (5)
O(5)–M–O(2)	102.1 (7)	106.4 (5)
O(5)–M–O(3)	100.3 (7)	101.0 (5)
O(5)–M–O(4)	105.9 (8)	108.9 (5)
O(1)–M–O(2)	87.2 (5)	86.7 (4)
O(2)–M–O(3)	89.1 (5)	88.3 (4)
O(3)–M–O(4)	88.1 (6)	86.4 (4)
O(4)–M–O(1)	87.5 (6)	86.8 (4)
O(1)–M–O(3)	163.1 (6)	160.4 (5)
O(2)–M–O(4)	151.9 (6)	144.7 (5)

Table VIII. Reference Least-Squares Planes for $[M(Me_3AsO)_5]^{2+}$ cations[a]

	Distance of atom from plane/Å	
	Plane I (M = Ni)	Plane II (M = Mg)
	For Atoms Included in Least-Squares Planes	
As(1)	0.223 (3)	0.232 (3)
As(2)	−0.080 (3)	−0.119 (3)
As(3)	0.047 (3)	0.099 (3)
As(4)	−0.069 (3)	−0.115 (3)
O(1)	−0.07 (1)	0.00 (1)
O(2)	−0.18 (1)	−0.19 (1)
O(3)	0.20 (2)	0.21 (1)
O(4)	−0.08 (2)	−0.12 (1)
	For Other Atoms	
M	0.359 (3)	0.454 (3)
As(5)	3.844 (3)	3.985 (3)
C(12)	0.38 (3)	0.40 (2)
C(22)	−0.42 (3)	−0.43 (2)
C(32)	0.09 (3)	0.17 (3)
C(42)	−0.04 (3)	−0.11 (2)

[a] Equations of planes referred to orthorhombic crystallographic axes X, Y, Z are atomic coordinates in Å: (I) $0.0382X + 0.9992Y - 0.0105Z = 2.6188$; (II) $0.0276X + 0.9996Y - 0.0020Z = 2.6408$.

While there are uncertainties about the exact nature of the M→L π bonding, evidence for electronic influence from the penultimate (P or As) atom in metal–oxo (R_3XO, X = P, As) bonding has been obtained from electronic spectra of a range of cobalt complexes.[27]

Note Added in Proof. A short "nonbonded" interaction between oxygen and tetrahedral arsenic atoms, of the same ~3.1 Å value found for the structures reported here, has recently been determined for a substituted triphenylarsonium cyclopentadienylide ion.[28]

Registry No. $[Ni(Me_3AsO)_5](ClO_4)_2$, 21508-99-6; $[Mg(Me_3AsO)_5](ClO_4)_2$, 57033-84-8.

Supplementary Material Available: Structure factor tables (18 pages). Ordering information is given on any current masthead page.

References and Notes

(1) J. Lewis, R. S. Nyholm, and G. A. Rodley, *Nature (London)*, **207**, 72 (1965).
(2) P. Pauling, G. B. Robertson, and G. A. Rodley, *Nature (London)*, **207**, 73 (1965).
(3) A. M. Brodie, S. H. Hunter, G. A. Rodley, and C. J. Wilkins, *Inorg. Chim. Acta*, **2**, 195 (1968).
(4) S. H. Hunter, R. S. Nyholm, and G. A. Rodley, *Inorg. Chim. Acta*, **3**, 631 (1969).
(5) D. M. L. Goodgame, M. Goodgame, and P. J. Hayward, *J. Chem. Soc. A*, 1352 (1970).
(6) F. Mani, *Inorg. Nucl. Chem. Lett.*, **7**, 447 (1971).
(7) M. W. G. de Bolster, I. E. Kortram, and W. L. Groeneveld, *J. Inorg. Nucl. Chem.*, **34**, 575 (1972).
(8) S. H. Hunter, K. Emerson, and G. A. Rodley, *Chem. Commun.*, 1398 (1969).
(9) G. B. Jameson and G. A. Rodley, *Inorg. Nucl. Chem. Lett.*, **11**, 547 (1975).
(10) R. Timkovich and A. Tulinsky, *J. Am. Chem. Soc.*, **91**, 4430 (1969).
(11) K. Ballschmiter and J. J. Katz, *J. Am. Chem. Soc.*, **91**, 2661 (1969).
(12) S. H. Hunter, Ph.D. Thesis, University of Canterbury, 1970.
(13) "International Tables for X-Ray Crystallography", Vol. III, Kynoch Press, Birmingham, England, 1962.
(14) Calculations were carried out at the University of Canterbury using a Burroughs B6718 computer. The data processing program HILGOUT is based on programs DRED (J. F. Blount) and PICKOUT (R. J. Doedens). Numerical absorption corrections are applied using program DABS which is a modified version of DATAPH (P. Coppens).
(15) Structure factor calculations and least-squares refinements were carried out using program CUCLS and Fourier summations using program FOURIER. These are highly modified versions of the well-known programs ORFLS (W. R. Busing, K. O. Martin, and H. A. Levy) and FORDAP (A. Zalkin), respectively. Other programs include local modifications of Busing and Levy's ORFFE function and error program, and Johnson's ORTEP thermal ellipsoid plotting program.
(16) D. T. Cromer and J. B. Mann, *Acta Crystallogr., Sect. A*, **24**, 321 (1968).
(17) R. F. Stewart, E. R. Davidson, and W. T. Simpson, *J. Chem. Phys.*, **42**, 3175 (1965).
(18) D. T. Cromer, *Acta Crystallogr.*, **18**, 17 (1965).
(19) M. J. Buerger, "Vector Space", Wiley, New York, N.Y., 1959, p 66.
(20) G. Ciani, M. Manassero, and M. Sansori, *J. Inorg. Nucl. Chem.*, **34**, 1760 (1972).
(21) J. S. Wood, *Prog. Inorg. Chem.*, **16**, 227 (1965).
(22) R. Morassi, I. Bertini, and L. Sacconi, *Coord. Chem. Rev.*, **11**, 343 (1973).
(23) B. A. Coyle and J. A. Ibers, *Inorg. Chem.*, **9**, 767 (1970).
(24) I. Lindquist, "Inorganic Adduct Molecules of Oxo-Compounds", Springer-Verlag, Berlin, 1963, p 69.
(25) C. I. Branden, *Acta Chem. Scand.*, **17**, 1363 (1963).
(26) F. A. Cotton and G. Wilkinson, "Advanced Inorganic Chemistry", Wiley, New York, N.Y., 1972, p 52.
(27) A. M. Brodie, S. H. Hunter, G. A. Rodley, and C. J. Wilkins, *J. Chem. Soc. A*, 2039 (1968).
(28) F. C. March, G. Ferguson, and D. Lloyd, *J. Chem. Soc., Dalton Trans.*, 1377 (1975).

Contribution from the Department of Chemistry, Arizona State University, Tempe, Arizona 85281

Crystal and Molecular Structure of Tetraisothiocyanatobis(2,2'-bipyridine)niobium(IV) and -zirconium(IV)

E. J. PETERSON, R. B. VON DREELE, and T. M. BROWN*

Received April 8, 1975 AIC502570

The crystal and molecular structures of the eight-coordinate complexes $Nb(NCS)_4(C_{10}H_8N_2)_2$ and $Zr(NCS)_4(C_{10}H_8N_2)_2$ have been determined from single-crystal x-ray intensity data collected by the θ–2θ scan technique. In both compounds the metal atoms are coordinated by eight nitrogen atoms, four belonging to the two bidentate 2,2'-bipyridine groups and four belonging to the isothiocyanate ligands. The niobium–nitrogen distances are 2.135 (3) and 2.318 (3) Å, respectively, for the M–NCS and M–2,2'-bpy bonds, while the zirconium–nitrogen distances are 2.182 (2) and 2.412 (2) Å, respectively. The coordination geometries around the metal for both complexes can be obtained by distortions from an idealized D_{2d} dodecahedron along a reaction pathway which retains D_2 symmetry. The degree of distortion correlates with the M–N bond lengths; the smaller niobium complex is sufficiently distorted from a dodecahedron to become a very nearly perfect D_4 square antiprism ($\delta = -2.1, 49.2°$) with the bidentate 2,2'-bipyridines bridging the square faces. The larger zirconium complex is significantly less distorted ($\delta = 4.2, 45.5°$) from the D_{2d} dodecahedron than the niobium complex. Each structure was solved by standard heavy-atom techniques and refined by full-matrix least-squares to final R values of 0.067 (1702 independent observed reflections) for $Nb(NCS)_4(C_{10}H_8N_2)_2$ and 0.056 (1833 independent observed reflections) for $Zr(NCS)_4(C_{10}H_8N_2)_2$. Both compounds crystallize in the orthorhombic space group $Pnnn$, $Z = 2$, with the lattice parameters $a = 7.720$ (4), $b = 13.179$ (7), $c = 13.113$ (4) Å for $Nb(NCS)_4(C_{10}H_8N_2)_2$ and $a = 7.646$ (6), $b = 13.407$ (11), $c = 13.245$ (11) Å for $Zr(NCS)_4(C_{10}H_8N_2)_2$.

Introduction

The elucidation of factors which govern the stereochemistry of eight-coordinate compounds has been the subject of a number of papers.[1-8] Some examples of discrete eight-coordinate complexes and their experimentally assigned stereochemistries are listed in Table I. In general, eight-coordinate complexes are usually classified as either a D_{2d}-$\bar{4}2m$ dodecahedron or a D_{4d}-$\bar{8}2m$ square antiprism. Recently, however, several authors have expressed consternation because many of the usual polyhedron-shape criteria neglect the possibility of a C_{2v} bicapped trigonal prism. Because of these objections, new criteria were proposed which relate the three most common polyhedra along a geometric reaction pathway.[7,8] Several theoretical studies have shown that both the D_{2d} and D_{4d} stereochemistries are equally likely on the basis of crystal field stabilization[3] or minimization of repulsions.[1,3,6] The MX_8 and MX_4Y_4 systems show predominantly dodecahedral stereochemistry, while the $M(A-A)_4$ compounds are divided between dodecahedral and square-antiprismatic structures. The latter observations have been explained in terms of the normalized ligand bite of the symmetrical bidentate ligands.[6] The structure of $Nb[(t\text{-}C_4H_9CO)_2CH]_4$ was recently investigated and found to be a distorted D_4 square antiprism.[9] This structure is significant because it is the first $M(A-A)_4$ system where the bidentate ligands span the l edges of an idealized antiprism.

Eight-coordinate complexes of the type $M(A-A)_2B_4$ are also of interest but have not been as extensively studied as the other systems. Most reported examples are dodecahedral and only a few compounds of this type which even closely approach a square antiprism have been reported, i.e., $W(CH_3)_4[O\text{-}N(CH_3)NO]_2$[10] and $Zr(SO_4)_2\cdot 4H_2O$.[11] Thus, in order to elucidate further the factors governing the stereochemical arrangement of ligands in eight-coordinate complexes,

Acta Crystallographica Section B 768499. B76783—JY384 SSP. Paper 337—Slip 1

Acta Cryst. (1977). B33, 000–000

Tri-μ-(trimethylarsine oxide)-hexakis(trimethylarsine oxide)dicalcium(II) Tetraperchlorate – a Dinuclear Calcium Complex

BY Y. S. NG, G. A. RODLEY AND WARD T. ROBINSON

Department of Chemistry, University of Canterbury, Christchurch, New Zealand

(*Received* 21 *May* 1976; *accepted* 2 *November* 1976)

Abstract. $Ca_2[(CH_3)_3AsO]_6(ClO_4)_4$, hexagonal, $P6_3/m$, $a = 11{\cdot}762\,(1)$, $c = 27{\cdot}279\,(2)$ Å; $M_r = 1702{\cdot}198$, $D_m = 1{\cdot}71$ (by flotation), $D_x = 1{\cdot}73$ g cm^{-3}, $Z = 2$; $F(000) = 1696$, μ(Cu $K\alpha$) = 91·91 cm^{-1}. Four-circle diffractometer intensity data were refined by the full-matrix least-squares method to give $R = 0{\cdot}061$ for 1072 data with $F_o^2 \geq 3\sigma(F_o^2)$. The structure consists of Ca atoms each coordinated to six trimethylarsine oxide ligands, three of which bridge to similar adjacent groups forming a dinuclear cationic complex with crystallographically imposed *m* symmetry. There are three crystallographically distinct perchlorate counter anions, two of which are disordered.

Introduction. Colourless, hexagonal crystals were recrystallized from powder samples (Jameson & Rodley, 1975, 1976) in methanol–triethyl orthoformate solution in the presence of acetonitrile vapour. Weissenberg and precession photography revealed the crystal to be hexagonal. Systematic absences ($00l$: l = odd) are consistent with space groups $P6_3$ and $P6_3/m$. On the basis of the statistical distribution of intensities, $P6_3/m$ was selected and successful refinement verified the choice.

The transparent crystal chosen for data collection had a maximum dimension of about 0·38 mm. Cell dimensions and their e.s.d.'s were determined from least-squares refinement of the setting angles of 12 carefully centred reflections. 1763 independent reflexions were collected in the range $0° \leq \theta \leq 57°$ on a Hilger & Watts diffractometer with Cu $K\alpha$ (Ni-filtered) X radiation. The data were corrected for Lorentz and polarization effects. Absorption corrections were not made because of difficulties in accurately defining the crystal habit. The structure was solved by normal Patterson and Fourier syntheses. Difficulties were encountered in attempting to locate the perchlorate O atoms.

Difference Fourier syntheses calculated through sections around the Cl atoms yielded peaks of the partially disordered perchlorate O atoms. Full-matrix positional and anisotropic temperature parameter refinement of all atoms converged at $R = 0{\cdot}057$. At this stage two of the three perchlorate anions had unreasonable stereochemistries. To resolve these problems, several models were investigated. The structure was refined in the non-centrosymmetric space group $P6_3$ to relieve the constraints on the perchlorate anions, but no electron densities for the O atoms were found at reasonable positions around the Cl atoms. The final model used described the perchlorate O atoms as tetrahedral rigid groups with a Cl–O distance of 1·44 Å in space group $P6_3/m$. Refinement converged with $R = 0{\cdot}061$. There are only negligible changes (in the order of 0·01 Å) in the cation geometry with different models for the perchlorate anions. The largest shift in the final cycle was $0{\cdot}27\sigma$. The highest peak from the final difference Fourier was about half the electron density of the most disordered perchlorate O atoms.

Programs used were modified versions of *ORFLS* (Busing, Martin & Levy, 1963), *FORDAP* (Zalkin, 1965) and *ORTEP* (Johnson, 1965). Calculations were carried out at the University of Canterbury on a Burroughs B6718 computer.

Atomic coordinates and temperature factors of all non-hydrogen atoms are listed in Tables 1 and 2. Selected bond distances and angles are given in Tables 3 and 4 respectively.*

Take in Tables 1, 2, 3, 4

Discussion. Various Ca and Mg complexes of substituted arsine and phosphine oxides were recently synthesized and characterized in this laboratory (Jameson & Rodley, 1975, 1976). X-ray powder photographs showed that the Ca analogue of $\{Mg[(CH_3)_3AsO]_5\}(ClO_4)_2$ did not have exactly the same structure as that reported for the Mg complex (Ng, Rodley & Robinson, 1976). The structure of the Ca arsine oxide complex was determined in order to gain further insight into the effects of metal ion character on the stereochemistries of Ca and Mg complexes.

The structure consists of discrete dimeric cationic units well separated in space. Fig. 1 shows an edge-on view of the dinuclear Ca cationic unit and illustrates the labelling scheme adopted in this paper. The structure is relatively 'open' and there are no interionic distances shorter than 3·3 Å (excluding H atoms). The perchlorate anions are symmetrically located around the cations as illustrated in Fig. 2. The Ca atoms are surrounded by six O atoms of the $(CH_3)_3AsO$ ligands in an approximately octahedral environment. There are two types of $(CH_3)_3AsO$ ligands present in the structure. Three crystallographically equivalent ligands form terminal groups with Ca–O bonds of 2·284 (7) Å. The other three symmetry-related ligands bridge the two Ca centres with a Ca–O distance of 2·424 (7) Å. The present structure appears to be the first of its kind to have been the subject of X-ray analysis. Closely related structures are $I_3NiI_3Bi[(Ph_3AsO)_3]$ (Lazarini & Golič, 1975), and the dimeric species $(Zn\,C_6H_4[(CH_3)_2AsO]_2\}_2)^{4+}$ (Hunter, Rodley & Emerson, 1976).

Take in Figs. 1, 2

Two of the three crystallographically independent perchlorate anions are disordered. The Cl atom at (0,0,0) is in an environment with $\bar{3}$ symmetry while that at $(0,0,\frac{1}{4})$ has $\bar{6}$ symmetry imposed on it. Each Cl atom may be considered to be at the centroid of two possible orientations for its bonded, tetrahedrally arranged O atoms. In the first case the overlapped arrangement is necessarily staggered, and in the second it is eclipsed. The high thermal motions exhibited by the associated perchlorate O atoms hindered further characterization of these disorders.

As–C bond lengths in the present structure are similar to those in $\{Mg[(CH_3)_3AsO]_5\}(ClO_4)_2$. However, in the Mg complex all the Mg–O distances are

* A list of structure factors has been deposited with the British Library Lending Division as Supplementary Publication No. SUP 32273 (5 pp.). Copies may be obtained through The Executive Secretary, International Union of Crystallography, 13 White Friars, Chester CH1 1NZ, England.

shorter than those in the present structure. The stronger Mg—O axial bond in the Mg complex possibly produces a '*trans*' effect (*via* strong $L \rightarrow M$ donation) (Ng, Rodley & Robinson, 1976) which favours the formation of a five-coordinate species. By contrast, the Ca ion is unlikely to exert this type of '*trans*' effect to produce five-coordination because $L \rightarrow M$ π bonding is less likely to occur for a significantly larger ion (ionic radii are: $Ca^{2+} = 0{\cdot}99$ and $Mg^{2+} = 0{\cdot}65$ Å). The larger size favours a higher coordination number than five. In fact, many Ca complexes with oxo ligands have coordination numbers of 7 or even 8 (Uchtman, 1972; Einspahr & Bugg, 1974; Kretsinger & Nelson, 1976).

We thank Dr F. C. March for his helpful comments on the solution of this structure and the New Zealand University Grants Committee for research equipment grants.

References

BUSING, W. R., MARTIN, K. O. & LEVY, H. A. (1963). *ORFLS*. Oak Ridge National Laboratory Report ORNL-TM-305.

EINSPAHR, H. & BUGG, C. E. (1974). *Acta Cryst.* B**30**, 1037–1043.

HUNTER, S. H., RODLEY, G. A. & EMERSON, K. (1976). *Inorg. Nucl. Chem. Lett.* **12**, 113–119.

JAMESON, G. B. & RODLEY, G. A. (1975). *Inorg. Nucl. Chem. Lett.* **11**, 547–551.

JAMESON, G. B. & RODLEY, G. A. (1976). *Inorg. Nucl. Chem. Lett.* **12**, 519.

JOHNSON, C. K. (1965). *ORTEP*. Oak Ridge National Laboratory Report ORNL-3974.

KRETSINGER, R. H. & NELSON, D. J. (1976). *Coord. Chem. Rev.* **18**, 29–124.

LAZARINI, F. & GOLIČ, L. (1975). *Acta Cryst.* A**31**, S140.

NG, Y. S., RODLEY, G. A. & ROBINSON, W. T. (1976). *Inorg. Chem.* **15**, 303–309.

UCHTMAN, V. A. (1972). *J. Phys. Chem.* **76**, 1304–1310.

ZALKIN, A. (1965). *FORDAP. A Fortran Program for Fourier Calculation*. Univ. of California, Berkeley.

A DINUCLEAR CALCIUM COMPLEX
A DINUCLEAR CALCIUM COMPLEX
A DINUCLEAR CALCIUM COMPLEX
A DINUCLEAR CALCIUM COMPLEX
A DINUCLEAR CALCIUM COMPLEX
A DINUCLEAR CALCIUM COMPLEX

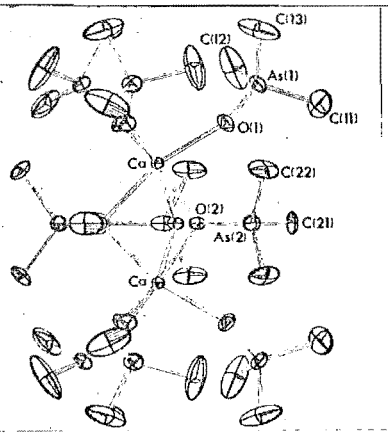

Fig. 1. A perspective view of the $\{Ca_2[(CH_3)_2AsO]_4\}^{4+}$ cation.

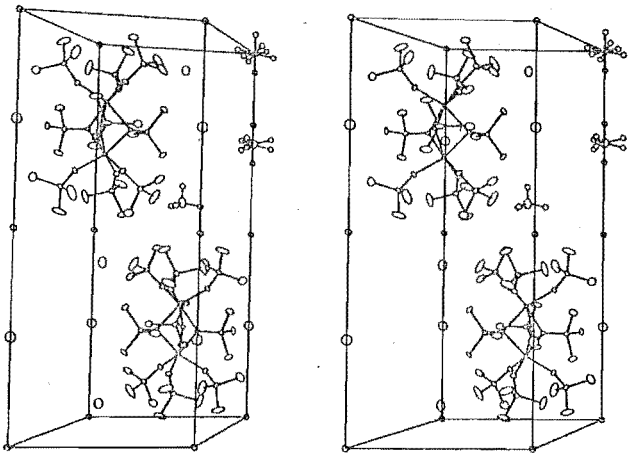

Fig. 2. Stereo diagram of the contents of the unit cell. For clarity only three perchlorate anions are shown with their O atoms attached.

Table 1. *Final parameters for non-group atoms*

Variable parameters have been multiplied by 10^4.

The form of the anisotropic temperature factor is $\exp[-(\beta_{11}h^2 + \beta_{22}k^2 + \beta_{33}l^2 + 2\beta_{12}hk + 2\beta_{13}hl + 2\beta_{23}kl)]$. Parameters without standard deviations are fixed by symmetry.

	x	y	z	β_{11}	β_{22}	β_{33}	β_{12}	β_{13}	β_{23}
Ca	$\frac{1}{2}$	$\frac{1}{2}$	1860 (1)	61 (2)	$\beta_{22}=\beta_{11}$	7 (0)	$2\beta_{12}=\beta_{11}$	0	0
As(1)	1205 (1)	3806 (1)	1018 (1)	112 (2)	106 (2)	14 (0)	37 (2)	−9 (1)	−15 (1)
As(2)	4677 (3)	4861 (3)	$\frac{1}{4}$	214 (4)	188 (4)	12 (0)	172 (3)	0	0
O(1)	1673 (8)	4984 (8)	1434 (3)	110 (10)	110 (10)	16 (1)	39 (9)	−7 (3)	−19 (3)
O(2)	3630 (10)	5409 (9)	$\frac{1}{4}$	110 (10)	60 (10)	7 (1)	50 (10)	0	0
C(11)	−230 (30)	2230 (20)	1224 (8)	470 (50)	150 (30)	36 (5)	10 (30)	40 (10)	−30 (10)
C(12)	2590 (20)	3510 (20)	850 (10)	200 (30)	390 (50)	100 (10)	170 (30)	−10 (10)	−120 (20)
C(13)	750 (30)	4250 (30)	430 (7)	720 (80)	430 (50)	24 (4)	390 (60)	−70 (10)	−40 (10)
C(21)	6460 (20)	6370 (30)	$\frac{1}{4}$	90 (30)	470 (60)	24 (5)	170 (40)	0	0
C(22)	4410 (20)	2790 (20)	1929 (5)	490 (50)	300 (40)	18 (3)	320 (40)	0 (10)	−23 (8)
Cl(1)	0	0	0	132 (7)	$\beta_{22}=\beta_{11}$	17 (1)	$2\beta_{12}=\beta_{11}$	0	0
Cl(2)	0	0	$\frac{1}{2}$	350 (20)	$\beta_{22}=\beta_{11}$	49 (4)	$2\beta_{12}=\beta_{11}$	0	0
Cl(3)	$\frac{1}{3}$	$\frac{1}{3}$	783 (7)	230 (10)	$\beta_{22}=\beta_{11}$	58 (4)	$2\beta_{12}=\beta_{11}$	0	0
O(31)	6640 (40)	2220 (30)	700 (10)	780 (80)	680 (90)	160 (20)	470 (80)	30 (30)	−150 (30)
O(32)	$\frac{1}{3}$	$\frac{1}{3}$	1210 (20)	800 (100)	$\beta_{22}=\beta_{11}$	100 (20)	$2\beta_{12}=\beta_{11}$	0	0

Table 2. *Final parameters for group atoms*

Positional parameters have been multiplied by 10^4.

	x	y	z	B
Perchlorate group 1				
O(11)	−1320 (10)	−810 (80)	−132 (0)	15 (1)
O(12)	0	0	528 (0)	17 (2)
Perchlorate group 2				
O(21)	−1110 (30)	80 (60)	2368 (0)	19 (1)
O(22)	0	0	3028 (0)	33 (6)

Table 3. *Selected interatomic distances* (Å)

Cation			
Ca–O(1)	2·284 (7)	As(1)–O(1)	1·657 (7)
Ca–O(2)	2·424 (7)	As(1)–C(11)	1·865 (20)
		As(1)–C(12)	1·886 (19)
Ca···Ca^{iv}	3·491 (6)	As(1)–C(13)	1·845 (20)
Ca···As(1)	3·800 (2)	As(2)–O(2)	1·649 (10)
Ca···As(2)	3·661 (2)	As(2)–C(21)	1·957 (26)
		As(2)–C(22)	1·926 (14)
Anion			
Cl(3)–O(31)	1·32 (3)	Cl(3)–O(32)	1·16 (6)

The Roman numeral superscripts represent the symmetry transformations given below. Where there is no further qualification, symmetry (i) is implied.

(i) x, y, z (iii) $y-x, -x, z$
(ii) $-y, x-y, z$ (iv) $x, y, \frac{1}{2}-z$

Table 4. *Selected bond angles* (°)

O(1)–Ca–O(1)^{ii}	96·4 (3)	O(1)–As(1)–C(11)	112·4 (7)	O(2)–As(2)–C(21)	108·4 (9)
O(1)–Ca–O(2)	99·2 (3)	O(1)–As(1)–C(12)	111·2 (7)	O(2)–As(2)–C(22)	110·2 (6)
O(1)–Ca–O(2)^{ii}	162·8 (3)	O(1)–As(1)–C(13)	112·5 (8)	C(21)–As(2)–C(22)	110·2 (8)
O(1)–Ca–O(2)^{iii}	89·1 (3)	C(11)–As(1)–C(12)	109·2 (12)	C(22)–As(2)–C(22)^{iv}	107·9 (11)
O(2)–Ca–O(2)^{ii}	73·9 (3)	C(12)–As(1)–C(13)	103·9 (14)	O(31)–Cl(3)–O(32)	100·3 (20)
Ca–O(1)–As(1)	148·8 (5)	C(13)–As(1)–C(11)	107·2 (13)		
Ca–O(2)–Ca^{iv}	92·1 (4)			O(31)–Cl(3)–O(31)^{ii}	116·9 (12)
Ca–O(2)–As(2)	127·0 (3)				

J. Appl. Cryst. (1977). **10**, –

A portable apparatus for mounting air-sensitive crystals

The mounting of air or moisture-sensitive crystals for X-ray analysis in an inert-atmosphere unit or a dry box can present considerable difficulties. In the course of a recent study of the compound $[Mg(Me_3PO)_5](ClO_4)_2$, an extremely moisture-sensitive compound, we developed a crystal-mounting apparatus which is easy to manipulate and inexpensive to make.

Fig. 1

A schematic view of the apparatus is shown in Fig. 1. The apparatus is made from a glass cylinder to which several side arms are attached. One end of the cylinder is sealed while the other end is covered by a removable plate which can be made airtight with greased ground-glass surfaces. The apparatus is 3 inches high and has a diameter of $4\frac{1}{2}$ inches. Each side arm is stoppered with a 'Suba-Seal' rubber cap. Air-sensitive crystals can be grown inside the apparatus or introduced into it [watch glass (*A*)] inside a dry box. (*B*) and (*C*) are containers for the drying agent and glue respectively. (*D*) is a rod in a tightly fitting grease-filled cylinder pierced through the rubber seal. A circular plate attached to the rod carries capillary tubes (Lindemann glass tubes) held by plasticine. (*E*) represents rods which have glass fibres attached and are used for selecting and mounting crystals. A considerable degree of laterial movement is possible because of the flexibility of the 'Suba-Seal' cap. Crystals are delivered into the tubes and the open ends are then sealed with glue before being removed from the apparatus. (*F*) is a spare side arm which could be used for fitting a vacuum line to the apparatus, or for some other purpose.

The attractive features are the easy manoeuvrability of the apparatus for selecting and mounting crystals that have been grown in an inert environment and the ability to view the crystals in an unimpaired manner under a microscope during mounting.

G. A. RODLEY
Y. S. NG

Department of Chemistry
University of Canterbury
Christchurch
New Zealand

(*Received* 13 *December* 1976; *accepted* 15 *January* 1977)

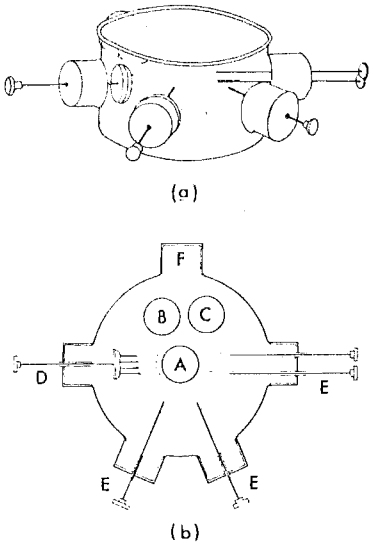

Fig. 1. Details of apparatus: (*a*) perspective view, (*b*) vertical plan.